THE MEGACRYST SUITE FROM THE SCHULLER KIMBERLITE, SOUTH AFRICA

by

Deon de Bruin

Thesis submitted in fulfilment of the requirements
for the degree of Doctor of Philosophy

Department of Geochemistry
University of Cape Town

August, 1991

DECLARATION

I hereby declare that all the work presented in this thesis is my own, except where otherwise stated in the text.

Signature Removed

Deon de Bruin
August, 1991

ABSTRACT

Clinopyroxene, orthopyroxene, garnet, ilmenite and olivine megacrysts from the Schuller kimberlite were analysed for major elements by electron microprobe and selected samples were analysed for trace elements by proton probe. In addition a number of clinopyroxene samples were analysed for Nd and Sr isotope compositions using mass spectrometry.

Clinopyroxene, orthopyroxene and garnet megacrysts from Schuller define unusually large compositional ranges. The clinopyroxene megacrysts plot as four distinct compositional groups which include: subcalcic, low Mg# (group 1), subcalcic, intermediate to high Mg# (group 2), calcic, low Mg# (group 3) and calcic, high Mg# (group 4) varieties. These compositions encompass and expand the range for both Cr-poor and Cr-rich clinopyroxene megacrysts from world-wide kimberlite localities. Major and trace element variations indicate that the respective clinopyroxene groups represent the products of crystallisation from a number of compositionally distinct magmas.

The trace element modelling of liquids in equilibrium with the group 1 clinopyroxene megacrysts cannot be reconciled with observed trends unless a small amount of a phase with a high Sr distribution coefficient, such as carbonate, is included with the megacryst crystallisation assemblage.

Combined Nd- and Sr isotopic data show overlapping initial Nd ratios for the various clinopyroxene megacryst groups but distinct initial Sr ratios between the groups. Consanguineity between major element and Sr isotope data for the clinopyroxene groups can be demonstrated at this locality. The group 1 clinopyroxene megacrysts (with intermediate Sr ratios) represent the crystallisation products of an "alkali-basaltic" magma of OIB affinity. The group 2 megacrysts (with unradiogenic Sr ratios) represent the product of interaction between a primary magma (such as represented by the group 1 clinopyroxenes) with a depleted MORB-type source followed by differentiation. Interaction of a similar primary magma with coarse peridotites, followed by crystallisation, would result in the group 4 megacrysts with radiogenic Sr ratios. The similarity in Sr isotopes of groups 1 and 3, and the extreme enrichment of incompatible elements in group 3 suggests that this material represent the products of extreme fractionation of the group 1 starting material.

The above interpretation would imply that the variation in megacryst magma compositions at different localities could be produced by varying amounts of lithospheric interaction with a primitive megacryst magma source followed by fractionation.

CONTENTS

CHAPTER 1: INTRODUCTION 1

1.1 LOCALITY DESCRIPTION 1

1.1.1 Geographic location 1
1.1.2 Mining history 1
1.1.3 General geology and previous work .. 2
1.1.4 Xenolith assemblage found at Schuller 3

1.2 AIMS OF THIS STUDY 4

CHAPTER 2: MEGACRYST REVIEW AND DESCRIPTION OF SAMPLES 6

2.1 REVIEW OF KIMBERLITIC MEGACRYSTS 6

2.2 DESCRIPTION OF SAMPLES 11

2.2.1 Garnet 12
2.2.2 Clinopyroxene 13
2.2.3 Orthopyroxene 13
2.2.4 Olivine 13
2.2.5 Ilmenite 14
2.2.5 Megacrysts with inclusions 14

2.3 ANALYTICAL METHODS 15

2.3.1 Electron microprobe 15
2.3.2 Proton microprobe 16
2.3.3 Radiogenic isotopes 16

CHAPTER 3: MINERAL CHEMISTRY 17

3.1 CLINOPYROXENE MEGACRYSTS 17

3.1.1 Introduction 17
3.1.2 Clinopyroxene megacryst compositions 18
3.1.3 Megacrysts from the Premier kimberlite 20
3.1.4 Comparison with Schuller lherzolite clinopyroxenes 23
3.1.5 Comparison between Premier clinopyroxene megacrysts and lherzolites 24
3.1.6 Comparisons with other localities .. 25
Northern Lesotho 26
Jagersfontein 26
Lekkerfontein 27
Orapa 28
Colorado-Wyoming 28
Mukorob 29
Eastern Griqualand 30
Hamilton Branch 30
Kimberley Group 31
Camutue 31
Witberg 32
3.1.7 Discussion 32

3.2 ORTHOPYROXENE MEGACRYSTS 39

3.2.1 Introduction 39
3.2.2 Orthopyroxene megacrysts compositions at Schuller 40
3.2.3 Comparison of megacryst orthopyroxenes with Schuller and Premier lherzolite orthopyroxenes .. 42
3.2.4 Comparisons with other localities .. 44
Monastery 44
Letseng-la-terae 44
Jagersfontein 45
Eastern Griqualand 45
Hamilton Branch 46
Sloan-Nix 46
3.2.5 Discussion 47

3.3 GARNET MEGACRYSTS 50

3.3.1 Introduction 50
3.3.2 Garnet megacryst compositions at Schuller 51
3.3.3 Comparison of megacryst garnets with Schuller and Premier lherzolite garnets 52
3.2.4 Comparisons with other localities .. 52
Monastery 53
Jagersfontein 53
Lekkerfontein 54
Orapa 54
Iron Mountain 55
Sloan-Nix 55
Mukorob 56
Eastern Griqualand 56
Hamilton Branch 56
Witberg 56
3.2.5 Discussion 56

3.4 OLIVINE MEGACRYSTS 58

3.5 ILMENITE MEGACRYSTS 58

3.6 DISCUSSION 60

3.6.1 The Schuller megacryst suite 60
3.6.2 Geothermobarometry 64
3.6.3 Regional megacryst compositional variations 67

CHAPTER 4: TRACE ELEMENT VARIATIONS 72

4.1 INTRODUCTION 72

4.2 SELECTION OF SAMPLES 74

4.1.2 Analytical 74

4.3 CLINOPYROXENE 75

4.3.1 Strontium 75
4.3.2 Zirconium 76
4.3.3 Gallium 76
4.3.4 Nickel 77
4.3.5 Zinc 78

4.4 ORTHOPYROXENE 78

4.5 GARNET 78

4.6 MODELLING 79

4.6.1 Introduction 79
4.6.2 Choice of Kd's 79
4.6.3 Description of model used for equilibrium crystallisation 80
4.6.4 Sr vs Zr 82
4.5.4 Ti vs Zr 84

4.7 DISCUSSION 84

CHAPTER 5: ND AND SR RADIOGENIC ISOTOPES **88**

5.1 INTRODUCTION 88

5.2 SAMPLE SELECTION 89

5.3 QUALITY OF ISOTOPIC RESULTS 90

5.3.1 Sm and Nd 90
5.3.2 Rb and Sr 90

5.4 ND ISOTOPE DATA 92

5.4.1 Nd and Sm concentrations 92
5.4.2 Nd isotopic ratios 93

5.5 SR ISOTOPE DATA 94

5.5.1 Sr and Rb concentrations 94
5.5.2 Sr isotopic ratios 95

5.6 DISCUSSION 98

CHAPTER 6: GENERAL CONCLUSIONS **101**

6.1 THE SCHULLER MEGACRYSTS 101

6.1.1 Introduction 101
6.1.2 Crystallisation conditions 101
6.1.3 Discussion 103

6.2 PREMIER 107

6.3 COMPARISONS WITH OTHER LOCALITIES 110

6.3.1 General 110
6.3.2 Regional variations 111

6.4 RELATIONSHIP BETWEEN MEGACRYSTS AND KIMBERLITE 112

ACKNOWLEDGEMENTS 117

REFERENCES 119

LIST OF FIGURES 129

FIGURES 135

LIST OF APPENDICES 199

APPENDICES 200

CHAPTER 1 : INTRODUCTION

1.1 LOCALITY DESCRIPTION

1.1.1 Geographic location

The Schuller kimberlite is situated in the Cullinan district of the Transvaal Province, South Africa, approximately 30 km east-northeast of Pretoria. The precise location of the mine is 25^{o} 45′ 37′′ south and 28^{o} 31′ 50′′ east, at an elevation of 1505 m above sea level. It is one of 11 kimberlite intrusions in the Premier cluster (Wagner, 1911), the largest of which is the well known Premier kimberlite (Figure 1.1).

1.1.2 Mining history

The first kimberlite discovered in the area was the Premier kimberlite in approximately 1891 by a prospector Thomas Cullinan. The farm owner prohibited prospecting on his farm, but Cullinan obtained some yellow ground by burying one of his oxen at the location from which he believed the alluvial diamonds on the farm Beyenestpoort emanated. This material was processed and shown to contain diamonds (Gerryts, 1951).

The Schuller and National kimberlites were discovered within the subsequent decade. They are separated by only 700 m. The National kimberlite is situated on the farm

Rietfontein whereas the Schuller kimberlite is traversed by the boundary between farms Rietfontein and Kaalfontein.

Both the Schuller and National pipes have been mined intermittently from the early part of this century. Records on diamond production exist from 1903 for the National kimberlite and from 1911 for the Schuller kimberlite. These records show that by 1926, 136 239 metric tons of kimberlite had been processed from Schuller for an average grade of 14.66 carat/100 ton whilst 44551 metric tons of kimberlite from the National kimberlite gave an average grade of 39.65 carat/100 ton. Wagner (1911) found diamonds at the Schuller mine to be dull lustreless stones, 90 % of which were cleavage fragments with numerous brown stones resembling those found at Premier.

1.1.3 General geology and previous work

The Schuller diatreme measures 150 x 90 m and consists of a core of massive hypabyssal kimberlite which is surrounded by more weathered kimberlite breccia. Blue tuffaceous kimberlite occurs on the southwestern side of the diatreme. The diatreme is intruded into quartzites of the Transvaal System.

Very little published work exists on Schuller. The geology has been described by Viljoen (1981) who also described the petrography of the Schuller kimberlite while garnet

and ilmenite macrocrysts were described by Underwood (1987). Eclogites and clinopyroxene megacrysts from Schuller have been described by de Bruin (1989, 1990) respectively. The presence of megacrysts and particularly ilmenite suggests that like Premier, Schuller is a Group I kimberlite (after Smith, 1983a).

No age determination exists for the Schuller kimberlite, itself but the immediately adjacent National kimberlite yields a Rb/Sr mica-age of 1180 +/- 30 my (Allsopp and Kramers, 1977). A closely similar Proterozoic age has also been established for the Premier diatreme by a number of techniques (Allsopp et al., 1967; Barrett and Allsopp, 1973; Kramers, 1979; Kramers and Smith, 1983; Smith, 1983b; Jones, 1987; Burgess et al., 1989). As kimberlites in the same cluster frequently have similar ages of emplacement and since the Schuller kimberlite has close similarities with both the National and Premier kimberlites it is strongly inferred that the Schuller kimberlite is also Proterozoic in age.

1.1.4 Xenolith assemblage found at Schuller

The collection of a large number of kimberlite xenoliths from the Schuller kimberlite was facilitated by a temporary period of mining between 1984 and 1987. All the xenoliths were collected from a 1 to 3 cm concentrate from the rotary pan separation in the mining process. As all kimberlite was crushed before treatment, no large

xenoliths were available. Concentrate dumps were continually reprocessed by further crushing so that very limited material was available during any particular visit to the mine. As the samples were collected during numerous visits over a long time span, the collection is thought to be representative of the Schuller kimberlite as a whole at this sampling horizon.

Xenoliths of coarse garnet-, garnet-spinel-, and spinel lherzolites, garnet websterites, websterites, eclogites, one garnet granulite and megacrysts of ilmenite, clinopyroxene, garnet, orthopyroxene and olivine were collected.

The xenolith suite found at the Schuller kimberlite is very similar to that found at Premier (personal observation). Although Danchin (1979) stated that garnet bearing peridotites are the predominant xenolith phase at Premier, it would appear in fact that similar to Schuller, the spinel peridotites are the most common xenolith phase (own observations, Bartlett personal communication).

1.2 AIMS OF THIS STUDY

A preliminary study of megacrysts from Schuller revealed an exceptionally large range in compositions, especially for the clinopyroxenes. The present study was directed to establish the full range in chemical compositions of the

megacryst suite present at Schuller inclusive of the phases clinopyroxene, orthopyroxene, garnet, ilmenite and olivine. Results from major and trace element compositions of megacrysts and Rb-Sr and Sm-Nd isotope compositions of clinopyroxene megacrysts will be used to define the petrogenesis of the megacrysts in terms of a single or separate group(s). The relationship between megacrysts and their host magma the kimberlite will also be addressed.

CHAPTER 2 : MEGACRYST REVIEW AND DESCRIPTION OF SAMPLES

2.1 REVIEW OF KIMBERLITIC MEGACRYSTS

Monomineralic crystals of large size (> 1 cm) are particularly abundant in many Group I kimberlites and have been referred to as megacrysts or discrete nodules. The megacryst suite includes olivine, orthopyroxene, clinopyroxene, garnet, ilmenite, phlogopite and minor zircon (Moore, 1986). These occur as single, almost always anhedral and chemically homogeneous crystals with occasional inclusions of another phase within the host. Coarse oriented intergrowths of ilmenite with clinopyroxene, and to a lesser extent with orthopyroxene, are often found. Garnet inclusions in ilmenite are quite common. Granular intergrowths of ilmenite and zircon have recently been described from Monastery, Moore (1986).

Megacrysts are distinguished from other xenoliths by virtue of their large size and distinct chemical composition. Despite numerous studies controversy still exists whether megacrysts are xenocrystal or phenocrystal in the kimberlite host (Smith, 1983b; Jones, 1984; Mitchell, 1986).

Two compositionally distinct suites are known from major element and physical characteristics : chrome-poor and chrome-rich megacrysts. The latter were first described

from the Colorado-Wyoming kimberlites by Eggler and MacCallum (1976). In addition to being high in chrome, chrome-rich megacrysts are distinct from the chrome-poor megacrysts in being more calcic and magnesian. Chrome-poor megacrysts predominate numerically in most megacryst bearing kimberlites although megacrysts of the chrome-rich suite have been found to be relatively abundant in the Sloan-Nix kimberlite, (Eggler et al., 1979) and to a lesser extent at Orapa (Shee and Gurney, 1979).

Megacrysts which do not readily fit in the above classification have also been described i.e. pyroxene megacrysts with coarse exsolution lamellae, (Jakob, 1977; Eggler et al., 1979; Aoki et al., 1980) and chrome-rich clinopyroxene 'Granny Smith' megacrysts which have chemical similarities to amphibole-free glimmerite xenoliths and are distinguished by the presence of ilmenite and the virtual absence of garnet and amphibole (Boyd et al., 1984).

Most models dealing with the formation of megacrysts have focused on the origin of chrome-poor megacrysts due to their predominance over chrome-rich megacrysts in kimberlites and the fact that their mineral compositions define excellent trends (Gurney et al., 1979) which can be readily interpreted. The chrome-rich megacrysts and exsolved megacrysts are not generally considered to be related to the chrome-poor megacrysts. Eggler et al.

(1979), however suggested that both the chrome-poor and chrome-rich suites could be formed by localised melting and crystallisation in a rising diapir. Hunter and Taylor (1984) proposed a model of a primary chrome-rich melt interacting with earlier formed 'fractionated' chrome-poor melt to account for the presence of the Cr-poor and Cr-rich megacryst suites and the reverse zoned rims on the ilmenite megacrysts from the Fayette County kimberlite.

The coarse grain size, major element variation trends and distinct mineral chemistry of chrome-poor megacrysts relative to peridotite xenoliths have been interpreted as the result of crystallisation from fractionating liquids at depths greater than 150 km (e.g. Gurney et al., 1979; Eggler et al., 1979; Garrison and Taylor, 1980; Harte and Gurney, 1981). The megacrysts are thought to represent phenocrysts or pegmatoidal phases derived from a magma at depth.

In contrast, Boyd and Nixon (1973) and Pasteris et al. (1979) have related the wide temperature and chemical variations found amongst megacrysts to formation from an interstitial melt at the top of the asthenosphere which is dispersed over a depth range of several tens of kilometres in the upper mantle with the magma showing decreasing temperature and Mg/(Mg+Fe) with decreasing depth.

Although wide ranges are found in the temperature estimates of megacrysts, the pressure estimates define a relatively narrow range. Gurney et al. (1979) thus related the formation of the Monastery megacrysts to isobaric differentiation of a uniformly cooling magmatic body of limited extent through the range of estimated megacryst temperatures. This model, which requires the slow cooling of megacrysts, is however not readily compatible with the absence of extensive exsolution features in high temperature subcalcic diopsides which is indicative of rapid eruption at high temperatures (McCallister and Nord, 1981).

A more detailed model for the formation of the chrome-poor megacryst suite was proposed by Harte and Gurney (1981) in which megacrysts form from a magma body of limited vertical extent as an intricate series of sheets. It was proposed that temperature differences between the hot magma and the relatively cooler country rocks would lead to heat convection and that differences in the relative motion of the liquid and crystals would promote differentiation of the magma to allow megacrysts of widely differing compositions and crystallisation temperatures to form simultaneously. This model allows the megacrysts sampled by kimberlites to show "frozen in" high temperature compositions preserved by rapid chilling whilst also allowing the development of a broad spectrum of temperatures of formation at the same pressure. The

formation of high-temperature deformed peridotite xenoliths was suggested to be associated with the development of the megacryst magma body by metasomatic exchange with the magma (Gurney and Harte, 1980).

The controversy regarding the origin of the megacryst suite largely revolves around the question of whether or not megacrysts are cognate to the kimberlite. Several researchers have proposed that megacrysts crystallised from a proto-kimberlite magma with megacrysts being early formed phenocrysts to the kimberlite (Haggerty and Boyd, 1975; Gurney et al., 1979; Eggler et al., 1979; Schulze, 1982a). These conclusions were supported by the presence of possible magmatic inclusions in certain megacryst phases. The conclusion of Eggler and Wendlandt (1979) that the megacryst phases (garnet, olivine, clinopyroxene and orthopyroxene) can co-exist with kimberlitic liquid at 50 - 60 kb pressures allows a cognate megacryst origin. A similar suite of minerals in alkali basalts are almost universally accepted as phenocrysts (Schulze, 1987).

Jones (1987) demonstrated that calculated model REE patterns for chrome-poor clinopyroxene and garnet megacrysts are unlike kimberlite but similar to primitive alkali basalts. Similar results were obtained by Harte (1983) who suggested on the basis of the forsterite content of megacryst olivines that the parental megacryst magma was picritic. In contrast the chrome-rich and Granny

Smith megacrysts have calculated REE patterns which are similar to the host kimberlites (Jones, 1987).

Various studies on the Sr and Pb isotopic compositions of megacrysts studies have concluded that megacrysts and the kimberlites in which they occur are not in equilibrium (Barrett, 1975; Kramers, 1979; Demaiffe and Fieremans, 1981; Ntanda et al., 1982; Smith, 1983b; Jones, 1987; Spriggs, 1988). Smith (1983b) concluded from isotopic studies of megacrysts and their host kimberlites that neither chrome-rich nor chrome-poor megacryst suites are in isotopic equilibrium with kimberlites and that megacrysts are true xenocrysts. [However his discussion assumes that kimberlite isotopic measurements are unmodified by interaction with the crust, which is not true.] Chrome-poor subcalcic clinopyroxene megacrysts from a spread of localities covering some million square kilometres across the Kalahari craton define a restricted field in terms of initial Sr and Nd ratios which is close to the mantle array and comparable in size with fields defined by many single ocean islands (White and Hofmann, 1982; Jones, 1987)

2.2 DESCRIPTION OF SAMPLES

Megacrysts were collected from Schuller mine between 1983 and 1987. As all were recovered from mine concentrate dumps, it was impossible to establish a relationship

between the samples and any particular kimberlite intrusive phase within the diatreme. The megacrysts occur in the following order of abundance garnet > clinopyroxene = ilmenite > orthopyroxene > olivine. Monomineralic crystals of > 1 cm covering the spectrum of physical characteristics i.e. colour and surface features for each megacryst phase, were selected for analyses. Initially, single thin sections were prepared for each megacryst, but at a later stage, edge and centre fragments of megacrysts were prepared as multiple grain mounts. In neither the thin sections nor the multiple grain mounts was significant chemical inhomogeneity detected by the electron microprobe.

2.2.1 Garnet

Two groups of garnet megacrysts may be identified from hand specimens :

i) Rounded megacrysts with smooth, unbroken surfaces ranging in size between 1 and 3 cm in the longest dimension. These megacrysts vary between deep red to orange with reddish shades.

ii) Garnets with typically conchoidally broken surfaces and colours ranging between lavender and red. These garnet megacrysts also seem to have a purplish surface coating which distinguishes them from the first group. The coatings are often found along fracture surfaces

penetrating the crystals and on the surface of broken crystals.

2.2.2 Clinopyroxene

Clinopyroxene megacrysts occur in colours ranging between pale green to bottle green. The chrome-rich specimens are generally bottle green although such samples are also found amongst the subcalcic samples. Sizes range between 1 cm to a sample of 3.5 cm in the longest dimension.

2.2.3 Orthopyroxene

The orthopyroxene megacrysts studied were all larger than 1 cm and specimens of up to 3.5 cm in the largest dimension were found. Most specimens are typical cleavage fragments similar to those described by Bloomer and Nixon (1973) and the well rounded surfaces seen amongst the garnets were not present. Two major colour variations are found which correspond to the bronzite and enstatite megacrysts described from Letseng-la-terae (Bloomer and Nixon, 1973): i) smoky brown colour and ii) grey-green glassy to almost yellow green.

2.2.4 Olivine

The olivine megacrysts were broken crystal fragments with a yellow brown to light brown colour. Only five samples were found.

2.2.5 Ilmenite

Ilmenite was very common. All ilmenite megacrysts selected for analyses were larger than 1 cm. Individual nodules are typically smooth and rounded although numerous broken fragments were also found. The overall appearance in hand specimen is similar to that described from other localities (e.g. Frick, 1973; Mitchell, 1973).

2.2.6 Megacrysts with inclusions

All megacrysts with inclusions were selected for analysis and these were prepared as single thin sections.

Two orthopyroxene megacrysts contain garnet as inclusions. In one (85/08) a single garnet inclusion measuring 1 by 0.5 mm was found while the other sample (86/118) contains a number of garnet inclusions. In the latter sample clinopyroxene was also found as small grains associated with garnet kelyphitic rims. Two further orthopyroxene megacrysts showed exsolution features, one exsolving garnet along cleavage and fractures (86/121) and the other exsolving clinopyroxene (86/103).

A clinopyroxene was found to co-exist with orthopyroxene (86/03). This sample contains unstrained megacrystalline clinopyroxene in contact with a strained and partially re-crystallised orthopyroxene. In one instance the orthopyroxene occurs as an inclusion within the clinopyroxene which would suggest that the clinopyroxene

crystallised after the orthopyroxene. Both the orthopyroxene and clinopyroxene portions have been invaded by alteration zones.

Two fresh occurrences of silicate / ilmenite associations were found. One with orthopyroxene, (86/114) and the other with clinopyroxene (86/83). A serpentinised clinopyroxene megacryst with ilmenite rods (86/150) was too altered for analysis. A number of ilmenite megacrysts were found to contain small pyroxene inclusions which were too altered for analysis.

2.3 ANALYTICAL METHODS

2.3.1 Electron microprobe

Initial electron microprobe analyses were done using a Cameca Camebax at the University of Cape Town. Appendix 1 lists the analytical conditions. Subsequent electron microprobe work was done at the South African Geological Survey using a Jeol 733 electron microprobe. Analytical conditions and standardisation techniques were similar. The analytical condition and standards used are also listed in Appendix 1.

Data for 76 clinopyroxene, 31 orthopyroxene, 40 garnet, 69 ilmenite and 5 olivine megacrysts together with the co-existing megacryst associations from the Schuller kimberlite are presented in Appendix 2.

In addition to the megacryst samples from the Schuller kimberlite, additional analyses of clinopyroxene megacrysts from Premier (69) and Orapa (29) were completed in this study to characterise the clinopyroxene megacryst suites from these kimberlites (Appendix 3).

2.3.2 Proton microprobe

The proton microprobe analyses were done by R.O. Moore using the HIAF facility at CSIRO, North Ryde, Australia. Analytical conditions were described by Griffin et al. (1988). The data are presented in Appendix 4.

2.3.3 Radiogenic isotopes

Selected clinopyroxene megacrysts were processed for Rb-Sr and Sm-Nd isotope analyses at the Bernard Price Institute of the University of the Witwatersrand under the supervision of C.B. Smith. The procedures used, analytical conditions together with the results are presented in Appendixes 5 and 6.

CHAPTER 3 : MINERAL CHEMISTRY

3.1 CLINOPYROXENE MEGACRYSTS

3.1.1 Introduction

Both the chrome-poor and chrome-rich clinopyroxene megacryst suites are well defined at Schuller. Minerals from both suites show a certain amount of chemical coherence with the same phases from other kimberlites at widely dispersed localities. Chrome-poor megacrysts from Monastery, described by Jakob (1977) and Gurney et al. (1979) and chrome-rich megacrysts from Sloan-Nix, described by Eggler et al. (1979) were generally considered as respective type examples.

Clinopyroxene megacrysts have been most frequently used for the definition of compositional groups as they display strong trends with readily recognised decreasing temperature (Eggler et al., 1987). These are not so easily identified in other megacryst minerals.

The clinopyroxene megacrysts found at Schuller display wide major element chemical variations which plot in a number of distinct chemical groups. These correspond to the chrome-poor, the chrome-rich and to some 'anomalous' megacrysts that have been partly characterised in the literature (Eggler et al., 1979). Clinopyroxene megacrysts from Premier are similar. Since the Schuller and Premier

kimberlites both have these very diverse chemically defined groups, previously described only from different localities, this Proterozoic kimberlite group is currently unique.

3.1.2 Clinopyroxene megacryst compositions

Based on major elements four distinct groups of clinopyroxene megacrysts are present at Schuller. The groups can be characterised on the basis of Ca#, Cr_2O_3 and Mg# (Figures 3.1.1 and 3.1.2) as :

Group

1 Subcalcic megacrysts with low chrome

2 Subcalcic megacrysts with intermediate chrome,

3 Calcic megacrysts with low chrome and

4 Calcic megacrysts with high chrome.

The group 1 clinopyroxenes have Ca# in the range 28.04 to 36.63 with low Mg# (79.30 - 86.45) and Cr_2O_3 concentrations (0.08 - 0.26 wt %). The Mg# and the Cr_2O_3 content decrease while Na_2O and TiO_2 increase linearly with increasing Ca# (Figures 3.1.1 to 3.1.4). These trends parallel those found in subcalcic clinopyroxene megacrysts described from Lesotho, (Nixon and Boyd, 1973) Monastery, (Jakob, 1977) and Lekkerfontein (Robey, 1981) but they are distinctly more Fe-rich at equivalent Ca#. In previous relevant studies (e.g. Schulze, 1987) it was found that

clinopyroxene megacrysts from world-wide localities have equivalent or higher Mg# and Cr concentrations than those at Monastery. In contrast the group 1 clinopyroxene megacrysts from Schuller have lower Mg# and Cr relative to Monastery Cr-poor megacrysts (or any other Cr-poor clinopyroxene megacrysts described from kimberlites). This extends the field for Cr-poor clinopyroxene megacrysts.

The subcalcic, intermediate chrome megacrysts (group 2) display a wider scatter of compositions with an overall increase in Mg# and Cr_2O_3 and decrease in Na_2O and TiO_2 with increasing Ca# (Figures 3.1.1 to 3.1.4). Although subcalcic, they contain distinctly higher Cr_2O_3 and Mg# than the group 1 clinopyroxene megacrysts at equivalent Ca#. Two apparent subpopulations can be distinguished : a lower Cr_2O_3, subcalcic and relatively iron-rich group (2a) and a higher Cr_2O_3, more calcic and magnesium-rich group (2b) (Figures 3.1.1 and 3.1.2). The group (2a) have chemical features closer to the subcalcic group 1 clinopyroxene megacrysts and the group (2b) have chemical features closer to the chrome-rich (group 4) group.

Twelve of the clinopyroxene megacrysts from Schuller are calcic (Ca# 44.29 to 45.97) with low Cr_2O_3 (0.24 to 0.39 wt %) (group 3). This group of megacrysts have Ca# within the range found in typical chrome-rich (group 4) megacrysts but the low Cr_2O_3 concentrations and Mg# (range 83.38 - 84.52) distinguish them from the former (Figures

3.1.1 and 3.1.2). Overlapping values of Cr_2O_3, TiO_2 and Na_2O do occur between groups 4 and 3 but group 3 generally contains higher Na_2O and lower Cr_2O_3 than group 4 (Figures 3.1.3 and 3.1.2).

In two samples where co-existing phases occur with clinopyroxene, (ilmenite: sample 86/83; orthopyroxene: sample 86/03), both clinopyroxenes are group 3.

The chrome-rich megacrysts (group 4) are calcic with Ca# of 43.51 to 45.89, high and constant Mg# (91.49 - 92.63) and high Cr_2O_3 values (1.10 to 1.45 wt %) (Figures 3.1.1 and 3.1.2). Na_2O and TiO_2 are within the range found in the other megacryst groups (Figures 3.1.3 and 3.1.4). These megacrysts are chemically similar to the chrome-rich clinopyroxene megacrysts described from Colorado-Wyoming, (Eggler et al., 1979) and Orapa, (Shee, 1978) although minor differences are apparent. In Colorado-Wyoming a distinctly lower Na_2O was reported for the chrome-rich megacrysts relative to the Cr-poor samples. This is not found at Schuller.

3.1.3 Megacrysts from the Premier kimberlite

The clinopyroxene megacrysts from Premier studied for comparison fall into at least three distinct compositional groups with respect to Ca#, Mg# and Cr_2O_3 contents which broadly correspond to groups 1, 2 and 4 at Schuller but they are not absolutely identical (Figures 3.1.5 and

3.1.6). They have been classified using the scheme proposed for Schuller into:

Group

1 Subcalcic megacrysts with low Mg# and chrome;

2 Subcalcic megacrysts with high Mg# and chrome;

4 Calcic megacrysts with high Mg# and intermediate chrome.

The group 1 clinopyroxene megacrysts found at Premier fall within the compositional field delineated by the group 1 clinopyroxene megacrysts from Schuller but a smaller range in compositions is found. These are equivalent to the intermediate to highly fractionated samples relative to Schuller.

For group 2, as at Schuller there are two compositional sub-groups. Three samples (group 2a) plot close to the group 1 field whereas the rest (group 2b) contain generally higher Mg# and chrome contents and lower titanium and sodium contents than the group 1 samples (Figures 3.1.5 to 3.1.8). The anomalously chrome-rich subcalcic diopside described from Premier by Smith (1983b) is chemically similar to the group (2b).

The calcic samples (group 4) (these are similar to group 4 at Schuller) plot as a dispersed group with high Mg# and TiO_2 contents and intermediate Cr_2O_3 contents. A broad

decrease in Cr_2O_3 and TiO_2 is found with increasing Ca# (Figures 3.1.6 and 3.1.7). Relative to similar samples from Schuller these calcic clinopyroxene megacrysts are actually intermediate in composition between the groups 3 and 4 with slightly lower Mg# and distinctly lower Cr_2O_3 contents. No clinopyroxene megacrysts with equivalent compositions to the calcic, magnesian Schuller samples (group 3) have been found at Premier.

Both Premier and Schuller contain multiple clinopyroxene megacryst groups. The subcalcic group (group 1) have overlapping compositions but differences are found for the group 2 and 4 megacrysts at the two localities. The relative proportions for the groups are not the same. Whereas 30 % of clinopyroxene megacrysts at Schuller are group 1 (subcalcic and Cr-poor), only 12% of group 1 samples are found at Premier. Similarly the calcic and magnesian group 4 constitute 28 % of the Schuller population but 65% at Premier. As noted above samples similar to the group 3 clinopyroxenes (16 % of the clinopyroxene population Schuller) are absent at Premier.

Note that the group 1 clinopyroxene megacryst compositions at Schuller and Premier overlap whereas readily identifiable differences are found in groups 2 and 4. This could indicate that group 1 reflect the composition of a primary melt whist the other groups have been affected in differing ways by more localised processes such as

variable degrees of partial melting, wall rock interaction or magma mixing.

3.1.4 Comparison with Schuller lherzolite clinopyroxenes

Although all the megacrysts that were analysed were larger than 1 cm in the longest dimension, the possibility exists that some could result from the disaggregation of coarse peridotites. Addressing this problem, Figures 3.1.9 to 3.1.12 depict comparisons between clinopyroxene megacryst compositions from Schuller, and clinopyroxenes from garnet lherzolites at the same locality. It is clear that the groups 1, 2 and 3 megacrysts cannot be from lherzolites.

Although some similarities between the major element composition of the Cr-rich megacrysts (group 4) and clinopyroxenes from garnet lherzolites are evident, especially with respect to Mg# (Figure 3.1.9), distinct differences are apparent in minor element contents i.e. the lherzolites have generally higher Cr_2O_3 (Figure 3.1.10) and lower TiO_2 (Figure 3.1.11). In general therefore the two populations are distinct. Four of the garnet lherzolites however have similar minor element chemistry. The clinopyroxenes of the spinel lherzolites (not shown) have higher Ca# and Mg# and lower TiO_2 concentrations relative to the chrome-rich clinopyroxene megacrysts. Therefore it is not likely that any of the selected megacrysts are from lherzolites.

3.1.5 Comparison between Premier clinopyroxene megacrysts and lherzolites

Analyses of clinopyroxene from both coarse and sheared peridotites are available from Premier (Boyd, unpublished data) which allow the direct comparison of lherzolite and megacryst clinopyroxene compositions from that locality.

Clinopyroxenes from coarse peridotites at Premier have distinctly higher Mg# (Figure 3.1.13) and chrome contents (Figure 3.1.14) than the calcic megacrysts (group 4). Although some overlap is found for TiO_2 and Na_2O between the two groups (Figures 3.1.15 and 3.1.16), the lherzolites generally have lower TiO_2 and higher Na_2O than the calcic, Mg-rich megacrysts (group 4) from Premier. Overall clinopyroxenes from the coarse peridotites are therefore quite distinct.

Clinopyroxenes from sheared lherzolites at Premier show some chemical similarities to the magnesian, chrome-rich subcalcic megacrysts (group 2) in terms of major constituents (Figure 3.1.13). Nonetheless despite some overlap, the sheared lherzolite clinopyroxenes generally have higher Mg#, Cr_2O_3 and Na_2O contents (Figures 3.1.13 3.1.14 and 3.1.16). The TiO_2 of the sheared lherzolite clinopyroxenes tend to plot in two distinct fields with higher TiO_2 values between 0.35 - 0.65 % (majority of samples) and a smaller group with TiO_2 contents below 0.2

wt % (Figure 3.1.15). The group 2 megacrysts plot as an intermediate group with TiO_2 contents between 0.12 to 0.4.

3.1.6 Comparisons with other localities

Clinopyroxene megacrysts from occurrences world-wide were re-evaluated in order to establish gross variations in compositions. Data were obtained from a number of published and unpublished sources for Letseng-la-terae, (Bloomer and Nixon, 1973) Thaba Putsoa and Solane (Nixon and Boyd, 1973), Monastery (Jakob, 1977), Iron Mountain (Smith, 1977), Kimberley Pool (Boyd and Nixon, 1978), Orapa (Shee, 1978; Tollo, 1982), Camutue (Boyd and Danchin, 1980), Lekkerfontein (Robey, 1981), Mukorob II (Jones, 1984), Hamilton Branch (Schulze, 1982b), Jagersfontein (Hops, 1989), State Line (Eggler, unpublished data), Eastern Griqualand (Boyd, unpublished data) and Witberg (de Bruin, unpublished data) kimberlites. Although Cr-poor clinopyroxene megacrysts were first described from the Northern Lesotho kimberlites by Nixon and Boyd (1973) the clinopyroxene megacrysts from Monastery display a greater abundance and a wider range in composition and can in this sense be considered the type locality of Cr-poor clinopyroxene megacrysts (Figure 3.1.17 a and b). In the ensuing discussions the compositions of the clinopyroxene megacrysts from Monastery will be used as a reference field.

Northern Lesotho

Clinopyroxene megacrysts from each locality appear to occupy distinctive positions in Ca# / Mg# and Ca# / Cr_2O_3 compositional space. Clinopyroxene megacrysts from Letseng-la-terae and Thaba Putsoa largely overlap with the Monastery field but are confined to compositions on the subcalcic end of the Monastery trend (Figure 3.1.18 a and b). The Thaba Putsoa and Letseng-la-terae trend are similar to each other although a smaller compositional range is evident from Thaba Putsoa. The sparse analyses from the Solane kimberlite plot in a very restricted field distinct from Thaba Putsoa and Letseng-la-terae. The Solane samples have lower Mg# ratios and Cr concentrations at equivalent Ca# relative to the other two trends. A clinopyroxene inclusion within an ilmenite host from Solane is compositionally equivalent to the group 3 clinopyroxene megacrysts at Schuller.

Jagersfontein

The clinopyroxenes from Jagersfontein described by Hops (1989) were made up of both Cr-poor and 'Granny Smith' megacrysts. The Cr-poor megacrysts form a trend of decreasing Mg# ratio and Cr_2O_3 content with increasing Ca# ratio (Figure 3.1.19 a and b). The most subcalcic clinopyroxene megacrysts yet described are found at this locality. At Jagersfontein the trend does not extend to more calcic 'cooler' compositions and the ilmenite/ clinopyroxene association is very rare. Ilmenite

megacrysts are also absent at this locality. On critical examination it would appear that the diffuse trend shown by the Jagersfontein Cr-poor suite might be two separate trends. The most subcalcic samples form a trend with equivalent or lower Mg# and Cr_2O_3 than the Monastery samples while the samples with intermediate to low Ca# ratio have equivalent Mg# but higher Cr_2O_3 contents relative to the Monastery samples. Seen in the light of multiple megacryst populations at Schuller the possibility of two or more separate but very similar trends at Jagersfontein should be closely examined.

Lekkerfontein

Clinopyroxene megacrysts from Lekkerfontein described by Robey (1981) follow the Monastery trend but the starting composition is more calcic (Figures 3.1.20 a and b). At this locality three distinct clinopyroxene populations were found by Robey (1981) : 1) discrete clinopyroxene megacrysts, 2) clinopyroxene with lamellar ilmenite lamellae and 3) clinopyroxene as inclusions in ilmenite megacrysts. The discrete clinopyroxenes plot in two clusters with respect to Ca# but are more subcalcic than the clinopyroxene associated with ilmenite. The samples containing lamellar intergrowths have compositions intermediate between the discrete and inclusion samples. The clinopyroxenes which occur as inclusions in ilmenite extends to lower Ca# values than found at Monastery.

Orapa

A compilation of clinopyroxene megacryst compositions from Orapa by Shee (1978), Tollo (1982) together with the additional samples analysed in this study (Appendix 3, Table 2), show a scatter of points with the majority of the subcalcic samples with equivalent Mg# but higher Cr_2O_3 at similar Ca# relative to Monastery (Figure 3.1.21 a and b). In this respect Orapa is similar to Jagersfontein (Figure 3.1.19). A small group of subcalcic samples however form a distinct trend of decreasing Mg# and Cr_2O_3 with decreasing Ca# at higher Mg# and Cr_2O_3 values. Thus multiple Cr-poor megacryst groups are also clearly present at Orapa. The calcic, Cr-rich samples at this locality plot as two distinct groupings with respect to Cr_2O_3. A group of calcic, Cr-poor and Fe-rich samples is similar in composition to the group 3 clinopyroxene megacrysts described from the Schuller kimberlite. Therefore multiple Cr-poor clinopyroxene megacryst suites are also present at Orapa, similar to Schuller and Premier. This underscores the fact that relatively large numbers of megacrysts need to be analysed to define megacryst populations at any particular locality.

Colorado-Wyoming

Clinopyroxene megacrysts from Iron Mountain form a linear trend from calcic and magnesian compositions extending to lower Cr_2O_3 and Mg# in a parallel trend to Monastery (Figure 3.1.22 a and b). The clinopyroxene megacrysts from

Sloan-Nix, (Figure 3.1.23) on the other hand from a trend which initiates at equivalent Ca# and Mg# but at higher Cr_2O_3 than the Iron Mountain samples. Note the separate compositional grouping of the two Cr-poor suites at Sloan-Nix (Figure 3.1.23). The 'anomalous' Cr-poor group as defined by Eggler et al. (1979), which included a number of co-existing mineral assemblages, show constant Mg# but decreasing Cr_2O_3 with increasing Ca#.

Mukorob

The clinopyroxene megacrysts from Mukorob analysed by Jones (1984) show a general trend of decreasing Mg# with increasing Ca# (Figure 3.1.24). The samples appear to plot as three distinct groupings when Cr_2O_3 is considered with Ca# (Figure 3.1.24 b). Four samples with the highest Cr_2O_3 contents are the most subcalcic specimens found at this locality. A compositional gap separates these samples from the rest, which have similar Ca# (range 40 to 46) and Mg# (range 84 to 86) but appear to form two groups with respect to Cr_2O_3 contents. The samples with the highest Cr_2O_3 form a general trend of decreasing Cr_2O_3 with increasing Ca# with the most subcalcic samples whereas those samples with lower Cr_2O_3 values appear to form a separate trend. The latter samples contain a number of ilmenite/clinopyroxene intergrowths.

Eastern Griqualand

Grouping localities together, clinopyroxene megacrysts from Eastern Griqualand kimberlites (Boyd, unpublished data) contain distinctly higher Mg# and Cr_2O_3 contents, and have less developed correlations with Ca# compared to Monastery (Figure 3.1.25 a and b). Samples from the individual kimberlites show better element associations as is expected from the demonstrated individuality of every locality studied in this project. Clinopyroxene megacrysts from Ramatseliso show decreasing Mg# and Cr_2O_3 with increasing Ca#. Samples from Abbotsford plot in at least two groups which correspond to a subcalcic high Cr_2O_3 group which has higher Cr_2O_3 at equivalent Ca# relative to Ramatseliso samples and a lower Cr_2O_3 group which falls within the field of the Ramatseliso samples. A single sample from Abbotsford has a composition which falls within the range found at Monastery.

Hamilton Branch

Clinopyroxene megacrysts from the Hamilton Branch kimberlite described by Schulze (1982b; 1984) form a broad diffuse trend where constant Mg# accompanies decreasing Ca# (Figure 3.1.26 a). Two sub-groups are apparent with respect to chrome; a higher Cr_2O_3, more subcalcic group where Cr_2O_3 decreases with increasing Ca# and a less subcalcic group with low but constant Cr_2O_3 and a range in Ca# (Figure 3.1.26 b). The range in Ca# with relatively constant Mg# found at this locality has been ascribed to

the early entry in the crystallising assemblage of ilmenite with it's high Fe content (Schulze, 1984).

Kimberley Group

Boyd and Nixon (1978) described a limited number of clinopyroxene megacrysts from the Kimberley Group of kimberlites; Kampfersdam, Kimberley, De Beers Bultfontein and Wesselton. These megacrysts were found to be more subcalcic relative to the Northern Lesotho types. The more calcic and relatively Fe-rich compositions, especially those intergrown with ilmenite were absent as at Jagersfontein. However discrete ilmenite megacrysts are abundant at all of the Kimberley localities but are exceedingly rare at Jagersfontein. The majority of the samples from the different Kimberley localities show compositional overlap (Figure 3.1.27 a and b). They partially overlap with Monastery but the starting compositions are shifted to more subcalcic and magnesian compositions. Two samples from Wesselton are magnesian, calcic and contain higher chrome. Both these clinopyroxenes occur as inclusions, together with garnet, within orthopyroxene.

Camutue

Clinopyroxene megacrysts from Camutue (Boyd and Danchin, 1980) define three distinct groups (Figures 3.1.28 a and b), two of which are subcalcic and the other calcic. Two separate trends are apparent amongst the subcalcic groups

both of which show scattered but general decreases in Mg# and Cr_2O_3 with increasing Ca#. These samples have compositions which are distinctly richer in Mg# and Cr_2O_3 relative to Monastery. The calcic group is comprised of clinopyroxene megacrysts with inclusions of garnet (one) and ilmenite (two) and are very similar in composition to the group 3 clinopyroxene megacrysts described from Schuller.

Witberg

Clinopyroxene megacrysts from Witberg (de Bruin unpublished data) form a broad diffuse trend of decreasing Mg# and Cr_2O_3 with increasing Ca# ratios (Figure 3.1.29 a and b). Both the Mg# ratios and Cr_2O_3 concentrations are higher than at Monastery at equivalent Ca# ratios. There is some indication that two different groupings can be seen with respect to Cr_2O_3 concentrations. The most subcalcic samples form a trend of sharply decreasing Cr_2O_3 with increasing Ca# whereas another trend is apparent with more gently decreasing Cr_2O_3. A group of 4 samples have distinctly higher Cr_2O_3 at equivalent Ca# .

3.1.7 Discussion

It is evident from the foregoing descriptions that the clinopyroxene megacryst suites at both the Schuller and Premier kimberlites are unusual in that multiple compositional groups are present in single kimberlites which covers and extends the range of known clinopyroxene

megacryst compositions. At least four different groups are found for Schuller, three at Premier. The very strong trends displayed by the subcalcic, low Cr (group 1) clinopyroxene megacrysts at Schuller undoubtedly represent the products from a fractionating magma. The concomitant decrease in Mg# and Cr_2O_3 with increasing Ca#, Na_2O and TiO_2 would strongly favour an igneous origin. Since TiO_2 increases with increasing Ca# (declining temperature) it is unlikely that ilmenite was a crystallising phase within the group 1 clinopyroxene megacrysts.

In contrast group 2 megacrysts cover a wide field and show no strong linear trends. It is unlikely that they represent a single simple fractionation event but would more probably reflect the results of a number of events or the differential involvement of more than one process. The igneous trends seen at other localities is not strong within this group which has been subdivided into two separate subgroups (2a and 2b) on the basis of mineral chemistry. The samples with the lower Mg- and Cr-contents (group 2a) show a scatter of points with broad decreases in Mg# and chrome with increasing Ca# (Figures 3.1.9 and 3.1.10). Although these samples plot within the compositional field of typical Cr-poor clinopyroxene megacrysts such as Monastery, they do not extend to such extreme Fe-rich compositions and in this respect are closer to examples from localities such as Jagersfontein, Kimberley and Northern Lesotho. The increase of TiO_2 with

increasing Ca# within this group (Figure 3.1.11) is also similar to the latter localities which would suggest that ilmenite was not a co-precipitating phase. The group 2b samples are unusually rich in chrome and magnesium relative to other Cr-poor megacryst suites and have no known chemical equivalents (with the exception of Premier). These samples show a large range in TiO_2 at relatively constant Ca# which could indicate crystallisation with ilmenite (Figure 3.1.11). From the major element data it appears that compositions amongst this group plot closer to clinopyroxenes in sheared lherzolites. This could suggest that that some interaction with host rock peridotite is reflected in these compositions. The large size of these samples and their unstrained nature is indicative of crystallisation from a liquid and preclude an origin as disaggregated lherzolites.

Group 3, the calcic megacrysts with low chrome have a few reported compositional equivalents at other localities such as Orapa, Camutue and Northern Lesotho although examples are very sparse. These samples differ from the Cr-rich group 4 by virtue of low chrome contents. No consanguineity between this group and the other megacryst groups can be demonstrated on the basis of major element compositions. At Schuller, the only co-existing megacryst phases with clinopyroxene occur within this group. These are orthopyroxene and ilmenite

The group 4 samples show a narrow spread in Ca# and Mg# and have compositions similar to typical Cr-rich clinopyroxene megacrysts such as found at Sloan-Nix (Eggler et al., 1979) and Orapa (Shee, 1978). These features have been ascribed due to buffering with peridotite wall-rock (Eggler et al., 1979). Eggler et al. (1979) alternatively suggested that the source peridotite from which the liquids resulting in the precipitation of the Cr-rich suite were extracted had been contaminated by contact with refractory lithosphere. Similar compositions could conceivably also be generated if these samples represent an older megacryst forming event which equilibrated to ambient mantle conditions.

Despite the close geographic association between the Schuller and Premier kimberlites, important differences can be seen in both the abundance of the various clinopyroxene megacryst groups and subtle variations in the chemical composition of similar groups. This individuality is a strong indication that megacryst formation is modified by localised processes. The fact that the group 1 clinopyroxene megacrysts from the two kimberlites overlap might indicate that the magma from which these megacrysts crystallised is the closest to a primary composition derived from a more generalised source. Other mechanisms such as magma mixing, contamination or assimilation might be invoked to explain

compositional differences for the group 2 and group 4 megacrysts.

From the comparisons with lherzolite clinopyroxenes it is evident that the 'anomalous' megacrysts are not likely to be disaggregated lherzolites. Some general correspondence with the lherzolites might however imply that interactions have occurred. The general tendency for the group 2 samples to have similarities with clinopyroxene from sheared lherzolites whereas the group 4 samples have similarities to clinopyroxene from coarse lherzolites might not be coincidental.

The fact that multiple megacryst populations are increasingly being recognised amongst the Cr-poor suite (e.g. Schuller; Premier; Orapa) would place additional constraints on the models proposed for megacryst genesis. Broad diffuse chemical trends exhibited at some localities (e.g. Jagersfontein; Witberg) might thus be made up of a series of smaller events under slightly different conditions, which when sampled by a kimberlite, would produce a broad generalised overall trend. These observations strongly argue against the practise of compositing megacryst suites from adjacent localities, however convenient it might be due to a lack of samples.

The necessity to analyse a large number of megacrysts from individual kimberlites has been demonstrated by the common

presence of multiple megacryst populations. These can require detailed attention as for example at Mukorob, Orapa and Witberg and in Eastern Griqualand.

Some of the megacryst suites show a certain amount of clustering around specific compositions with compositional gaps between clusters (e.g. Mukorob, Lekkerfontein and Abbotsford). It is not clear whether this is a function of sampling or an indication of specific formation processes, but the latter idea is favoured.

Within the southern African context it is remarkable that localities from within the Kalahari Craton have Cr-poor clinopyroxene compositions that largely overlap in terms of Ca#, Mg# and Cr_2O_3 contents but that compositions from localities from off-craton or near craton edges generally have higher Mg# and Cr_2O_3 at equivalent Ca# contents.

Cr-poor clinopyroxene megacrysts from the on-craton kimberlites Monastery, Jagersfontein, Kimberley, Northern Lesotho all have very similar trends in terms of Ca#, Mg# and Cr_2O_3 compositions. Differences seen could easily be accounted for by the extent of fractionation occurring at any particular locality. For instance the clinopyroxene compositions at Jagersfontein and Kimberley do not extend to such Fe-rich compositions as at Monastery and neither are clinopyroxene-ilmenite intergrowths found at these localities.

The Cr-poor clinopyroxene megacrysts from the circum-craton localities, Eastern Griqualand, Mukorob and Witberg kimberlites show variable enrichment in Cr_2O_3 and Mg# relative to the on-craton kimberlites discussed above. The only exception to the above observations is the off-craton Lekkerfontein kimberlite where the Cr-poor clinopyroxene compositions largely follow Monastery in terms of Cr_2O_3 and Mg#, but the trend starts at lower Ca#.

At Orapa, which is situated within the boundaries of the Kalahari craton, multiple Cr-poor megacryst populations are found. The 'main' clinopyroxene trend is similar to the on-craton trend e.g. Monastery. The subsidiary trend is weakly developed and distinctly Mg# and Cr-rich.

The Cr-poor clinopyroxene megacrysts from the United States and Angolan kimberlites have characteristics similar to those found for the off-craton southern African kimberlites; enrichment of Mg# and chrome content is found at equivalent Ca# relative to Monastery. Each of the kimberlites however display an individuality in the observed trends.

Relative to known megacryst compositions from world-wide occurrences it appears that clinopyroxene megacrysts from within the boundaries of the Kalahari craton are significantly different from the circum-cratonic Kalahari-, the Northern American- and Angolan kimberlites.

The reason for this is not presently understood but it could either be a reflection of the nature of the source regions or interactions with specific mantle components.

A model based on major element, trace element and isotopic data, primarily from the clinopyroxene megacrysts will be considered in Chapter 6.

3.2 ORTHOPYROXENE MEGACRYSTS

3.2.1 Introduction

Although orthopyroxene is generally less abundant than clinopyroxene in megacryst bearing kimberlites, exceptions do occur such as at Letseng-la-terae where orthopyroxene predominates (Mitchell, 1986). At Monastery orthopyroxene is greatly subordinate to clinopyroxene (Jakob, 1977; Moore, 1986). Boyd and Danchin (1980) noted the absence of orthopyroxene megacrysts from the Angolan localities and Orapa but ascribed their absence to the secondary effect of the greater susceptibility of orthopyroxene to weathering and alteration compared to garnet and clinopyroxene. Orthopyroxenes belonging to the Cr-rich suite have only been described from the Colorado-Wyoming (Eggler et al., 1979) and Fayette County (Hunter and Taylor, 1984) kimberlites. All other samples belong to the Cr-poor suite.

3.2.2 Orthopyroxene megacryst compositions at Schuller

Like the clinopyroxenes, the orthopyroxene megacrysts from the Schuller kimberlite show a very wide compositional spread which extends beyond the range of compositions found prior to this study by others for Cr-poor orthopyroxene megacrysts suites world-wide.

Two major distinct chemical groups correspond to two observed colour groups. Those with the brown colour (group 1) contain distinctly lower amounts of Cr_2O_3 and have lower Mg# than the green coloured megacrysts (group 2). In addition, samples with distinct chemistry to the major groups were also found. Two orthopyroxene megacrysts (samples 86/16 and 86/14) with very low Mg# (80.38 - 81.22) are compositionally distinct from other groups (group 3). Similar orthopyroxene megacryst compositions have not yet been reported.

The Fe-rich orthopyroxene megacrysts (group 1) display chemical similarities to the group I orthopyroxene megacrysts described from Monastery (Jakob, 1977), and to discrete orthopyroxene megacrysts from Jagersfontein (Hops, 1989) and Letseng-la-terae (Nixon and Boyd, 1973). Decreasing CaO, Al_2O_3 and Cr_2O_3 contents correlate with decreasing Mg# (range 87.7 to 83.4) (Figures 3.2.1 to 3.2.3). With decreasing Mg# the TiO_2 initially increases from 0.1 to 0.28 wt % TiO_2 in three samples (Figure 3.2.4). A scattered group with a restricted TiO_2 content

(range 0.16 to 0.22 wt% TiO_2) are found at lower Mg# which displays a general decrease in TiO_2 with decreasing Mg#. This would suggest that ilmenite co-precipitated with orthopyroxene following on TiO_2 enrichment in the magma. Although the trend is remarkably similar to that described at Monastery by Jakob (1977), no intergrowths with ilmenite were found in the samples from the Schuller kimberlite.

The more magnesian (group 2) orthopyroxenes have a larger spread in Mg# (range 88 to 92) and show, as a whole, a general increase in TiO_2 (Figure 3.2.4) and decrease in Cr_2O_3 (Figure 3.2.3) with decreasing Mg#. The generally lower CaO and Al_2O_3 (Figures 3.2.5 and 3.2.6) found for the most magnesian samples would however be contrary to expected fractionation. This will be further discussed in Section 3.2.5.

Four of the orthopyroxene megacrysts are associated with other megacryst phases, two contain inclusions of garnet (samples 85/08 and 86/118) and one each is associated with ilmenite (sample 86/114) and clinopyroxene (sample 86/3). The samples associated with garnet and ilmenite fall within the group 2 orthopyroxene megacrysts at intermediate Mg# except for lower CaO (Figure 3.2.1). The sample associated with clinopyroxene plots within the field delineated by the group 1 orthopyroxene megacrysts (Figures 3.2.1 to 3.2.4).

Two orthopyroxene megacrysts associated with exsolution of garnet and clinopyroxene (samples 86/121 and 86/103) are separated from the others by their distinctly higher Mg# and Cr_2O_3 and lower CaO, Al_2O_3 and TiO_2 (Figures 3.2.1 to 3.2.4). These are chemically similar to the group II lamellar enstatites described from Monastery (Jakob, 1977).

3.2.3 Comparison of megacryst orthopyroxenes with Schuller and Premier lherzolite orthopyroxenes

Orthopyroxene from the Schuller coarse lherzolites contain distinctly lower CaO and generally higher Al_2O_3 and Cr_2O_3 and lower TiO_2 than the megacrysts (Figures 3.2.5 to 3.2.8). The megacrysts are thus compositionally distinct from lherzolite orthopyroxenes at Schuller, and qualitatively have formed at higher temperatures and pressures since they have more clinopyroxene and garnet in solid solution.

No sheared lherzolites have been found at Schuller, which is most probably a sampling problem. In lieu of the lack of suitable lherzolitic samples from Schuller and orthopyroxene megacrysts from Premier, comparisons between the Schuller megacrysts and orthopyroxene from coarse and sheared lherzolites from the nearby Premier pipe (Boyd, unpublished data) were made.

Orthopyroxene from Premier coarse lherzolites are distinctly more magnesian and contain lower CaO (Figure 3.2.5) and TiO_2 (Figure 3.2.8) contents than the megacrysts. Relative to the Premier data, the lherzolite orthopyroxene compositions from Schuller extend to less magnesian values which leads to a greater overlap in composition with the more magnesian megacrysts. This is due to two samples from Schuller which are consistently more Fe-rich than the Premier samples.

Orthopyroxenes from the Premier sheared lherzolites show some overlap in Mg# with the more magnesian (group 2) Schuller orthopyroxene megacrysts but contain distinctly higher CaO and Al_2O_3 at equivalent Mg# (Figures 3.2.5 and 3.2.6). Larger overlap is found for TiO_2 and Cr_2O_3 contents but the lherzolitic orthopyroxene compositions extend to higher concentrations than are found in the megacrysts (Figures 3.2.8 and 3.2.7). As with the clinopyroxenes it is found that the more magnesian orthopyroxene megacrysts (group 2) have greater similarities to the orthopyroxenes from the sheared lherzolites. The lherzolite orthopyroxenes are however distinctly Ti-rich relative to the megacrysts at equivalent Mg#.

3.2.4 Comparisons with other localities

Compositions of orthopyroxene megacrysts from the Monastery (Jakob, 1977; Moore, 1986), Letseng-la-terae (Bloomer and Nixon, 1973), Jagersfontein (Hops, 1989), Eastern Griqualand kimberlites (Boyd, unpublished data), Hamilton Branch (Schulze, 1982b) and Sloan-Nix (Eggler, unpublished data) are shown in Figures 3.2.9 to 3.2.14.

Monastery

The discrete orthopyroxene megacrysts from Monastery (Group I of Jakob, 1977) occupy two fields which correspond to a high and a low temperature group which are separated by a compositional gap in terms of CaO and Mg# (Figure 3.2.9 a). Orthopyroxene megacrysts associated with ilmenite plots within this gap but towards the higher temperature group. The lower Ca group appear to plot as a separate field on the Cr_2O_3 vs. Mg# plot (Figure 3.2.9 b).

Letseng-la-terae

Overall orthopyroxene megacrysts from the Letseng-la-terae (Figure 3.2.10 a and b) form a trend of decreasing CaO, and Cr_2O_3 with decreasing Mg# similar to that found at Monastery. This is generally considered to be the 'normal' trend of fractional crystallisation with decreasing temperature. Three samples from Letseng-la-terae, termed enstatite (Bloomer and Nixon, 1973) plot off the main trend and have compositions similar to the Mg-rich (group 2) orthopyroxene megacrysts from Schuller.

Jagersfontein

Orthopyroxene megacrysts from Jagersfontein define trends of decreasing CaO and Cr_2O_3 (Figures 3.2.1 a and b) with decreasing Mg#, and define a compositional field very similar to that found at Monastery. The orthopyroxene megacrysts from both Jagersfontein and Letseng-la-terae are thus very close in composition to orthopyroxene megacrysts from Monastery as are the clinopyroxenes (refer to Figures 3.1.18 and 3.1.19 a and b).

Eastern Griqualand

Orthopyroxene megacrysts from the Eastern Griqualand kimberlites, Ramatseliso and Abbotsford are distinctly Mg-rich and Cr-rich relative to samples from Monastery (Figure 3.2.12 a and b). The orthopyroxene megacrysts from Ramatseliso plot in a restricted field with respect to CaO content but show a wide spread in Cr_2O_3, whereas the samples from Abbotsford occupy a scattered field with respect to CaO and Cr_2O_3 compositions and are Mg-rich relative to Ramatseliso samples. Orthopyroxene megacrysts from Eastern Griqualand and Mukorob are however significantly different to on-craton occurrences by their very high Al_2O_3 contents (Eastern Griqualand range 2.05 to 2.52 wt % (Boyd and Nixon, 1980) and Mukorob range 2.2 to 4.7 wt % (Mitchell, 1987)). Higher Al_2O_3 contents in orthopyroxenes have been attributed to lower pressure of equilibration (e.g. McGregor, 1974).

Hamilton Branch

Orthopyroxene megacrysts from Hamilton Branch are very similar in character to samples from Eastern Griqualand being distinctly Mg- and Cr-rich relative to samples from Monastery (Figure 3.2.13 a and b).

Sloan-Nix

As with the clinopyroxene megacryst suite at Sloan-Nix, Eggler et al. (1979) describe three distinct orthopyroxene megacryst suites. These were established via mineral inclusion comparisons. The chrome-poor orthopyroxene megacrysts fall in two distinct chemical groups (Cr-poor and 'anomalous' Cr-poor) characterised by relatively higher and lower CaO and Cr_2O_3 contents (Figure 3.2.14 a and b). The Cr-poor group plot along a trend parallel to the Monastery, Letseng-la-terae and Jagersfontein samples which is displaced to more magnesium-rich compositions. The 'anomalous' Cr-poor group which includes discrete orthopyroxene megacrysts and megacrysts associated with inclusions, shows a spread of Mg# but limited variation in other components. The third group of chrome-rich orthopyroxene megacrysts from this locality have magnesium-rich compositions with high Cr_2O_3 (Figure 3.2.14 b) and low TiO_2 (not shown) relative to the chrome-poor orthopyroxene megacrysts in general.

3.2.5 Discussion

From the previous comparisons by locality it is evident that no Cr-rich orthopyroxene megacrysts have been described from southern African localities.

The comparison of orthopyroxene megacryst and lherzolite orthopyroxenes from Schuller and Premier compositions illustrates that the megacrysts are not merely derived from the disaggregation of lherzolite. Some compositional overlaps exist for some elements of the more Mg-rich megacryst samples, with orthopyroxene from sheared lherzolite but not with coarse lherzolite. This is similar to the situation found in comparisons between megacryst and lherzolite clinopyroxenes where the more Cr-rich, subcalcic and magnesian megacryst compositions tend towards sheared lherzolitic clinopyroxene compositions. Whereas the megacryst compositions plot as narrow restricted fields, much larger chemical variations are found for lherzolitic orthopyroxene compositions.

Similar to the clinopyroxene megacrysts at Schuller, the megacryst orthopyroxenes show a very large compositional range and four distinct groups are apparent; Fe-rich (group 1), Mg-rich (group 2), anomalously Fe-rich (group 3) and exsolved megacrysts.

The Fe-rich (group 1) orthopyroxenes are similar in composition and show similar compositional trends to

orthopyroxene megacrysts from Monastery, Letseng-la-terae and Jagersfontein (e.g. Figures 3.29; 3.2.10; 3.2.11). The general decrease in CaO, Al_2O_3 and Cr_2O_3 with decreasing Mg# is compatible with differentiation and the co-precipitation of garnet and clinopyroxene and possibly olivine similar to that described from Monastery (Jakob, 1977). The initial increase in TiO_2 followed by a decrease with decreasing Mg# is also similar to that found at Monastery and would indicate that ilmenite became a co-precipitating phase at a later stage in the differentiation.

The Mg-rich (group 2) orthopyroxenes as a whole show increasing CaO and Al_2O_3 and TiO_2 and decreasing Cr_2O_3 with decreasing Mg#. The linear increases in CaO and Al_2O_3 with decreasing Mg# are contrary to expected fractionation trends. These increases could conceivably be generated in a scenario where orthopyroxene and possibly olivine crystallises without garnet and clinopyroxene. Under such circumstances Ca and Al would act as incompatible elements and increase in the liquid with differentiation. If the rises in concentration of these elements are greater than the fall in temperature, a situation might arise with orthopyroxene showing increasing Ca and Al with decreasing temperature and fractionation. This possibility can however be discounted as co-existing garnet inclusions in orthopyroxenes indicate that garnet was a precipitating phase with the group 2 orthopyroxenes.

It is also apparent from the comparisons by locality that large variations in orthopyroxene compositions are found on a world-wide scale. Orthopyroxenes from single localities largely plot in restricted fields but trends which are more magnesian than Monastery (e.g. Eastern Griqualand, Hamilton Branch and Sloan-Nix kimberlites) are also relatively enriched in chrome. Fractionation trends at such localities are parallel to Monastery but shifted to more magnesian compositions. Clinopyroxene megacryst compositions at these localities also contain higher Mg# and chrome contents. In view of these observations, and the presence of multiple clinopyroxene megacryst populations at Schuller, the variations in the Mg-rich (group 2) orthopyroxenes are interpreted as a number of parallel, weakly developed trends with 'normal' fractionation similar to those found elsewhere. The least magnesian of the group 2 orthopyroxenes contain the highest CaO and Al_2O_3 which would translate into higher temperatures of crystallisation. The most magnesian orthopyroxenes would similarly have crystallised at lower temperatures on the basis of their CaO and Al_2O_3 contents. The proposed relations for the orthopyroxenes would thus be similar to that observed for clinopyroxenes where the most magnesian (highest Mg#) samples have compositions which tend towards mineral phases observed in sheared lherzolites. Such compositions also have higher Ca/(Ca+Mg) and therefore lower estimated equilibration temperatures and are relatively enriched in Mg# and chrome.

The inter-kimberlite orthopyroxene megacryst comparisons clearly illustrate that general fractionation trends similar to that found at Monastery occur at other localities where decreasing trends of CaO and Cr_2O_3 correspond to decreasing Mg#. At localities where clinopyroxene megacrysts are compositionally similar to Monastery (e.g. Jagersfontein and Letseng-la-terae) the orthopyroxene megacryst compositions are also similar and show the same trends. However, where the initial orthopyroxene compositions are richer in Cr_2O_3 relative to Monastery, it is found that the fractionation trends are shifted to more magnesian compositions (e.g. Eastern Griqualand, Hamilton Branch and Sloan-Nix). It is also evident that these compositional shifts follow those observed in the previous section for the clinopyroxene megacrysts. For instance the records of lower temperature and higher Cr-content in the clinopyroxene megacrysts from Sloan-Nix, and Eastern Griqualand are also seen in orthopyroxene compositions from these localities.

3.3 GARNET MEGACRYSTS

3.3.1 Introduction

Garnet megacrysts are very common as a megacryst phase in kimberlites and examples have been described from numerous localities. Although both Cr-rich and Cr-poor varieties have been described from the Sloan-Nix kimberlites (Eggler et al., 1979) and the Fayette County kimberlites, (Hunter

and Taylor, 1984) no Cr-rich samples are known from the southern African region. The definition of megacryst suites on the basis of garnet is complicated by the fact that compositional trends might not be apparent with falling temperature (Eggler et al., 1987).

3.3.2 Garnet megacryst compositions at Schuller

The garnet megacrysts display a range in Mg# from 84 to 77. CaO (Figure 3.3.1) and Cr_2O_3 (Figure 3.3.2) decreases while TiO_2 (Figure 3.3.3) increases with decreasing Mg#. The Na_2O content varies between 0.06 and 0.11 wt % and shows a weak scattered increase with decreasing Mg# (Figure 3.3.4). Garnets found as inclusions in orthopyroxene plot within the fields delineated by the discrete megacrysts. Three samples are chemically distinct with markedly higher CaO at equivalent Mg# (Figure 3.3.1) relative to the rest of the samples.

The physical characteristics of the garnets can be correlated approximately with the compositions. Rounded garnets with smooth unbroken surfaces (group 1; Mg# < 80) contain lower CaO and Cr_2O_3 and higher TiO_2 and Na_2O than conchoidally broken red to lavender fragments (group 2; Mg# > 80). The overall trends of decreasing Cr_2O_3 and increasing TiO_2 is compatible with fractionation as has been found for other garnet megacryst suites (Jakob, 1977; Shee, 1978; Hops, 1989). Apart from three anomalous samples which have Ca# > 16 (group 3), the majority of the

garnets have Ca# between 14 and 16. This has been interpreted as an indication of the buffering of Ca and Mg due to co-precipitation of orthopyroxene and clinopyroxene with garnet at constant pressure (Jakob, 1977).

3.3.3 Comparison of megacryst garnets with Schuller and Premier lherzolite garnets

In Figures 3.3.5 and 3.3.6 garnet megacryst and garnets from coarse peridotites from Schuller and coarse and sheared peridotites from Premier are compared in terms of their Mg#, Cr_2O_3 and TiO_2 contents. Garnets from the Schuller coarse lherzolites show some overlap in Mg# with the most magnesian megacrysts but contain generally lower Cr_2O_3 (at equivalent Mg#) and distinctly lower TiO_2 than the megacrysts. Garnets from both the coarse and sheared lherzolites from Premier show some overlap with the most magnesian megacrysts but show much wider variations in both Cr_2O_3 and TiO_2 than the megacrysts. It is concluded from the above data that the megacrysts are not derived from the disaggregation of lherzolites.

3.3.4 Comparison with other localities

The compositions of chrome-poor garnet megacrysts from Iron Mountain (Smith, 1977), Orapa (Shee, 1978; Tollo, 1982), Lekkerfontein (Robey, 1981), Hamilton Branch (Schulze, 1982b), Mukorob 2 (Jones, 1984), Jagersfontein (Hops, 1989), Sloan-Nix (Eggler, unpublished data), Eastern Griqualand (Boyd, unpublished data) and Witberg

(de Bruin, unpublished data) kimberlites have been compared to the Cr-poor garnet megacrysts from the Monastery kimberlite (Jakob, 1977) in terms of Mg# ratio and the TiO_2 and Cr_2O_3 contents (Figures 3.3.7 to 3.3.16).

Monastery

The garnet megacrysts from Monastery described by Jakob (1977) show a decrease in Cr_2O_3 with decreasing Mg# with very low Cr_2O_3 contents for those samples associated with ilmenite Figures 3.3.7 a). Two samples do not follow this trend and plot at distinctly higher Cr_2O_3 which might be an indication of the existence of a separate garnet megacryst population. TiO_2 increases for the discrete monomineralic group with decreasing Mg#. This is followed by decreasing TiO_2 with a further decrease in Mg# for the samples associated with ilmenite (Figure 3.3.7 b). These trends have been ascribed to fractional crystallisation in an evolving magma where TiO_2 decrease in the silicate phases as ilmenite becomes a crystallising phase (Jakob, 1977).

Jagersfontein

Garnet megacrysts from Jagersfontein plot as a scattered trend which is initiated at higher Mg# relative to Monastery and shows a decrease in Cr_2O_3 and an increase in TiO_2 with decreasing Mg# (Figure 3.3.8 a and b). The ilmenite association is not found at this locality (Hops, 1989). The broad scattered nature of the Cr_2O_3 vs Mg# plot

can be interpreted as a series of subparallel trends. It appears from co-existing clinopyroxene / garnet data that one sample with higher Mg# relative to the Monastery trend can be correlated to a clinopyroxene composition which also appeared to form a separate trend. It would thus appear probable that at Jagersfontein two compositional trends are described by both garnet and clinopyroxene compositions.

Lekkerfontein

Garnet megacrysts compositions from Lekkerfontein are very similar to Monastery with respect to Cr_2O_3 and TiO_2 although the starting compositions are slightly more Mg-rich (Figure 3.3.9 a and b). Like Monastery TiO_2 shows an initial increase followed by a decrease with decreasing Mg# which is indicative of the co-precipitation of ilmenite with garnet for the more Fe-rich compositions (Figure 3.3.9 b). The absolute TiO_2 content for the Lekkerfontein garnets is however lower than that at Monastery.

Orapa

Garnet megacrysts from Orapa are more widely scattered than Monastery. The majority of the samples are relatively Cr-rich. Orapa garnets do however show decreasing Cr_2O_3 and increasing TiO_2 with decreasing Mg# (Figure 3.3.10 a and b). A few samples form a weaker trend at lower Cr_2O_3 contents similar to the Monastery trend. Thus as with the

clinopyroxene data at this locality, the garnet megacrysts show the existence of multiple garnet megacryst groups, poorly defined probably due to incomplete sampling.

Iron Mountain

Samples from Iron Mountain show a large spread in compositions but with starting compositions distinctly more Mg- and Cr-rich relative to Monastery. The TiO_2 content shows a weak parabolic relation, similarly to Monastery but at lower absolute values (Figure 3.3.11 a and b) and therefore ilmenite was a co-precipitating phase with garnet at this locality. Two samples, both of which are associated with ilmenite form a separate trend to the rest of the samples with respect to Cr_2O_3 and TiO_2.

Sloan-Nix

The Cr-poor garnet megacrysts from Sloan-Nix show two separate populations, both of which are relatively Cr-rich in comparison to Monastery. The Cr-poor garnet megacrysts form a small group showing decreasing Cr_2O_3 and increasing TiO_2 with decreasing Mg# (Figures 3.3.12 a and b). The Cr-poor 'anomalous' garnet megacrysts as defined by Eggler et al. (1979) display a wider scatter of points with are distinctly richer in Cr_2O_3 and poorer in TiO_2 than the above group.

Mukorob

Garnet megacrysts from Mukorob 2 show scattered trends generally following the Monastery trend but are distinctly Ti-poor (Figure 3.3.13 a and b).

Eastern Griqualand

Garnet megacryst from the Eastern Griqualand kimberlites are generally Mg- and Cr-rich relative to Monastery. Samples from specific localities plot in restricted but overlapping fields (Figure 3.3.14 a and b).

Hamilton Branch

Garnet megacrysts from Hamilton Branch show a narrow spread in Mg# but are again Cr-rich (similar to clinopyroxene and orthopyroxene megacrysts) relative to Monastery (Figure 3.3.15 a and b).

Witberg

Garnet megacrysts from Witberg plot in two groups which correspond to a high-Cr, high Mg# and a low-Cr, low Mg# group. The general trends are similar to those found at Monastery but once again commence at higher chrome and Mg# values (Figure 3.3.16 a and b).

3.2.5 Discussion

From the above it appears that the garnet megacrysts at Schuller have few exact equivalents compared to reported data. The garnets with lower Mg# (group 1) are equivalent

to samples from Orapa while those with the highest Mg# (group 2) are somewhat similar to Eastern Griqualand and some samples from Hamilton Branch although differences exist (Figure 3.3.17 a and b). All the garnet megacrysts are distinctly Cr-rich relative to Monastery.

As with the clinopyroxene and orthopyroxene, comparisons of megacryst garnets and garnets in lherzolites show that the most magnesian garnets megacrysts show some similarity in compositions with garnets from the sheared lherzolites, but the latter fill larger and more scattered fields.

Multiple megacryst compositional groups are evident at several localities, particularly Orapa and possibly Jagersfontein and Monastery.

It would appear that increasing Cr-content is accompanied by an increasingly magnesian nature of starting compositions. These relations are shown clearly when garnet compositions at localities such as the Eastern Griqualand, Iron Mountain and Sloan-Nix kimberlites are compared to the compositions of garnet megacrysts from Monastery, Jagersfontein and Lekkerfontein. Similar trends have already been observed for clinopyroxene and orthopyroxene (where available) at these localities.

3.4 OLIVINE MEGACRYSTS

The olivines at Schuller are very iron-rich with forsterite contents varying between 79.5 and 81.4 and with NiO concentrations between 0.14 and 0.17 wt % (Appendix 2, Table 5). These correspond to the iron-rich olivines described from Monastery by Jakob (1977) and Gurney et al. (1979). Moore (1986) re-investigated these iron-rich olivines and found that they are associated with zircon, ilmenite and phlogopite. This raises the possibility that such an association could also be present at Schuller. However no zircon megacrysts have been found at Schuller nor have they been reported from Premier despite the use of Sortex instruments in the diamond recovery. Therefore they are thought to be absent.

3.5 ILMENITE MEGACRYSTS

The ilmenite megacrysts found at Schuller occur as discrete megacrysts, graphic intergrowths with pyroxenes and ilmenite hosting small pyroxene inclusions. Only two samples of graphic intergrowths with pyroxenes were found, one each with orthopyroxene (sample 86/114) and clinopyroxene (sample 86/83). The pyroxenes which occur as inclusions in the ilmenite were too altered for meaningful analysis.

The discrete megacrysts are picroilmenites (geikelite contents range between 25 and 52 %). The majority of the monomineralic ilmenites (80 %) plot as a group with MgO varying between 7 and 11 wt % and relatively constant Cr_2O_3 between 0.5 and 0.7 wt %, (Figure 3.5.1). These lie in the trough of kimberlite ilmenites as defined by Haggerty (1975). A smaller group show increasing Cr_2O_3 (0.9 to 1.5 wt%) with decreasing MgO while four samples with high MgO (12 to 14 wt %) and Cr_2O_3 (1.2 to 2.2 wt %) correspond to the Mg-rich limb of the parabolic curve of African ilmenites defined by Haggerty (1975) (Figure 3.5.1). The ilmenite which occurs as a graphic intergrowth with orthopyroxene and one of the ilmenites with pyroxene inclusions plot on the the Mg-rich limb whereas the rest of the ilmenites with pyroxene inclusions plot on the Mg-rich end of the main group.

These variations are similar to ilmenites from the Hamilton Branch (Schulze, 1984) although not as many data points are available for Schuller. Schulze (1984) found a broad correspondence between texture and ilmenite mineral compositions at Hamilton Branch where graphic intergrowths with pyroxenes contain higher Cr_2O_3 and MgO than small pyroxene intergrowths with ilmenite whereas monomineralic ilmenites tend to contain lower MgO contents. This is broadly similar to that found at Schuller.

Overall trends of decreasing Al (Figure 3.5.2) and increasing Fe3+ (Figure 3.5.3) are found with decreasing $Mg/Mg+Fe^{2+}$. The decreasing Al with fractionation would suggest that a silicate phase (possibly phlogopite ?) was crystallising with the ilmenite throughout the sequence. Increasing Fe^{3+} with decreasing Mg# is compatible with differentiation, similar to that found for monomineralic ilmenites by Agee et al. (1982).

3.6 DISCUSSION

3.6.1 The Schuller megacryst suite

It is evident from the previous discussions that a distinct number of compositional groups are present amongst the clinopyroxene and orthopyroxene megacrysts at Schuller. It is not clear however from the major element relations whether or not similar multiple compositional groups are present amongst the garnet and ilmenite megacrysts. As very few co-existing phases with inclusions are present amongst the samples studied, it is difficult to correlate, with certainty, co-precipitating megacryst phases.

It was found from the comparisons between the Schuller megacryst compositions and minerals from the sheared lherzolites from Premier that some clinopyroxene (group 2b), orthopyroxene (group 2b) and the most magnesian garnet megacryst compositions (Mg# 80 to 84) approach the

mineral compositions of the sheared lherzolites (refer to Figures 3.1.13, 3.1.14 for clinopyroxene, Figures 3.2.5 and 3.2.7 for orthopyroxene and Figures 3.3.5 and 3.3.6 for garnet). Arguments based on the large size of the megacrysts and the fact that the sheared lherzolite minerals occupy much larger compositional fields than the megacrysts have been used to discount the possibility of megacryst derivation from lherzolite disaggregation. Nevertheless these compositional characteristics argue for an association between the most magnesian megacryst phases and the deformed high temperature peridotites. All of the above clinopyroxene, orthopyroxene and garnet megacrysts have high magnesium contents, are enriched in chrome and contain low titanium compared to other megacrysts. This consistency also supports the above grouping. The two orthopyroxene megacrysts with inclusions of garnet have very similar compositions (refer to Figures 3.2.1 to 3.2.4) and fall within the compositional fields for orthopyroxenes and garnets discussed above. In addition, an orthopyroxene associated with ilmenite, has a very similar composition to the orthopyroxenes associated with garnet. This would suggest that at that point orthopyroxene, garnet and ilmenite (possibly clinopyroxene and olivine as well) were liquidus phases. The relatively Cr-rich and Mg-rich nature of the melt from which these assemblages have crystallised is illustrated by the high MgO and Cr_2O_3 content of the ilmenite (Figure 3.5.1). The

silicates within this group were found to have similarly high Mg# and chrome contents.

The higher calcium contents in the group 2a orthopyroxene megacrysts, and their more iron-rich nature, relative to the group 2b orthopyroxene megacrysts are (Figure 3.2.1) compatible with similar features found for the group 2a clinopyroxene megacrysts (Figure 3.1.1). In addition, both sub-sets are intermediate in composition between the most Fe-rich and most Mg-rich clinopyroxene and orthopyroxene megacrysts. These samples also contain intermediate Cr_2O_3 contents relative to the Mg- and Fe-rich end members. The Fe-rich garnets (Mg# 77 to 80) could have been in equilibrium with these orthopyroxene and clinopyroxene subgroups. It should be remembered that both the orthopyroxene and clinopyroxene megacrysts associated with this grouping do not have the very sharp differentiation trends often seen at other localities or found for the group 1 samples at Schuller. This feature has previously been interpreted to represent a number of fractionation events which are closely related rather than a single trend.

The group 1 clinopyroxene megacrysts at Schuller are the most Fe-rich megacrysts described for kimberlites in general. Their fractionation trends are sharp and coherent. TiO_2 increases with decreasing Mg# and Ca# and ilmenite could not have been a significant crystallising

phase with the group 1 clinopyroxenes (Figures 3.1.9 and 3.1.10). No garnet megacrysts with sufficiently high iron nor low chrome were found at Schuller to co-exist with this group. The Fe-rich group of orthopyroxene megacrysts (group 1) have sufficiently high Fe to have co-existed with this group. However the pronounced decrease in TiO_2 at Mg# 85 (Figure 3.3.4) for the group 1 orthopyroxenes and the absence of such decrease amongst the group 1 clinopyroxenes (Figure 3.1.11) would not support the idea that the respective group 1 orthopyroxenes and clinopyroxenes co-precipitated over the full extent of their compositional ranges. It is possible however that the three group 1 orthopyroxenes which show an increase in TiO_2 with decreasing Mg# have crystallised with the group 1 clinopyroxenes. The rest of the group 1 orthopyroxenes which show a decrease in TiO_2 with decreasing Mg# could have crystallised together with ilmenite after the group 1 clinopyroxene crystallisation ceased. It is also possible that the two orthopyroxene megacrysts which have extreme Fe-rich compositions (group 3) could have co-existed with the group 1 clinopyroxene megacrysts.

No silicate phases with sufficiently high Cr_2O_3 contents were found at Schuller to have co-existed with the group 4 clinopyroxenes. Whereas the Cr-rich clinopyroxenes described from Sloan-Nix (Eggler et al., 1979) and Elliot County (Hunter and Taylor, 1982) were associated with similar Cr-rich garnets and orthopyroxenes this has not

been found within southern Africa. Shee (1978) and Tollo (1982) described Cr-rich clinopyroxenes from Orapa but not other megacryst phases which were similarly Cr-rich. In general neither Cr-rich orthopyroxene nor garnet megacrysts have as yet been described from southern African Group 1 kimberlites.

The group 3 clinopyroxene megacrysts were found to co-exist with ilmenite and iron-rich orthopyroxene respectively. The ilmenites associated with the clinopyroxenes were found to be very Mn-rich which is thought to be indicative of secondary alteration. The orthopyroxene is Fe-rich and fall within the compositional field delimited by the Fe-rich group 1 orthopyroxenes. The very Fe-rich nature of the clinopyroxenes could be indicative of high levels of fractionation. This would be supported by the low equilibration temperatures indicated by the calcic nature of the clinopyroxenes and by the co-existence of ilmenite.

3.6.2 Geothermobarometry

The application of geothermometers to single mineral crystals can be attempted using the diopside-enstatite solvus (Ca/(Ca+Mg)) determined by Lindsley and Dixon (1976) and others for clinopyroxenes and the empirical method of Boyd and Nixon (1973) for orthopyroxenes. The application of these two methods to monomineralic minerals is based on the assumption of co-precipitation of

clinopyroxene and orthopyroxene in the megacryst assemblage in general. If the assumption about equilibrium with orthopyroxene is wrong, then temperatures obtained for clinopyroxenes using the diopside solvus would be minimum temperatures (Boyd and Nixon, 1973).

Hops (1989) found in a comparative geothermometer study on deformed peridotites from Jagersfontein that temperatures obtained using the Boyd and Nixon (1973) (BN73) and Lindsley and Dixon (1976, 20 kbar) (LD76) were equivalent and suggested that comparisons between equilibration temperatures obtained by these methods could be valid.

Applying the the LD76 thermometer to the group 1 clinopyroxene megacrysts, a temperature range of 1479 to 1324 deg C is obtained. The three group 1 orthopyroxene megacrysts which have been inferred to have crystallised with the group 1 clinopyroxenes have a BN73 temperatures between 1360 to 1270 deg C. This falls within the lower range of the temperatures obtained by LD76 for the clinopyroxenes, consistent with the above grouping. The rest of the group 1 orthopyroxenes, which have decreasing TiO_2 with decreasing Mg# (Figure 3.2.4) and which had been inferred earlier in this thesis to have crystallised with ilmenite after the group 1 clinopyroxene crystallisation had ceased, have BN73 calculated temperatures in the range 1290 to 1180 deg C. These temperatures are lower than

suggested for group 1 clinopyroxenes and are consistent with that earlier interpretation.

The group 2a clinopyroxenes have LD76 temperatures in the range 1426 to 1264 deg C while the group 2a orthopyroxenes have BN73 temperatures in the range 1310 - 1200 deg C. The group 2b clinopyroxenes have LD76 temperatures in the range 1289 to 1185 deg C whilst the group 2b orthopyroxenes have BN73 temperatures in the range 1250 to 1200 deg C. Both groups 2a and 2b have clinopyroxene and orthopyroxene temperature estimates that overlap, which supports their grouping.

The group 3 samples have LD76 temperatures in the range 1090 to 817 deg C. The one sample which contains a group 3 clinopyroxene in association with a group 1 orthopyroxene is a disequilibrium assemblage. The clinopyroxene has a LD76 temperature of 1011 deg C whilst the NB73 empirical thermometer when applied to the orthopyroxene gives a temperature estimate of 1270 deg C. The fact that the orthopyroxene shows effects of strain and re-crystallisation whist the clinopyroxene do not is also an indication of disequilibrium. This association is not presently understood.

The co-existence of any other megacryst phases with the Cr-rich group 4 clinopyroxene megacrysts cannot be

demonstrated. The LD76 thermometer however gives temperature range of 1123 to 1009 deg C when applied.

Pressures can be calculated for garnet/orthopyroxene pairs using the Nickel and Green (1985) geobarometer with a temperature estimate from the orthopyroxene composition using the Boyd and Nixon (1973) empirical geothermometer. The two orthopyroxene megacrysts with co-existing garnet were found to give pressure estimates of 53 kb (85/08) and 50 kb (86/118) respectively. If the above pairing of groups are assumed to be correct then pressure calculations can be done for corresponding orthopyroxene - garnet pairs. For instance the most magnesian garnet and orthopyroxenes (assigned as group 2b : samples 86/22 & SE30) give a pressure estimate of 54.7 kb whereas the least magnesian garnet and orthopyroxene (group 2a : samples OPX1 & GA16) give a pressure estimate of 53.5 kb.

3.6.3 Regional megacryst compositional variations

Individual kimberlites have been found to contain distinct megacryst assemblages. Such distinctions can be seen in terms of the proportions of the phases or in terms of mineral compositions. For instance ilmenite is very rare at Jagersfontein (Hops, 1989) and abundant at Monastery (Jakob, 1979) and Lekkerfontein (Robey, 1981). Differences can also be found in the order of crystallising assemblages. Schulze (1984) noted the early crystallisation of ilmenite at Hamilton Branch kimberlite

and the effect it had on the fractionation patterns of clinopyroxene. Similarly Mitchell (1987) has shown that that kimberlites within the same cluster (Gibeon) have different crystallising assemblages. Clinopyroxene intergrowths with ilmenite occurs at the high temperature end at Deutche Erde 1 but at the low temperature end at the adjacent Mukorob 2. Compositional trends also vary from locality to locality. For example Eggler et al. (1987) subdivided the chrome-poor megacrysts from North America into a "Sloan-Nix trend" and a "Monastery trend" on the basis of mineral chemical variation.

The distinctions in terms of megacryst mineral compositions at specific localities have been clearly illustrated in this study. For instance, clinopyroxene megacrysts from Ramatseliso and Abbotsford plot in distinct compositional fields where the samples from Abbotsford are clearly richer in Cr_2O_3 than those of Ramatseliso (Figure 3.1.25 b). Similarly it can be shown that garnet megacrysts from Clarkton and Abbotsford plot as distinct groups (Figures 3.3.14 a and b). Larger regional variations have also been shown to exist. As a whole the megacrysts from the peripheral cratonic Eastern Griqualand kimberlites are distinctly enriched in Mg# and Cr_2O_3 relative to cratonic megacrysts (Nixon, 1987). Inter-kimberlite distinctions in megacryst assemblages are also manifested in that multiple megacryst compositional

groups are clearly present at some kimberlites (Schuller, Premier and Orapa).

Megacryst mineral compositions from kimberlite localities from within the boundaries of the Kaapvaal Craton are remarkably similar. It can be seen from the comparisons by locality that the Monastery, Jagersfontein, the Northern Lesotho and Kimberley kimberlites contain megacryst compositions that overlap. All the clinopyroxenes from these localities contain similar Cr_2O_3 and Mg# at equivalent Ca#. Similarly it can be shown that orthopyroxenes (where found) contain similar CaO, Al_2O_3 and Cr_2O_3 at equivalent Mg# while garnets have similar ranges in Mg# and Cr_2O_3.

In contrast, it appears that the megacryst mineral compositions from the circum-cratonic kimberlites have consistently different and more variable compositions. The clinopyroxenes from the Eastern Griqualand, Mukorob and Witberg kimberlites are decidedly enriched in Mg# and Cr_2O_3 relative to sources from within the boundaries of the Kaapvaal discussed above. In addition the compositions are much more variable than the above. For instance at an equivalent Ca# the clinopyroxenes from Eastern Griqualand are more magnesium-rich than that at Witberg. Similarly it is found that orthopyroxene megacrysts from Eastern Griqualand and garnet megacrysts from Eastern Griqualand

and Witberg are distinctly enriched in Cr_2O_3 and Mg# relative to that of the within craton kimberlites.

In contrast to the above observations of Cr- and Mg-enrichments found in the megacrysts of off-craton kimberlites, it is found that the clinopyroxene and garnet compositions of off-craton Lekkerfontein are similar to Monastery and the other on-craton kimberlites. The orthopyroxene megacrysts from both Eastern Griqualand and Gibeon kimberlites contain higher Al_2O_3 than the on-craton kimberlites which has been interpreted as lower pressure crystallisation. However orthopyroxene megacrysts from Lekkerfontein have relatively low Al_2O_3 (0.93 to 1.04 wt % (Robey, 1981)) with resulting pressure calculations of 50 kb. This is similar to that found for Monastery by Gurney et al. (1979). This would indicate that the formation conditions for the Lekkerfontein megacrysts must have been very similar to that of the on-craton kimberlites.

The megacryst compositions from kimberlites such as Kentucky and Sloan-Nix have dissimilar composition to those from kimberlites from within the Kaapvaal craton but are similar to those of the circum-cratonic Kaapvaal kimberlites as shown by the variability in mineral compositional fields and enrichment in Mg# and Cr_2O_3. This could indicate that the variability in megacryst compositions is normal and that very special circumstances

must have prevailed under the Kaapvaal craton to have formed such consistent crystallising assemblages.

CHAPTER 4 : TRACE ELEMENT VARIATIONS

4.1 INTRODUCTION

There is very little available data on the trace element variations in megacrysts from kimberlites and the mineral purification procedures. Rare earth element (REE) and trace element concentrations have been determined for ilmenite-clinopyroxene xenoliths, (Gurney et al., 1973; Mitchell et al., 1973b) and ilmenites (Mitchell et al., 1973a) while REE variations of garnet and clinopyroxene megacrysts were reported from Sloan-Nix (Eggler et al., 1979) and the Monastery kimberlite (Jones, 1984). Shimizu and Allegre (1978) have determined some trace element concentrations in single clinopyroxene and garnet megacrysts from Monastery using secondary ion mass spectrometry (SIMS) ion-microprobe. Apart from the above some data on the Rb, Sr, Sm, Nd, U, K and Pb concentrations of megacrysts were published in conjunction with radiogenic isotope studies on selected megacrysts (Barrett, 1975; Shimizu, 1975; Kramers, 1977,1979; Kramers et al., 1981; Smith et al., 1982; Smith, 1983b; Jones, 1984; Spriggs, 1988; Hops, 1989; Winterburn, 1989).

Eggler et al. (1979) determined REE in both Cr-poor and Cr-rich clinopyroxene and garnet megacrysts from the Sloan-Nix kimberlites. It was found that the Cr-rich diopsides are enriched in light and intermediate REE and

that both the Cr-rich diopside and garnet are depleted in heavy REE relative to the Cr-poor megacrysts. It was also found that the Cr-poor and Cr-rich megacrysts had REE patterns similar to mineral separates from Lesotho sheared and granular garnet lherzolites respectively as reported by Shimizu (1974).

Jones (1984) determined the REE concentrations of a number of Cr-poor clinopyroxene megacrysts from the Monastery kimberlite. He found that the total REE contents increase with increasing Ca# which is in line with differentiation of a laterally zoned host magma chamber. The calculated REE content of the liquid in equilibrium with the Cr-poor clinopyroxene megacrysts was found to be dissimilar to kimberlite but similar to a primitive alkali-basalt.

Shimizu and Allegre (1978) found that a clinopyroxene megacryst from Monastery had similar Sr and Zr concentrations to that found in clinopyroxenes from sheared lherzolites from a number of localities, including Premier. In contrast distinctly higher Sr and Zr concentrations were found in clinopyroxene and garnets from coarse lherzolites. Extreme enrichment of Sr and Zr were found in clinopyroxenes from coarse lherzolites containing metasomatically introduced minerals such as phlogopite and K-richterite.

4.2 SELECTION OF SAMPLES

In this study megacryst samples were selected to cover the compositional ranges and to represent each of the previously defined chemical groups as determined from major elements. Figures 4.1 and 4.2 illustrate the major element variations for the selected clinopyroxene (21 samples) megacrysts. Care was taken to select fresh samples with the aim to use a subset of these samples for isotope work. The compositional ranges for megacrysts of orthopyroxene (15 samples) and garnet (14 samples) on which trace element analyses were done are shown in Figures 4.3 and 4.4 respectively.

4.2.1 Analytical

The trace element analyses were made on sample chips mounted in a araldite disk with the proton probe at the CSIRO Heavy Ion Analytical Facility laboratory at North Ryde, New South Wales as described by Griffin et al. (1988). Analyses were done by R.O. Moore. Trace element results for clinopyroxene, orthopyroxene and garnet megacrysts are listed in Appendix 4. A standardless reduction technique was used and results were normalised against the Fe contents as determined by electron microprobe. A comparison between the Sr concentrations obtained by proton probe and isotope dilution mass spectrometry (Appendix 6, Table 1) are in excellent

agreement, giving confidence in the accuracy of the proton probe data.

4.3 CLINOPYROXENE

4.3.1 Strontium

There is a large overall variation in the strontium content of clinopyroxene megacrysts from Schuller between 70 and 170 ppm (Figures 4.5 and 4.6). Samples from the previously defined groups have distinct ranges in Sr concentration. The group 1 samples have the lowest concentrations (70 - 100 ppm). Group 2 samples have intermediate concentrations (90 - 110 ppm) while group 4 has the highest concentrations (120 - 170 ppm). The small number of group 3 samples show a scattered distribution of Sr concentrations with 2 samples at 90 ppm and a third at 120 ppm. The Sr concentration in the group 1 clinopyroxene megacrysts increases linearly with both increasing Ca# (Figure 4.5) and decreasing Mg# (Figure 4.6) which is indicative of fractional crystallisation. Although a linear increase in Sr is found between the group 1 and 2 samples with increasing Ca#, separate trends are found for the group 1, group 2a and group 2b when plotted against Mg#. This would indicate that the group 2 samples cannot be a continuation of the group 1 fractionation trend but that these samples crystallised from a magma with a lower Fe/Mg ratio. Similarly, it can also be shown that the group 2b samples do not form a continuation of the group

2a samples as they represent crystallisation from a magma with an even lower Fe/Mg ratio.

Whereas the groups 1 and 2 clinopyroxene megacrysts have Sr contents similar to sheared peridotites, the group 4 samples have Sr contents closer to coarse garnet peridotites free of metasomatically introduced phases from Bultfontein, Liqhobong and Matsoku as determined by Shimizu and Allegre (1978).

4.3.2 Zirconium

The zirconium content of the clinopyroxene megacrysts show similar relationships to those described for Sr (Figures 4.7 and 4.8). A range of concentrations are found (4 to 123 ppm) with group 1 samples having the lowest concentrations (range 4 to 13 ppm), group 2 with intermediate concentrations (range 6 to 14 ppm) and group 4 with higher concentrations (range 20 to 42 ppm). The group 3 samples are however distinct from the other groups with exceptionally high Zr values (range 62 to 123 ppm). Similar relations between Zr and Ca# and Mg# are found (Figures 4.7 and 4.8) as for Sr.

4.3.3 Gallium

The absolute Ga concentration for all groups with exception of group 3 clinopyroxene megacrysts fall in the range of 4 to 11 ppm (Figure 4.9). The group 3 samples have a markedly higher concentration of 16 to 19 ppm. The

group 1 megacrysts show a linear increase in Ga content from 4 to 11 ppm with increasing Ca# which is compatible with differentiation. The Ga concentration in the groups 1, 2 and 4 clinopyroxenes are generally higher than reported in clinopyroxene from two porphyroclastic (2.9 and 1.3 ppm Ga) and one coarse (3.5 ppm Ga) garnet lherzolites from the Bultfontein Floors (McKay and Mitchell, 1988). Wedepohl (1969) however states that gallium enrichment occurs in situations where volatile components are important in formation processes. The very much higher gallium concentrations found in the group 3 clinopyroxene megacrysts might thus attest to this process. It is known that ilmenite crystallised with these megacrysts which must mean high Ti in the melt. This could indicate extreme fractionation and hence would be consistent with elevated volatile contents.

4.3.4 Nickel

Nickel is a compatible trace element in clinopyroxene and a linear decrease is found with increasing differentiation in group 1 clinopyroxene megacrysts from 671 to 423 ppm (Figure 4.10). All the group 2 samples plot in a narrow band between 417 and 518 ppm which is within the range found for the most differentiated, lower temperature group 1 samples. The group 3 samples are clearly distinct from all other samples with low Ni contents of 248 to 151 ppm. The group 4 samples have a similar Ni content to the group 2 samples but extend to lower values of 317 ppm.

4.3.5 Zinc

The clinopyroxene megacrysts shows large variations in zinc (Figure 4.11). Excellent discrimination is found between the different clinopyroxene groups with group 1 samples with the highest Zn (range 31 to 40), group 2 samples intermediate concentrations (range 17 to 26) and group 4 samples the lowest concentrations (Zn range 12 to 17). Zn shows a very strong correlation with FeO (Figure 4.12).

4.4 ORTHOPYROXENE

In the orthopyroxene megacrysts trace element data are only available for Ni and Zn. Both these elements show linear correlations with Mg#. Ni decreases (Figure 4.13) and Zn increases (Figure 4.14) with decreasing Mg#. Other elements were below detection.

4.5 GARNET

The trace elements in garnets plot in a haphazard scattered fashion and do not show the regular variations observed in the clinopyroxenes. The Y concentration in garnet varies between 15 and 33 ppm but the majority of samples plot in a narrow range between 15 and 22 ppm (Figure 4.15). The Zr content varies between 45 and 90 ppm although one anomalous sample has a higher concentration of 160 ppm (Figure 4.16). The Ni content defines a broad

scattered band which varies between 90 and 120 ppm throughout the range of Mg# (Figure 4.17). The Zn concentration also shows a broad scatter of increasing concentration from 14 to 25 ppm with decreasing Mg# (Figure 4.18).

4.6 MODELLING

4.6.1 Introduction

The trace element data of the megacrysts (present study), together with published crystal-liquid distribution coefficients (Kd) can be used to calculate the composition of the magma in equilibrium with the megacrysts.

4.6.2 Choice of Kd's

Green et al. (1989) experimentally determined the partition coefficients of Sr, Zr and Y between garnet, clinopyroxene and orthopyroxene and basaltic glass at high pressure and temperature using a proton microprobe. The partitioning of Sr was determined on enriched glass whereas those for Zr and Y were determined in natural minerals. The observed Kd's determined for Sr and Zr between garnet, clinopyroxene and orthopyroxene were found to be close to those determined by previous workers. The Kd's determined for Y by Green et al. (1989) were found to be generally higher than previously found by Pearce and Norry (1979). The data of Green et al. (1989) were determined at 20 to 25 kb whereas Pearce and Norry's

(1979) data were produced at lower pressure and temperature. These Kd's determined by Green et al. (1989) are considered to be the most up to date results on an appropriate system (basaltic).

The distribution coefficient of Ti for clinopyroxene was calculated from the data presented by Green et al. (1989). This value of 0.43 is higher than that proposed by Pearce and Norry (1979) of 0.3.

4.6.3 Description of model used for equilibrium crystallisation

The concentration of the liquid/magma in equilibrium with the megacrysts can be calculated using the following formulation:

$$Kd = C_{solid} / C_{melt} \quad \ldots\ldots\ldots\ldots\ldots (1)$$

where Kd is the distribution coefficient, C_{melt} the concentration of the trace element in the liquid and C_{solid} the concentration of the trace element in the crystallising phase. The use of a model that assumes equilibrium between the interiors of the crystals and the melt (equilibrium crystallisation) is justified on the ground that major elements do not show any core to rim zonation. This would imply that the cooling of the magma and the diffusion processes in the minerals were such that the interiors of the crystals maintained equilibrium with the melt. The calculation of liquid compositions in

equilibrium with a series of fractionating crystals allows the modelling of the evolving magma.

The samples which represent the highest temperature group 1 megacrysts have lowest incompatible element concentrations and the highest compatible element concentrations. Such samples provide the best estimate of crystallisation near the liquidus and are the most likely to represent liquidus composition. The sharp fractionation trends and rapid trace element depletions and enrichments shown by the group 1 megacrysts is suggestive of small volume of liquid which was continuously changing, although not fast enough to result in zoning of the crystals.

The equilibrium crystallisation equation can be used to compare modelled trends to observed trend.

$$C_L = C_i / (F + D_S(1-F)) \quad \ldots\ldots\ldots\ldots\ldots\ldots (2)$$

where: C_i = concentration of trace element in original melt

C_L = concentration of trace element in differentiated liquid

F = fraction of liquid remaining

D_S = bulk distribution coefficient

The concentration of C_i can be calculated from the trace element concentration of the least differentiated (highest

temperature) sample. As neither the nature of the crystallising phases nor their proportions are known various assumptions about the bulk distribution coefficient (Kd) have to be made in the modelling exercise. From the calculation of liquid compositions the rate of depletion or enrichment of a particular trace element can give a reasonable estimate of the bulk Kd.

4.6.4 Sr vs Zr

Figure 4.19 shows the calculated Sr and Zr concentrations in a melt in equilibrium with the group 1 clinopyroxene megacrysts using a Kd of 0.06 and 0.1 for Sr and Zr respectively. A general increase in both Sr and Zr is observed with differentiation from 1230 ppm Sr and 43 ppm Zr for the highest temperature most subcalcic sample and 1640 ppm Sr and 92 ppm Zr for the lowest temperature most differentiated sample.

Assuming that the liquid composition calculated to be in equilibrium with the highest temperature samples, represents the initial liquid composition, the evolution of liquid lines of descent can be calculated for different bulk Kd's using Equation 2. From Figure 4.19 it can be seen that the majority of samples fall in an envelope described by Sr Kd's between 0.5 and 0.7 assuming a Zr Kd of 0.1. Amongst the megacryst phases at Schuller, the Sr Kd for clinopyroxene is the highest at 0.06 (see Green et al., 1989). Thus irrespective of the proportions of phases

crystallising, the bulk Kd for the megacryst assemblage should be less than 0.06. The observed C_L^{Sr} trend (between 0.5 and 0.7) thus grossly overestimates (by a factor of 10) any reasonable Kd.

As all other commonly observed megacryst phases have Sr distribution coefficients smaller than clinopyroxene it would be necessary to have a crystallising phase with a high Kd to generate the observed trend. In order to increase the bulk Kd from 0.06 to 0.6 the Kd can be calculated for a theoretical phase crystallising at different proportions. For example, for 10 % of a crystallising phase, a calculated Sr liquid Kd of 5.4 would be required or for 5% of a crystallising phase then a Kd of 10.9 would be needed to generate the rate of enrichment seen in the strontium content of the calculated magma composition with differentiation.

Carbonate is a phase that might be appropriate. Eggler and Wendlandt (1979) predicted that a carbonate phase (magnesite or dolomite) should be a megacryst phase, although carbonate has never been found as such. Schulze (1984) proposed that carbonate could be a megacryst phase in the Hamilton Branch megacryst suite to explain the general lack of Mg-enrichment for megacryst phases accompanied by ilmenite precipitation. Kirkley et al. (1989) interpreted elliptical to spherical calcite segregations together with other material within ilmenite

megacrysts from Monastery to be of a primary nature. These inclusions are believed to have crystallised from fluids that were trapped during ilmenite megacryst crystallisation.

4.6.5 Ti vs Zr

The modelling of liquid compositions of Ti and Zr in equilibrium with the group 1 clinopyroxene megacrysts are shown in Figure 4.20 using clinopyroxene liquid Kd's of 0.43 and 0.1 for Ti and Zr respectively. Equilibrium crystallisation modelling of liquid lines of descent shows that a bulk distribution coefficient of 0.4 and 0.1 closely approximates that for the calculated liquid. The range in compositions would be adequately described by 70 to 80 percent crystallisation.

4.7 DISCUSSION

The group 1 clinopyroxene megacrysts display excellent linear trends where the incompatible elements (Sr, Zr, Ga and Zn) increase and the compatible element (Ni) decreases with increasing Ca# and decreasing Mg# ratios. This is strong evidence that the group 1 clinopyroxene megacrysts are the products of a fractionating magma, as indicated by numerous other criteria.

Much fewer samples are available for the group 2 clinopyroxene megacrysts and less developed trends are

present. The group 2a clinopyroxene megacrysts show similar trace element relations to the group 1 clinopyroxene megacrysts but at a lower Fe/Mg ratio. This could indicate that these samples were precipitated from a different magma than the group 1 samples. Although similar in character to group 2a samples, the group 2b samples crystallised from yet another different magma in view of their even lower Fe/Mg ratio. This indicates that the clinopyroxene megacryst suite at Schuller consists of a series of fractionating magmas with different initial compositions. These observations would indicate that the group 2 samples do not represent a large fractionation sequence, but are represented by a series of smaller events which fractionated separately. Similar conclusions were reached on the basis of major element chemical variations.

The group 3 samples are exceptionally enriched in Zr and Ga and depleted in Ni. The high Ca# and low Mg# previously noted for these samples together with the observations that ilmenite was a co-precipitating phase and the high levels of incompatible- and low levels of compatible elements would indicate extreme levels of fractionation.

The trace elements from the different groups have distinct patterns generally with group 1 and group 4 at the two extremes and group 2 intermediate between the two. Shimizu and Allegre (1978) have shown that garnet lherzolites fall

in three distinct groups on the basis of trace elements in clinopyroxene and garnet. These groups were found to correspond to sheared peridotite, unmetasomatised coarse peridotite and metasomatised peridotite. In comparison with the Schuller clinopyroxene megacrysts it transpires that groups 1 and 2 fall within the range of the sheared peridotite clinopyroxenes in terms of Sr and Zr whilst group 4 are close to coarse peridotite clinopyroxenes. The trace element variations thus follow that found for the major elements where group 2 megacrysts were found to approach sheared lherzolite compositions whereas group 4 megacrysts were found to be similar to coarse peridotites. The group 3 samples have Zr concentration in the range of granular metasomatised lherzolite clinopyroxenes.

The trace element variations for garnets do not follow simple patterns but appear to plot in a haphazard way. No regular variations are seen with the major element chemistry. Jones (1984) also found that REE concentrations in garnet megacrysts from Monastery do not correlate with major elements and suggested that the trace element variations might be affected by other processes such as assimilation or changing crystal-liquid distribution coefficient values with magma composition. Alternatively, in view of the presence of multiple compositional clinopyroxene groups at Schuller it is possible a similar situation exists for garnets which is not reflected by

major element variations. Additional trace element data on a larger suite of garnet megacrysts is needed to resolve this problem.

The modelling of Sr liquid compositions cannot be reconciled with observed trends. It is thus inferred that an additional carbonate phase with a high Sr liquid Kd would be required as a precipitating phase. Eggler and Wendlandt (1979) predicted that carbonate should be a liquidus phase. In the past the presence of calcite inclusions in megacrysts (Rawlinson and Dawson, 1979; Schulze, 1985) have been used as evidence in support that megacrysts are phenocrysts in kimberlites and that the trapped material represent kimberlite material. However, on the basis of the above modelling it becomes a strong possibility that carbonate is in actual fact a megacryst phase.

CHAPTER 5 : ND AND SR RADIOGENIC ISOTOPES

5.1 INTRODUCTION

The radiogenic isotopic characterisation of kimberlitic megacryst minerals could potentially place important constraints on their origin and affinities and is important evidence in the search of their ultimate source. Whereas earlier studies examined megacrysts from a number of localities (Barrett, 1975; Kramers et al., 1979; Smith, 1983b) later studies have placed greater emphasis on suites of megacrysts from single localities such as Monastery (Jones, 1984), Jagersfontein (Hops, 1989) and Kaalvallei (Smith and Schulze, unpublished data). All of these kimberlites are however Cretaceous or younger. The present study concentrates on clinopyroxene megacrysts from the Proterozoic Schuller and Premier kimberlites.

The clinopyroxene megacryst suites at Schuller and Premier represent an unusual situation where a number of distinct populations (based on major constituents) are found in a single kimberlite. The compositional spread at these localities is equivalent to that observed for clinopyroxene megacrysts on a world-wide scale. The isotopic characterisation of the different groups could place constraints on the processes leading to megacryst formation.

In the isotopic analysis of mantle derived material there are contamination problems due to the higher concentrations of Rb, Sr, Nd and Sm in the kimberlite relative to the entrained xenoliths. This requires the analysis of ultra pure mineral separates which can only be achieved by laborious hand selection. Sample fragments were therefore processed while immersed in ethanol to ensure that each grain was free from cracks, alteration or inclusions which could affect the measured isotope ratios.

5.2 SAMPLE SELECTION

Sample selection for combined Sr and Nd isotope work depended on the freshness and the large size of a particular sample to yield sufficient material for isotope work. Major element relations of the selected samples from Schuller are shown in Figure 5.1. Three group 1 clinopyroxene samples (CPX 3, CPX 32 and CPX 24) were selected to represent the high-, intermediate- and low temperature portions of the differentiation sequence. The four group 2 samples (CPX 17, CPX 26, CPX 6 and CPX 11) were selected to represent the largest possible compositional variation within this group. Two samples (86/2 and CPX 25) from the group 3 megacrysts and three group 4 samples (CPX 18, CPX 43 and CPX 21) were chosen to represent ranges in composition in these respective groups. In addition three samples from Premier (P46, P6 and P3) were selected to represent the group 1, 2 and 4

clinopyroxene megacryst populations at this adjacent kimberlite locality (Figure 5.2).

Sample preparation techniques and analytical procedures that were used are listed in Appendix 5. The Nd and Sr isotopic results are listed in Appendix 6, Tables 2 and 3.

5.3 QUALITY OF ISOTOPIC RESULTS

5.3.1 Sm and Nd

Repeat dissolutions of different portions of sample CPX 21 yielded $^{143}Nd/^{144}Nd$ ratios which were found to be within the internal 2 standard deviations of the running mean (Appendix 6, Table 3). Isotope dilution concentration results for Sm and Nd on repeat dissolutions (samples P46, CPX 21 and P3) are also in good agreement.

5.3.2 Rb and Sr

The Rb concentrations in all the megacrysts analysed were low (within blank ranges) thus the measured present $^{87}Sr/^{86}Sr$ ratios are essentially initial ratios.

Two samples (P46 and CPX 21) yielded measured $^{87}Sr/^{86}Sr$ isotopic ratios within the internal 2 standard deviations of the running mean on repeat dissolutions (Appendix 6, Table 2). Comparative inter-laboratory isotopic measurements on portions of sample P46 at the Bernard Price Institute (BPI) and the Geological Survey are in

good agreement. A slightly lower ratio was obtained on sample CPX 21 at the Geological Survey (0.70240) relative to BPI results (0.70258).

A more problematic and unexplained trend resulted from the $^{87}Sr/^{86}Sr$ isotopic measurement of spiked and natural splits of the same sample. On three of the ten samples where data were obtained on both isotope dilution (ID) and isotope concentration (IC) splits, (CPX 6, 86/2 and CPX 25) the measured ID ratio was found to be significantly higher than that of the measured IC ratio. The remainder of the results are within the error limits. In cases where such a discrepancy exists the results from the IC split are used since the IC results would appear to be more consistent. For instance the high ID result for CPX 6 of 0.70264 contrasts sharply with the four other results for group 2 megacrysts which range between 0.70202 to 0.70214. Similar low results were also obtained for the Premier group 2 clinopyroxene megacrysts. In addition the IC results for the two group 3 clinopyroxene megacrysts are identical whereas the ID results are significantly higher. The processing of ID samples involves the addition of a spike solution which is not the case for the IC samples. The extra processing step could potentially be the source for the observed discrepancy.

5.4 ND ISOTOPE DATA

5.4.1 Nd and Sm concentrations

Sm concentrations for the Schuller megacrysts range between 1.10 to 2.03 ppm whereas the Nd concentrations vary between 3.77 and 14.05 ppm. The group 1 clinopyroxene megacrysts show a linear relation between Sm and Nd (Figure 5.3). This corresponds to an increase in REE content with fractionation which is similar to the relationship found for clinopyroxene megacrysts from Monastery by Jones (1984). The increase of incompatible elements with fractionation was also noted for the group 1 clinopyroxenes previously. The group 2 megacrysts plot in a very narrow field which partially overlaps with the group 1 samples. A linear relation between Sm and Nd is also found for the group 4 megacrysts but these plot as a separate field generally at higher Sm and Nd concentrations. The two group 3 samples have the highest Sm and Nd concentrations. These results are similar to the other incompatible trace element results discussed previously and are consistent with very high levels of fractionation. The three clinopyroxene megacrysts from Premier plot within the respective compositional fields delineated for the compositionally equivalent Schuller clinopyroxene megacrysts. The chondrite normalised values show an enrichment of Nd relative to Sm which is similar to clinopyroxene data from Monastery (Jones, 1987) and Jagersfontein (Hops, 1989).

5.4.2 Nd isotopic ratios

The initial $^{143}Nd/^{144}Nd$ ratio calculated at 1198 Ma for the Schuller clinopyroxene megacrysts varies between 0.51109 and 0.51132. A plot of initial $^{143}Nd/^{144}Nd$ ratio and Nd concentration (Figure 5.4) do not show any linear trends but megacrysts from the various groups plot in distinctive fields. The three clinopyroxene megacrysts from Premier plot within the appropriate fields delineated by the Schuller megacrysts, adding further justification to the group classification.

A number of Nd isotopic measurements are available for megacrysts from Premier. Jones (1984; 1987) analysed three clinopyroxene and two garnet megacrysts and found a narrow range of initial $^{143}Nd/^{144}Nd$ ratios of 0.51135 to 0.51139 for four of the five samples with one garnet with a lower ratio of 0.51127. This data allowed Jones (1984; 1987) to determine an isochron age of 1198 Ma for megacrysts of the Premier kimberlite.

Winterburn (1989) analysed two clinopyroxene, one orthopyroxene and three garnet megacrysts and found an initial $^{143}Nd/^{144}Nd$ isotopic range of 0.51122 to 0.51156

From previous comparisons between Nd isotopic ratios between megacrysts and their host kimberlites, it was generally found that their $^{143}Nd/^{144}Nd$ ratios are similar. Jones (1984) found that Cr-poor, Cr-rich megacrysts and

kimberlites have similar Nd ratios. Hops (1989) also found overlapping Nd ratios for Cr-poor megacrysts, Granny Smith megacrysts and the host kimberlite at Jagersfontein. Spriggs (1988) found equally large variations in clinopyroxene and garnet megacrysts from the Gibeon province kimberlites which overlapped but which did not coincide with the kimberlite. The $^{143}Nd/^{144}Nd$ initial ratios of the kimberlites were found to be generally lower than the megacrysts.

Whereas the initial $^{143}Nd/^{144}Nd$ isotopic ratios for clinopyroxenes from sheared (0.51133; Walker et al., 1989) and coarse peridotites (0.51135; Winterburn, 1989) from Premier are within experimental error, distinct differences are apparent in the absolute REE concentrations (sheared Nd=5.37, Sm=0.939 and coarse Nd=36.1, Sm=3.9 ppm).

5.5 Sr ISOTOPE DATA

5.5.1 Sr and Rb concentrations

The Sr results were previously discussed in the trace element section. Appendix 6, Table 1 lists a comparison between the Sr concentration obtained by isotope dilution and PIXE which are in excellent agreement. All Rb concentrations were found to be within blank ranges.

5.5.2 Sr isotopic ratios

The $^{87}Sr/^{86}Sr$ ratios for the clinopyroxene megacrysts from Schuller vary from 0.70202 to 0.70264. Such a large spread negates the possibility that all the clinopyroxene megacrysts could have originated from the same source. No overall correlation is seen between Sr concentration and Sr isotopic ratios of these megacrysts (Figure 5.5) which indicates that a simple mixing hypothesis is not tenable.

If the Sr isotope ratios are considered in conjunction with the previously defined major element groupings, it becomes evident that the within group Sr isotopic variation is remarkably small. Three of the group 1 samples all have $^{87}Sr/^{86}Sr$ ratios between 0.70217 to 0.70219 despite the large apparent temperature interval (110 deg C) represented by these samples (Figure 5.5). The group 2 samples have a larger spread of $^{87}Sr/^{86}Sr$ ratios which varies between 0.70202 to 0.70214 with an average of the four samples of 0.70209. This is lower than that found for the group 1 samples. The group 4 clinopyroxene megacrysts have a narrow spread in $^{87}Sr/^{86}Sr$ ratios (0.70255 to 0.70264) which is significantly higher than that of either group 1 or group 2 clinopyroxene megacrysts. The conflicting ID and IC results of the group 3 clinopyroxene megacrysts makes these samples difficult to interpret but the preferred value of 0.70222 is close to that of the group 1 samples (Appendix 6, Table 2).

The three samples from Premier show similar relations to those found for Schuller clinopyroxene megacrysts. Sample P46 which is similar in composition to the group 1 clinopyroxene megacrysts has a $^{87}Sr/^{86}Sr$ ratio of 0.70222 while the group 2 sample P6 has a ratio of 0.70204 (Figure 5.5). These values are in excellent agreement with those obtained for the Schuller megacrysts. The group 4 sample (P3) has a $^{87}Sr/^{86}Sr$ ratio of 0.70233 which is lower than that found for the Schuller group 4 samples but is still significantly higher than the group 1 and group 2 samples.

A number of clinopyroxene megacrysts from Premier were previously analysed for their Sr isotopic compositions by Smith (1983b), Jones (1984) and Winterburn (1989). Major element compositions were given for the single specimen analysed by Smith (1983b) but not for the samples analysed by Jones (1984) and Winterburn (1989). The lack of the major element compositions of these clinopyroxenes, prohibits their classification into a group and thus complicates direct comparisons between the published isotope determinations and the present results.

The megacryst analysed by Smith (1983b) has a high K and Rb content with a resulting initial ratio calculated at 1198 Ma of 0.70218. This sample is similar to the group 2 clinopyroxene megacrysts in major element composition whereas the isotopic composition falls within the group 1 range. The clinopyroxene megacryst of unreported major

element- or Sr-composition analysed by Jones (1984) has a ratio of 0.70225 which is similar in isotopic composition to the group 1 sample analysed from Premier in this work. The low Sm and Nd concentrations in this sample is comparable with those in either groups 1 or 2. Winterburn (1989) quotes isotopic results of two megacrysts from Premier (samples were not analysed for major element compositions) with resulting $^{87}Sr/^{86}Sr$ initial ratios of 0.70260 and 0.70143 respectively. These megacrysts have Rb concentrations of 0.224 and 3.904 ppm respectively which could indicate that the mineral separates were not perfectly free of kimberlitic or alteration material. The sample with the higher ratio is close in isotopic composition to the group 4 samples. The very low initial $^{87}Sr/^{86}Sr$ ratio of 0.70143 of the other sample could possibly be the result of an overestimation of the Rb content.

The complexity shown by the $^{87}Sr/^{86}Sr$ ratios of clinopyroxene megacrysts from Schuller and Premier would indicate that care should be taken to fully characterise megacryst suites with major element data at particular localities before attempting to interpret the isotopic results. The comparison of Sr isotope data from the literature with that obtained in this study could also be complicated by the fact that different techniques have been used at the different isotope laboratories. Clinopyroxene megacrysts are very susceptible to

contamination from the kimberlite due to their low Rb and Sr contents relative to kimberlite. Different criteria have also been applied at different laboratories as to what constitute "pure" unaltered clinopyroxene material suitable for isotopic analysis. In addition the different leaching and processing procedures could also result in disparate results. The importance of working with ultra-pure material in isotope studies of mantle derived material was aptly shown by the work of Richardson et al. (1985) on garnets from peridotites. However, the present results from Schuller and Premier clinopyroxene megacrysts are from a well characterised suite of samples. All samples were furthermore scrupulously selected and processed under identical conditions. The results are internally consistent.

5.6 DISCUSSION

From the combined eNd and eSr plot of the megacrysts from both Schuller and Premier (Figure 5.6) it can be seen that there is a large spread in values for clinopyroxene megacrysts from either locality which is comparable in size to the field for the combined Cretaceous clinopyroxene megacrysts as determined by Smith (1983b) and Jones (1984). However, clinopyroxene megacrysts from the specific compositional groups defined on the basis of major elements at Schuller and Premier plot in restricted isotopic fields. The discrimination between such fields is

predominantly due to differences in the Sr isotopic component as the Nd results show complete overlap. The megacrysts all plot in the depleted quadrant of the eNd-eSr plot which indicates a time integrated depleted source. This could either indicate that the various megacrysts groups are derived from distinct isotopic source areas or that some interaction process resulted in the spread now observed.

In detail, the group 1 samples occupy a central position with the group 2 samples having relatively more depleted and the group 4 samples more enriched Sr-isotopic signatures (Figure 5.6). Such correlations between major-, trace- and isotopic compositions have never before been demonstrated.

Previous work has shown that Cr-rich megacrysts generally have Sr isotopic compositions which are enriched relative to the Cr-poor megacryst compositions but depleted relative to the host kimberlite (Jones, 1984; Hops, 1989). The higher $^{87}Sr/^{86}Sr$ in the Cr-rich megacrysts was ascribed to isotopic modification by the kimberlite subsequent to megacryst crystallisation (Smith, 1983b; Jones 1984). Although the higher $^{87}Sr/^{86}Sr$ ratios in the group 4 megacrysts can be explained by an analogous process, the lower $^{87}Sr/^{86}Sr$ in the group 2 megacrysts cannot, as the group 1 megacrysts unquestionably represent a fractionating magma. The lower $^{87}Sr/^{86}Sr$ in the group 2

megacrysts relative to the group 1 megacrysts would require a source with a lower $^{87}Sr/^{86}Sr$ composition in a mixing scenario.

Hops (1989) investigated the isotopic characteristics of megacrysts and high temperature deformed peridotites at Jagersfontein and found that although the $^{87}Sr/^{86}Sr$ of clinopyroxenes overlap, the peridotite clinopyroxenes generally had lower $^{87}Sr/^{86}Sr$ ratios than the Cr-poor megacrysts (Figure 5.7). This would indicate that the deformed peridotites have isotopic characteristics closer to a mid ocean ridge basalt (MORB) type source whereas the megacrysts have characteristics similar to an ocean island basalt (OIB) type source.

CHAPTER 6 : GENERAL CONCLUSIONS

6.1 THE SCHULLER MEGACRYSTS

6.1.1 Introduction

The clinopyroxene megacrysts at Schuller, which fall into distinct major element and Sr isotopic units, can be used to constrain the megacryst formation model at this locality. It is believed that the compositional variations observed reflect interactions between deep seated primitive magmas and distinct mantle lithologies.

It is proposed here that at least four separate crystallising events took place to form the megacryst suite at Schuller. Clinopyroxene was present in all four events and it is thus useful to typecast such events using the clinopyroxene data. The following reconstruction of crystallisation sequences is based on phases hosting inclusions, geothermobarometry, fractionation trends and isotopic results as discussed in previous chapters.

6.1.2 Crystallisation conditions

Crystallisation of the group 1 clinopyroxenes initiated at 1479 deg C and continued down to 1324 deg C. Trace element modelling shows that a phase with a high Sr distribution coefficient also crystallised together with the group 1 clinopyroxenes, possibly a carbonate. The group 1 orthopyroxenes co-precipitated in the range 1360 to 1324

deg. C and carried on to 1270 deg C. At the cessation of the group 1 clinopyroxene crystallisation, the degree of fractionation was of the order of 75 - 80 %. From the element variation trends of the orthopyroxenes it is apparent that orthopyroxene continued to crystallise after the cessation of crystallisation of group 1 clinopyroxenes, together with ilmenite in the temperature range 1290 to 1270 deg C and probably on to 1180 deg C. The Sr isotope ratios indicate that as crystallisation proceeded the group 3 clinopyroxenes formed together with ilmenite in the temperature range 1090 - 817 deg C. At this stage the degree of fractionation must have been very high as shown by the high concentrations of incompatible trace elements in the group 3 clinopyroxenes. Based on the extent enrichment of Zr in the group 3 clinopyroxenes, the degree of fractionation could be generated by in excess of 90 % equilibrium crystallisation.

Group 2a clinopyroxene and orthopyroxene megacrysts crystallised together with Fe-rich garnets in the temperature range 1426 to 1264 deg C at 54 kb. Ilmenite was either a minor crystallising phase or was absent.

Groups 2b clinopyroxene and orthopyroxene megacrysts respectively, together with Mg-rich garnets and ilmenites, were co-precipitated over the temperature range 1289 to 1185 deg C for clinopyroxenes and 1250 and 1200 deg C for the orthopyroxenes. The pressure estimate varies between

50 to 55 kb. This large variation is probably due to the inaccuracy of the calculations rather than a real difference.

The group 4 clinopyroxenes crystallised over a temperature range of 1123 to 1009 deg C. No indications of co-precipitating phases were found.

The inferred sequence of crystallising events are pictorially represented against a calculated temperature in Figure 6.1.

6.1.3 Discussion

The group 1 clinopyroxenes clearly crystallised from a fractionating magma at depth as testified by coherent major and trace element variations. This magma appears to be primitive with OIB isotopic characteristics and is therefore asthenospheric. Mineral compositions are Cr- and Ti-poor and are the most Fe-rich kimberlitic megacrysts described to date. The trace element contents are also compatible with asthenospheric derived melts. The uniform Sr isotopic results for three samples representing a relatively large temperature interval indicate that this fractionation occurred within a closed system without any mixing processes. A similar result was found at Monastery where a high temperature clinopyroxene megacryst analysed by Smith (1983b) and a lower temperature clinopyroxene intergrown with ilmenite analysed by Shimizu (1975) had

$^{87}Sr/^{86}Sr$ ratio within experimental error. Spriggs (1988) however suggested from isotopic data on clinopyroxenes from the Gibeon kimberlites that the composition of the melt would progressively change toward that of the wall rock with megacryst differentiation. It should however be borne in mind that Spriggs (1988) analysed twelve megacrysts from seven different kimberlites. In lieu of the complexities shown by megacryst suites at a single locality such as Schuller, the comparisons of major element and isotopic data from megacrysts from separate, although adjacent localities, should be treated with circumspection.

The similarity in Sr isotope ratios between the group 1 and group 3 clinopyroxenes indicate that these could have crystallised from the same magma but that a break occurred in clinopyroxene precipitation. Orthopyroxene and ilmenite crystallised after the cessation of group 1 clinopyroxene crystallisation and was followed by the calcic, Cr-poor and relatively Fe-rich group 3 clinopyroxenes at very high levels of fractionation where clinopyroxene crystallised with ilmenite. Analyses of sparse samples of similar clinopyroxenes have been listed in the literature (Nixon and Boyd, 1973; Shee, 1978) prior to the description of a large suite of similar samples from Monastery (Moore et. al., in prep.). The latter co-exists with olivine, phlogopite, ilmenite and zircon. This would indicate that extreme differentiation of the megacryst magma has

occurred at a number of localities. In addition it shows that extreme megacryst differentiation results in very Fe-rich compositions. This is distinct from the more magnesian compositions found in early formed phenocrysts in kimberlites and is strong support for a xenocrystic origin of megacrysts in kimberlites.

The group 2 megacrysts do not show the clear major and trace element igneous trends normally associated with megacrysts. At least two subgroups have been identified, each of which appear to represent a number of smaller crystallisation events. Some of these samples have chemical compositions equivalent to typical Cr-poor megacrysts e.g. Monastery, (group 2a) whereas others are enriched in Cr_2O_3 and Mg# and have compositions that tend towards, and partially overlap, with clinopyroxenes from sheared lherzolites (group 2b). The Sr isotope ratios of all the group 2 samples are however significantly lower than in the group 1 megacrysts. It is impossible to generate the observed low $^{87}Sr/^{86}Sr$ isotopic compositions by the mixing of an asthenospherically derived magma with enriched subcratonic mantle such as represented by the coarse lherzolites.

The group 2 clinopyroxene megacrysts can be generated by the mixing of a primary asthenospheric magma of OIB origin with material of more depleted Sr isotopic compositions. This material is thought to be represented by some high

temperature peridotites. Minerals separated from high temperature peridotites have been found with Nd and Sr ratios similar to MORB (i.e. more depleted than OIB type magmas) (Shimizu, 1975; Allegre et al., 1982; Richardson et al., 1985). At Jagersfontein, Hops (1989) also found generally lower $^{87}Sr/^{86}Sr$ ratios in clinopyroxenes from high temperature peridotites relative to Cr-poor clinopyroxene megacrysts which would also support a MORB type source for some high temperature peridotites.

The interaction between a primary OIB magma with more depleted MORB wall-rock would result in a magma with less radiogenic Sr compared to the original starting magma. The group 2 clinopyroxene megacrysts at Schuller do not follow a broad coherent trend such as that found at Monastery for instance, but rather plot in a more scattered fashion. They are therefore interpreted to represent a series of smaller isolated fractionation events. This would indicate that interactions between the primary magma and the wall rock is variable and very localised. The group 2b clinopyroxene megacrysts contain distinctly higher Cr_2O_3 contents relative to the group 2a and are envisaged to represent a greater amount of wall rock interaction followed by subsequent crystallisation.

The group 4 Mg-rich megacrysts have Sr concentrations and isotopic compositions which are closer to cool coarse common peridotites. The group 4 megacrysts could be the

consequence of pristine magma interacting with common peridotites which would explain the higher $^{87}Sr/^{86}Sr$ ratios and the higher Sr and Zr concentrations seen in them.

These facts demonstrate that one kimberlite sampled at least three different megacryst populations with different Sr isotopic characteristics and is additional evidence that megacrysts are not true phenocrysts in the kimberlite in which they occur.

Various factors, which are difficult to quantify such as the size of the intrusion, the magma composition and state of evolution, the temperature difference between magma and wall rock and the composition of the wall-rock must have an influence on the composition of resulting megacrysts and the extent of fractionation which occurs. The time period before sampling by a passing kimberlite can also influence the extent of fractionation.

6.2 PREMIER

The comparative study of clinopyroxene megacrysts from Schuller and Premier shows that multiple megacryst suites are also present at Premier but that the two megacryst suites are not exactly equivalent in terms of compositional relations and abundances. Four groups are found at Schuller and three at Premier.

The major element compositions and Sr-isotopes of the respective group 1 clinopyroxenes from Schuller and Premier overlap, although the samples from Premier do not show as large a compositional spread as those from Schuller. Thus although the magma composition at the two localities is similar, the extent of fractionation of the group 1 clinopyroxene megacrysts at Premier is less than that at Schuller. The absence of the group 3 clinopyroxenes at Premier, which at Schuller have been interpreted as products of extreme fractionation of the group 1 clinopyroxene magma, also supports the premise that less fractionation occurred at Premier for the group 1 clinopyroxene megacrysts.

Differences are found in both the abundance and compositions of the groups 2 and 4 clinopyroxene Schuller and Premier megacrysts. Whereas the group 4 clinopyroxenes constitute 65 % of the clinopyroxene megacryst population at Premier, it forms only 28 % at Schuller. In addition to the above, clear compositional differences are found between the compositional fields of the group 4 clinopyroxenes from Premier and Schuller. The samples from Premier contain relatively lower chrome and lower Mg#. The one sample from Premier which was analysed for Sr isotopes also has a lower $^{87}Sr/^{86}Sr$ ratio (0.70233) than the Schuller group 4 samples (range 0.70255 to 0.70264). Although more samples from Premier are needed to corroborate this trend, the lower chrome contents and Mg#

ratios together with the lower $^{87}Sr/^{86}Sr$ might be an indication of relatively lower amounts of interaction between the primary magma (such as represented by the group 1 clinopyroxene megacrysts) and coarse cold lithospheric peridotites at Premier relative to Schuller.

The group 2b clinopyroxene megacrysts at Premier are more abundant than equivalent samples at Schuller. This also indicates differences in the megacrysts sources sampled by the respective kimberlites.

The compositional and isotopic similarities between the group 1 clinopyroxenes from Schuller and Premier support the idea that these samples represent the products from a primary magma. The compositional differences found for the other clinopyroxene megacryst groups are interpreted to represent variable amounts of interaction between the primary megacryst magma and available wall rocks. These observations would support the proposal that megacryst formation occur as small localised events (Harte and Gurney, 1981; Harte, 1983; Mitchell, 1987)

Given the close implied temporal and known spatial association of the Schuller and Premier kimberlites this would suggest that the formation of megacrysts is restricted to local processes and reflect local interactions.

6.3 COMPARISON WITH OTHER LOCALITIES

6.3.1 General

It has been shown in this study that multiple Cr-poor megacryst populations are more common in single kimberlites than hitherto believed. Although multiple megacryst populations have clearly been shown at Sloan-Nix (Eggler et al., 1979), their presence has largely been ignored in most megacryst models. This study confirms the presence of multiple clinopyroxene megacryst compositional groups at localities such as Orapa and Witberg. At other localities such as Jagersfontein they may also be present. Here the fractionation trends are broad and can be interpreted as a number of fractionation events forming under slightly differing conditions. These would be mixed together by the kimberlite which transports them to the surface as was suggested by Mitchell (1987). The presence of multiple populations in kimberlitic megacryst suites needs to be incorporated in general megacryst formation models.

Care needs to be taken in the study of megacrysts in that a large enough population is analysed to establish the true compositional range. Megacrysts from different kimberlites should also not be composited as it is now firmly established that megacrysts from specific localities tend to have specific characteristics (e.g. this work; Mitchell, 1987; Hops et al., 1991; Davis et

al., 1991). Samples for isotope work should also be carefully selected after the compositional ranges have been established.

6.3.2 Regional variations

In the comparison between megacryst compositions from different southern African localities it was noticed that megacryst compositions from localities situated within the boundaries of the Kalahari Craton differ significantly from megacryst compositions from localities situated within the mobile belts surrounding the craton or localities situated in marginal craton settings.

Clinopyroxene megacryst compositions from localities from within the craton have compositions that are remarkably similar and constant. Such compositions generally plot within the field demarcated by the Monastery samples where the fractionation trend is extensive as was established by Jakob (1977) and Gurney et al. (1979). Differences between localities can easily be accounted for by differing degrees of fractionation and differences in the proportions of crystallising phases. This indicates a very uniform source for such megacrysts and may have contributed to the idea that megacrysts represent a continuous horizon in the upper mantle.

Relative to on-craton localities, off craton localities have distinct and rather more variable megacryst

compositions. These are relatively uniformly enriched in chrome and Mg#. Similar trends were noticed by Nixon (1987) for the Eastern Griqualand kimberlites.

The megacrysts from other on-craton localities where data are available from such as Colorado-Wyoming and Angola do not follow the general trend shown by megacrysts from within the boundaries of the Kalahari craton but tend to be more variable and in general distinctly chrome and Mg# rich.

6.4 RELATIONSHIP BETWEEN MEGACRYSTS AND KIMBERLITE

Cr-poor megacrysts are a ubiquitous feature of Group 1 kimberlites. The fact that the magma from which the Cr-poor megacryst suite crystallised existed immediately prior to kimberlite eruption is clearly established. This is confirmed by the presence of sub-microscopic pigeonite exsolution in subcalcic clinopyroxenes which is indicative of rapid cooling from high temperatures at low pressures (McCallister and Nord, 1981). The large grain size of megacrysts, their lack of aggregation and the general coherent differentiation trends are indications that they crystallised at depth from magmas. Age dating of megacrysts also generally corresponds with pipe emplacement ages (Smith, 1983b; Jones, 1984; Winterburn, 1989).

The question whether one specific magma gave rise to the megacrysts and to the eventual kimberlite has not been satisfactorily resolved. Experimental work by Eggler and Wendlandt (1979) and Brey et al. (1983) supports the co-existence of the typical megacryst assemblage with kimberlitic liquids at depth. Inclusions with kimberlite mineralogy within megacryst minerals have been interpreted as trapped melt inclusions (Gurney et al., 1979; Gurney and Harte, 1980; Schulze, 1985) which also favour a phenocrystal origin of megacrysts in kimberlite. However, given the infiltrative powers of kimberlitic fluids, as often seen in lherzolite xenoliths, and the commonly cracked and veined appearance of megacrysts in general, such trapped inclusions could merely represent infiltration by kimberlite.

Other evidence, however, indicates that the Cr-poor megacrysts are xenocrysts in the kimberlite. Jones (1984) found that calculated model REE profiles of liquids which would have crystallised the Cr-poor megacrysts at Monastery have dissimilar profiles to those observed in kimberlite but are similar to REE profiles of primitive alkali basalts. Harte (1983) similarly showed on the basis of trace elements that the calculated liquid in equilibrium with a subcalcic clinopyroxene megacryst is very similar to a basanite. Harte (1983) also noted that the maximum Mg# for megacryst olivines of approximately 0.9 is compatible with that expected for picritic-basaltic

primary magmas. This would indicate that the megacryst magma is closer in composition to alkali-basalt rather than kimberlite.

Pasteris (1980) and Hunter and Taylor (1984) have noted that distinct rim zonations found in ilmenite megacrysts indicate that such minerals were not in equilibrium with the kimberlite and cannot be phenocrysts. The zonations are magnesium- and chrome-rich compared to relative Fe-rich megacrysts cores. In the present study it was also found that extreme fractionation results in Fe-enrichments at low temperatures (group 3 samples). Such compositions are unlike early kimberlitic phenocrysts which are magnesian and chromian.

Both megacrysts and Group I kimberlites have Nd and Sr systematics which indicate derivation from a time integrated slightly depleted source relative to bulk earth. This is similar in scale and size to single ocean island basalts (Jones, 1984). However the Cr-poor megacrysts and the Group I kimberlites are not in Sr isotopic equilibrium. It is found that the Cr-poor megacrysts have lower $^{87}Sr/^{86}Sr$ in general than their host kimberlites (Smith, 1983b; Jones, 1984; Spriggs, 1988). The Cr-rich and Granny Smith megacrysts have higher $^{87}Sr/^{86}Sr$ than the Cr-poor megacrysts with values that overlap with that of the kimberlite (Jones, 1984; Hops, 1989). Although favouring a xenocrystic model for Cr-poor

megacrysts on the basis of isotopes, Smith (1983b) suggested that it was possible to reconcile the Sr-isotopic discrepancy between the megacrysts and the kimberlites if the kimberlite formed by the assimilation of lithospheric material (with radiogenic Sr) after crystallisation of the megacrysts. Jones (1984, 1987) similarly proposed a cognate model for the Cr-poor megacrysts by a process of assimilation-fractional-crystallisation (AFC) followed by incorporation of radiogenic lithospheric material to change the magma composition from basaltic to kimberlitic.

Spriggs (1988) showed with Pb isotope work on clinopyroxene megacrysts and kimberlites from Gibeon that the megacrysts and kimberlite are not in Pb isotopic equilibrium. In addition the Pb isotopic compositions do not support an AFC mixing model as has been proposed on the basis of the Sr isotopes. Spriggs (1988) found that the kimberlite and lithospheric material have radiogenic and un-radiogenic Pb respectively with megacrysts having an intermediate value. This would thus negate the possibility of an AFC mixing model where kimberlite is generated from a megacryst magma which assimilated some subcontinental lithospheric material. The Pb isotopes thus do not support the idea that megacrysts are phenocrysts within the kimberlite or that the magma from which the megacrysts crystallised was altered by lithospheric

assimilation to generate the kimberlite as was proposed by Smith (1983b) and Jones (1984).

On the basis of the above it is proposed that megacrysts in kimberlites crystallise from "alkali basalts" with OIB isotopic characteristics. Although such magmas could have been generated in the same broad cycle of igneous activity in which the kimberlite was generated these magmas are not considered to be a proto-kimberlitic magma. The presence of multiple compositional and isotopic megacryst groups within single kimberlites suggests that megacryst formation occurs on a small scale. Interactions between the megacryst magma and lithospheric and/or asthenospheric material would have a profound affect on the resulting megacryst compositions. Whether single or multiple megacryst populations are present at any particular locality is thus dependent on the complexity of the lithosphere in the region where the megacrysts crystallise.

The results of this study are compatible with those by Pasteris (1980) who suggested that megacrysts crystallised from melts unrelated to kimberlite. Kimberlitic melts would disrupt pockets of crystallising magma and both the crystallising megacrysts together with interstitial liquid would be incorporated into the kimberlite. Various megacryst populations can thus be accounted for.

ACKNOWLEDGEMENTS

I guess Leon Daniels had a lot to do with my interest and involvement in kimberlites and mantle xenoliths. It started in 1980 when he invited me to accompany him on a vacation job to sample some of the Karoo kimberlites for John Gurney. My introduction to the Schuller kimberlite was by Nok Frick and Schalk Strauss in 1983. It was meant to be a short term project.

As for this thesis, John Gurney my supervisor, is thanked for constant support and encouragement from the initial proposed M.Sc. project, the eventual conversion into the present format up to the last paragraph. John also made F.R.D. funds available for the initial probe work.

My employer, the Geological Survey, is thanked for allowing me (and paying me) to have worked on this project. I was also fortunate to be given the opportunity to present parts of this work at conferences in Beijing, P.R. China and Araxa, Brazil. My colleagues at the Laboratory have always supported me in this work. Special thanks are due to Feo Walraven for assistance with isotope work, Martin Kohler and Charlie Mabuela for photographic services and Nok Frick for encouragement and general interest. Martin Lekotoko and David Kgaditse produced brilliant polished thin sections and disks.

The staff and past and present students of the Geochemistry Department at UCT were always helpful and provided support. Thanks are due to Rory, Jenny, Melissa, Marshall and Leon. Dick Rickard taught me a lot about the electron microprobe and provided invaluable assistance to get the electron microprobe at the Geological Survey up and running. Rory Moore was mostly always available to listen to my woes and kindly produced the proton probe trace element data presented in this thesis.

It was indeed a privilege to have learned some of the intricacies of isotope work and mineral picking from an enthusiast such as Craig Smith at BPI at the University of the Witwatersrand. Craig also proof read sections of this thesis and made valuable suggestions. Thanks to the BPI stalwarts Janet, Alastair, Moose, Ingeborg, Trevor and Erika for teaching me about columns, their calibration, bead loading, clean lab procedures and other such stuff.

Patrick Bartlett provided valuable samples from the Premier kimberlite and ensured pleasant visits to the mine. The staff at AARL always showed interest and were available to discuss new data.

A lot of people contributed directly to this thesis by unselfishly making unpublished analyses of megacrysts and

related material available. In this regard thanks to Joe Boyd, Dave Eggler, Dan Schulze and Jenny Hops

My mother and my family in Cape Town provided shelter and encouragement during my working visits to UCT. Thank you very much.

Finally special thanks to my wife, Michelle and my daughter Janine who understood that this goal was very important to me and allowed me to pursue it over many Saturdays.

REFERENCES

AGEE J.J., GARRISON J.R. and TAYLOR L.A. 1982. Petrogenesis of oxide minerals in kimberlite, Elliot County, Kentucky. American Mineralogist 67, 28-42.

ALLEGRE C.J., SHIMIZU N. and ROUSSEAU D. 1982. History of the continental lithosphere recorded by ultramafic xenoliths. Nature 296, 732-735.

ALLSOPP H.L. and KRAMERS J.D. 1977. Rb-Sr and U-Pb age determinations on southern African kimberlite pipes. Extended Abstract Second International Kimberlite Conference Santa Fe.

ALLSOPP H.L., BURGER, A.J. and VAN ZYL C. 1967. A minimum age for the Premier kimberlite pipe yielded by biotite Rb-Sr measurements, with related galena isotopic data. Earth and Planetary Science Letters 3, 161-166.

AOKI K.I., FUJIMAKI H. and KITAMURA M. 1980. Exsolved garnet-bearing pyroxene megacrysts from some South African kimberlites. Lithos 13, 269-279.

BARRETT D.R. 1975. The genesis of kimberlites and associated rocks: Strontium isotopic evidence. Physics and Chemistry of the Earth 9, 637-653.

BARRETT D.R. and ALLSOPP H.L. 1973. Rubidium-strontium age determinations on southern African kimberlite pipes. Extended Abstract First International Kimberlite Conference University of Cape Town 23-25

BLOOMER A.G. and NIXON P.H. 1973. The geology of the Letseng-la-terae Kimberlite Pipes. In: Nixon P.H. ed., Lesotho Kimberlites, pp 20-32. Lesotho National Development Corporation, Maseru.

BOYD F.R. 1989. Where do we go from here? In: Kimberlites and related rocks, Volume 2: Their mantle/crust setting, diamonds and diamond exploration. Geological Society of Australia Special Publication 14, pp 1239-1251. Blackwell.

BOYD F.R. and DANCHIN R.V. 1980 Lherzolites, eclogites and megacrysts from some kimberlites in Angola. American Journal of Science 280-A, 528-549.

BOYD F.R. and NIXON P.H. 1973. Origin of the ilmenite-silicate nodules in kimberlites from Lesotho and South Africa. In: Nixon P.H. ed., Lesotho Kimberlites, pp 254-268. Lesotho National Development Corporation, Maseru.

BOYD F.R. and NIXON P.H. 1978. Ultramafic nodules from the Kimberley pipes, South Africa. Geochimica et Cosmochimica Acta 42, 1367-1382.

BOYD F.R. and NIXON P.H. 1980. Discrete nodules from the kimberlites of East Griqualand, southern Africa. Carnegie Institution of Washington Yearbook 79, 296-301.

BOYD F.R., DAWSON J.B. and SMITH J.V. 1984. Granny Smith diopside megacrysts from the kimberlites of the Kimberley area and Jagersfontein, South Africa. Geochimica et Cosmochimica Acta 48, 381-384.

BREY G., BRICE W.R., ELLIS D.J., GREEN D.H., HARRIS K.L. and RYABCHIKOV I.D. 1983. Pyroxene-carbonate reactions in the upper mantle. Earth and Planetary Science Letters 62, 63-74.

BURGESS R., TURNER G., LAWRENZI M. and HARRIS J.W. 1989. 40Ar-39Ar laser probe dating of individual clinopyroxene inclusions in Premier eclogitic diamonds. Earth and Planetary Science Letters 94, 22-28.

DANCHIN R.V. 1979. Mineral and bulk chemistry of garnet lherzolite and garnet harzburgite xenoliths from the Premier Mine, South Africa. In: Boyd F.R. and Meyer H.O.A. eds., The Mantle Sample: Inclusions in kimberlites and other volcanics, pp 104-126. American Geophysical Union, Washington.

DAVIES G.R., SPRIGGS A.J., NIXON P.H. and REX D.C. 1991. A non-cognate origin for the Gibeon kimberlite megacryst suite. Extended Abstracts Fifth International Kimberlite Conference, Araxa, pp 63-65

DE BRUIN D. 1989. Mantle eclogites from the Schuller kimberlite, Transvaal, South Africa. South African Journal of Geology 92, 134-135.

DE BRUIN D. 1990. Clinopyroxene megacrysts from the Schuller kimberlite, Transvaal, South Africa (abstract). 15 th General Meeting of the International Mineralogical Association held in Beijing, P.R. China, V. 2, 791-792.

DEMAIFFE D. and FIEREMANS M. 1981. Strontium-isotopic geochemistry of the Mbuji Mayi and Kundelungu kimberlites (Zaire, central Africa). Chemical Geology 31, 311-323.

DROOP, G.T.R. 1987. A general equation for estimating Fe3+ concentrations in ferromagnesian silicates and oxides from microprobe analyses, using stoichiometry criteria. Mineralogical Magazine 51, 431-435.

EGGLER D.H. and WENDLANDT R.F. 1979. Experimental studies on the relationship between kimberlite magmas and partial melting of peridotite. In: Boyd F.R. and Meyer H.O.A. eds., Kimberlites, Diatremes and Diamonds: Their geology, petrology, and geochemistry. pp 330-338. American Geophysical Union, Washington.

EGGLER D.H.and McCALLUM M.E. 1976. A geotherm from megacrysts in the Sloan kimberlite pipes, Colorado. Carnegie Institution of Washington Yearbook 75, 538-541.

EGGLER D.H., McCALLUM M.E. and SMITH C.B. 1979. Megacryst assemblages in kimberlite from northern Colorado and southern Wyoming: petrology, geothermometry-barometry and areal distribution. In: Boyd F.R. and Meyer H.O.A. eds., The Mantle Sample, pp 213-226. American Geophysical Union, Washington.

EGGLER D.H., McCALLUM M.E. and KIRKLEY, M.B. 1987. Kimberlite-transported nodules from Colorado-Wyoming: a record of enrichment of shallow portions of an infertile lithosphere. In: Mullen, E. and Pasteris, J.D. eds., Geological Society of America Special Paper, 215, pp 77-90.

FRICK C. 1973. Kimberlitic ilmenites. Transactions of the Geological Society of South Africa 76, 84-94.

GARRISON J.R.(Jnr) and TAYLOR L.A. 1980. Megacrysts and xenoliths in kimberlite, Elliott County, Kentucky: A mantle sample from beneath the Permian Appalachian Plateau. Contributions to Mineralogy and Petrology 75, 27-42.

GERRYTS E. 1951. The petrology of the kimberlites at the Premier (Transvaal) diamond mine, South Africa. Unpublished Ph.D., McGill University.

GREEN T.H., SIE S.H., RYAN C.G. and COUSENS D.R. 1989. Proton microprobe-determined partitioning of Nb, Ta, Zr, Sr and Y between garnet, clinopyroxene and basaltic magma at high pressure and temperature. Chemical Geology 74, 201-216.

GRIFFIN W.L., JAQUES, A.L., SIE, S.H., RYAN, C.G., COUSENS, D.R. and SUTTER, G.F. 1988. Conditions of diamond growth: a proton microprobe study of inclusions in West Australian diamonds. Contributions to Mineralogy and Petrology 99, 143-158.

GRIFFIN W.L., SMITH D., BOYD F.R., COUSENS D.R., RYAN C.G., SIE S.H. and SUTTER G.F. 1989. Trace-element zoning in garnets from sheared mantle xenoliths. Geochimica et Cosmochimica Acta 53, 561-567.

GURNEY J.J. and HARTE B. 1980. Chemical variations in upper mantle nodules from southern African kimberlites. Philosophical Transactions of the Royal Society of London A297, 273-293.

GURNEY J.J., FESQ H.W. and KABLE E.J.D. 1973. Clinopyroxene ilmenite intergrowths from kimberlite: A re-appraisal. In: Nixon P.H. ed., Lesotho Kimberlites, pp 238-253. Lesotho National Development Corporation, Maseru.

GURNEY J.J., JAKOB W.R.O. and DAWSON J.B. 1979. Megacrysts from the Monastery kimberlite pipe, South Africa. In: Boyd F.R. and Meyer H.O.A. eds., The Mantle Sample, pp 227-243. American Geophysical Union, Washington.

HAGGERTY S.E. 1975. The chemistry and genesis of opaque minerals in kimberlites. Physics and Chemistry of the Earth 9, 295-307.

HAGGERTY S.E. and BOYD F.R. 1975. Kimberlite in an olivine megacryst from Monastery. Long Abstracts, Kimberlite Symposium, London.

HARTE B. 1983. Mantle peridotites and processes - the kimberlite sample. In: Hawkesworth C.J. and Norry M.J. eds., Continental basalts and mantle xenoliths, pp 46-99. Shiva Publishing Limited, Cheshire.

HARTE B. and GURNEY J.J. 1981. The mode of formation of chromium-poor megacryst suites from kimberlites. Journal of Geology 89, 749-753.

HOPS J.J. 1989. Some aspects of the geochemistry of high-temperature peridotites and megacrysts from the Jagersfontein kimberlite pipe, South Africa. Unpublished Ph.D., University of Cape Town.

HOPS J.J., GURNEY J.J., HARTE B. and WINTERBURN P. 1989. Megacrysts and high temperature nodules from the Jagersfontein kimberlite pipe. In: Kimberlites and related rocks, Volume 2: Their mantle/crust setting, diamonds and diamond exploration. Geological Society of Australia Special Publication 14, pp 759-770. Blackwell.

HOPS J.J., MOORE R.O. and GURNEY J.J. 1991. The individuality of on- and off-craton megacryst suites in southern Africa. Extended Abstracts Fifth International Kimberlite Conference, Araxa, pp 177-179.

HUNTER R.H. and TAYLOR L.A. 1984. Magma-mixing in the low velocity zone: kimberlitic megacrysts from Fayette County, Pennsylvania. American Mineralogist 69, 16-29.

JAKOB W.R.O. 1977. Geochemical aspects of the megacryst suite from the Monastery kimberlite pipe. Unpublished M.Sc., University of Cape Town.

JAROSEWICH E., NELEN J.A. and NORBERG J.A. 1980. Reference standards for electron microprobe analysis. Geostandards Newsletter 4, 43-47.

JONES R.A. 1984. Geochemical and isotopic studies of some kimberlites and included ultrabasic xenoliths from southern Africa. Unpublished Ph.D., University of Leeds.

JONES R.A. 1987. Strontium and neodymium isotopic and rare earth element evidence for the genesis of megacrysts in kimberlites of southern Africa. In: Nixon P.H. ed., Mantle Xenoliths, pp 711-724. J.Wiley & Sons, New York.

KIRKLEY M.B., SMITH H.S. and GURNEY J.J. 1989. Kimberlite carbonates - a carbon and oxygen stable isotope study. In: Kimberlites and related rocks, Vol. 1 Their composition, occurrence origin and emplacement pp. 264-281, Geological Society of Australia Special Publication No. 14, Blackwell.

KRAMERS J.D. 1977. Lead and strontium isotopes in Cretaceous kimberlites and mantle-derived xenoliths from southern Africa. Earth and Planetary Science Letters 34, 419-431.

KRAMERS J.D. 1979. Lead, Uranium, Strontium, Potassium and Rubidium in inclusion-bearing diamonds and mantle-derived xenoliths from southern Africa. Earth and Planetary Science Letters 42, 58-70.

KRAMERS J.D. and SMITH C.B. 1983. A feasibility study of U- Pb and Pb-Pb dating of kimberlites using groundmass mineral fractions and whole rock samples. Isotope Geoscience 1, 23-35.

KRAMERS J.D., RODDICK, J.C.M., DAWSON, J.B. and Boyd, F.R. 1979. Pb, Sr and Nd studies of xenoliths of the MARID suite and deep-seated clinopyroxene megacrysts, and their implications. (abstact) Kimberlite Symposium II, Cambridge.

KRAMERS J.D., SMITH C.B., LOCK N.P., HARMON R.S. and BOYD F.R. 1981. Can kimberlites be generated from ordinary mantle? Nature 291, 53-56.

LINDSLEY D.H. and DIXON S.A. 1976. Diopside-enstatite equilibria at 850 oC to 1400 oC, 5 to 35 kbars. American Journal of Science 276, 1285-1301.

McKAY D.B. and MITCHELL R.H. 1988. Abundance and distribution of gallium in some spinel and garnet lherzolites. Geochimica et Cosmochimica Acta 52, 2867-2870.

McCALLISTER R.H. and NORD G.L.(Jnr) 1981. Subcalcic diopsides from kimberlites: Chemistry, exsolution microstructures and thermal history. Contributions to Mineralogy and Petrology 78, 118-125.

McGREGOR I.D. 1974. The system MgO-Al2O3-SiO2: Solubility of Al2O3 in enstatite for spinel and garnet peridotite compositions. Amerian Mineralogist 59, 110-119

MITCHELL R.H. 1973. Magnesian ilmenite and its role in kimberlite petrogenesis. Journal of Geology 81, 301-311.

MITCHELL R.H. 1986. Kimberlites: Mineralogy, Geochemistry, and Petrology. Plenum Press New York and London 442 pp.

MITCHELL R.H. 1987. Megacrysts in kimberlites from the Gibeon field, Nambibia. Neues Jahrbuch Miner. Abh. 157, 267-283.

MITCHELL R.H., BRUNFELT A.O. and NIXON P.H.. 1973a. Trace elements in magnesian ilmenites from Lesotho kimberlites. In: Nixon P.H. ed., Lesotho Kimberlites, pp 230-234. Lesotho National Development Corporation, Maseru.

MITCHELL R.H., CARSWELL D.A. and BRUNFELT A.O. 1973b. Mineralogy and rare earth geochemistry of an ilmenite-clinopyroxene xenolith from the Monastery Mine. In: Nixon P.H. ed., Lesotho Kimberlites, pp 224-229. Lesotho National Development Corporation, Maseru.

MOORE R.O. 1986. A study of the kimberlites, diamonds and associated rocks and minerals from the Monastery Mine, South Africa. Unpublished Ph.D., University of Cape Town.

NICKEL K.G. and GREEN D.H. 1985. Empirical geothermobarometry for garnet peridotites and implications for the nature of the lithosphere, kimberlites and diamonds. Earth and Planetary Science Letters 73, 158-170.

NIXON P.H. 1987. Kimberlitic xenoliths and their cratonic setting. In: Nixon P.H. ed., Mantle Xenoliths, pp 215-239. J.Wiley & Sons, New York.

NIXON P.H. and BOYD F.R. 1973. The discrete nodule association in kimberlites from northern Lesotho. In: Nixon P.H. ed., Lesotho Kimberlites, pp 67-76. Lesotho National Development Corporation, Maseru.

NOBLE S.R., LIGHTFOOT P.C. and SCHARER U. 1989. A new method for single-filament isotopic analysis of Nd using in situ reduction. Chemical Geology 79, 15-19.

NTANDA M., MEYER H.O.A. and MOREAY, J. 1982. Garnet and cpx megacrysts from Kasai (abstract). Terra Cognita 2, 223.

PASTERIS J.D. 1980. The significance of groundmass ilmenite and megacryst ilmenite in kimberlites. Contributions to Mineralogy and Petrology 75, 315-325.

PASTERIS J.D., BOYD F.R. and NIXON P.H. 1979. The ilmenite association at the Frank Smith mine, R.S.A. In: Boyd F.R. and Meyer H.O.A. eds., The Mantle Sample, pp 256-278. American Geophysical Union, Washington.

PEARCE J.A. and NORRY M.J. 1979. Petrogenetic implications of Ti, Zr, Y and Nb variations in volcanic rocks. Contributions to Mineralogy and Petrology 69, 33-47.

RAWLINSON P.J. and DAWSON J.B. 1979. A quench pyroxene-ilmenite xenolith from kimberlite: Implications for pyroxene-ilmenite intergrowths. In: Boyd F.R. and Meyer H.O.A. eds., The Mantle Sample, pp 292-299. American Geophysical Union, Washington.

RICHARD P., SHIMIZU N. and ALLEGRE C.J. 1976. $^{143}Nd/^{146}Nd$, a natural tracer: an application to oceanic basalts. Earth and Planetary Science Letters 31, 269-278.

RICHARDSON S.H., ERLANK A.J. and HART S.R. 1985. Kimberlite-borne garnet peridotite xenoliths from old enriched subcontinental lithosphere. Earth and Planetary Science Letters 75, 116-128.

ROBEY J.vA. 1981. Kimberlites of the Central Cape Province, R.S.A. Unpublished Ph.D., University of Cape Town.

SCHULZE D.J. 1982a. Megacrysts from the Hamilton Branch kimberlite, Kentucky: discrete nodules and cumulate rocks. Terra Cognita 2, 254-256.

SCHULZE D.J. 1982b. The petrology of ultramafic xenoliths from the Hamilton Branch kimberlite pipe, Elliot Country, Kentucky. Unpublished Ph.D. University of Texas.

SCHULZE D.J. 1984. Cr-poor megacrysts from the Hamilton Branch kimberlite, Elliott County, Kentucky. In: Kornprobst J. ed., Kimberlites IIB: The mantle and crust-mantle relationships, pp 97-108. Elsevier Science Publishers.

SCHULZE D.J. 1985. Evidence for primary kimberlitic liquids in megacrysts from kimberlites in Kentucky, U.S.A. Journal of Geology 93, 75-79.

SCHULZE D.J. 1987. Megacrysts from alkalic volcanic rocks. In: Nixon P.H. ed., Mantle Xenoliths, pp 433-451. J.Wiley & Sons, New York.

SHEE S.R. 1978. The mineral chemistry of xenoliths from the Orapa kimberlite pipe, Botswana. Unpublished M.Sc., University of Cape Town.

SHEE S.R. and GURNEY J.J. 1979. The mineralogy of xenoliths from Orapa, Botswana. In: Boyd F.R. and Meyer H.O.A. eds., The Mantle Sample, pp 37-49. American Geophysical Union, Washington.

SHIMIZU N. 1974. Rare earth elements (REE) in garnets and clinopyroxenes from garnet lherzolite nodules in kimberlite. Carnegie Institution of Washington Yearbook 73, 954-961.

SHIMIZU N. 1975. Rare earth elements in garnets and clinopyroxenes from garnet lherzolite nodules in kimberlites. Earth and Planetary Science Letters 25, 26-32.

SHIMIZU N. and ALLEGRE C.J. 1978. Geochemistry of transition elements in garnet lherzolite xenoliths in kimberlites. Contributions to Mineralogy and Petrology 67, 41-50.

SMITH C.B. 1977. Kimberlite and mantle derived xenoliths at Iron Mountain, Wyoming. Unpublished M.Sc, Colorado State University.

SMITH C.B. 1983a. Pb, Sr and Nd isotopic evidence for sources of southern African Cretaceous kimberlites. Nature 304, 51-54.

SMITH C.B. 1983b. Rubidium-strontium, uranium-lead and samarium-neodymium isotopic studies of kimberlite and selected mantle-derived xenoliths. Unpublished Ph.D., University of the Witwatersrand.

SMITH C.B., McCALLUM M.E. and HEDGE C.E. 1982. Rb/Sr isotopic ratios in selected lower crust-upper mantle nodules from Colorado-Wyoming kimberlites. United States Geological Survey Open File Report 82-178, 22p.

SOBOLEV N.V., LAURENT'EV YU G., POKHILENKO N.P. and USOVA L.V. 1973. Chrome-rich garnets from the kimberlites of Yakutia and their parageneses. Contributions to Mineralogy and Petrology 40, 39-52.

SPRIGGS A.J. 1988. An isotopic and geochemical study of kimberlites and associated alkaline rocks from Nambibia. Unpublished Ph.D. University of Leeds.

TOLLO P.T. 1982. Petrography and mineral chemistry of ultramafic and related inclusions from the Orapa A/K-1 kimberlite pipe, Botswana. Unpublished M.Sc. University of Massachusetts.

UNDERWOOD D.T. 1987. Geochemistry and petrology of the Premier satellite kimberlite pipes. Unpublished B.Sc.(Hons) report. University of the Witwatersrand.

VILJOEN E.A. 1981. The kimberlite occurrences from the vicinity of Rayton, south of Premier Mine, and from East Lynne, east of Pretoria. Unpublished M.Sc. University of Pretoria.

WAGNER P.A. 1911. Petrological notes on the kimberlite occurrences in the Pretoria district. Transactions of the Geological Society of South Africa 14, 43-63.

WALKER R.J., CARLSON R.W., SHIRLEY S.B. and BOYD F.R. 1989. Os, Sr, Nd, and Pb isotope systematics of southern African peridotite xenoliths: Implications for the chemical evolution of subcontinental mantle. Geochimica et Cosmochimica Acta 53, 1583-1595.

WHITE W.M. and HOFMANN A.W. 1982. Sr and Nd isotope geochemistry of oceanic basalts and mantle evolution. Nature 296, 821-825.

WINTERBURN P.A. 1989. Isotopic studies of the peridotite xenoliths and megacrysts from the Premier kimberlite pipe, S. Africa. CSIR Internal Report: EMA-I 8928, Pretoria, South Africa. pp19.

WEDEPOHL K.H. 1969. Handbook of Geochemistry. Springer-Verlag.

LIST OF FIGURES

1 Locality map for the Premier cluster kimberlites.

3.1.1 Plot of Ca# vs Mg# for clinopyroxene megacrysts from Schuller.

3.1.2 Plot of Ca# vs Cr_2O_3 for clinopyroxene megacrysts from Schuller.

3.1.3 Plot of Ca# vs TiO_2 for clinopyroxene megacrysts from Schuller.

3.1.4 Plot of Ca# vs Na_2O for clinopyroxene megacrysts from Schuller.

3.1.5 Plot of Ca# vs Mg# for clinopyroxene megacrysts from Premier.

3.1.6 Plot of Ca# vs Cr_2O_3 for clinopyroxene megacrysts from Premier.

3.1.7 Plot of Ca# vs TiO_2 for clinopyroxene megacrysts from Premier.

3.1.8 Plot of Ca# vs Na_2O for clinopyroxene megacrysts from Premier.

3.1.9 Plot of Ca# vs Mg# for clinopyroxene megacrysts and coarse lherzolite clinopyroxenes from Schuller.

3.1.10 Plot of Ca# vs Cr_2O_3 for clinopyroxene megacrysts and coarse lherzolite clinopyroxenes from Schuller.

3.1.11 Plot of Ca# vs TiO_2 for clinopyroxene megacrysts and coarse lherzolite clinopyroxenes from Schuller.

3.1.12 Plot of Ca# vs Na_2O for clinopyroxene megacrysts and coarse lherzolite clinopyroxenes from Schuller.

3.1.13 Plot of Ca# vs Mg# for clinopyroxene megacrysts and coarse and sheared lherzolite clinopyroxenes from Premier.

3.1.14 Plot of Ca# vs Cr_2O_3 for clinopyroxene megacrysts and coarse and sheared lherzolite clinopyroxenes from Premier.

3.1.15 Plot of Ca# vs TiO_2 for clinopyroxene megacrysts and coarse and sheared lherzolite clinopyroxenes from Premier.

3.1.16 Plot of Ca# vs Na_2O for clinopyroxene megacrysts and coarse and sheared lherzolite clinopyroxenes from Premier.

3.1.17 Plots of Ca# vs Mg (a) and Cr_2O_3 (b) in clinopyroxene megacrysts from Monastery.

3.1.18 Plots of Ca# vs Mg (a) and Cr_2O_3 (b) in clinopyroxene megacrysts from Northern Lesotho.

3.1.19 Plots of Ca# vs Mg (a) and Cr_2O_3 (b) in clinopyroxene megacrysts from Jagersfontein.

3.1.20 Plots of Ca# vs Mg (a) and Cr_2O_3 (b) in clinopyroxene megacrysts from Lekkerfontein.

3.1.21 Plots of Ca# vs Mg (a) and Cr_2O_3 (b) in clinopyroxene megacrysts from Orapa.

3.1.22 Plots of Ca# vs Mg (a) and Cr_2O_3 (b) in clinopyroxene megacrysts from Iron Mountain.

3.1.23 Plots of Ca# vs Mg (a) and Cr_2O_3 (b) in clinopyroxene megacrysts from Sloan-Nix.

3.1.24 Plots of Ca# vs Mg (a) and Cr_2O_3 (b) in clinopyroxene megacrysts from Mukorob.

3.1.25 Plots of Ca# vs Mg (a) and Cr_2O_3 (b) in clinopyroxene megacrysts from Eastern Griqualand.

3.1.26 Plots of Ca# vs Mg (a) and Cr_2O_3 (b) in clinopyroxene megacrysts from Hamilton Branch.

3.1.27 Plots of Ca# vs Mg (a) and Cr_2O_3 (b) in clinopyroxene megacrysts from Kimberley.

3.1.28 Plots of Ca# vs Mg (a) and Cr_2O_3 (b) in clinopyroxene megacrysts from Camutue.

3.1.29 Plots of Ca# vs Mg (a) and Cr_2O_3 (b) in clinopyroxene megacrysts from Witberg.

3.2.1 Plot of Mg# vs CaO for orthopyroxene megacrysts from Schuller.

3.2.2 Plot of Mg# vs Al_2O_3 for orthopyroxene megacrysts from Schuller.

3.2.3 Plot of Mg# vs Cr_2O_3 for orthopyroxene megacrysts from Schuller.

3.2.4 Plot of Ca# vs Ti2O for orthopyroxene megacrysts from Schuller.

3.2.5 Plot of Mg# vs CaO for orthopyroxene megacrysts, coarse and sheared lherzolite orthopyroxenes from Premier and coarse lherzolite orthopyroxenes from Schuller.

3.2.6 Plot of Mg# vs Al_2O_3 for orthopyroxene megacrysts, coarse and sheared lherzolite orthopyroxenes from Premier and coarse lherzolite orthopyroxenes from Schuller.

3.2.7 Plot of Mg# vs Cr_2O_3 for orthopyroxene megacrysts, coarse and sheared lherzolite orthopyroxenes from Premier and coarse lherzolite orthopyroxenes from Schuller.

3.2.8 Plot of Mg# vs Cr_2O_3 for orthopyroxene megacrysts, coarse and sheared lherzolite orthopyroxenes from Premier and coarse lherzolite orthopyroxenes from Schuller.

3.2.9 Plots of Mg# vs CaO (a) and Cr_2O_3 (b) in orthopyroxene megacrysts from Monastery.

3.2.10 Plots of Mg# vs CaO (a) and Cr_2O_3 (b) in orthopyroxene megacrysts from Letseng-la-terae.

3.2.11 Plots of Mg# vs CaO (a) and Cr_2O_3 (b) in orthopyroxene megacrysts from Jagersfontein.

3.2.12 Plots of Mg# vs CaO (a) and Cr_2O_3 (b) in orthopyroxene megacrysts from Eastern Griqualand.

3.2.13 Plots of Mg# vs CaO (a) and Cr_2O_3 (b) in orthopyroxene megacrysts from Hamilton Branch.

3.2.14 Plots of Mg# vs CaO (a) and Cr_2O_3 (b) in orthopyroxene megacrysts from Sloan-Nix.

3.3.1 Plot of Mg# vs CaO for garnet megacrysts from Schuller.

3.3.2 Plot of Mg# vs Cr_2O_3 for garnet megacrysts from Schuller.

3.3.3 Plot of Mg# vs TiO_2 for garnet megacrysts from Schuller.

3.1.4 Plot of Mg# vs Na_2O for garnet megacrysts from Schuller.

3.3.5 Plot of Mg# vs Cr_2O_3 for garnet megacrysts, coarse and sheared lherzolite garnets from Premier and coarse lherzolite garnets from Schuller.

3.3.6 Plot of Mg# vs TiO_2 in garnet megacrysts, coarse and sheared lherzolite garnets from Premier and coarse lherzolite garnets from Schuller.

3.3.7 Plots of Mg# vs Cr_2O_3 (a) and TiO_2 (b) in garnet megacrysts from Monastery.

3.3.8 Plots of Mg# vs Cr_2O_3 (a) and TiO_2 (b) in garnet megacrysts from Jagersfontein.

3.3.9 Plots of Mg# vs Cr_2O_3 (a) and TiO_2 (b) in garnet megacrysts from Lekkerfontein.

3.3.10 Plots of Mg# vs Cr_2O_3 (a) and TiO_2 (b) in garnet megacrysts from Orapa.

3.3.11 Plots of Mg# vs Cr_2O_3 (a) and TiO_2 (b) in garnet megacrysts from Iron Mountain.

3.3.12 Plots of Mg# vs Cr_2O_3 (a) and TiO_2 (b) in garnet megacrysts from Sloan-Nix.

3.3.13 Plots of Mg# vs Cr_2O_3 (a) and TiO_2 (b) in garnet megacrysts from Mukorob.

3.3.14 Plots of Mg# vs Cr_2O_3 (a) and TiO_2 (b) in garnet megacrysts from Eastern Griqualand.

3.3.15 Plots of Mg# vs Cr_2O_3 (a) and TiO_2 (b) in garnet megacrysts from Hamilton Branch.

3.3.16 Plots of Mg# vs Cr_2O_3 (a) and TiO_2 (b) in garnet megacrysts from Witberg.

3.5.1 Plot of MgO vs Cr_2O_3 in ilmenite megacrysts from Schuller.

3.5.2 Plot of Mg# vs Al in ilmenite megacrysts from Schuller.

3.5.3 Plot of Mg# vs Fe^{3+} in ilmenite megacrysts from Schuller.

4.1 Plot of Ca# vs Mg# in clinopyroxene megacrysts Schuller analysed in trace elements.

4.2 Plot of Ca# vs Cr_2O_3 in clinopyroxene megacrysts from Schuller analysed for trace elements.

4.3 Plot of Mg# vs CaO in orthopyroxene megacrysts from Schuller analysed for trace elements.

4.4 Plot of Mg# vs Cr_2O_3 in garnet megacrysts from Schuller analysed for trace elements.

4.5 Plot of Ca# vs Sr in clinopyroxene megacrysts from Schuller.

4.6 Plot of Mg# vs Sr in clinopyroxene megacrysts from Schuller.

4.7 Plot of Ca# vs Zr in clinopyroxene megacrysts from Schuller.

4.8 Plot of Mg# vs Zr in clinopyroxene megacrysts from Schuller.

4.9 Plot of Ca# vs Ga in clinopyroxene megacrysts from Schuller.

4.10 Plot of Ca# vs Ni in clinopyroxene megacrysts from Schuller.

4.11 Plot of Ca# vs Zn in clinopyroxene megacrysts from Schuller.

4.12 Plot of FeO vs Zn in clinopyroxene megacrysts from Schuller.

4.13 Plot of Mg# vs Ni in orthopyroxene megacrysts from Schuller.

4.14 Plot of Mg# vs Zn in orthopyroxene megacrysts from Schuller.

4.15 Plot of Mg# vs Y in garnet megacrysts from Schuller.

4.16 Plot of Mg# vs Y in garnet megacrysts from Schuller.

4.17 Plot of Mg# vs Ni in garnet megacrysts from Schuller.

4.18 Plot of Mg# vs Zn in garnet megacrysts from Schuller.

4.19 Plot of calculated Zr vs Sr in magma in equilibrium with the group 1 clinopyroxene megacrysts.

4.20 Plot of calculated Zr vs Ti in magma in equilibrium with the group 1 clinopyroxene megacrysts.

5.1 Plot of Ca# vs Mg# in clinopyroxene megacrysts from Schuller analysed for Sr and Nd isotopes.

5.2 Plot of Ca# vs Mg# in clinopyroxene megacrysts from Premier analysed for Sr and Nd isotopes.

5.3 Plot of Sm vs Nd in clinopyroxene megacrysts from Schuller and Premier.

5.4 Plot of the reciprocal of Nd vs $^{143}Nd/^{144}Nd$ in clinopyroxene megacrysts from Schuller and Premier.

5.5 Plot of the reciprocal of Sr vs $^{87}Sr/^{86}Sr$ in clinopyroxene megacrysts from Schuller and Premier.

5.6 Plot of epsilon Sr vs epsilon Nd in clinopyroxene megacrysts from Schuller and Premier.

5.7 Plot of epsilon Sr vs epsilon Nd in clinopyroxene megacrysts and high temperature lherzolite clinopyroxenes from Jagersfontein.

6.1 A pictorial description of the various sequences of phases crystallising at Schuller relative to calculated temperature.

Figure 1.1

Locality map for the Premier cluster of kimberlites.

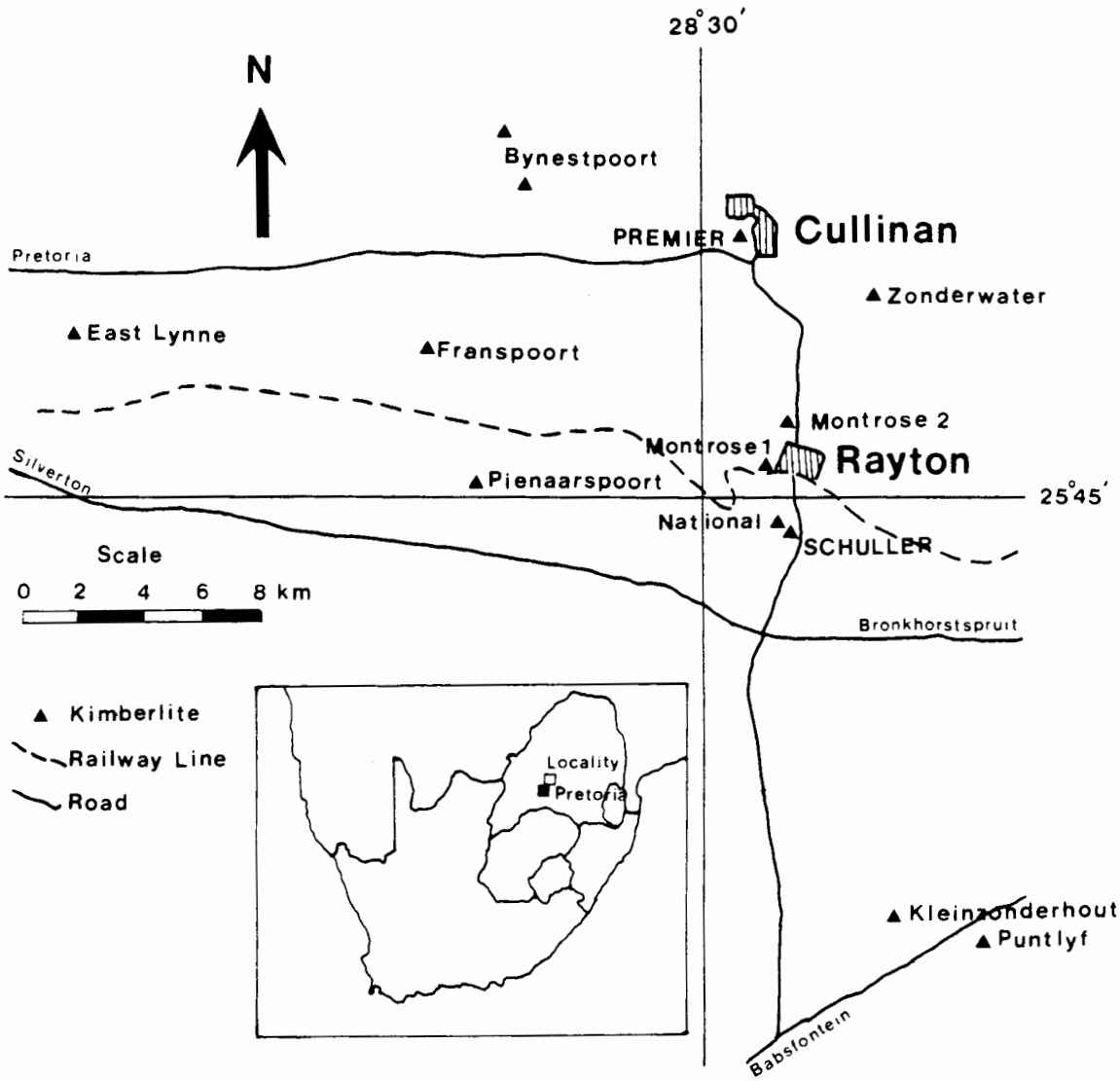

Figure 3.1.1

Ca# (atomic) versus Mg# (atomic) in clinopyroxene megacrysts from the Schuller kimberlite. The symbols 1, 2, 3, 4 refer to the compositional groups discussed in the text. I = association with ilmenite, O = association with orthopyroxene.

Figure 3.1.2

Ca# (atomic) versus Cr_2O_3 (wt%) in clinopyroxene megacrysts from the Schuller kimberlite. Symbols as in Figure 3.1.1.

Figure 3.1.1

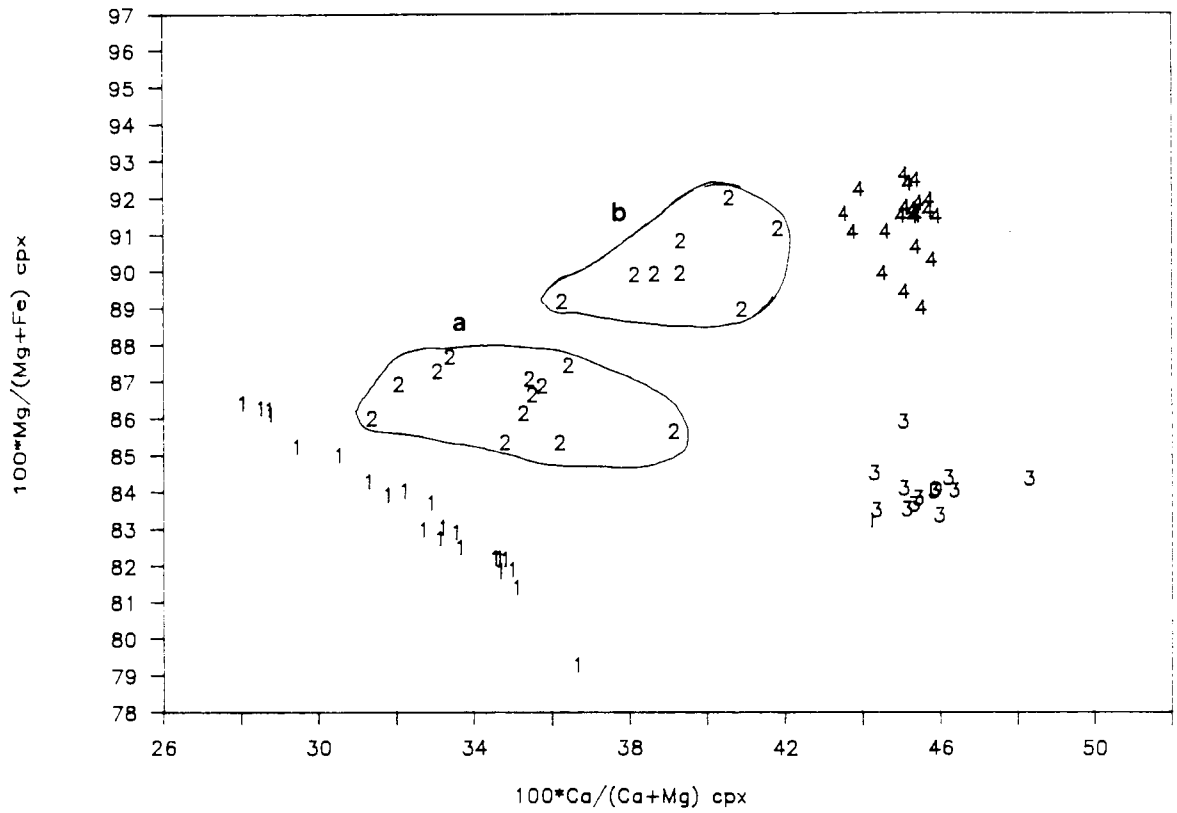

Figure 3.1.2

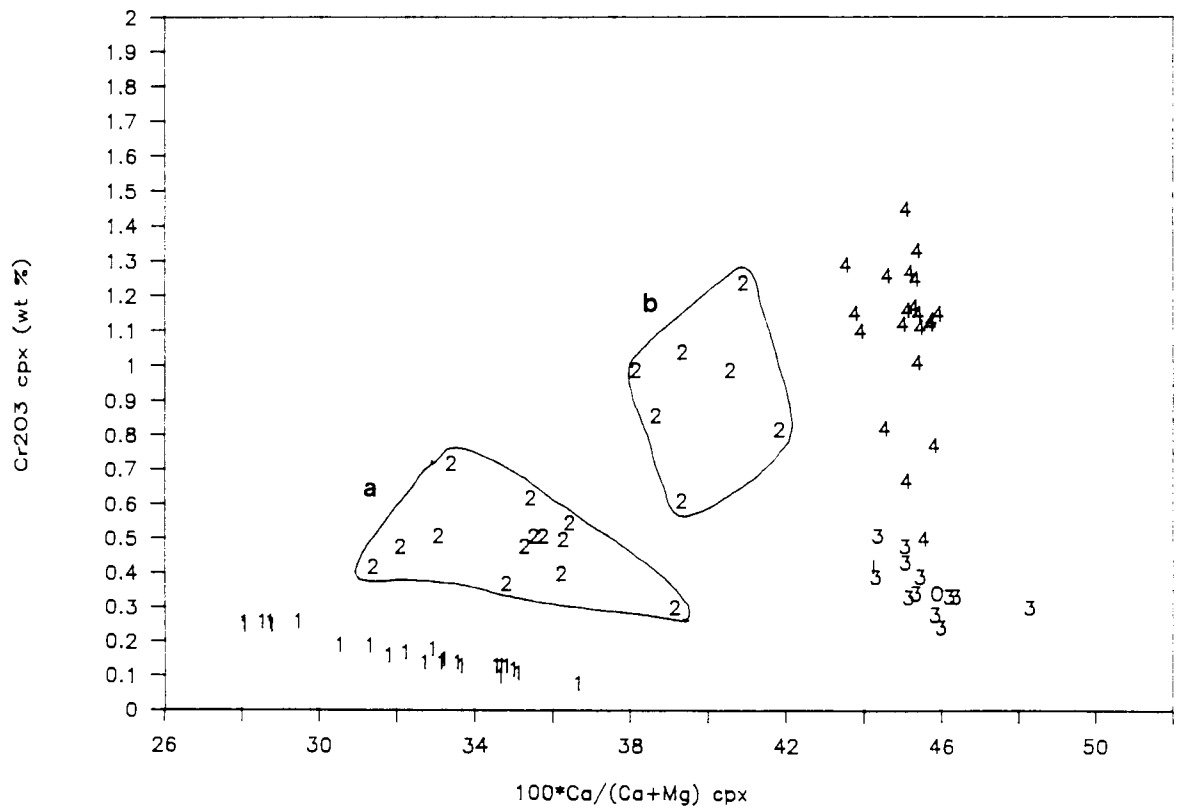

Figure 3.1.3

Ca# (atomic) versus TiO_2 (wt%) in clinopyroxene megacrysts from the Schuller kimberlite. Symbols as in Figure 3.1.1.

Figure 3.1.4

Ca# (atomic) versus Na_2O (wt%) in clinopyroxene megacrysts from the Schuller kimberlite. Symbols as in Figure 3.1.1.

Figure 3.1.3

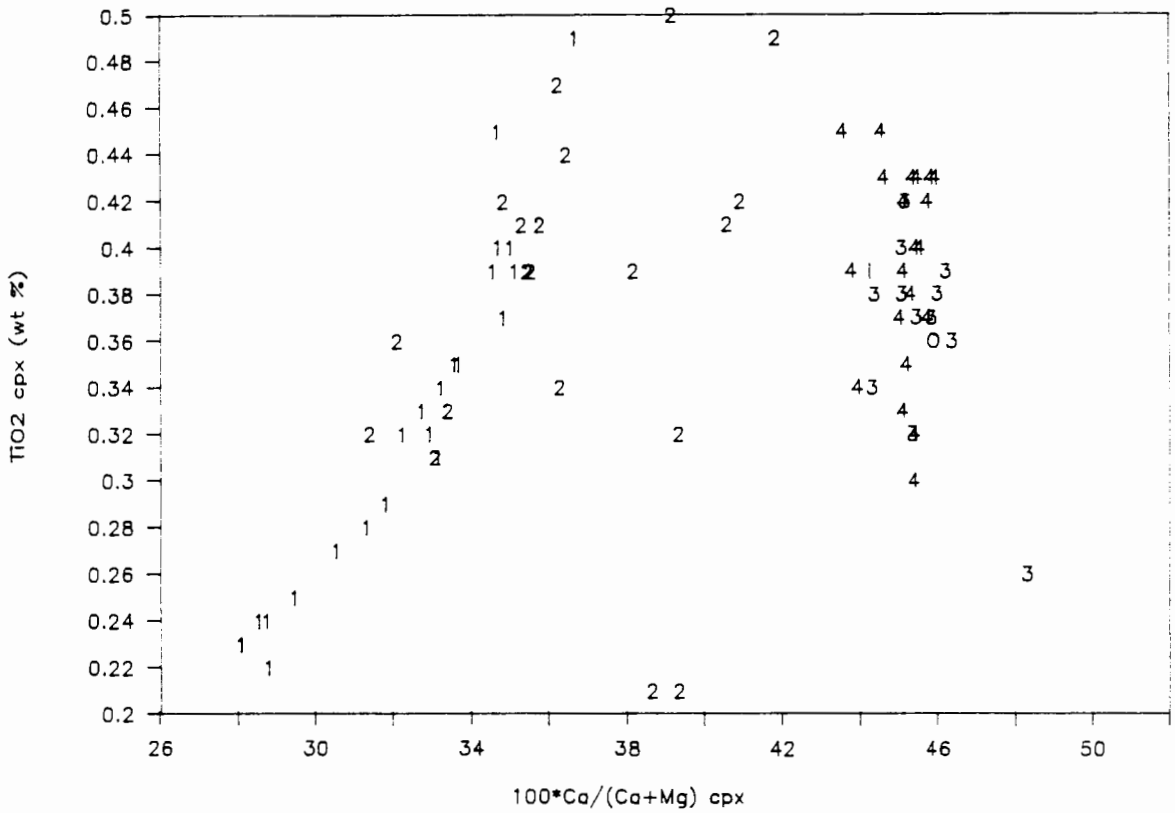

Figure 3.1.4

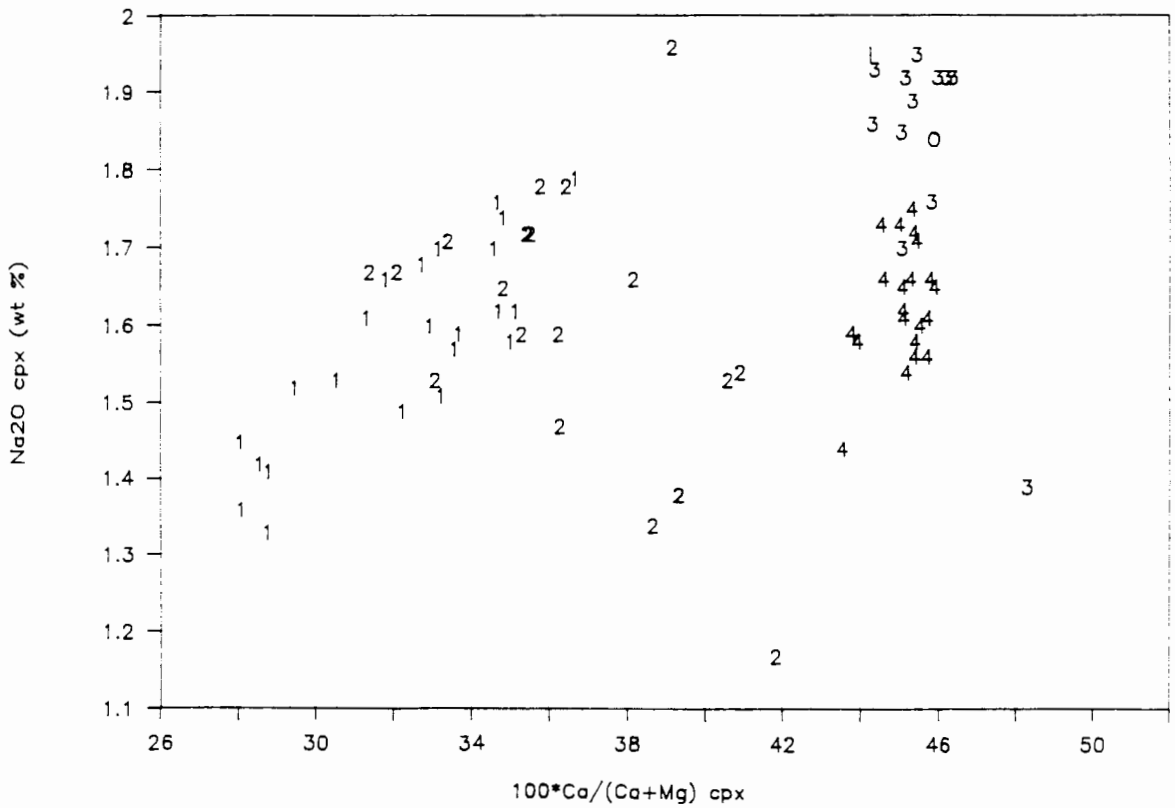

Figure 3.1.5

Ca# (atomic) versus Mg# (atomic) in clinopyroxene megacrysts from the Premier kimberlite. The symbols 1, 2, 2a, 4 refer to the compositional groups discussed in the text.

Figure 3.1.6

Ca# (atomic) versus Cr_2O_3 (wt%) in clinopyroxene megacrysts from the Premier kimberlite. Symbols as in Figure 3.1.5.

Figure 3.1.5

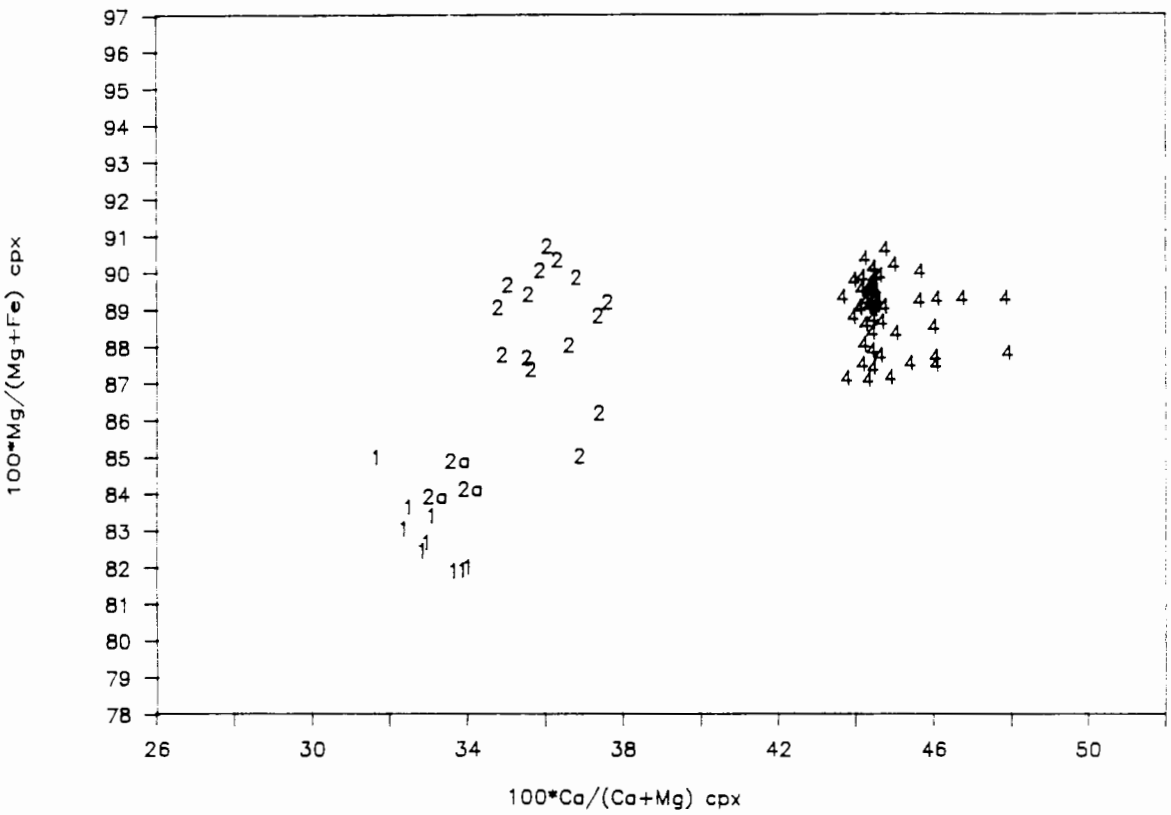

Figure 3.1.6

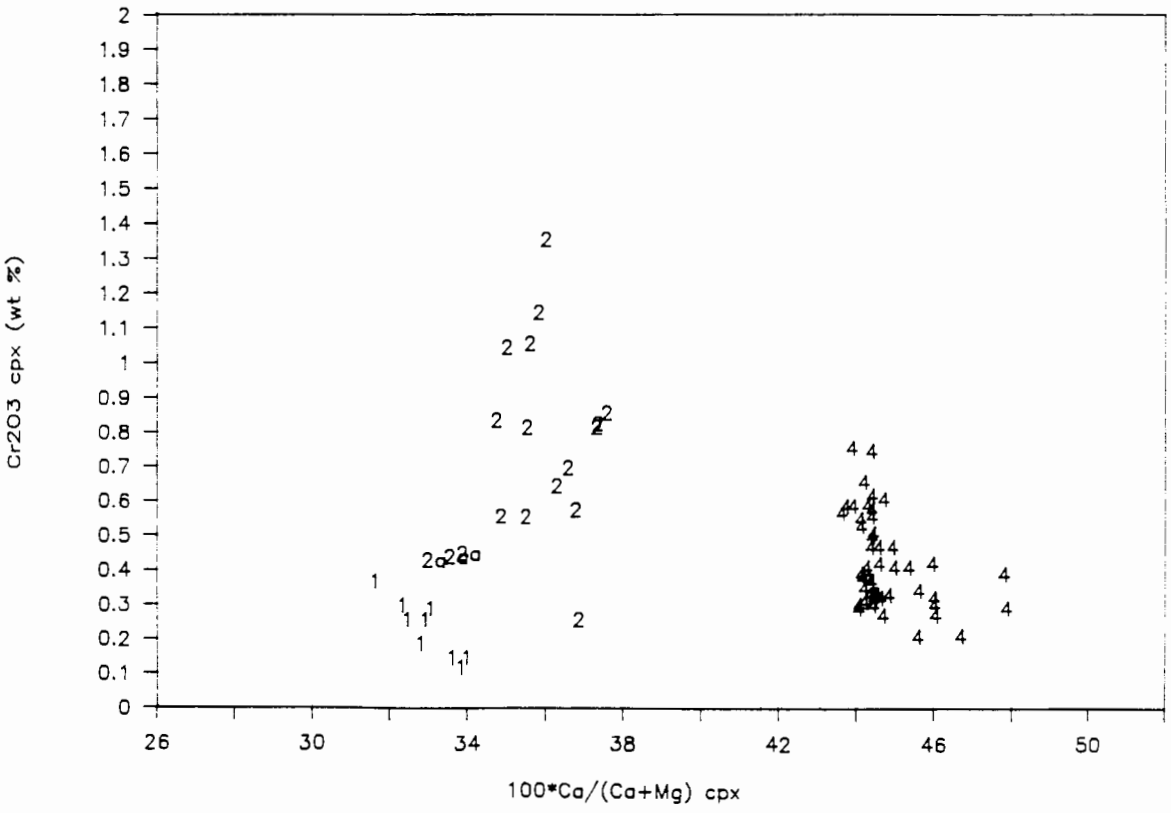

Figure 3.1.7

Ca# (atomic) versus TiO_2 (wt%) in clinopyroxene megacrysts from the Premier kimberlite. Symbols as in Figure 3.1.5.

Figure 3.1.8

Ca# (atomic) versus Na_2O (wt%) in clinopyroxene megacrysts from the Premier kimberlite. Symbols as in Figure 3.1.5.

Figure 3.1.7

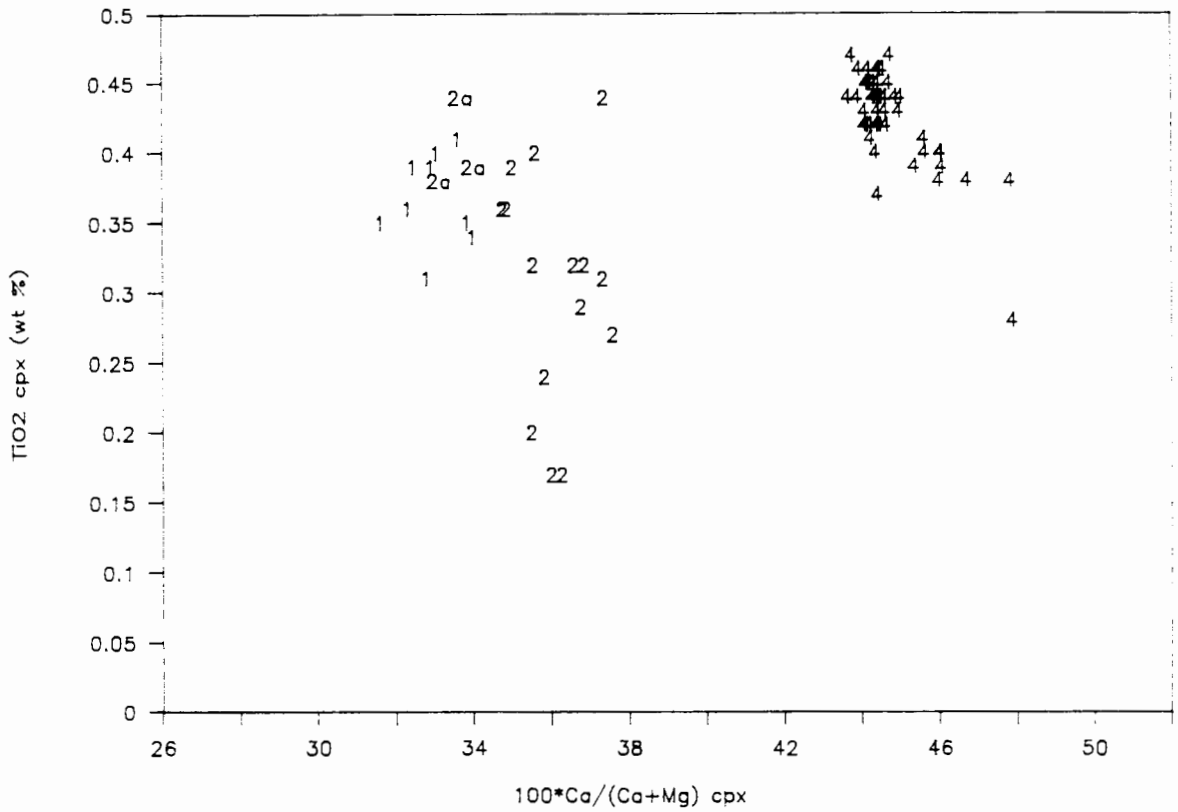

Figure 3.1.8

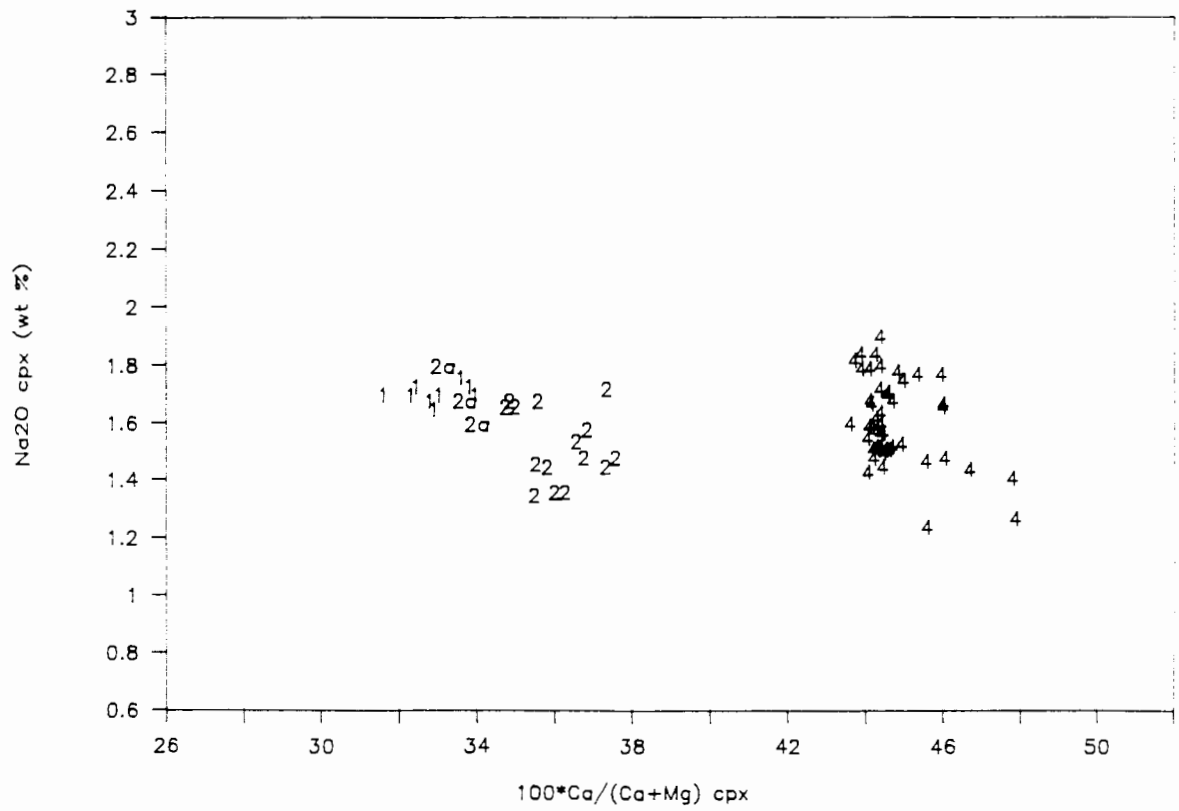

Figure 3.1.9

Ca# (atomic) versus Mg# (atomic) in clinopyroxene megacrysts (symbols as in Figure 3.1.1) and clinopyroxenes in coarse garnet lherzolites (outlined field) from the Schuller kimberlite (de Bruin, unpublished data).

Figure 3.1.10

Ca# (atomic) versus Cr_2O_3 (wt%) in clinopyroxene megacrysts (symbols as in Figure 3.1.1) and clinopyroxenes in coarse garnet lherzolites (outlined field) from the Schuller kimberlite (de Bruin, unpublished data).

Figure 3.1.9

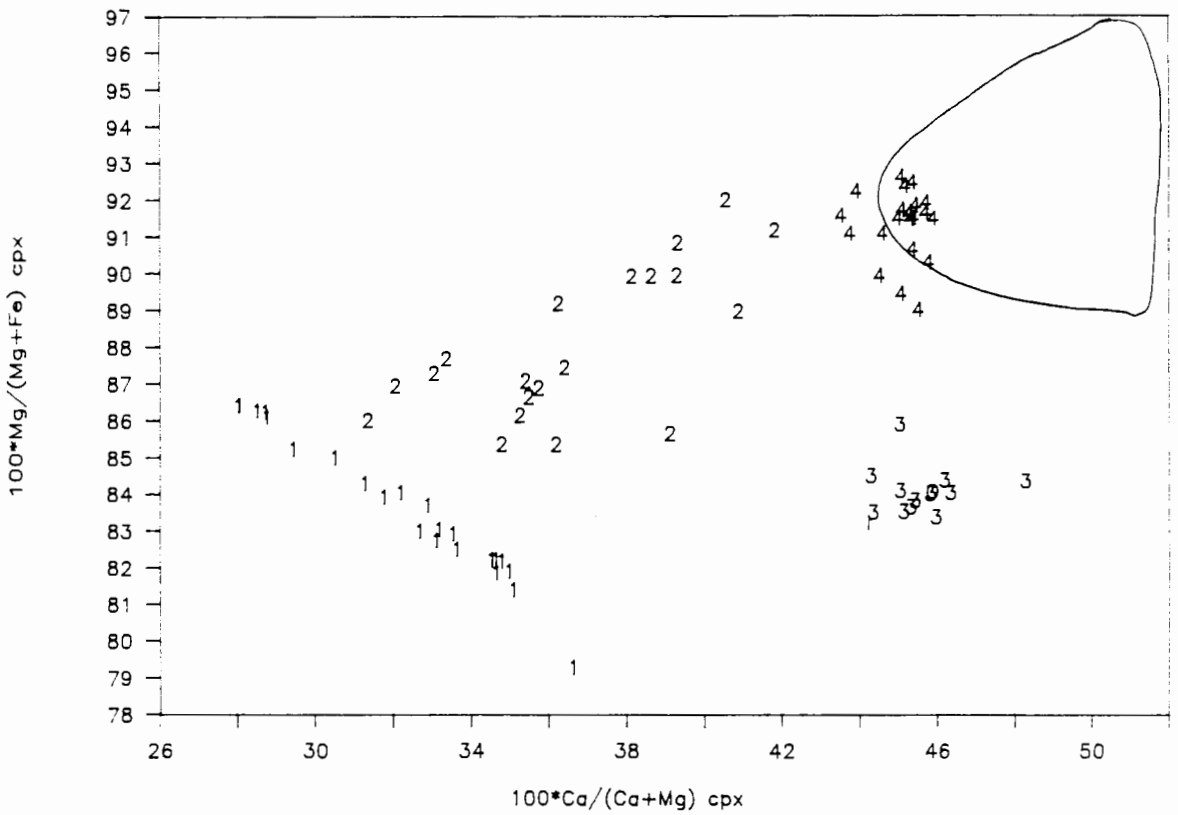

Figure 3.1.10

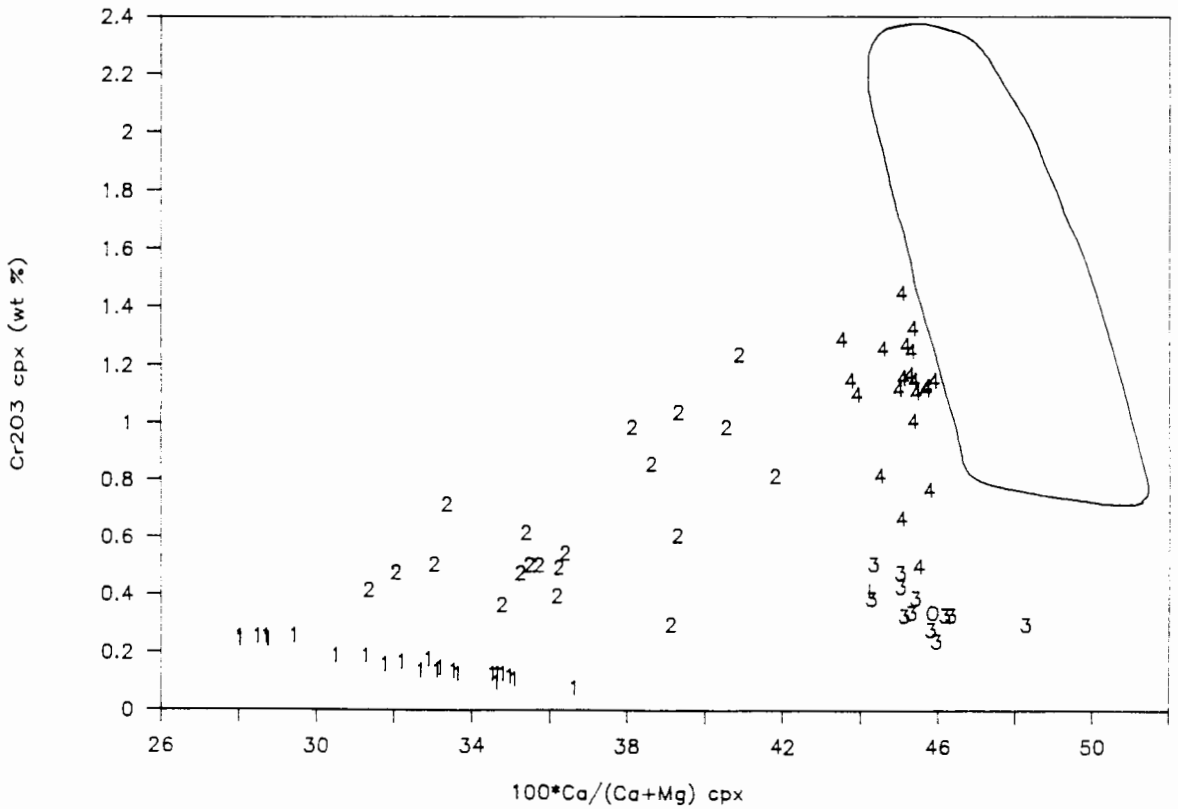

Figure 3.1.11

Ca# (atomic) versus TiO_2 (wt%) in clinopyroxene megacrysts (symbols as in Figure 3.1.1) and clinopyroxenes in coarse garnet lherzolites (outlined field) from the Schuller kimberlite (de Bruin, unpublished data).

Figure 3.1.12

Ca# (atomic) versus Na_2O (wt%) in clinopyroxene megacrysts (symbols as in Figure 3.1.1) and clinopyroxenes in coarse garnet lherzolites (outlined field) from the Schuller kimberlite (de Bruin, unpublished data).

Figure 3.1.11

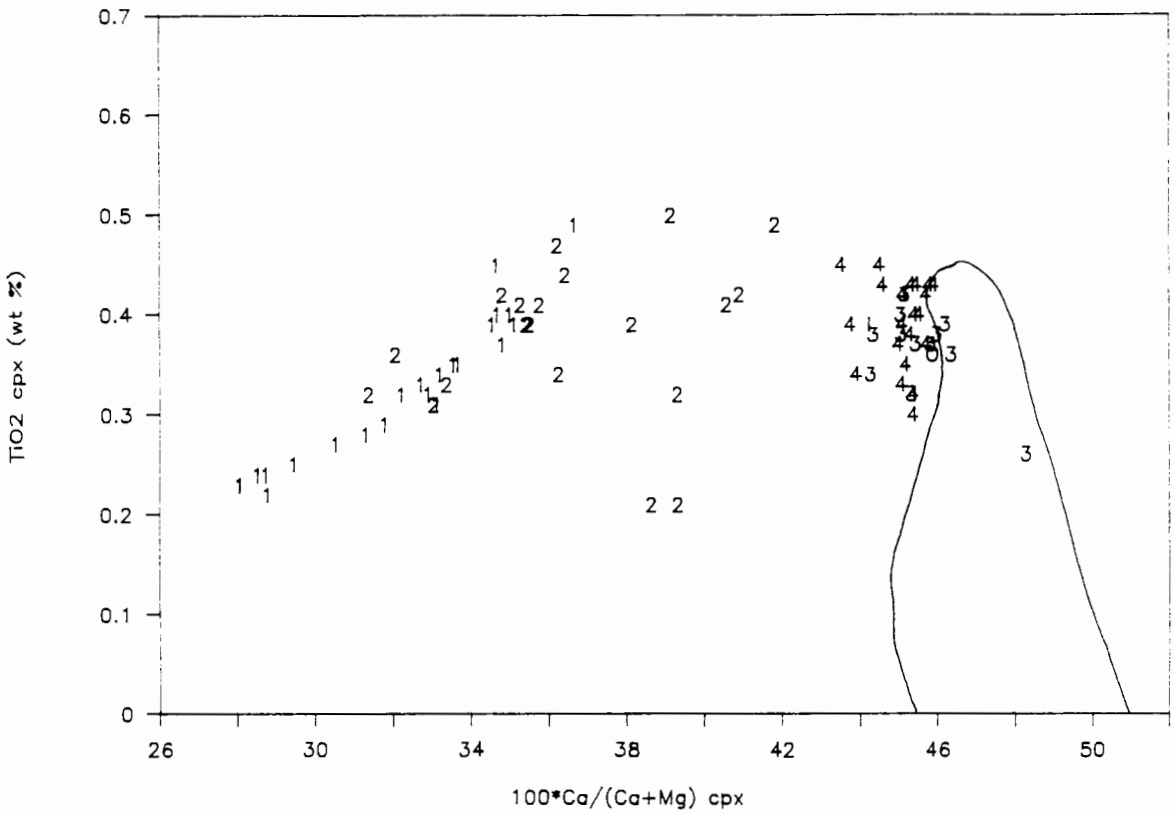

Figure 3.1.12

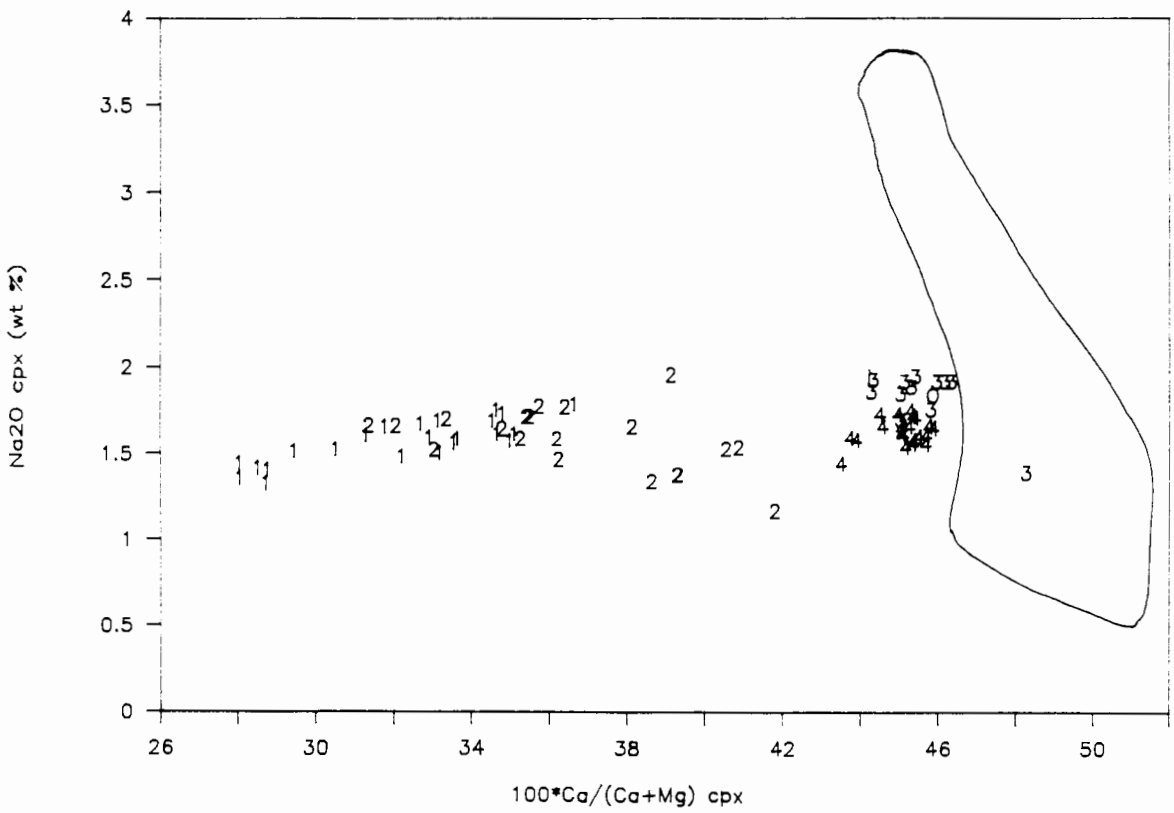

Figure 3.1.13

Ca# (atomic) versus Mg# (atomic) in clinopyroxene megacrysts (symbols as in Figure 3.1.5), clinopyroxenes in coarse garnet lherzolites (solid line) and deformed garnet lherzolites (broken line) from the Premier kimberlite (Boyd, unpublished data).

Figure 3.1.14

Ca# (atomic) versus Cr_2O_3 (wt%) in clinopyroxene megacrysts (symbols as in Figure 3.1.5), clinopyroxenes in coarse garnet lherzolites (solid line) and deformed garnet lherzolites (broken line) from the Premier kimberlite (Boyd, unpublished data).

Figure 3.1.13

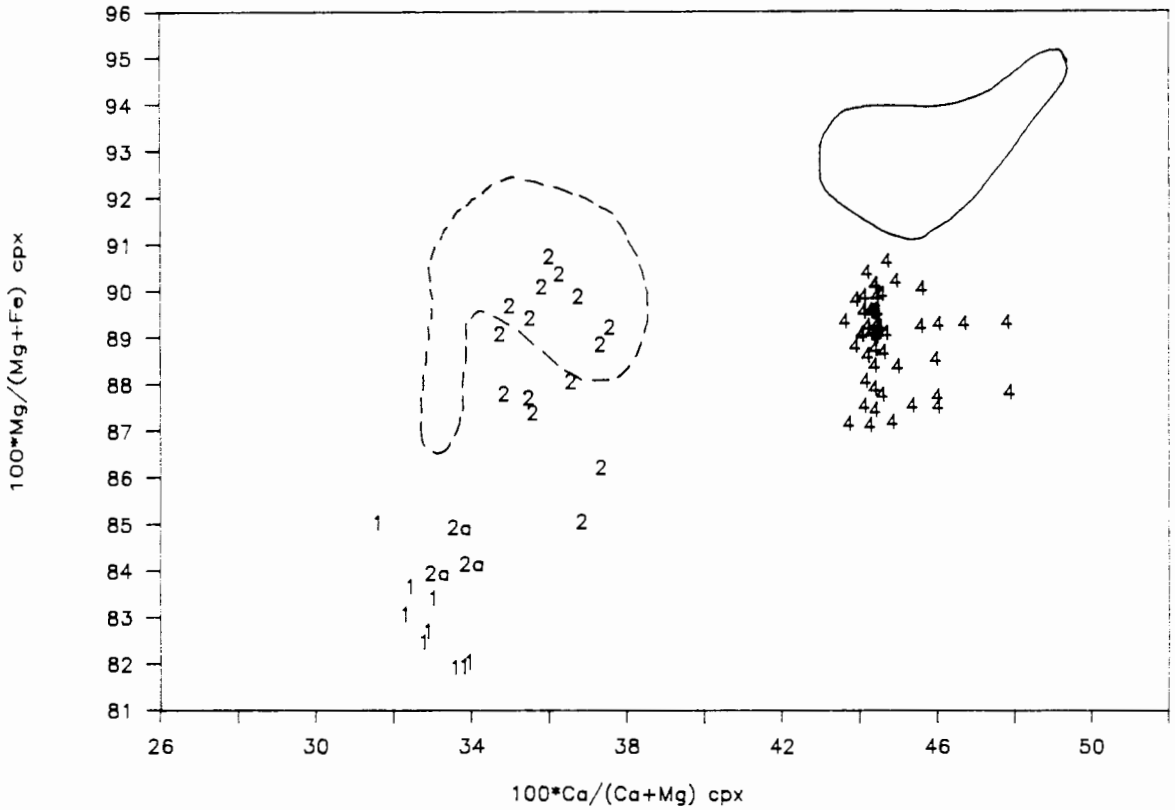

Figure 3.1.14

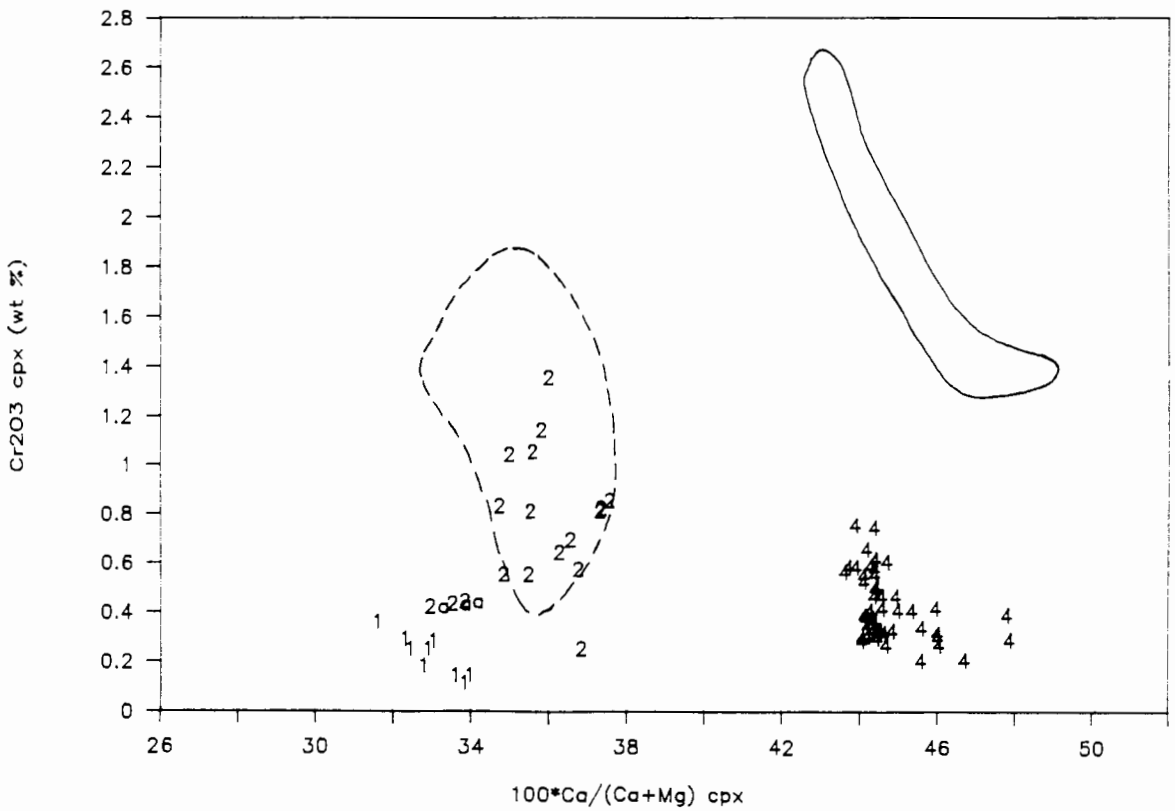

Figure 3.1.15

Ca# (atomic) versus TiO_2 (wt%) in clinopyroxene megacrysts (symbols as in Figure 3.1.5), clinopyroxenes in coarse garnet lherzolites (solid line) and deformed garnet lherzolites (broken line) from the Premier kimberlite (Boyd, unpublished data).

Figure 3.1.16

Ca# (atomic) versus Na_2O (wt%) in clinopyroxene megacrysts (symbols as in Figure 3.1.5), clinopyroxenes in coarse garnet lherzolites (solid line) and deformed garnet lherzolites (broken line) from the Premier kimberlite (Boyd, unpublished data).

Figure 3.1.15

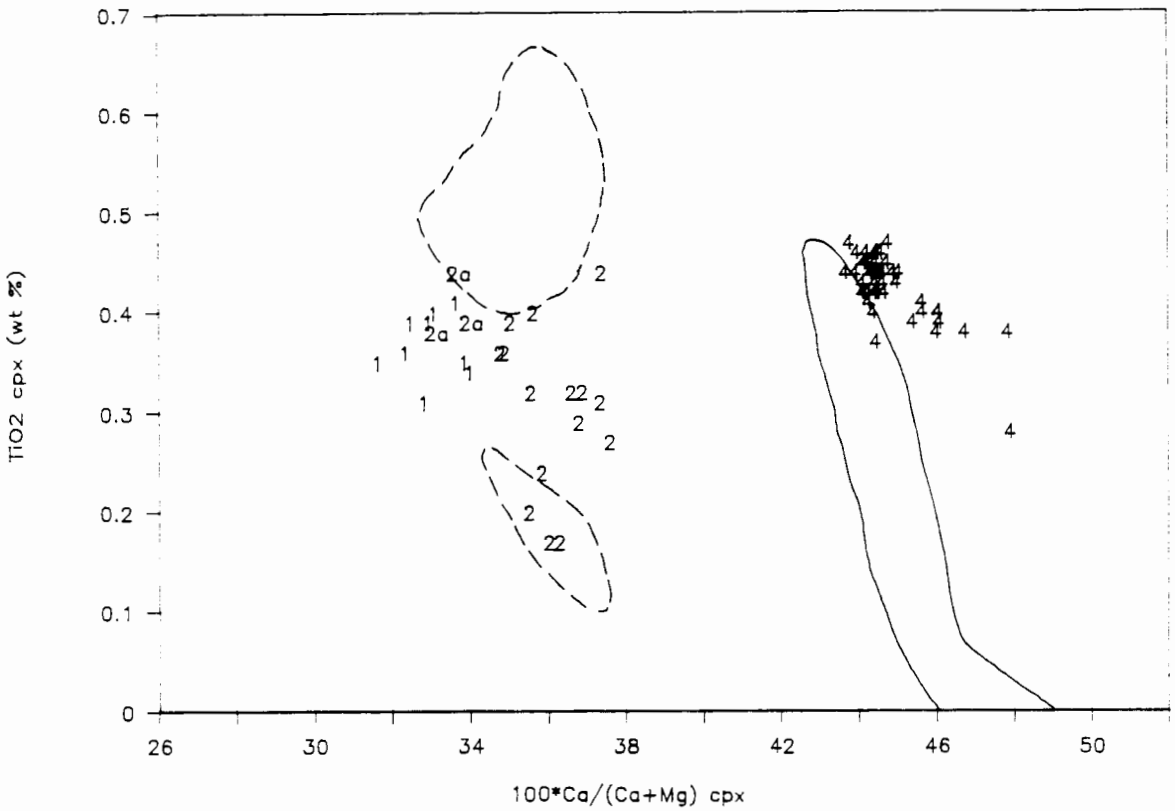

Figure 3.1.16

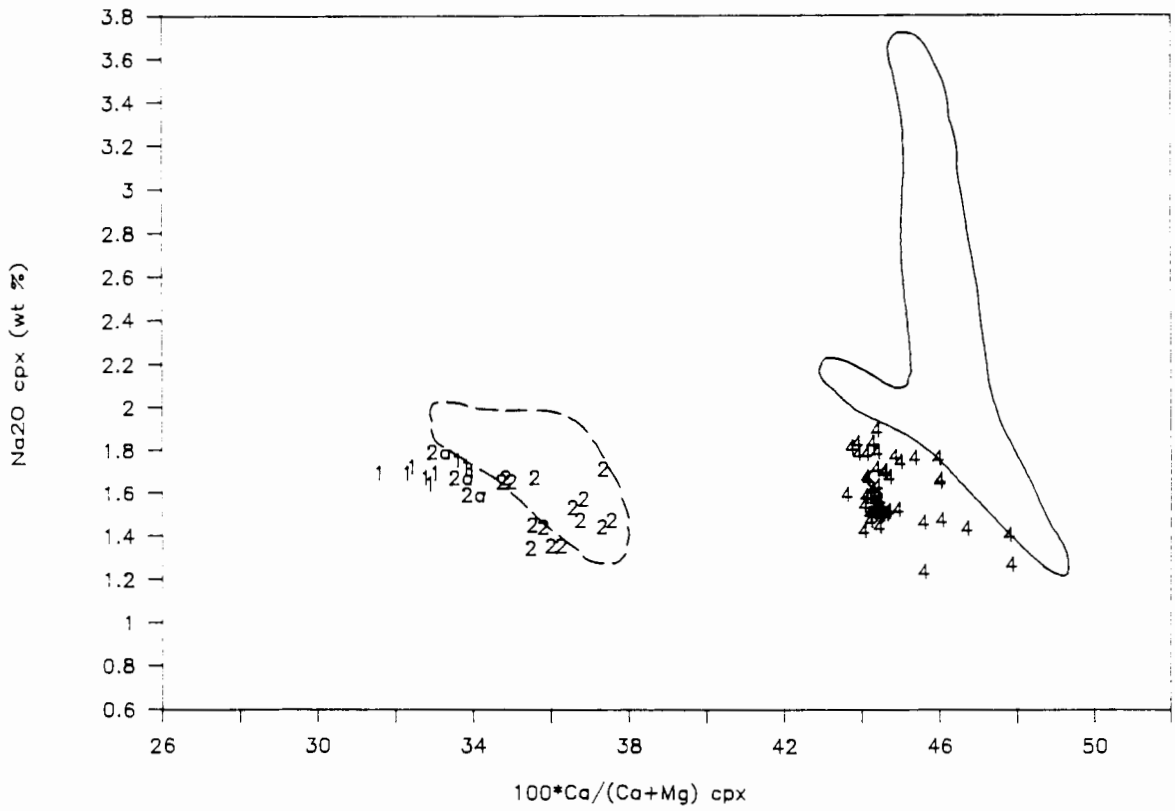

Figure 3.1.17 a and b

Ca# (atomic) versus Mg# (atomic) (a) and Cr_2O_3 (wt%) (b) in clinopyroxene megacrysts from Monastery (Jakob, 1977). M = discrete; m = ilmenite association. Lower case letters denotes either inclusions in megacrysts or megacrysts hosting inclusions.

Figure 3.1.17 (a)

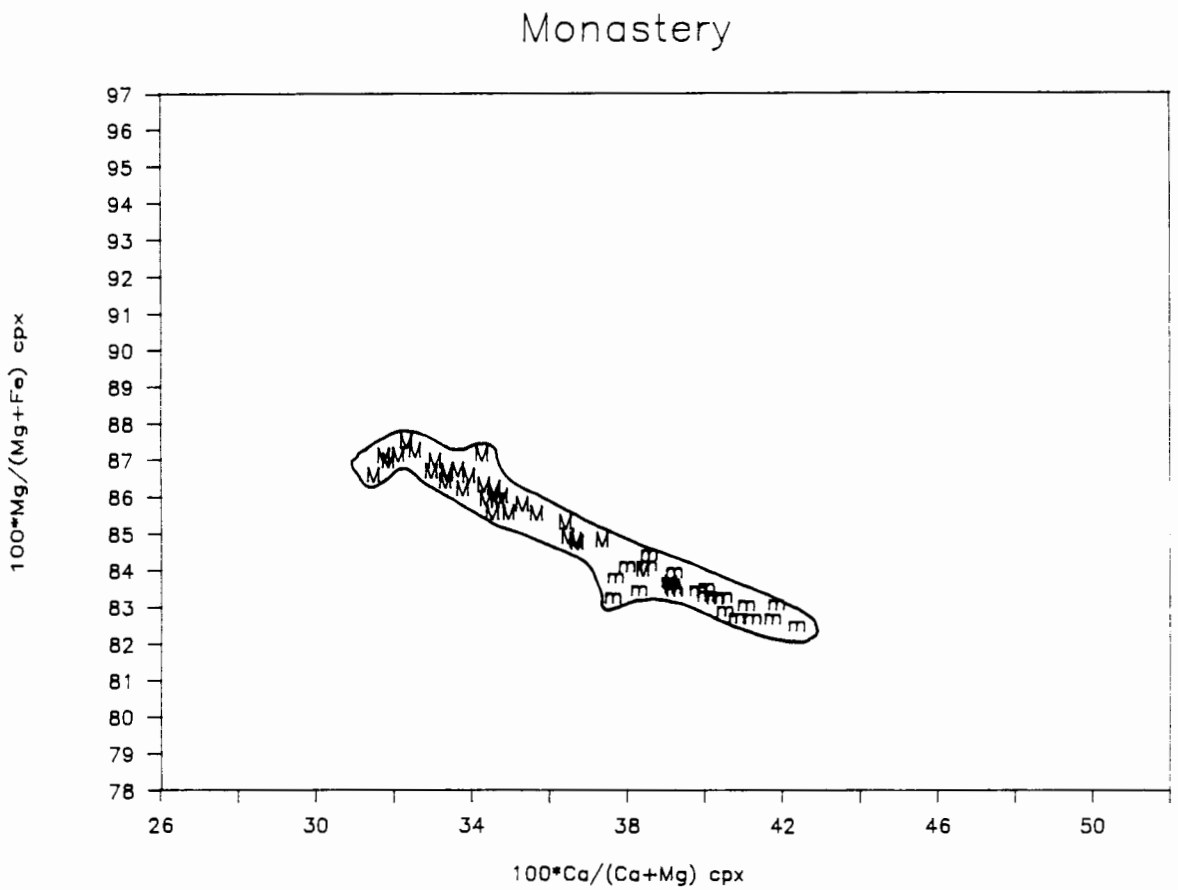

Figure 3.1.17 (b)

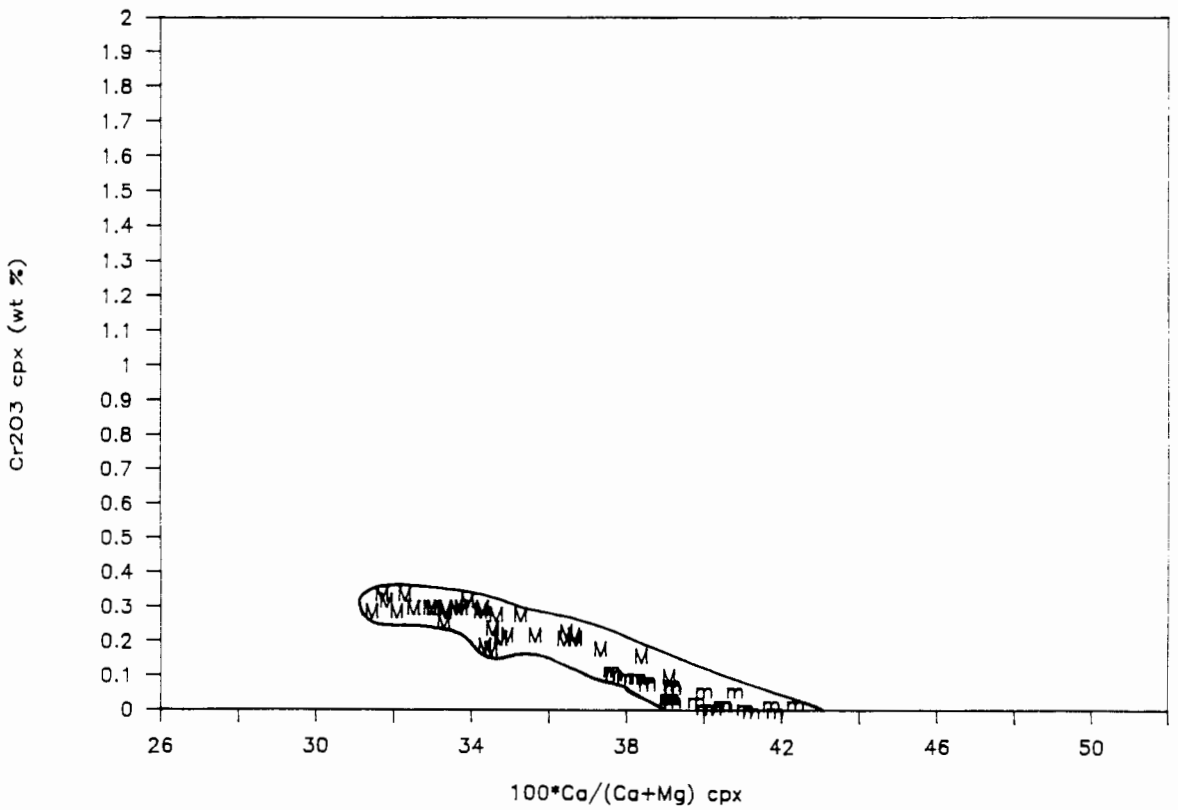

Figure 3.1.18 a and b

Ca# (atomic) versus Mg# (atomic) (a) and Cr_2O_3 (wt%) (b) in clinopyroxene megacrysts from the Northern Lesotho kimberlites (Nixon and Boyd, 1973; Bloomer and Nixon, 1973). L = Letseng-la-terae; S = Solane; T = Thaba Putsoa. The outlined field depicts the compositional range found at Monastery as shown in Figures 3.1.17 (a and b).

Figure 3.1.18 (a)

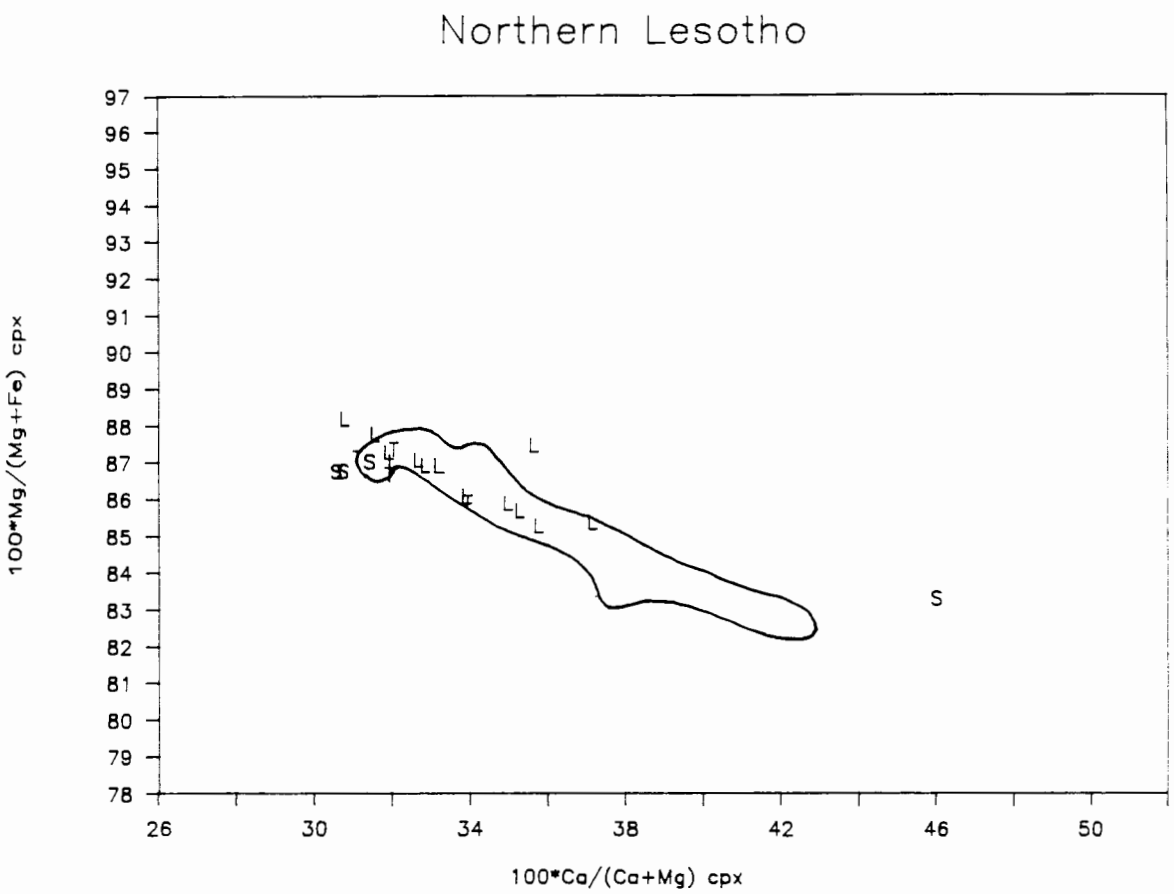

Figure 3.1.18 (b)

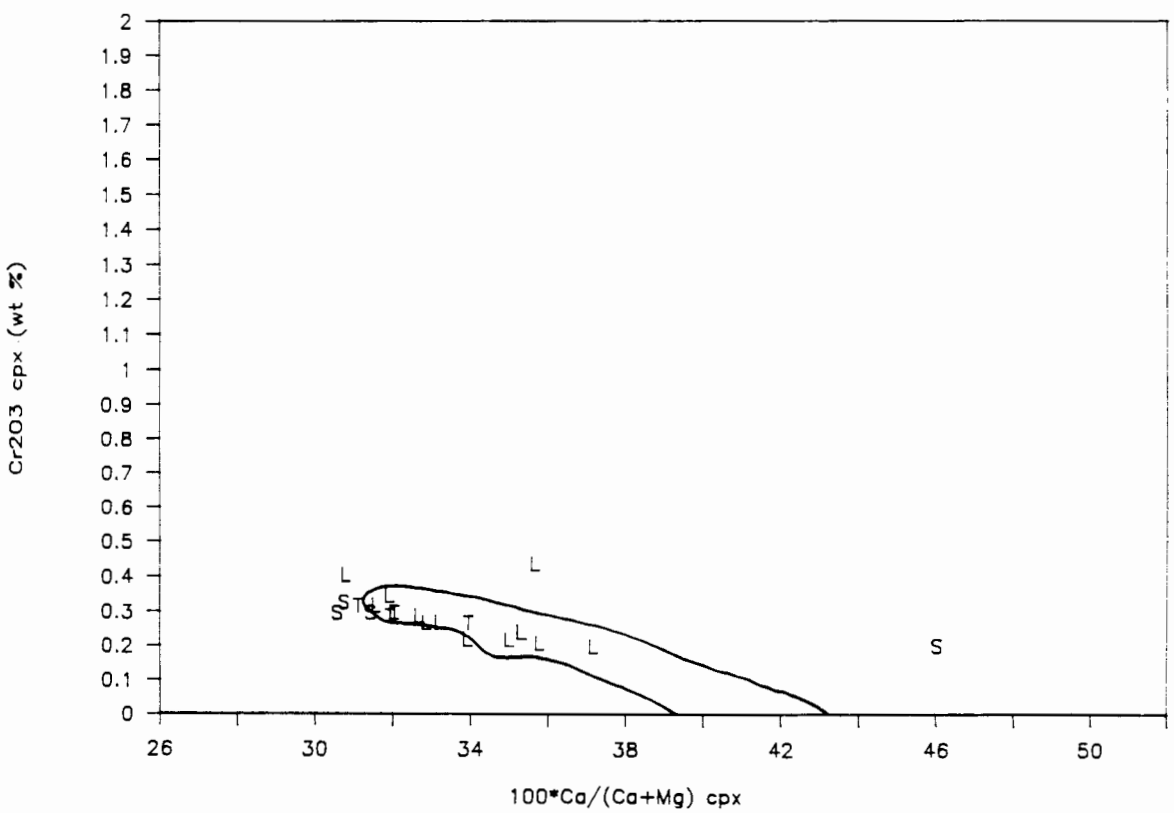

Figure 3.1.19 a and b

Ca# (atomic) versus Mg# (atomic) (a) and Cr_2O_3 (wt%) (b) in clinopyroxene megacrysts from Jagersfontein (Hops, 1989). J = discrete; j = Granny Smith. The outlined field depicts the compositional range found at Monastery as shown in Figures 3.1.17 (a and b).

Figure 3.1.19 (a)

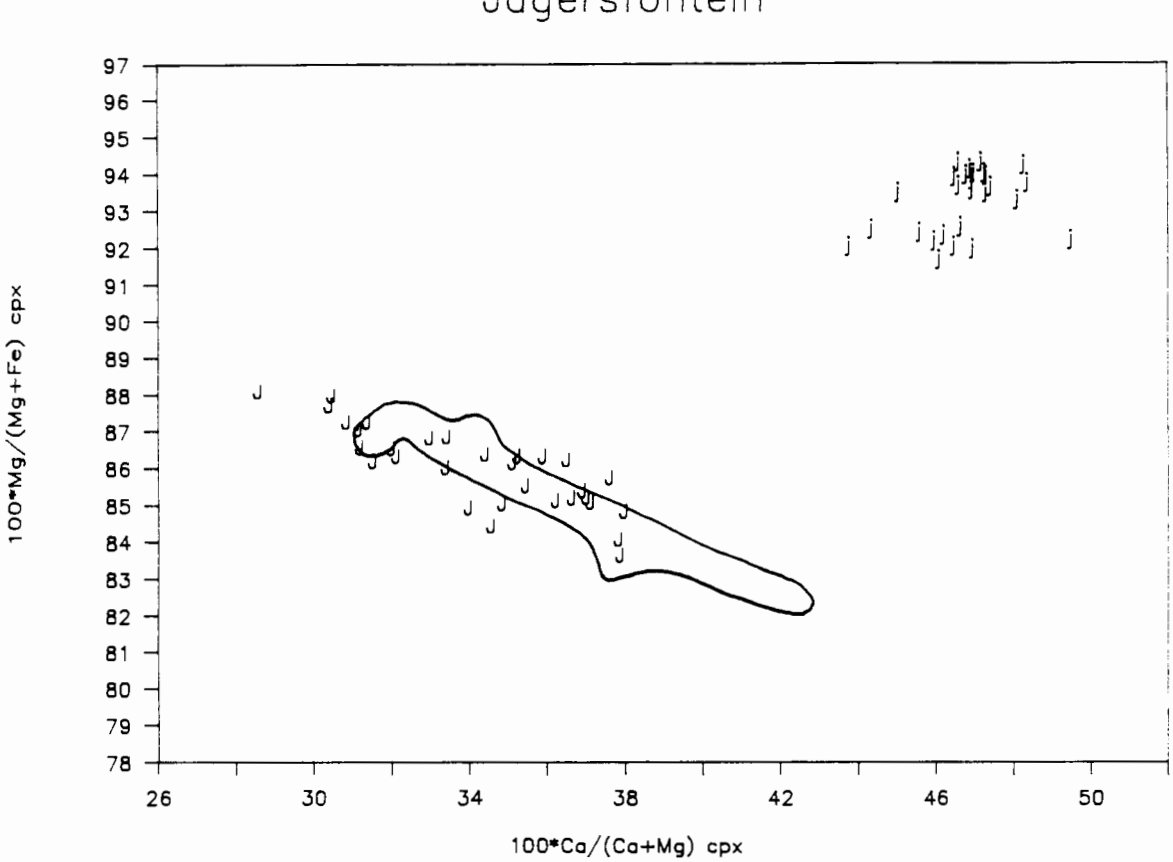

Figure 3.1.19 (b)

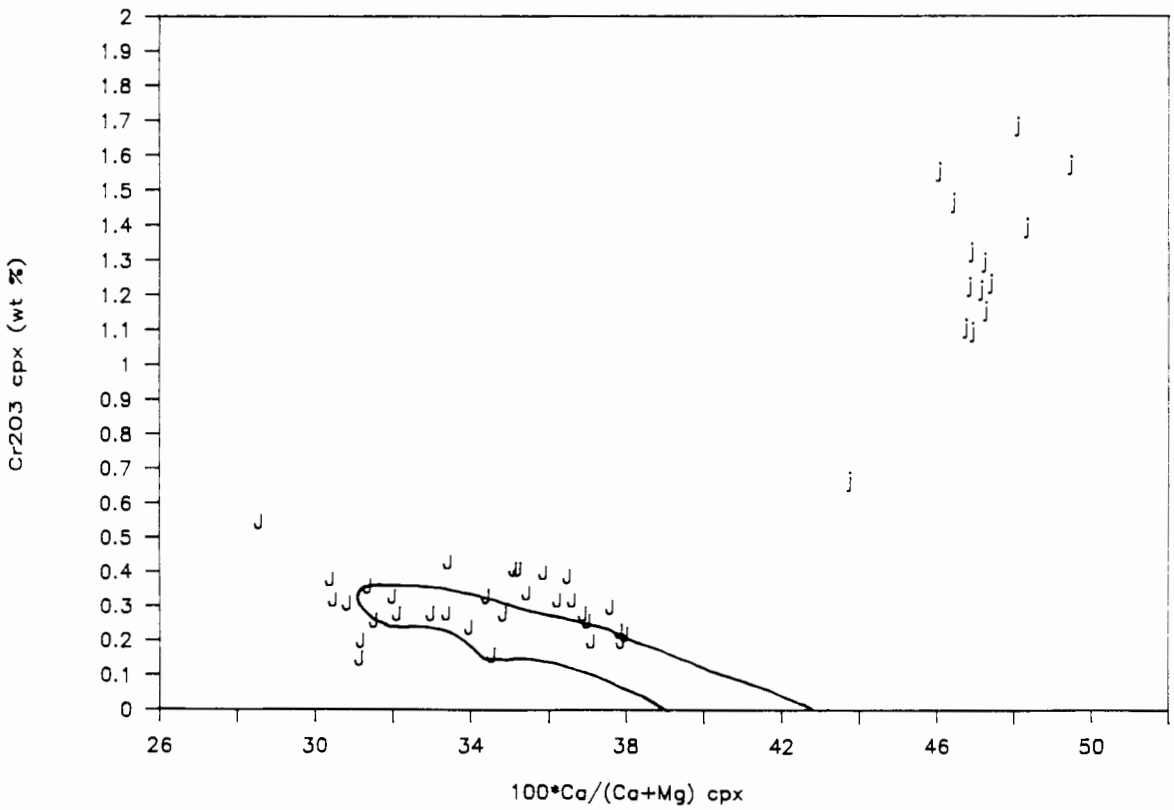

Figure 3.1.20 a and b

Ca# (atomic) versus Mg# (atomic) (a) and Cr_2O_3 (wt%) (b) in clinopyroxene megacrysts from Lekkerfontein (Robey, 1981). L = discrete; l = lamellar ilmenite intergrowth; i = inclusions in ilmenite. The outlined field depicts the compositional range found at Monastery as shown in Figures 3.1.17 (a and b).

Figure 3.1.20 (a)

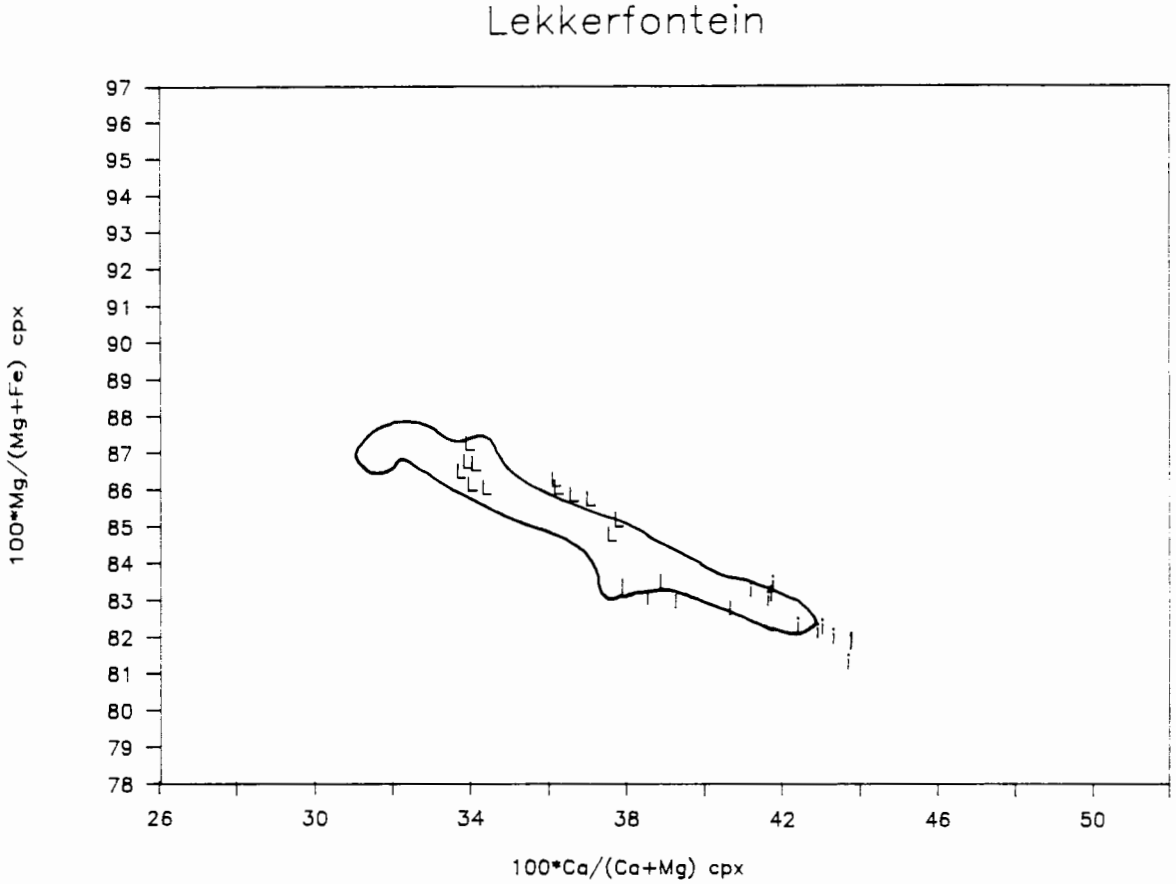

Figure 3.1.20 (b)

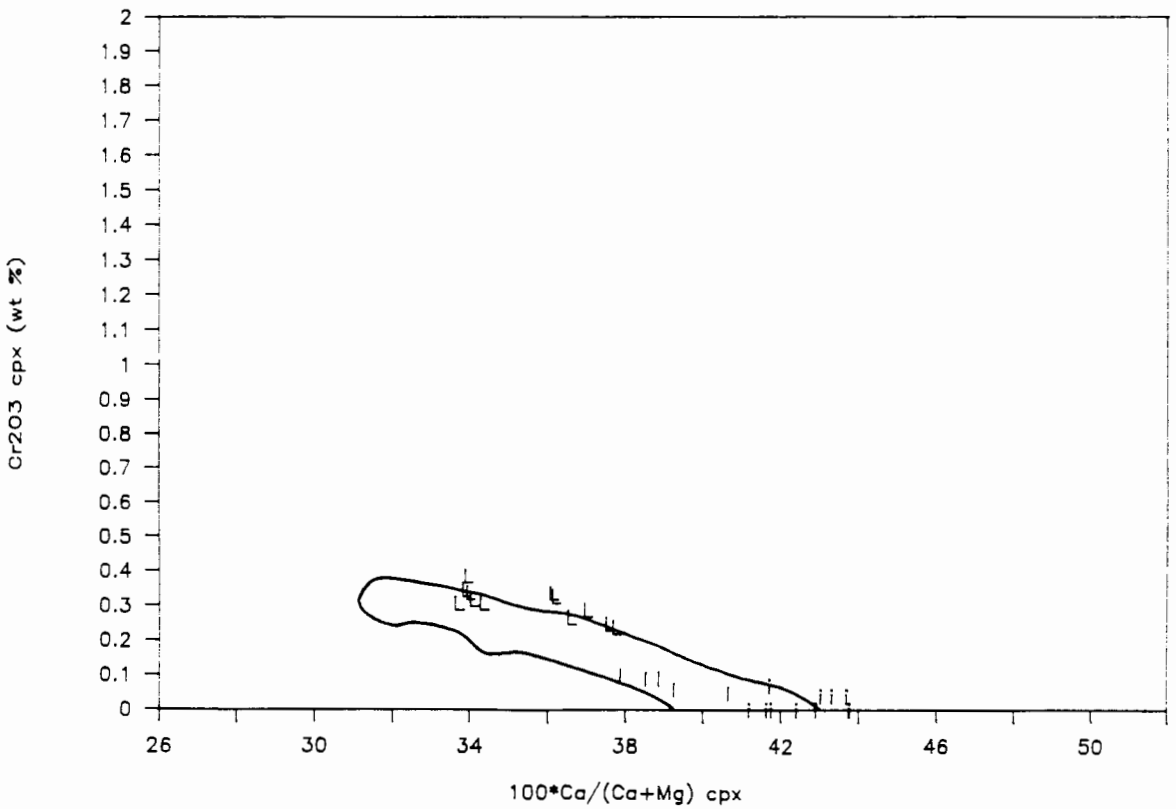

Figure 3.1.21 a and b

Ca# (atomic) versus Mg# (atomic) (a) and Cr_2O_3 (wt%) (b) in clinopyroxene megacrysts from Orapa (Shee, 1978; Tollo, 1982; Appendix 3, Table 2). O = data from Shee; o = data from Tollo; C = Appendix 3, Table 2. The outlined field depicts the compositional range found at Monastery as shown in Figures 3.1.17 (a and b).

Figure 3.1.21 (a)

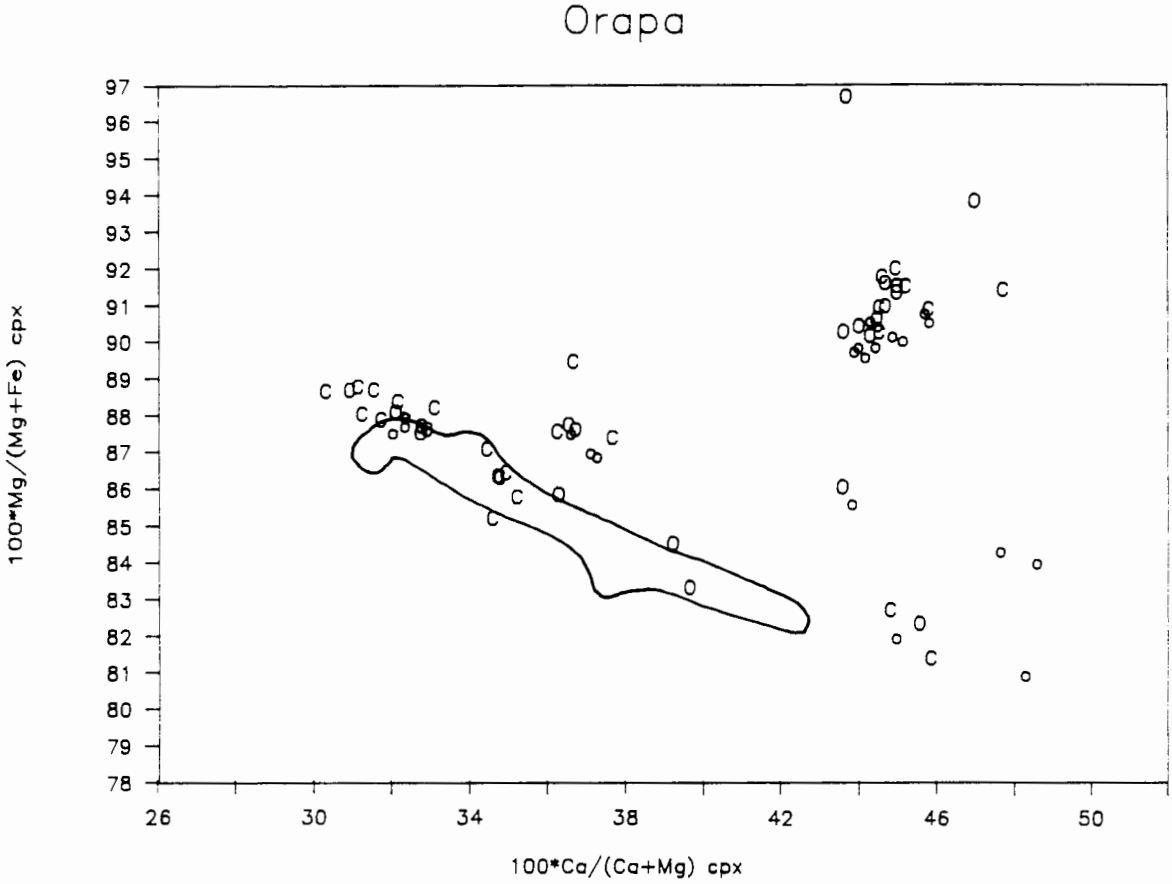

Figure 3.1.21 (b)

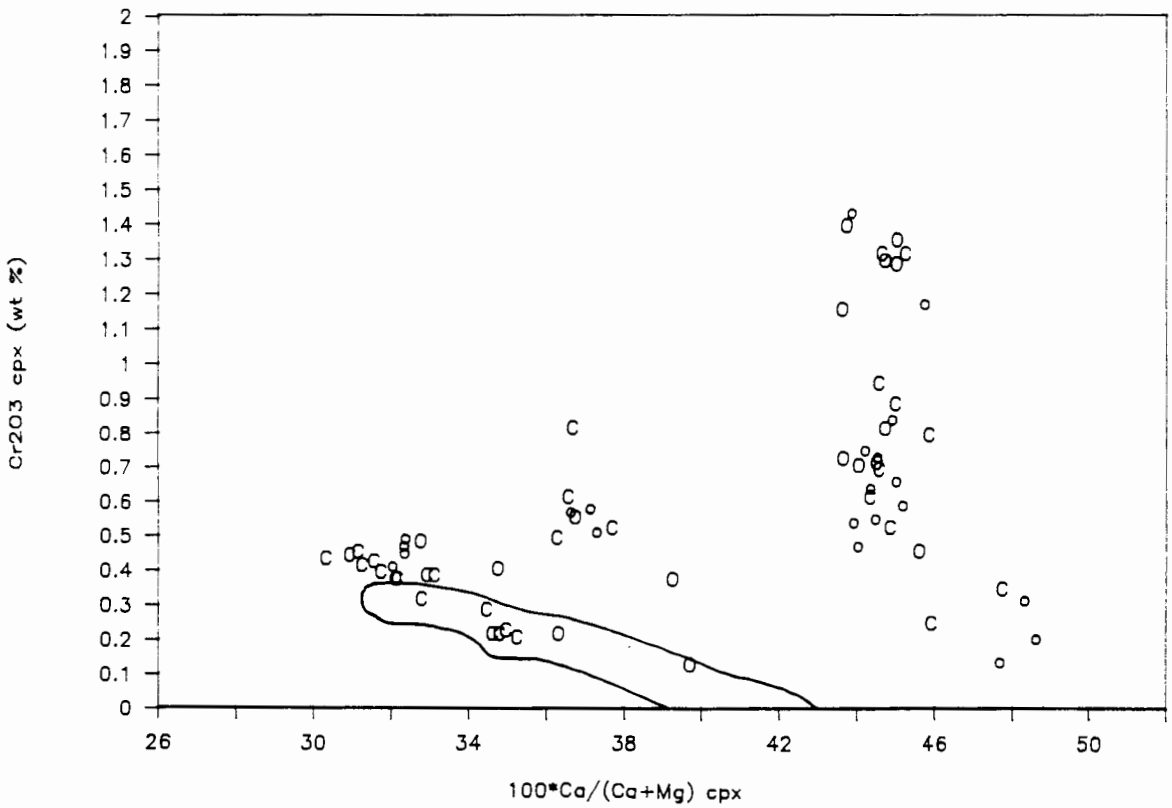

Figure 3.1.22 a and b

Ca# (atomic) versus Mg# (atomic) (a) and Cr_2O_3 (wt%) (b) in clinopyroxene megacrysts from Iron Mountain (Smith, 1977). I = discrete; i = ilmenite association. The outlined field depicts the compositional range found at Monastery as shown in Figures 3.1.17 (a and b).

Figure 3.1.22 (a)

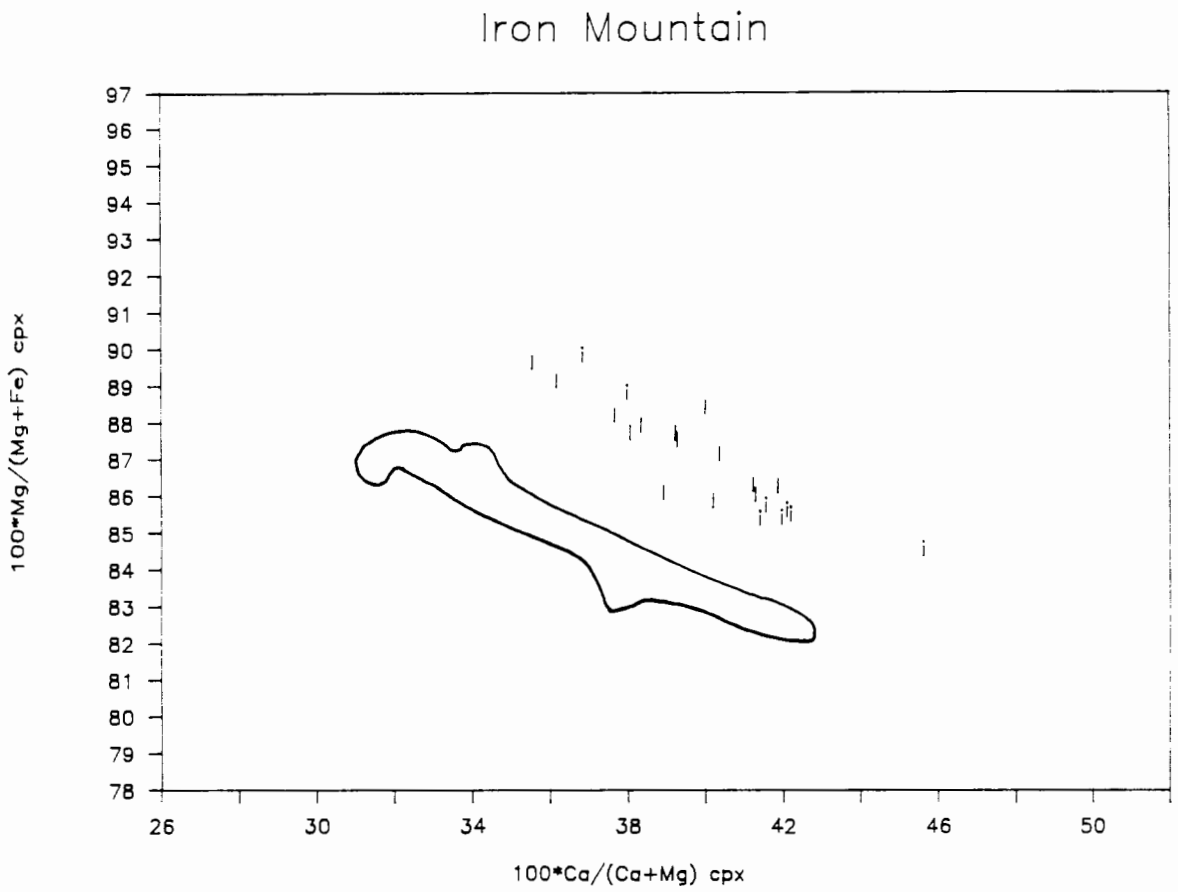

Figure 3.1.22 (b)

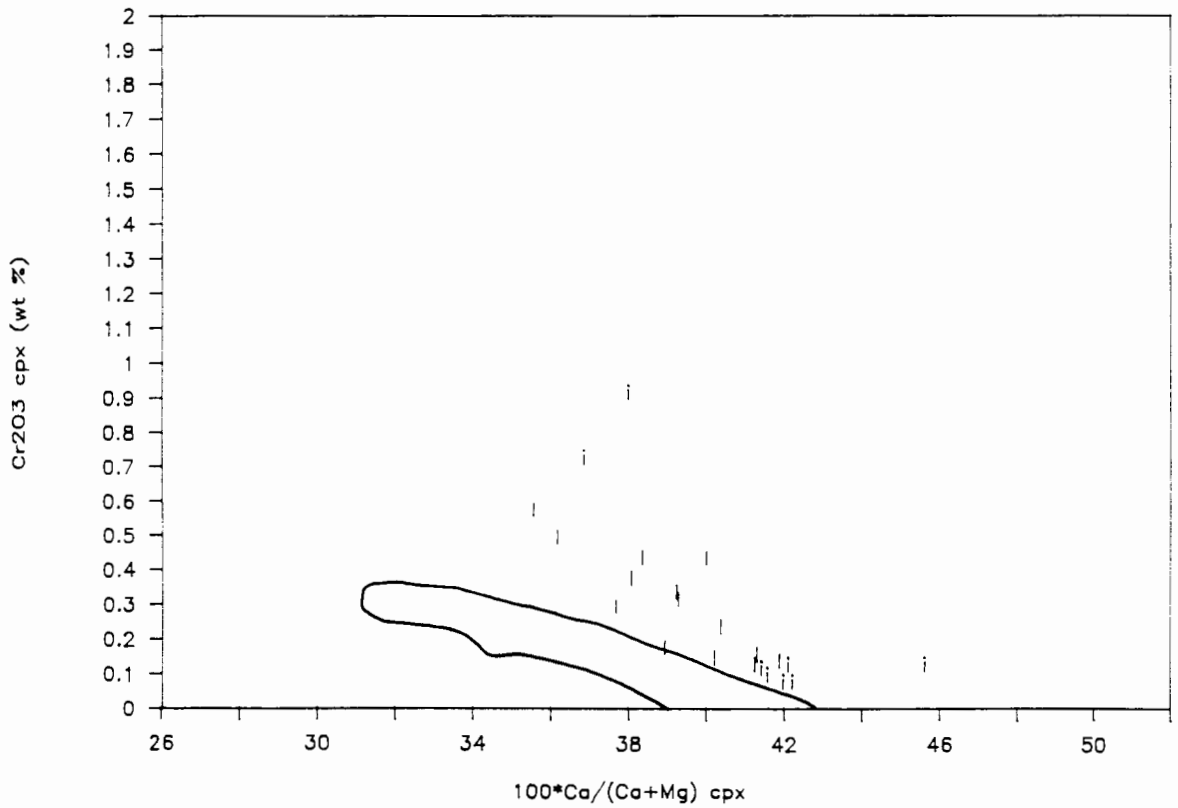

Figure 3.1.23 a and b

Ca# (atomic) versus Mg# (atomic) (a) and Cr_2O_3 (wt%) (b) in clinopyroxene megacrysts from Sloan-Nix (Eggler, unpublished data). S = discrete, Cr-poor; s = inclusions, Cr-poor; C = discrete, Cr-rich; c = inclusions, Cr-rich. The outlined field depicts the compositional range found at Monastery as shown in Figures 3.1.17 (a and b).

Figure 3.1.23 (a)

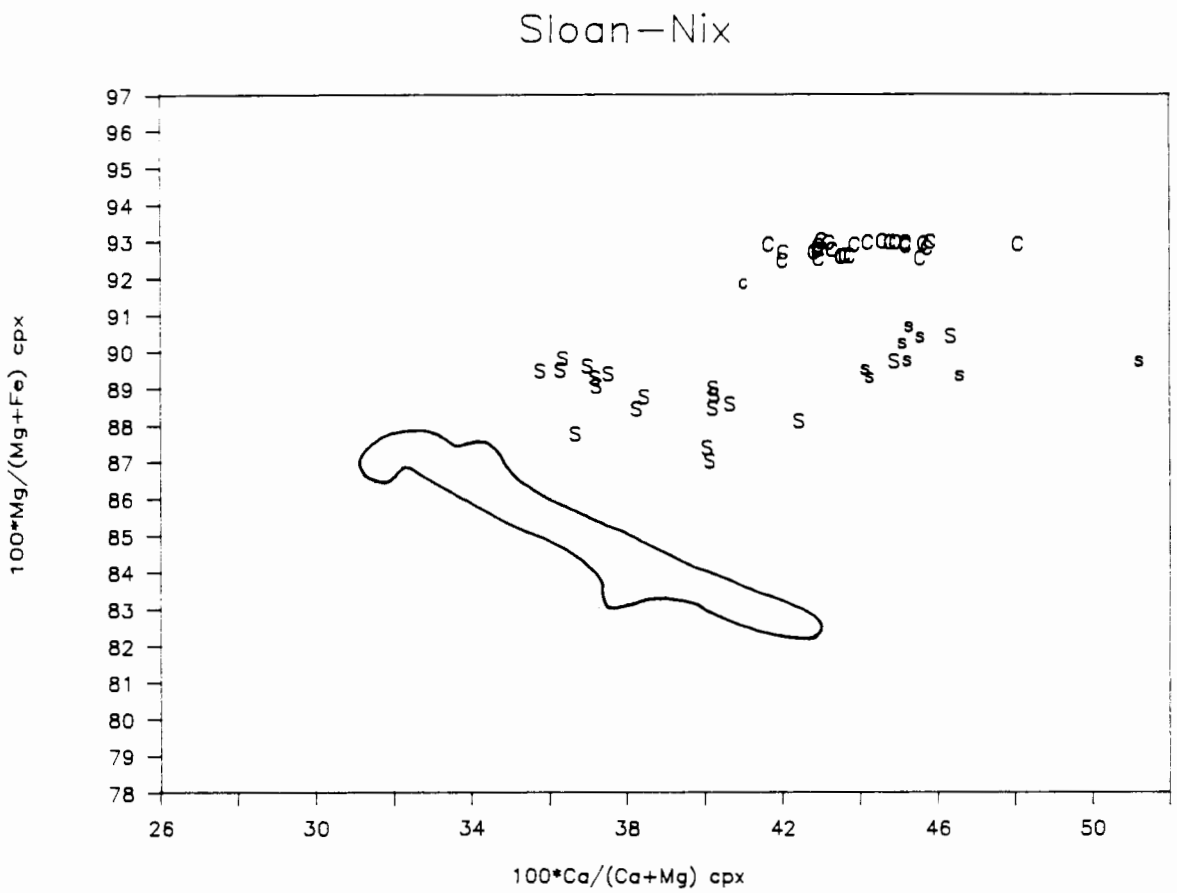

Figure 3.1.23 (b)

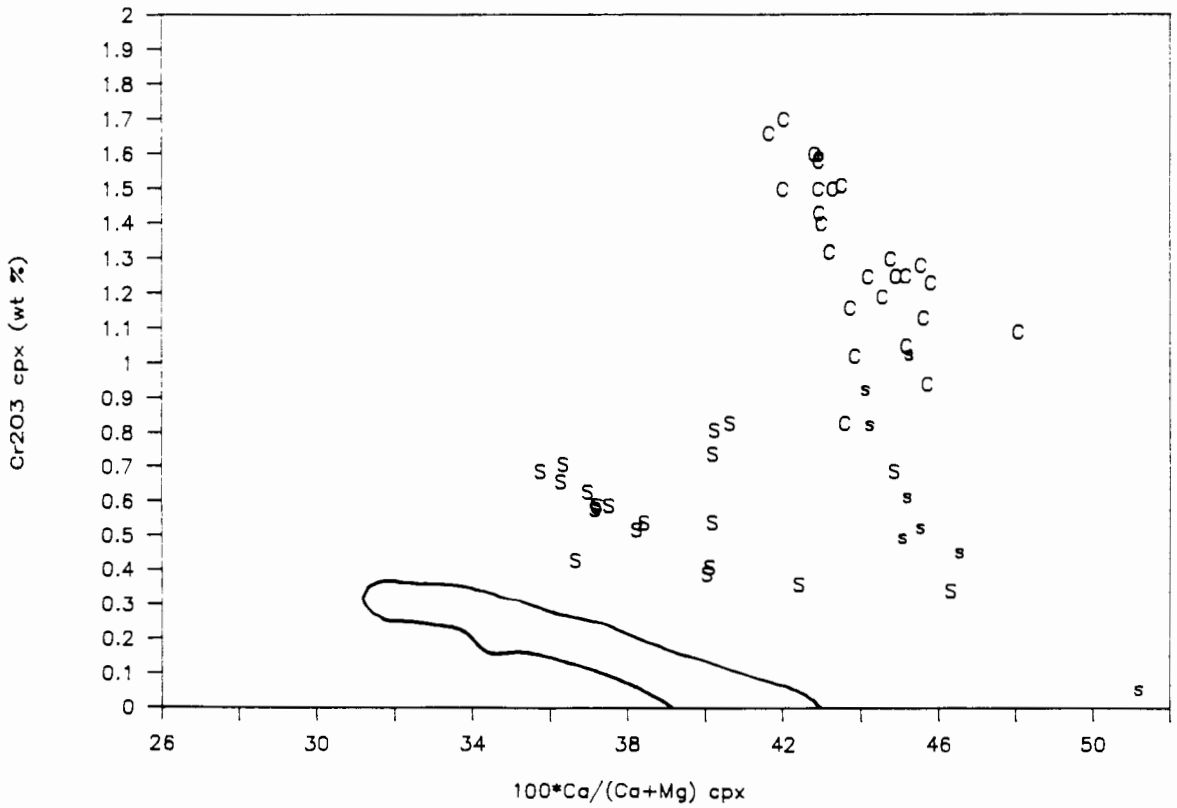

Figure 3.1.24 a and b

Ca# (atomic) versus Mg# (atomic) (a) and Cr_2O_3 (wt%) (b) in clinopyroxene megacrysts from Mukorob 2 (Jones, 1984). U = discrete; g = inclusions in garnet; i = inclusions in ilmenite. The outlined field depicts the compositional range found at Monastery as shown in Figures 3.1.17 (a and b).

Figure 3.1.24 (a)

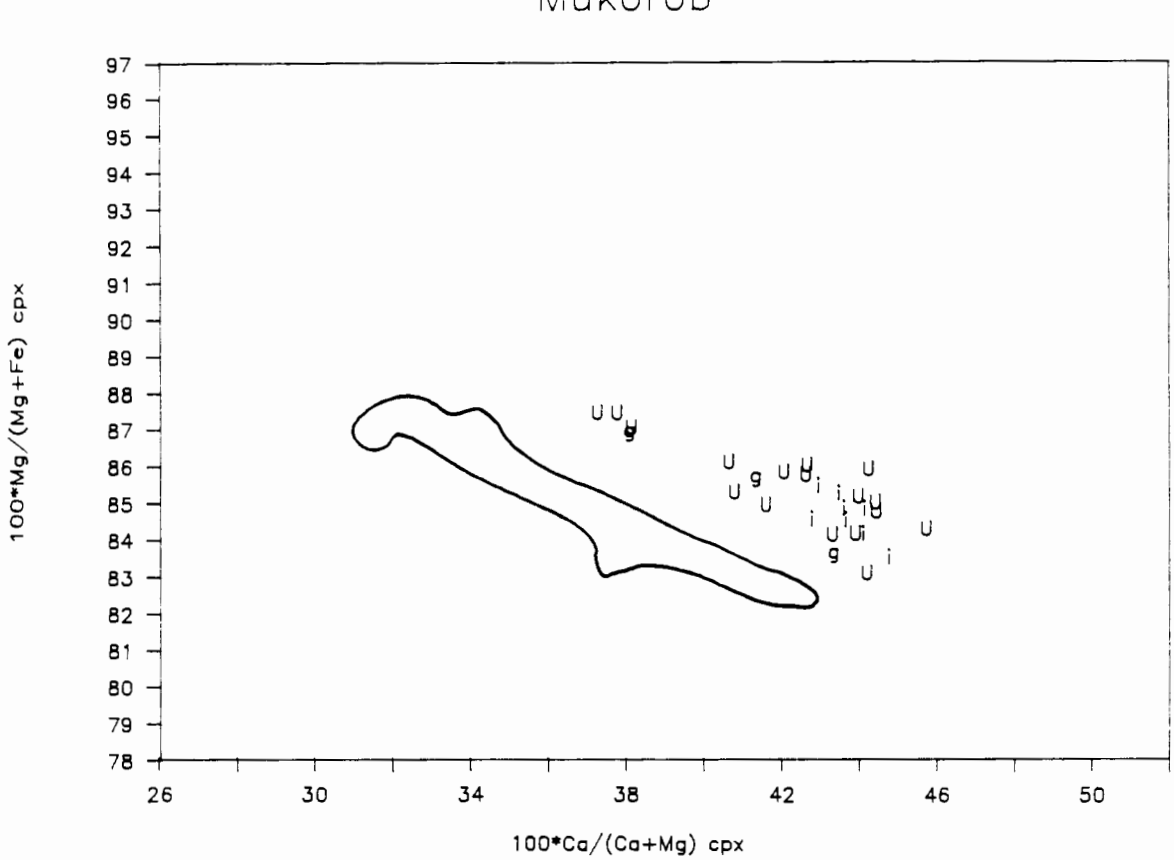

Figure 3.1.24 (b)

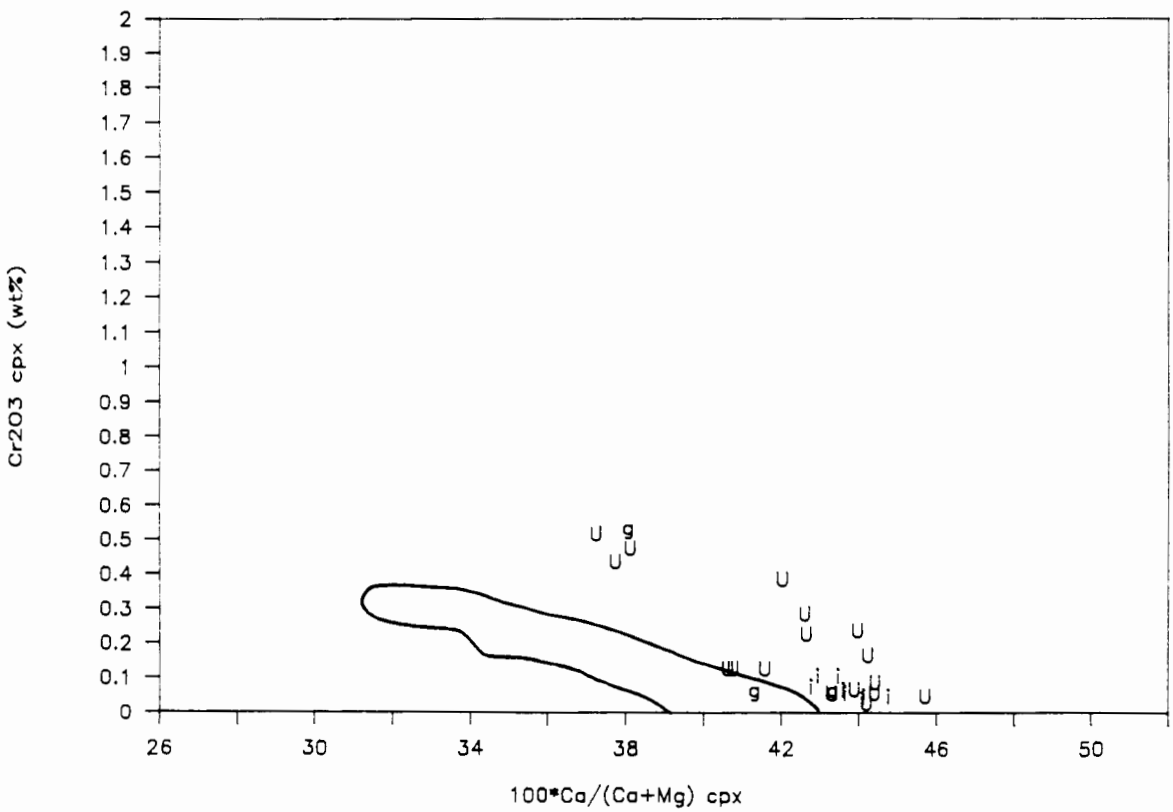

Figure 3.1.25 a and b

Ca# (atomic) versus Mg# (atomic) (a) and Cr_2O_3 (wt%) (b) in clinopyroxene megacrysts from the Eastern Griqualand kimberlites (Boyd, unpublished data). A = Abbotsford; R = Ramatseliso; Z = Zeekoegat. The outlined field depicts the compositional range found at Monastery as shown in Figures 3.1.17 (a and b).

Figure 3.1.25 (a)

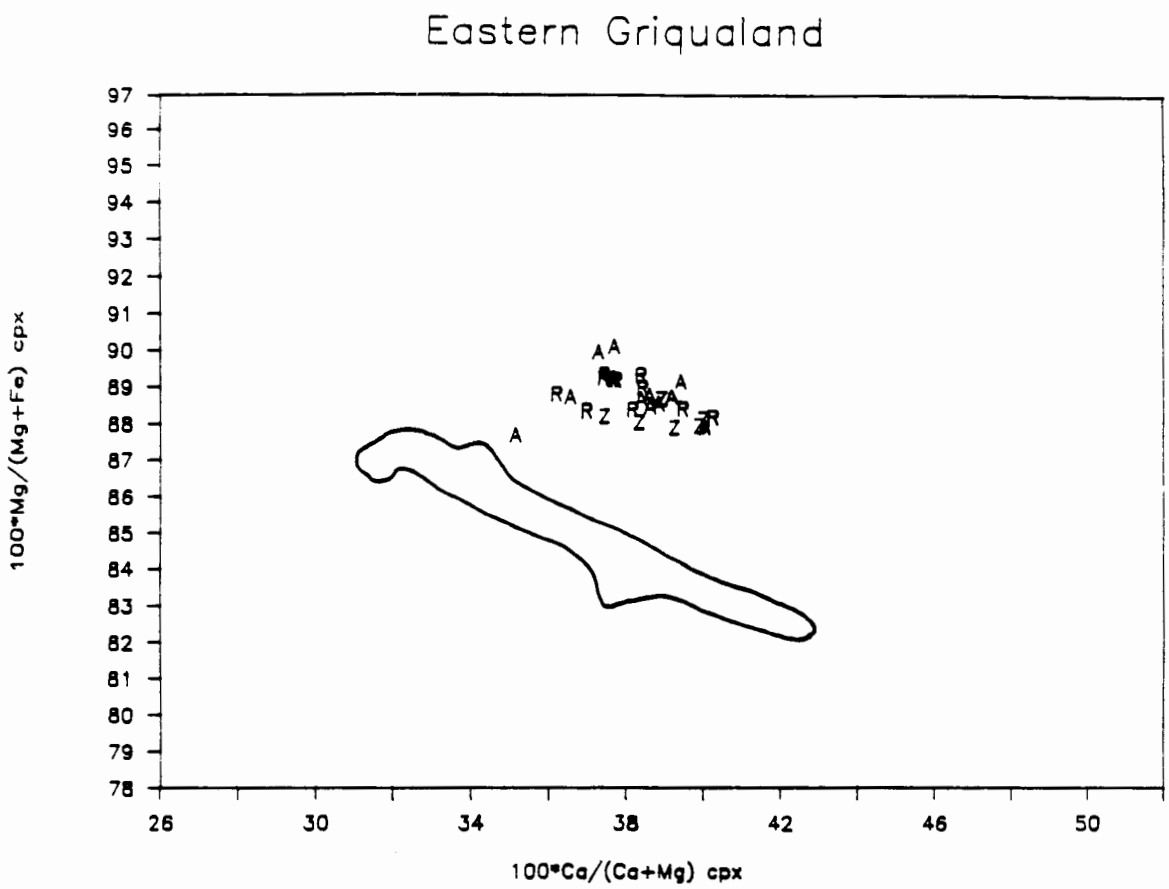

Figure 3.1.25 (b)

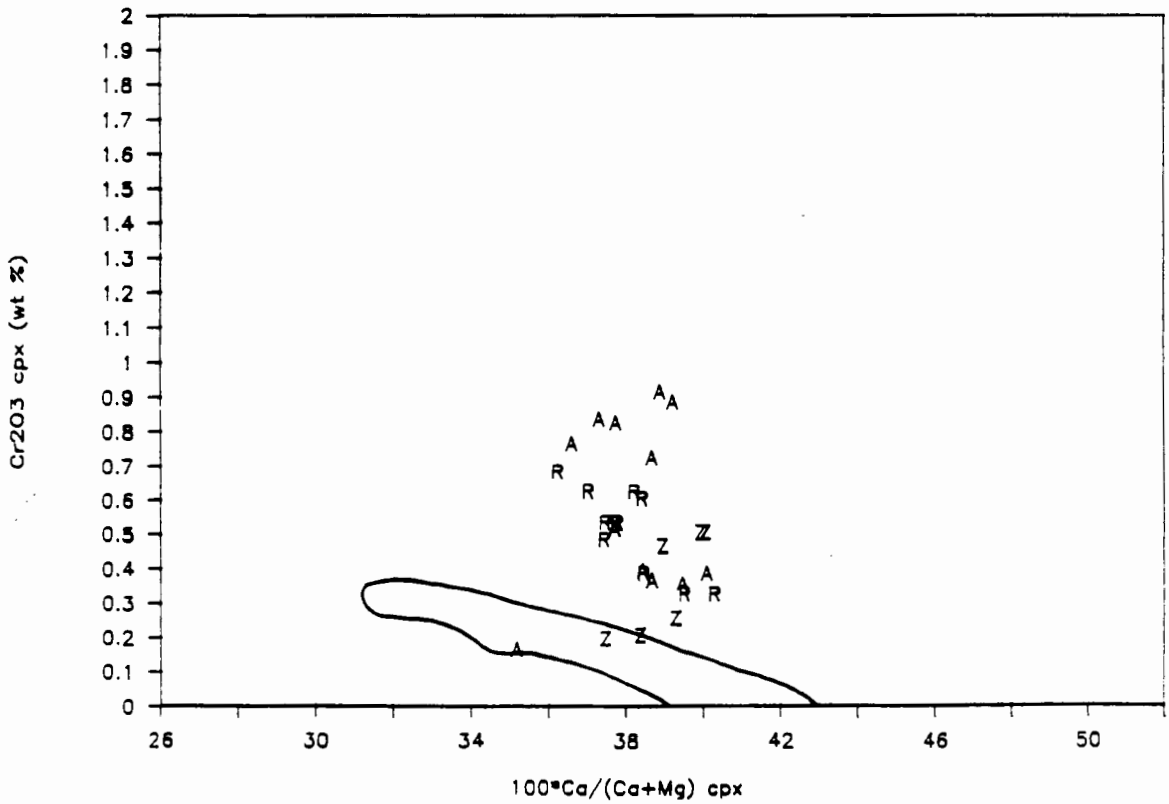

Figure 3.1.26 a and b

Ca# (atomic) versus Mg# (atomic) (a) and Cr_2O_3 (wt%) (b) in clinopyroxene megacrysts from Hamilton Branch (Schulze, 1982b). K = discrete; g = garnet association; i = ilmenite association as inclusions; l = ilmenite association as lamellar intergrowths. The outlined field depicts the compositional range found at Monastery as shown in Figures 3.1.17 (a and b).

Figure 3.1.26 (a)

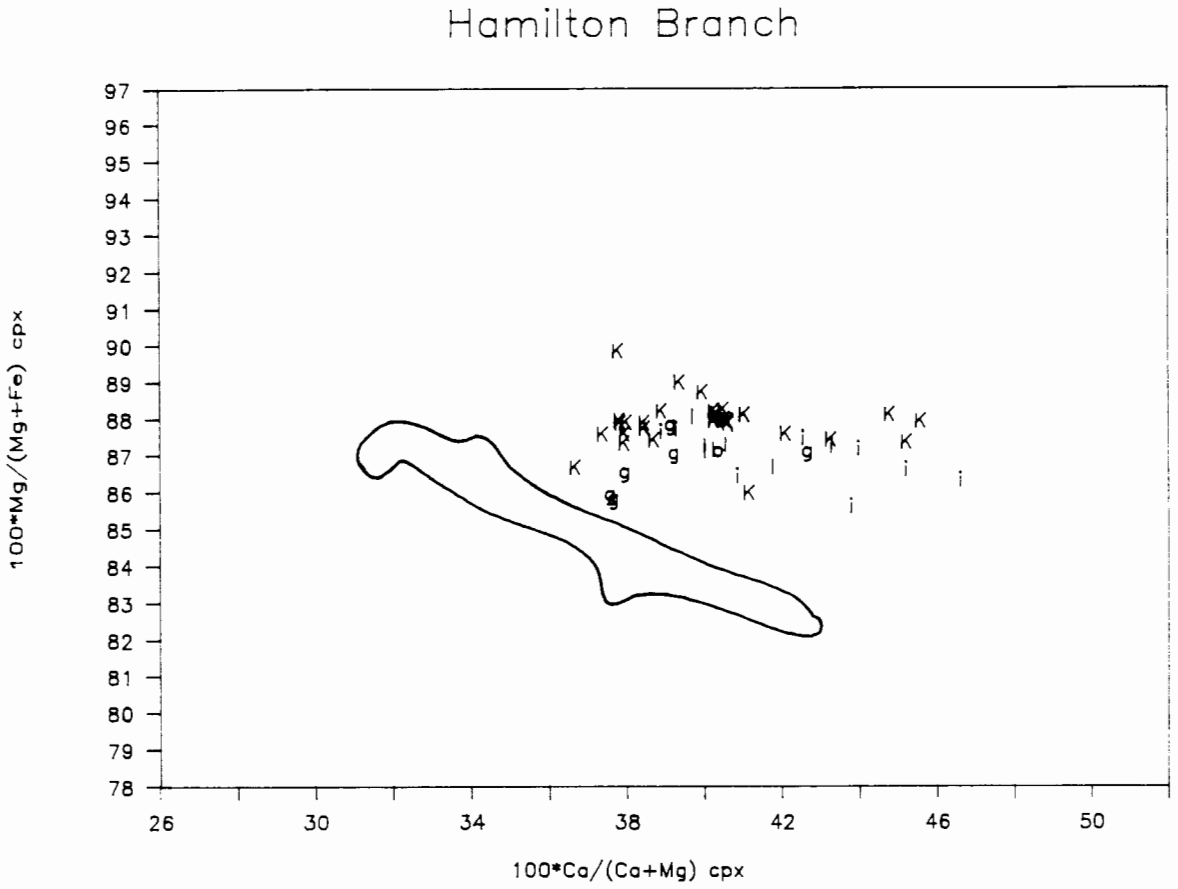

Figure 3.1.26 (b)

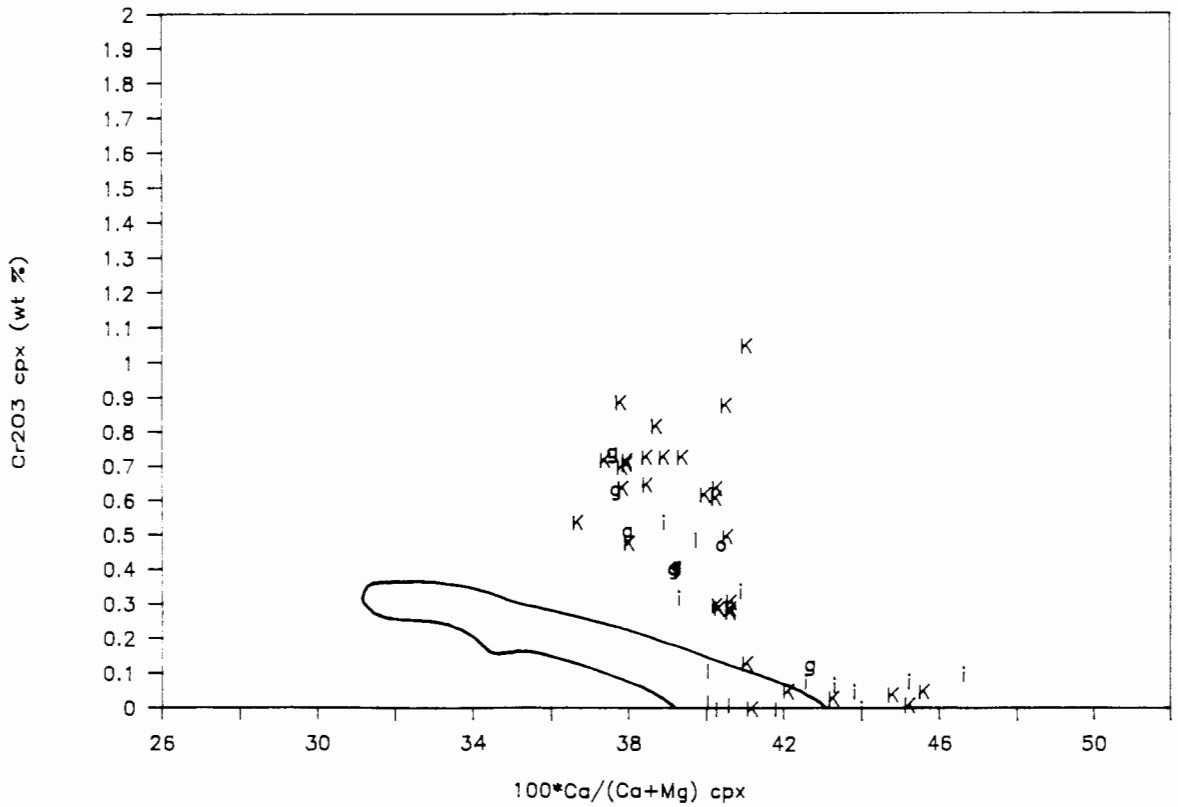

Figure 3.1.27 a and b

Ca# (atomic) versus Mg# (atomic) (a) and Cr_2O_3 (wt%) (b) in clinopyroxene megacrysts from the Kimberley Pool kimberlites (Boyd and Nixon, 1978). F = Kampfersdam; Y = Kimberley; D = De Beers; B = Bultfontein; W = Wesselton. The outlined field depicts the compositional range found at Monastery as shown in Figures 3.1.17 (a and b).

Figure 3.1.27 (a)

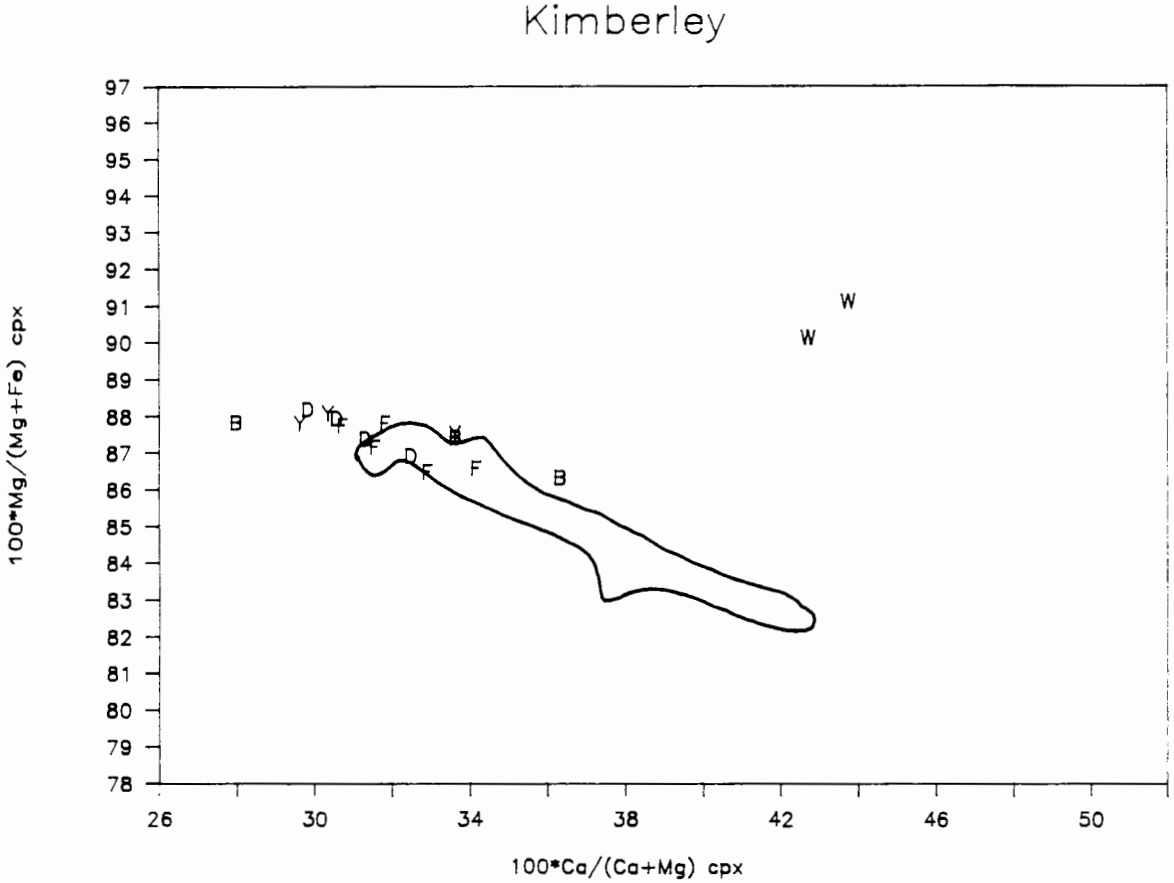

Figure 3.1.27 (b)

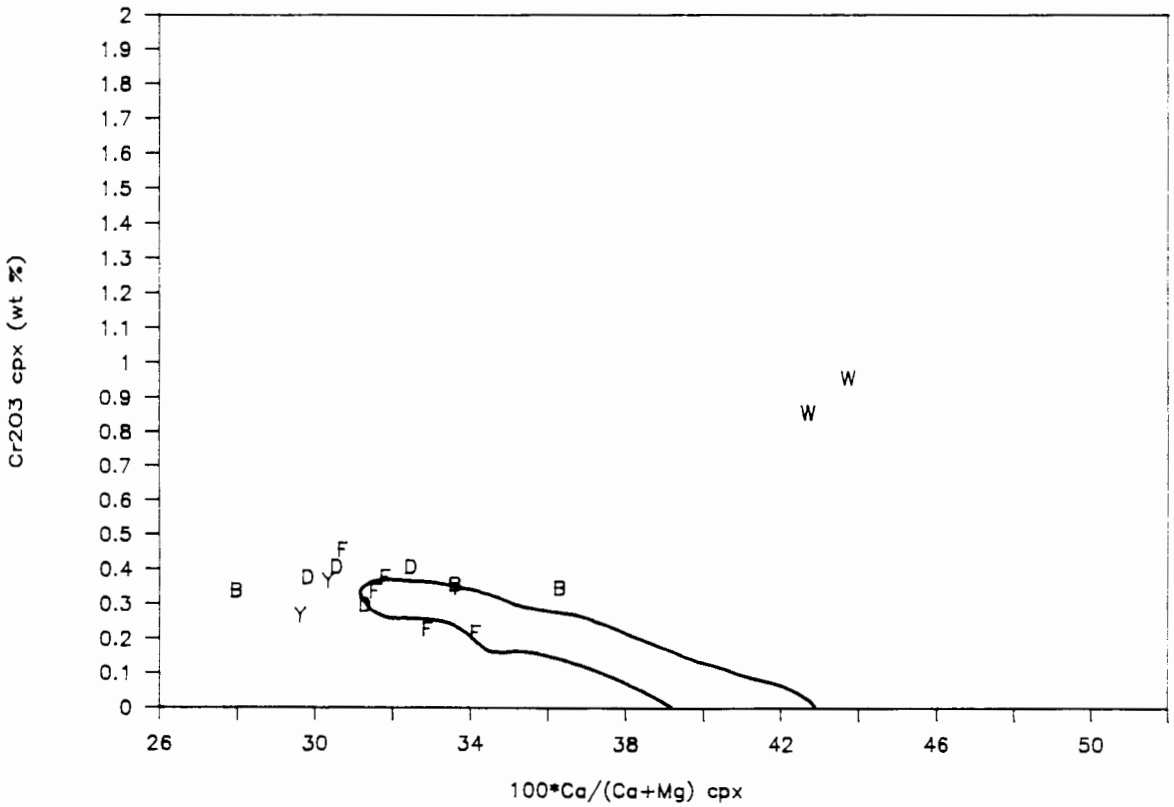

Figure 3.1.28 a and b

Ca# (atomic) versus Mg# (atomic) (a) and Cr_2O_3 (wt%) (b) in clinopyroxene megacrysts from Camutue (Boyd and Danchin, 1980). C = discrete, G = with inclusions of garnet, g = clinopyroxene inclusions in discrete garnets, i = discrete clinopyroxene with inclusions of ilmenite. The outlined field depicts the compositional range found at Monastery as shown in Figures 3.1.17 (a and b).

Figure 3.1.28 (a)

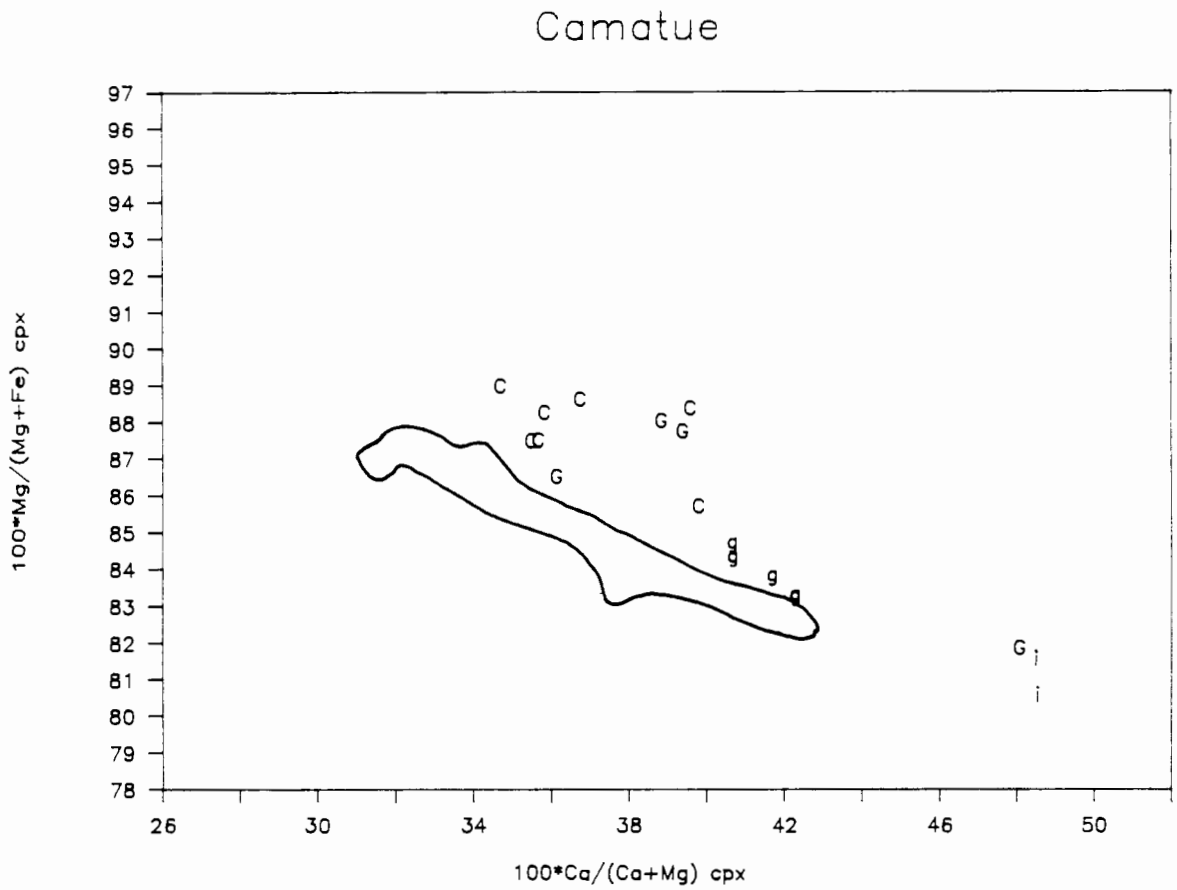

Figure 3.1.28 (b)

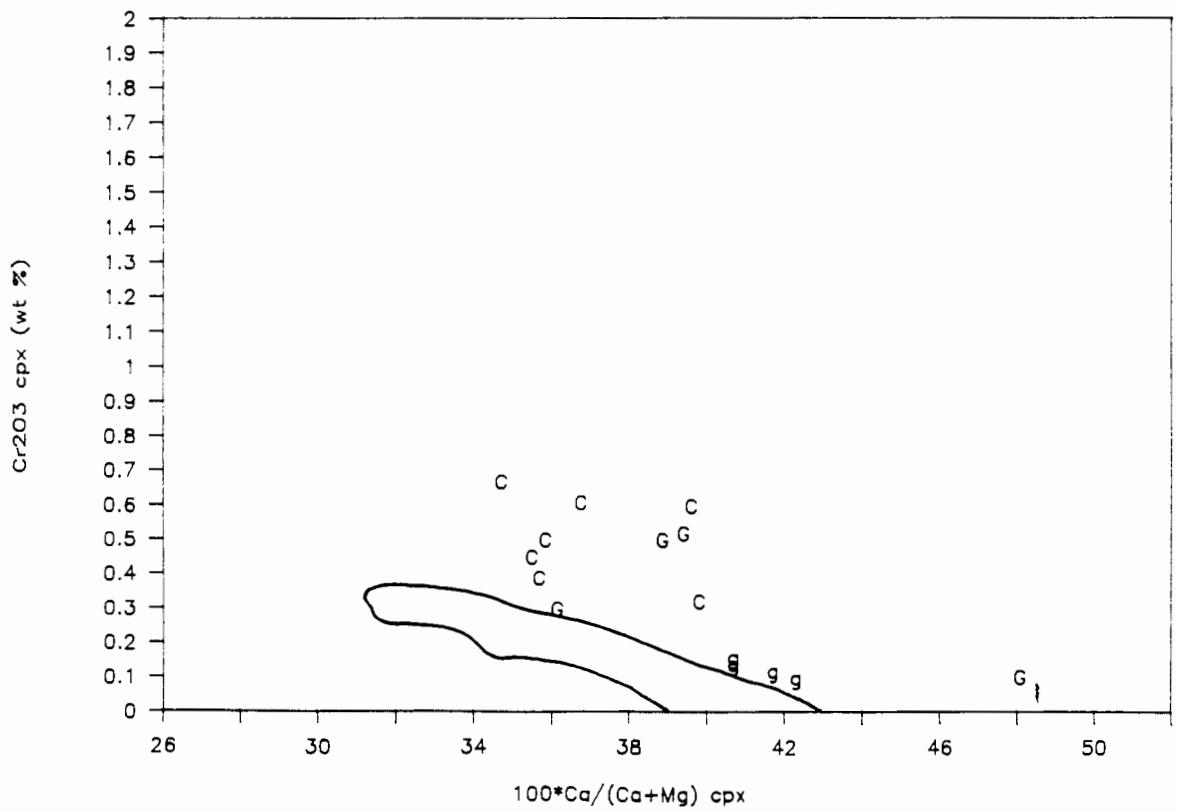

Figure 3.1.29 a and b

Ca# (atomic) versus Mg# (atomic) (a) and Cr_2O_3 (wt%) (b) in clinopyroxene megacrysts from Witberg (de Bruin, unpublished data). These samples have been subdivided into two compositional groups: o = Cr-poor; w = relatively enriched in chrome and Mg#. The outlined field depicts the compositional range found at Monastery as shown in Figures 3.1.17 (a and b).

Figure 3.1.29 (a)

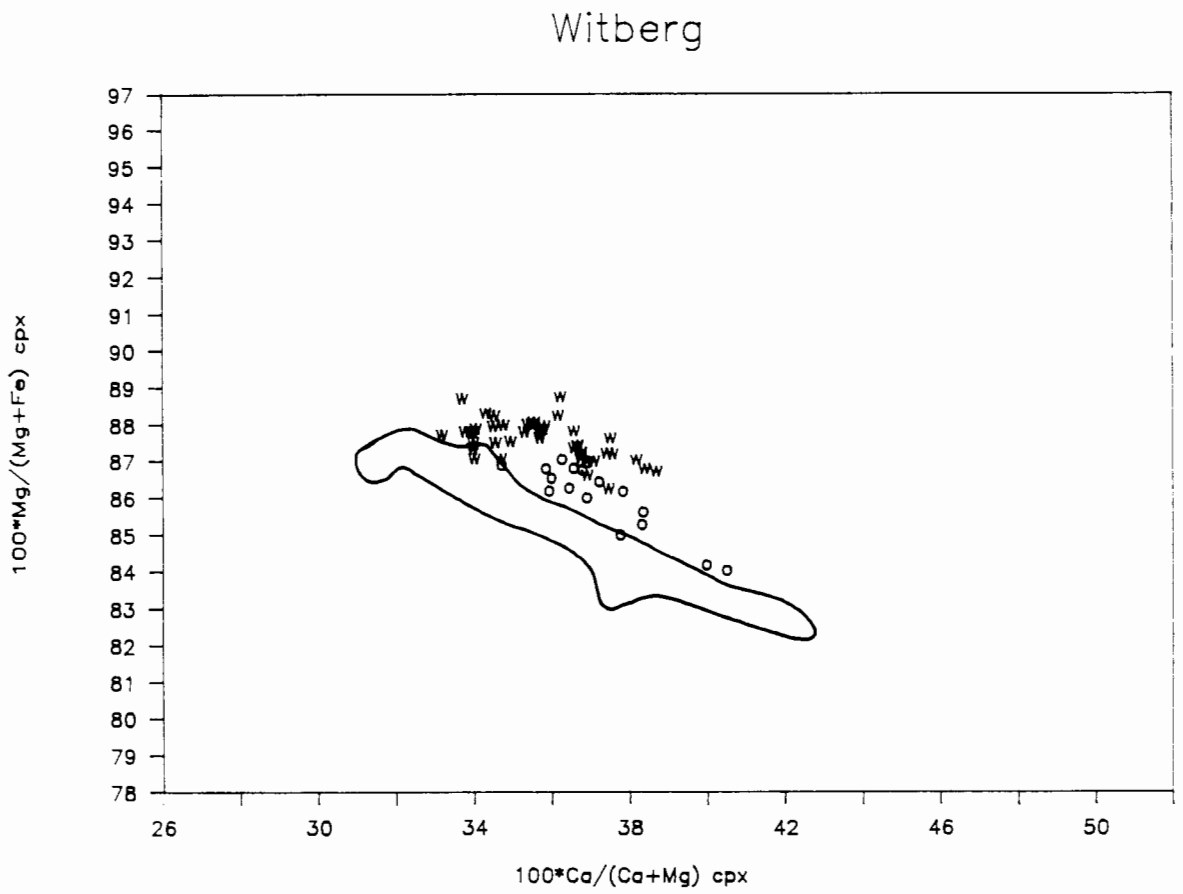

Figure 3.1.29 (b)

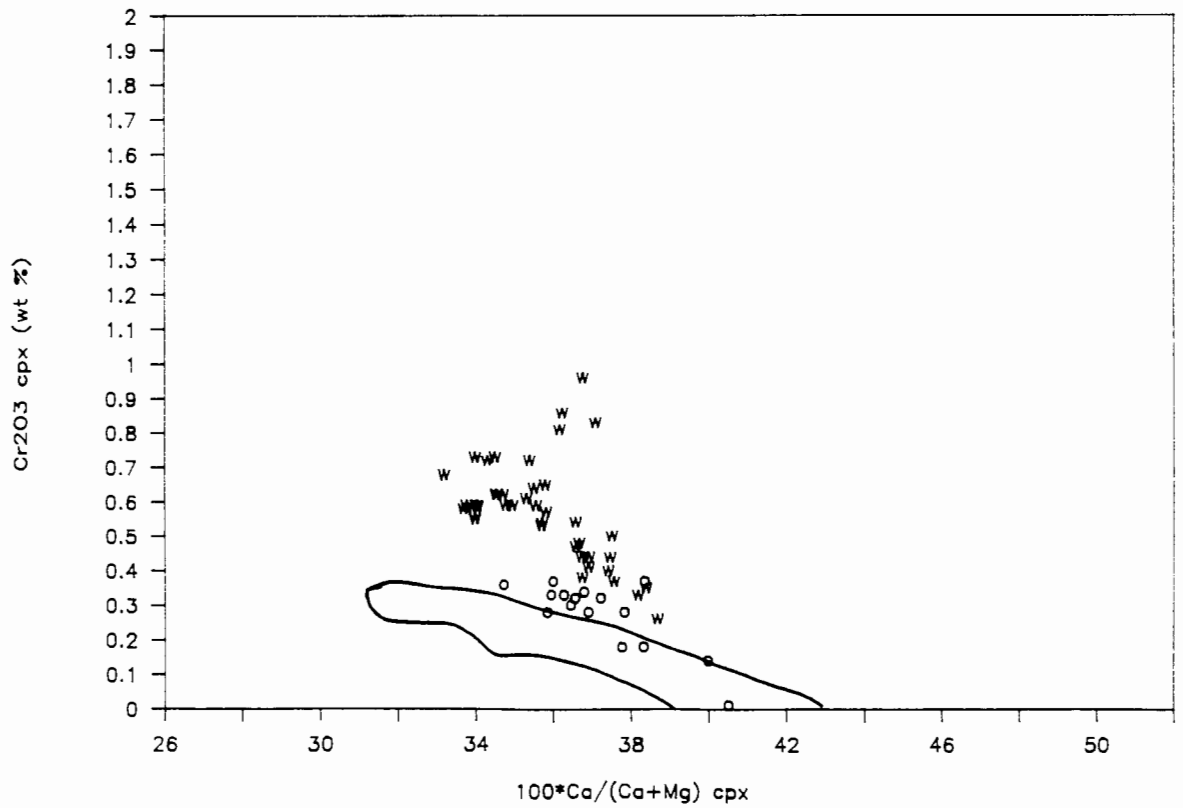

Figure 3.2.1

Mg# (atomic) versus CaO (wt%) in orthopyroxene megacrysts from the Schuller kimberlite. The symbols 1, 2, 3 refer to the compositional megacryst groups discussed in the text. X = exsolved megacrysts. Association with other megacryst phases are indicated within brackets where c = clinopyroxene; g = garnet; i = ilmenite association.

Figure 3.2.2

Mg# (atomic) versus Al_2O_3 (wt%) in orthopyroxene megacrysts from the Schuller kimberlite. Symbols as in Figure 3.2.1

Figure 3.2.1

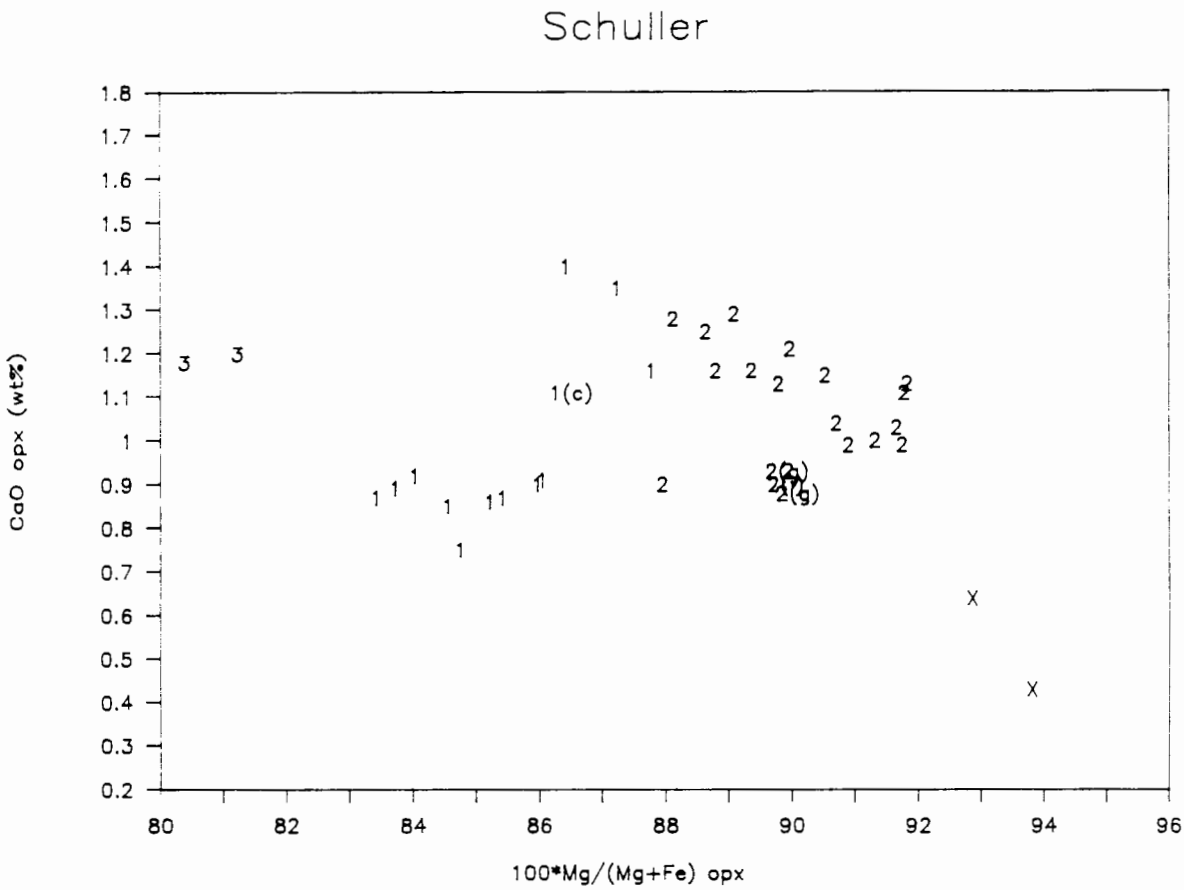

Figure 3.2.2

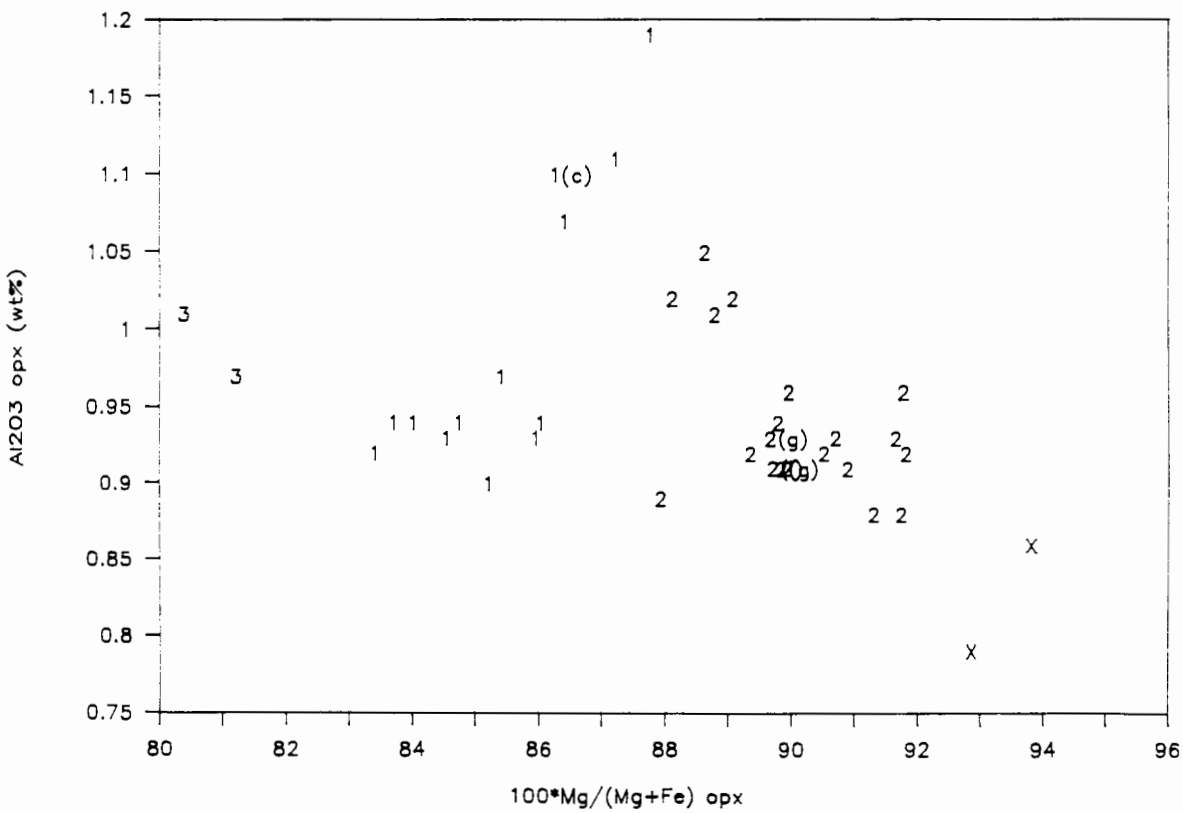

Figure 3.2.3

Mg# (atomic) versus Cr_2O_3 (wt%) in orthopyroxene megacrysts from the Schuller kimberlite. Symbols as in Figure 3.2.1

Figure 3.2.4

Mg# (atomic) versus TiO_2 (wt%) in orthopyroxene megacrysts from the Schuller kimberlite. Symbols as in Figure 3.2.1

Figure 3.2.3

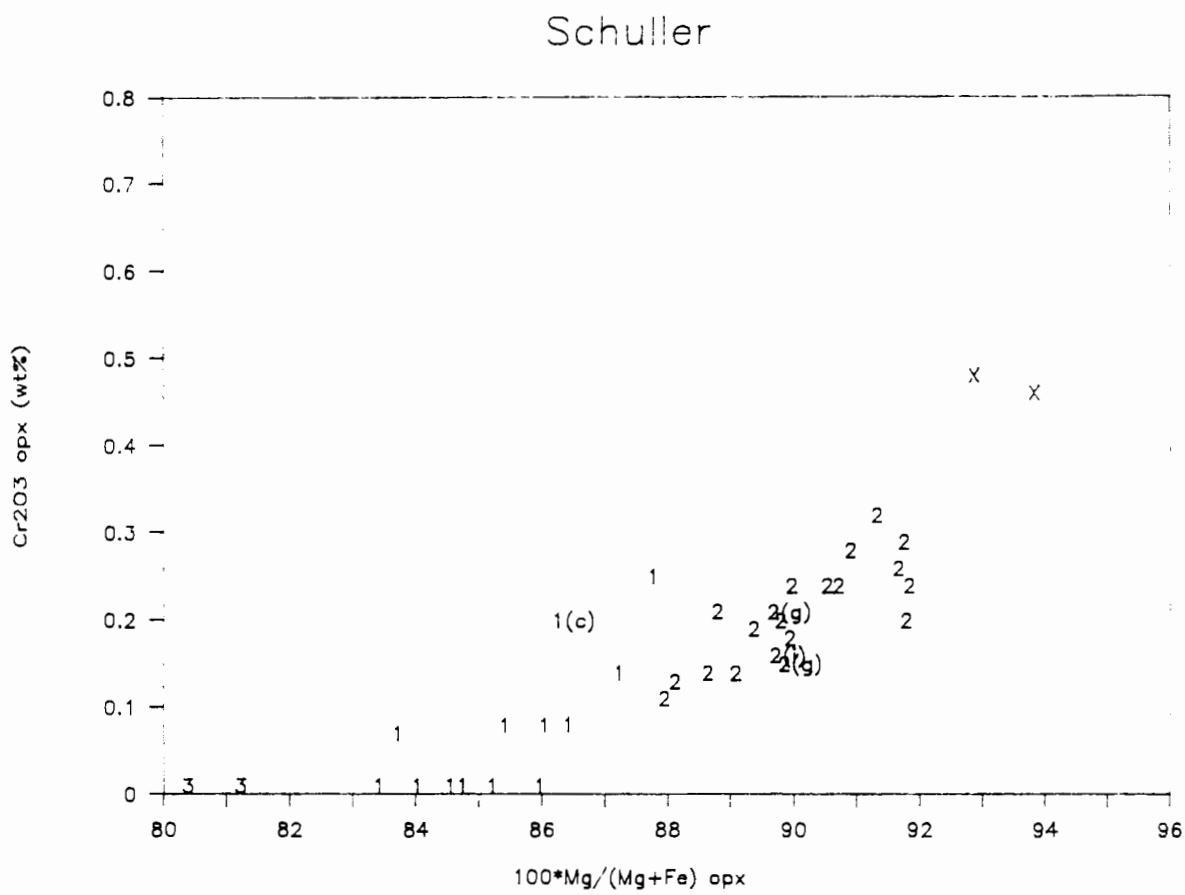

Figure 3.2.4

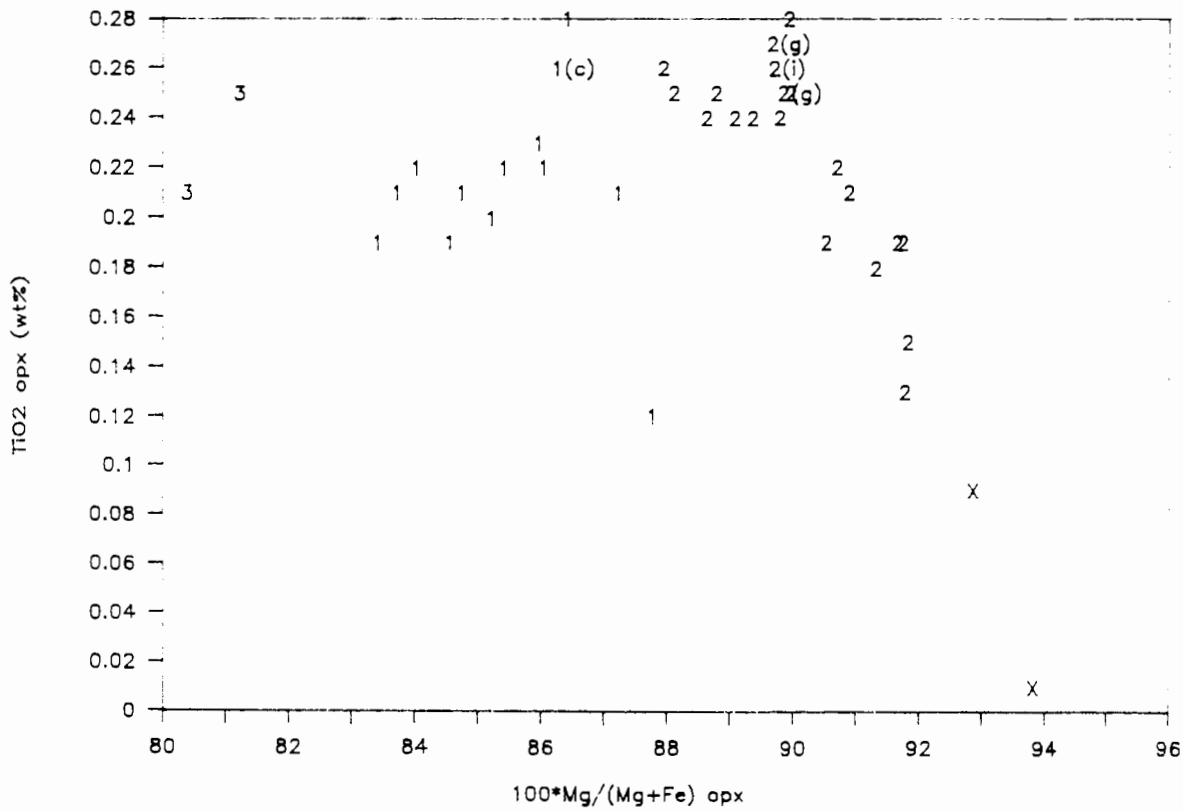

Figure 3.2.5

Mg# (atomic) versus CaO (wt%) in orthopyroxene megacrysts from the Schuller kimberlite and the compositional fields of orthopyroxene in deformed (solid line) and coarse (broken line) garnet lherzolites from Premier (Boyd, unpublished data) and Schuller coarse garnet lherzolites (stippled) (de Bruin, unpublished data). Symbols for megacrysts as in Figure 3.2.1

Figure 3.2.6

Mg# (atomic) versus Al_2O_3 (wt%) in orthopyroxene megacrysts from the Schuller kimberlite and the compositional fields of orthopyroxene in deformed (solid line) and coarse (broken line) garnet lherzolites from Premier (Boyd, unpublished data) and Schuller coarse garnet lherzolites (stippled) (de Bruin, unpublished data). Symbols for megacrysts as in Figure 3.2.1

Figure 3.2.5

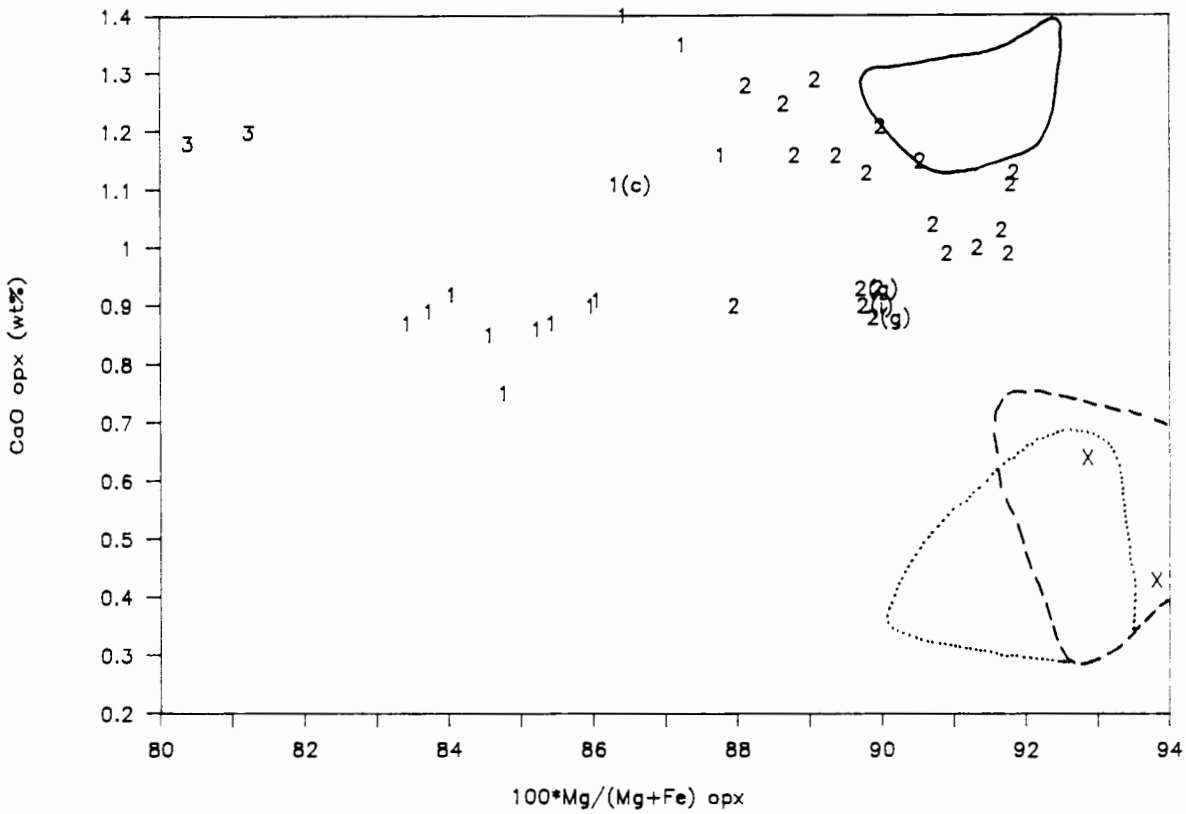

Figure 3.2.6

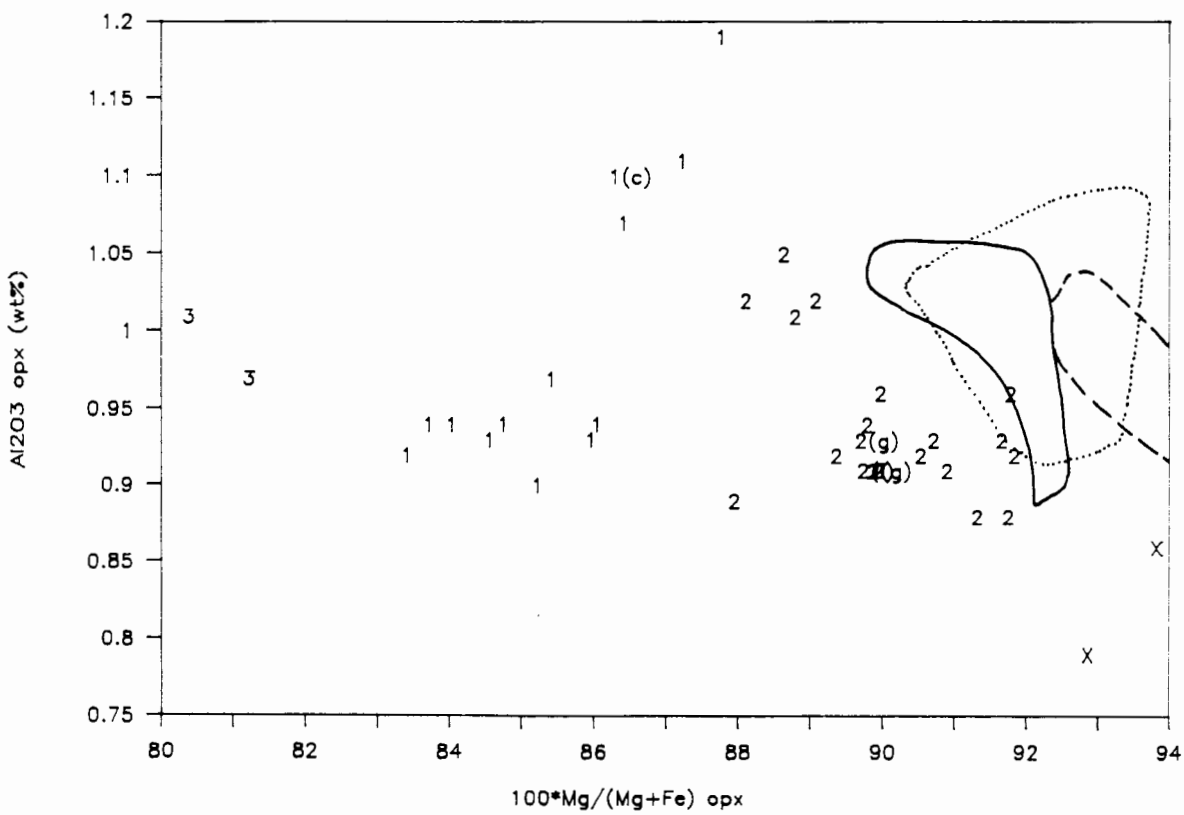

Figure 3.2.7

Mg# (atomic) versus Cr_2O_3 (wt%) in orthopyroxene megacrysts from the Schuller kimberlite and the compositional fields of orthopyroxene in deformed (solid line) and coarse (broken line) garnet lherzolites from Premier (Boyd, unpublished data) and Schuller coarse garnet lherzolites (stippled) (de Bruin, unpublished data). Symbols for megacrysts as in Figure 3.2.1

Figure 3.2.8

Mg# (atomic) versus TiO (wt%) in orthopyroxene megacrysts from the Schuller kimberlite and the compositional fields of orthopyroxene in deformed (solid line) and coarse (broken line) garnet lherzolites from Premier (Boyd, unpublished data) and Schuller coarse garnet lherzolites (stippled) (de Bruin, unpublished data). Symbols for megacrysts as in Figure 3.2.1

Figure 3.2.7

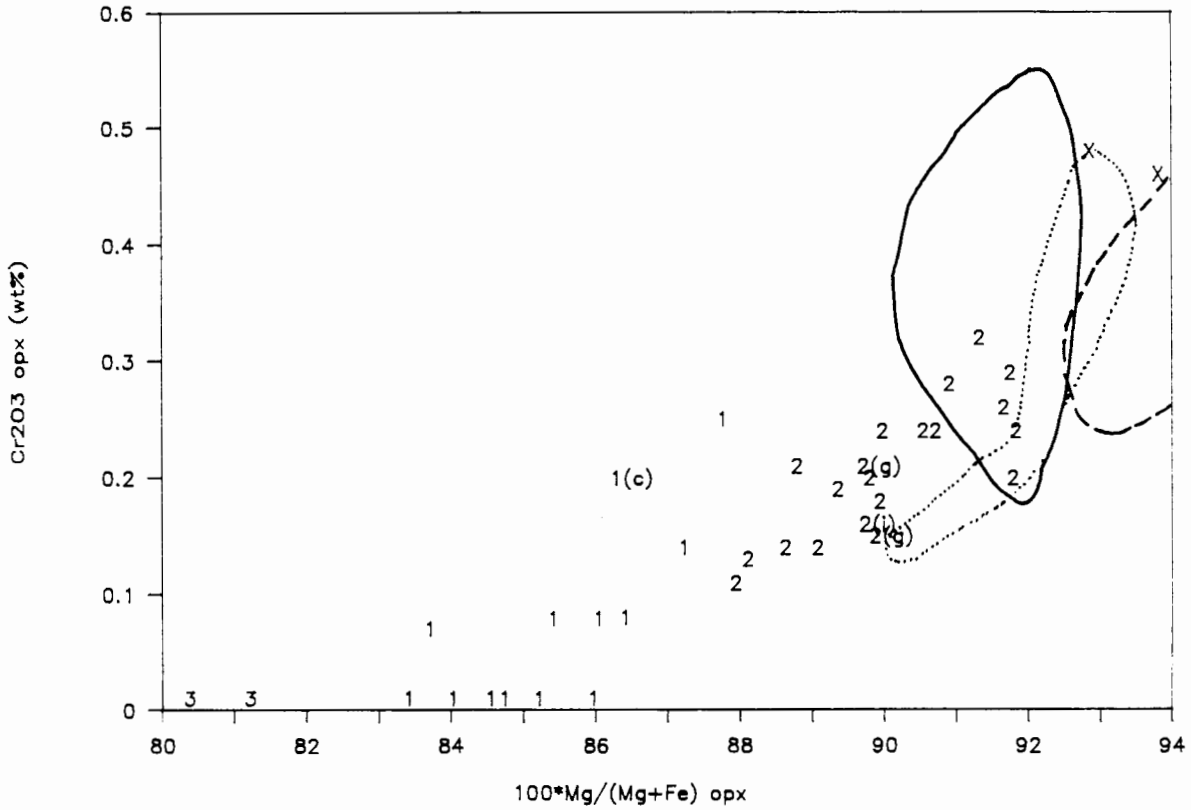

Figure 3.2.8

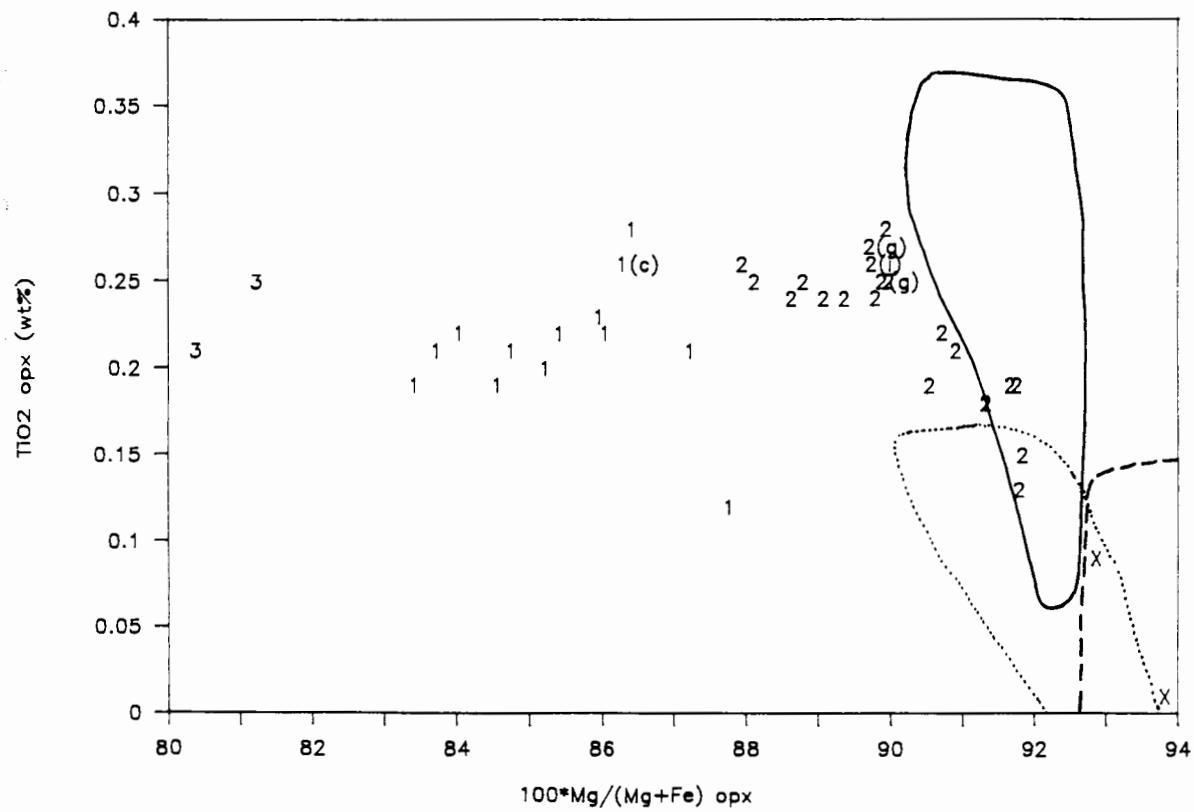

Figure 3.2.9 a and b

Mg# (atomic) versus CaO (wt%) (a) and Cr_2O_3 (wt%) (b) in orthopyroxene megacrysts from Monastery (Jakob, 1977) and orthopyroxene in megacrystalline xenoliths (Moore, 1986) . M = discrete; m = ilmenite association (Jakob, 1977) and R = megacrystalline (Moore, 1986).

Figure 3.2.9 (a)

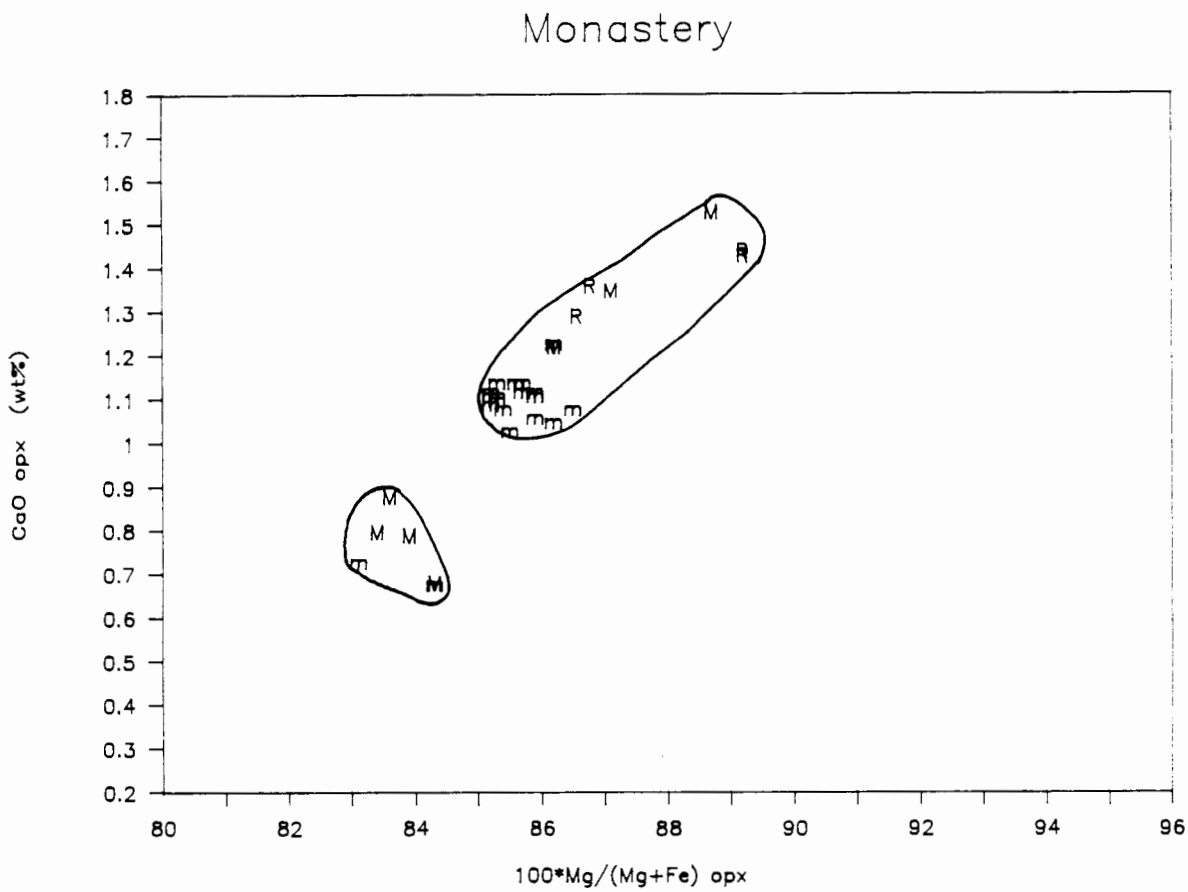

Figure 3.2.9 (b)

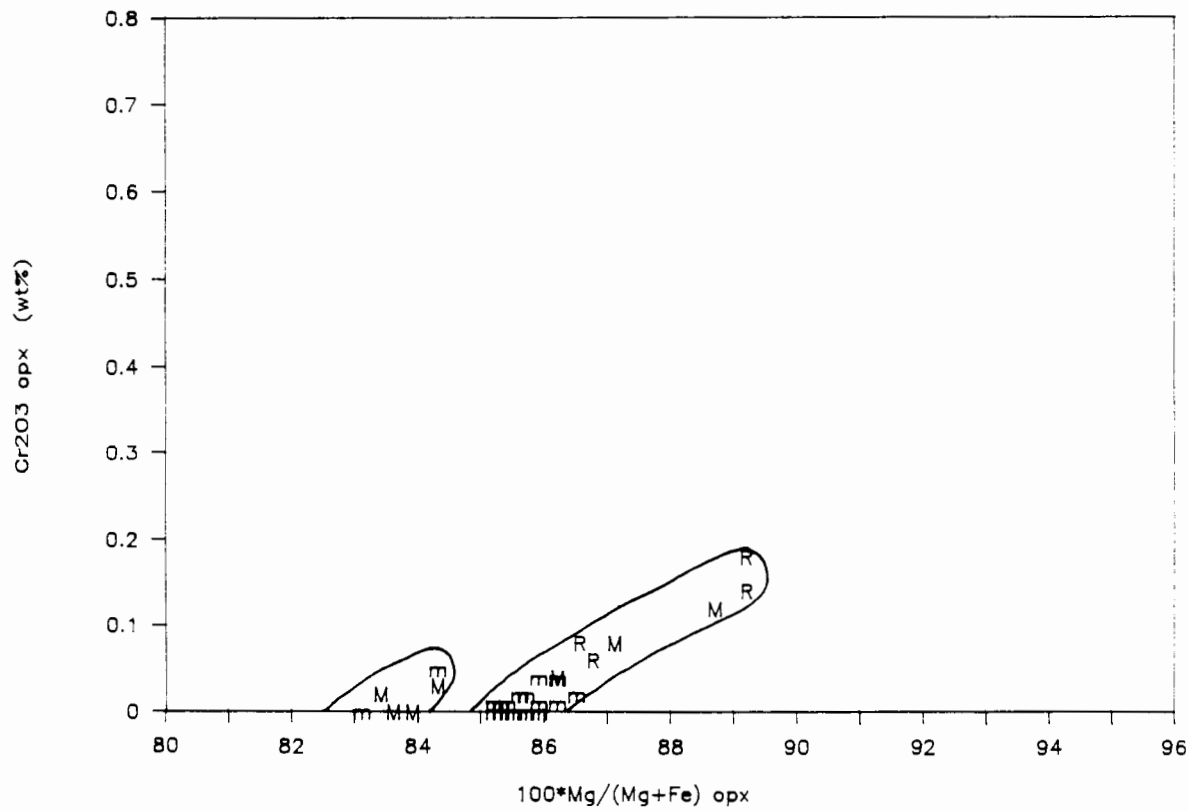

Figure 3.2.10 a and b

Mg# (atomic) versus CaO (wt%) (a) and Cr_2O_3 (wt%) (b) in orthopyroxene megacrysts from Letseng-la-terae (Bloomer and Nixon, 1973) (E = Enstatites; B = bronzites). The compositional fields of orthopyroxene megacrysts from Monastery (Figures 3.2.9 a and b) are shown.

Figure 3.2.10 (a)

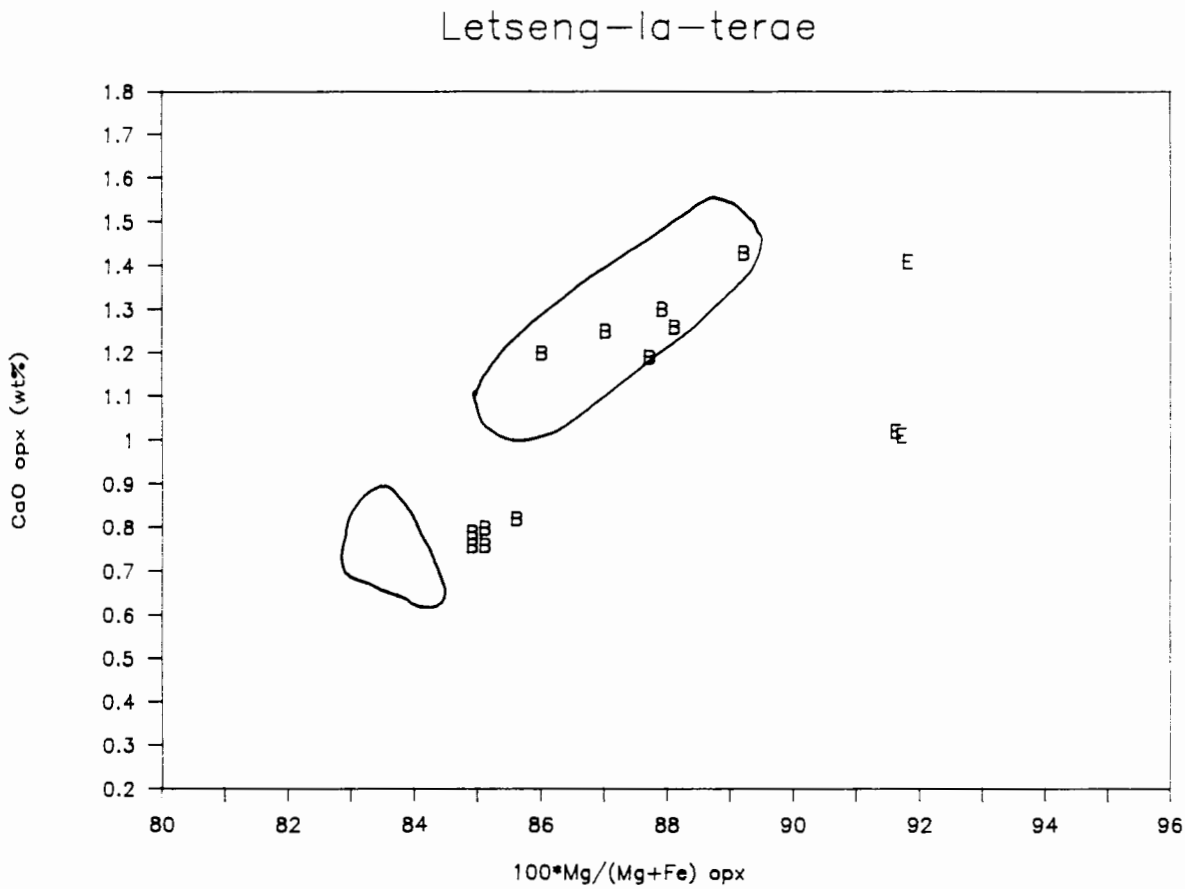

Figure 3.2.10 (b)

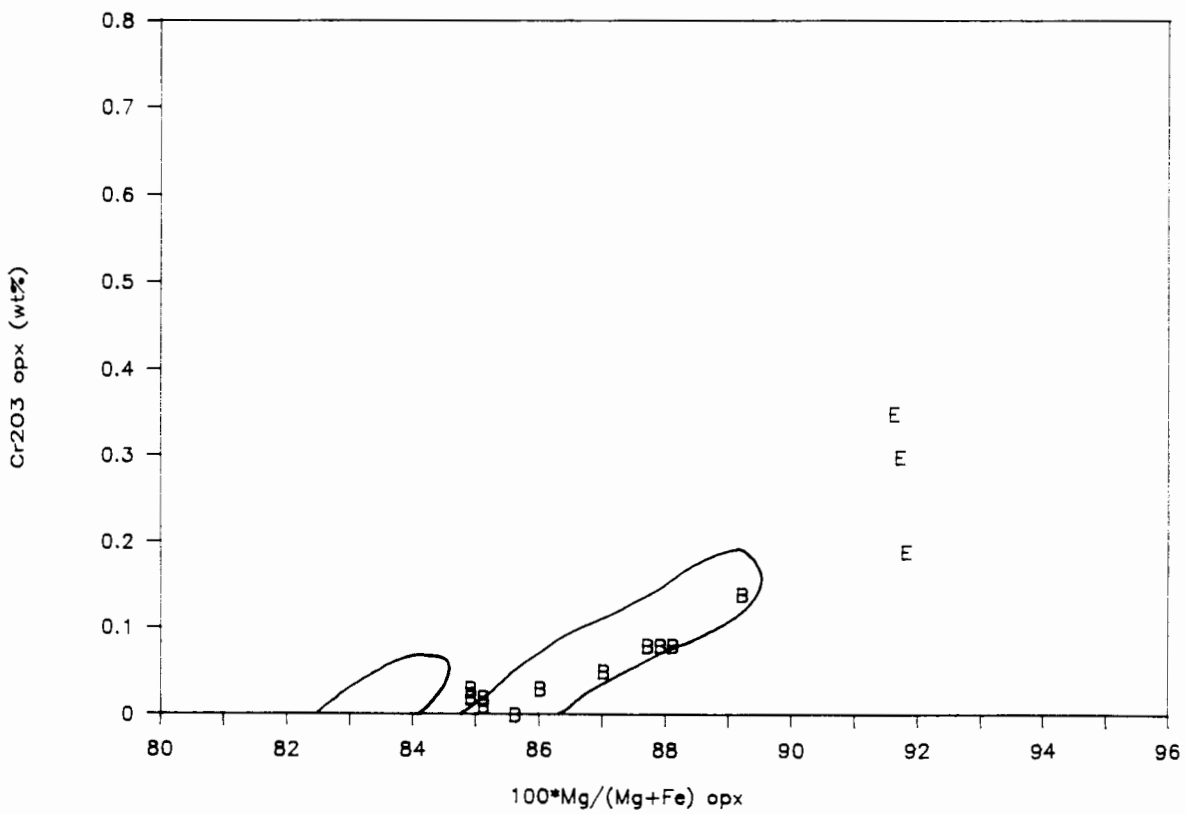

Figure 3.2.11 a and b

Mg# (atomic) versus CaO (wt%) (a) and Cr_2O_3 (wt%) (b) in orthopyroxene megacrysts from Jagersfontein (Hops, 1989). The compositional fields of orthopyroxene megacrysts from Monastery (Figures 3.2.9 a and b) are shown.

Figure 3.2.11 (a)

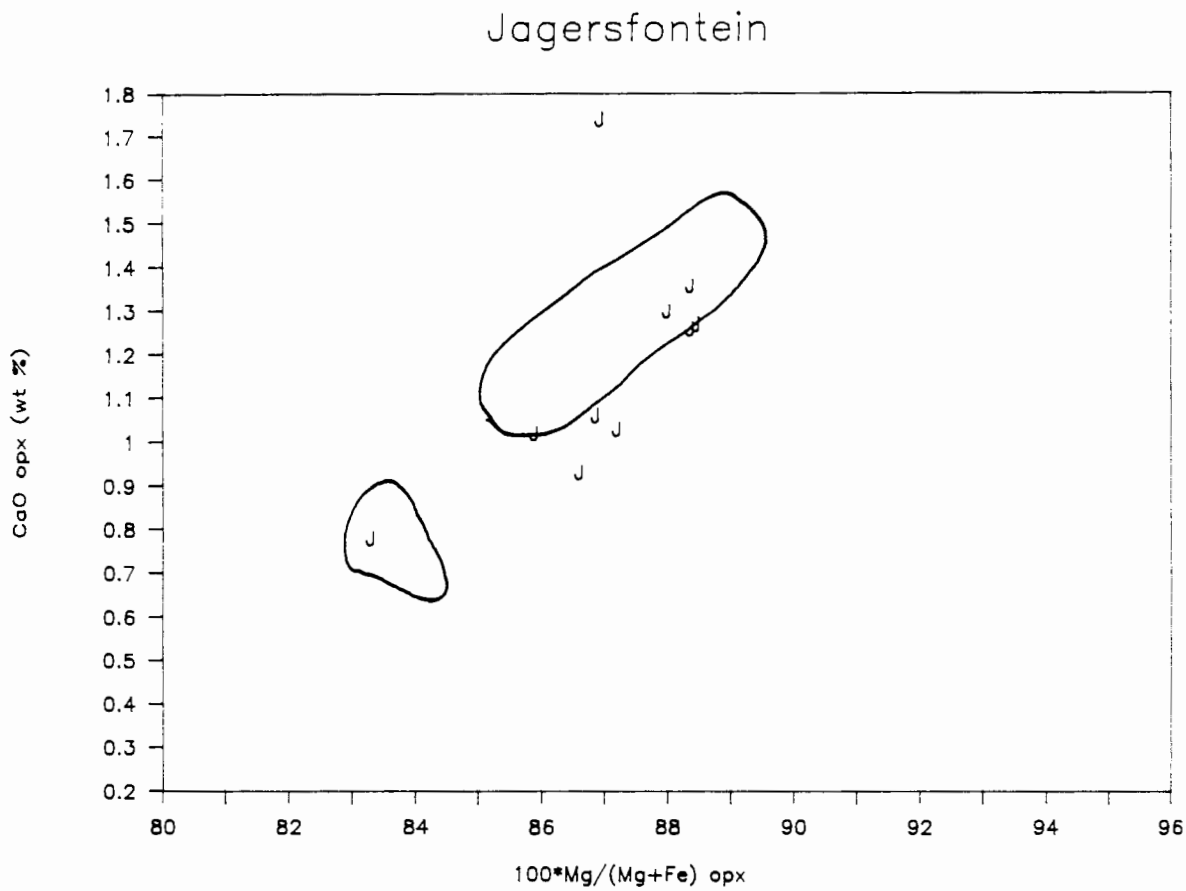

Figure 3.2.11 (b)

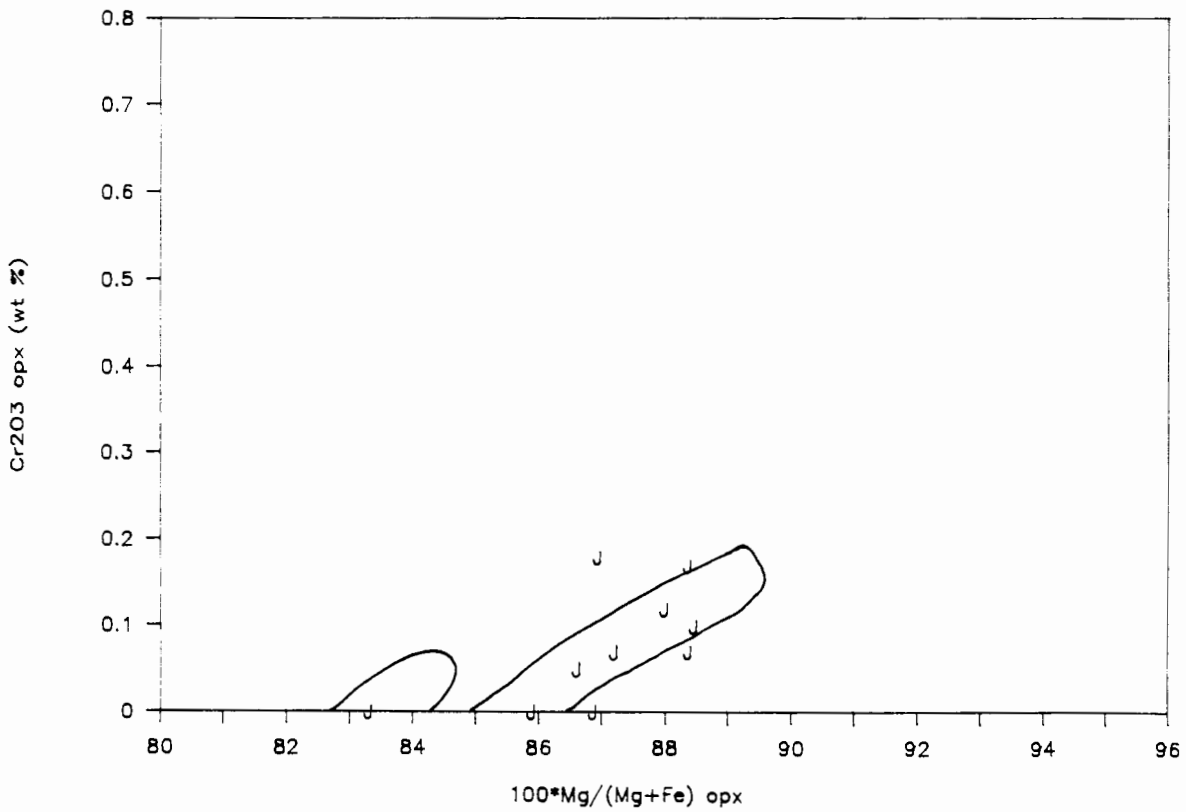

Figure 3.2.12 a and b

Mg# (atomic) versus CaO (wt%) (a) and Cr_2O_3 (wt%) (b) in orthopyroxene megacrysts from the Eastern Griqualand kimberlites (Boyd, unpublished data). R = Ramatseliso; A = Abbotsford; Z = Zeekoegat. The compositional fields of orthopyroxene megacrysts from Monastery (Figures 3.2.9 a and b) are shown.

Figure 3.2.12 (a)

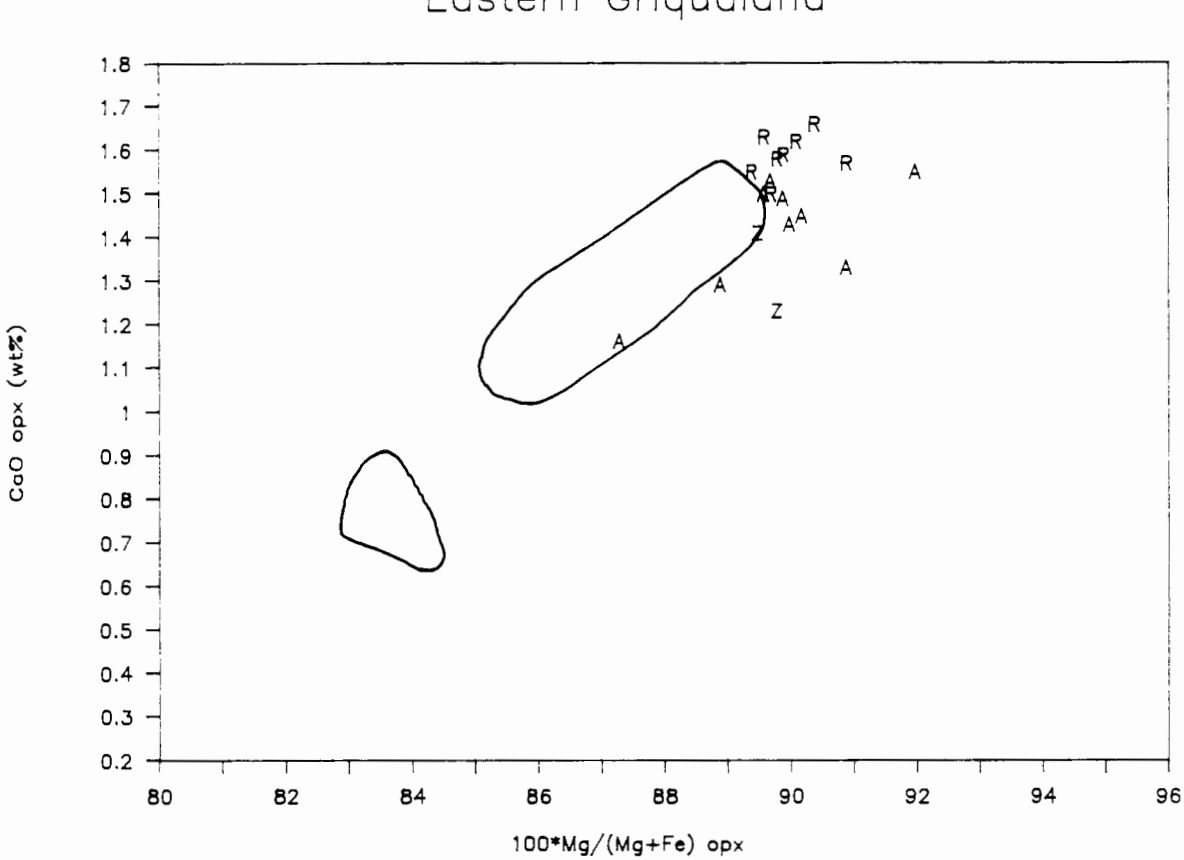

Figure 3.2.12 (b)

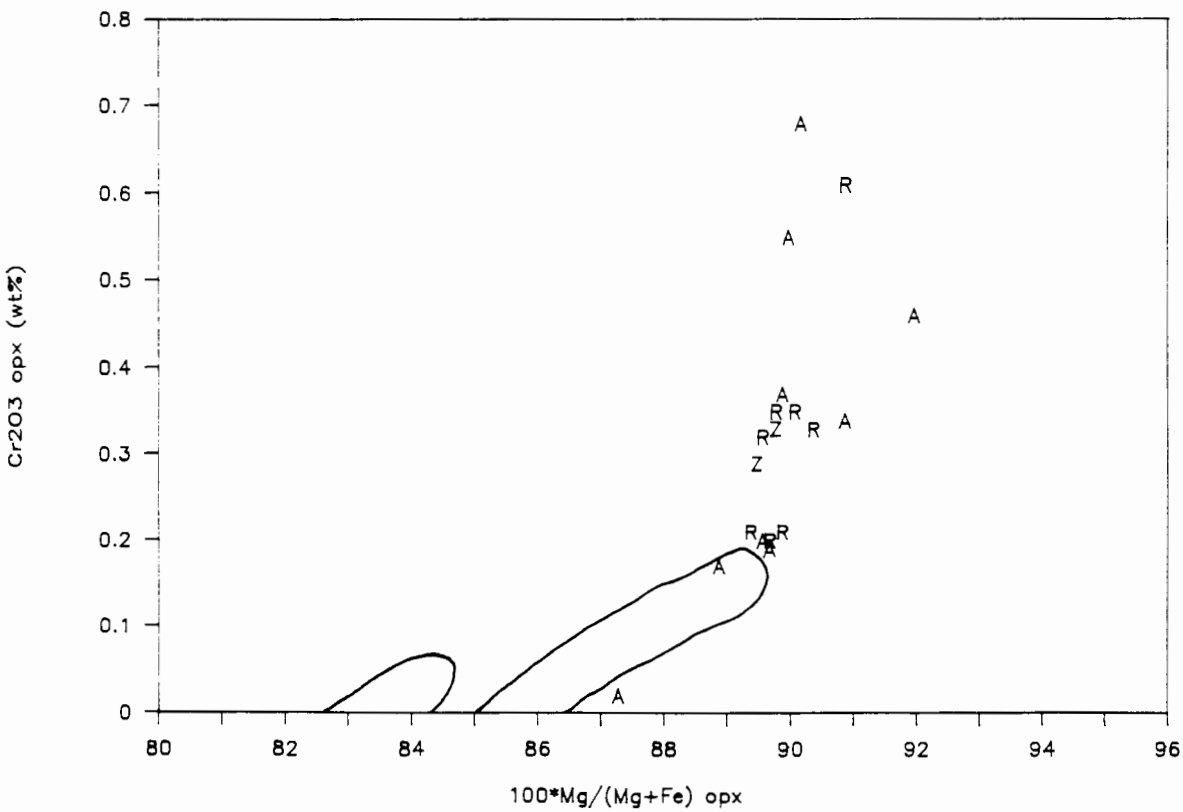

Figure 3.2.13 a and b

Mg# (atomic) versus CaO (wt%) (a) and Cr_2O_3 (wt%) (b) in orthopyroxene megacrysts from Hamilton Branch (Schulze, 1982b). The compositional fields of orthopyroxene megacrysts from Monastery (Figures 3.2.9 a and b) are shown.

Figure 3.2.13 (a)

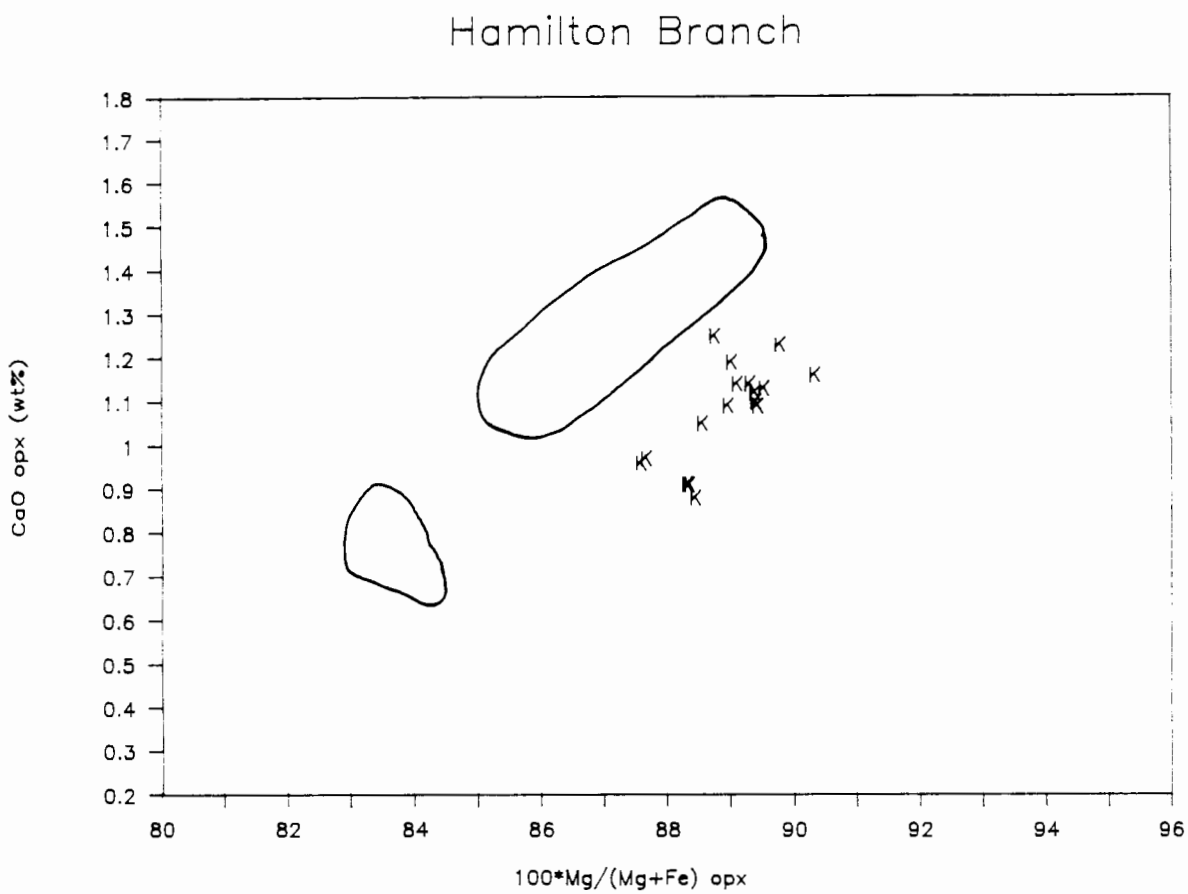

Figure 3.2.13 (b)

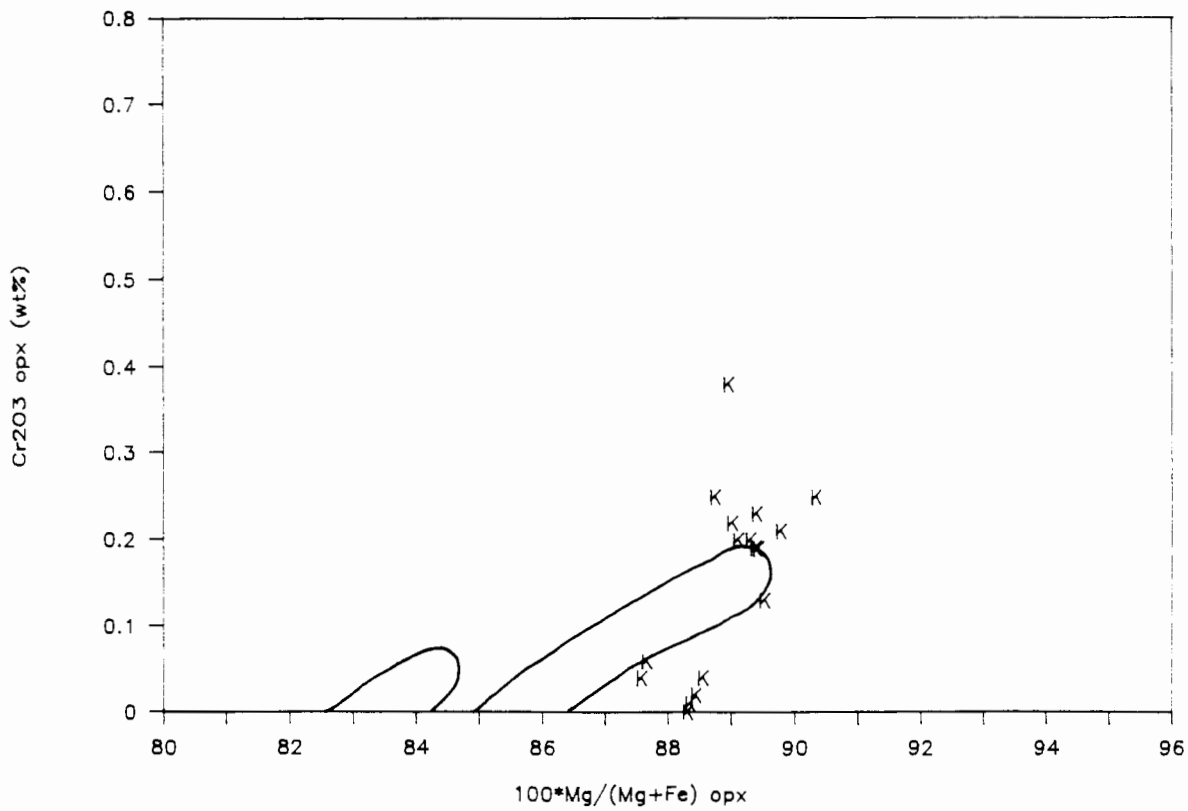

Figure 3.2.14 a and b

Mg# (atomic) versus CaO (wt%) (a) and Cr_2O_3 (wt%) (b) in orthopyroxene megacrysts from Sloan-Nix (Eggler, unpublished data). S = Cr-poor discrete; s = Cr-poor as inclusions; C = Cr-rich; c = Cr-rich as inclusions. The compositional fields of orthopyroxene megacrysts from Monastery (Figures 3.2.9 a and b) are shown.

Figure 3.2.14 (a)

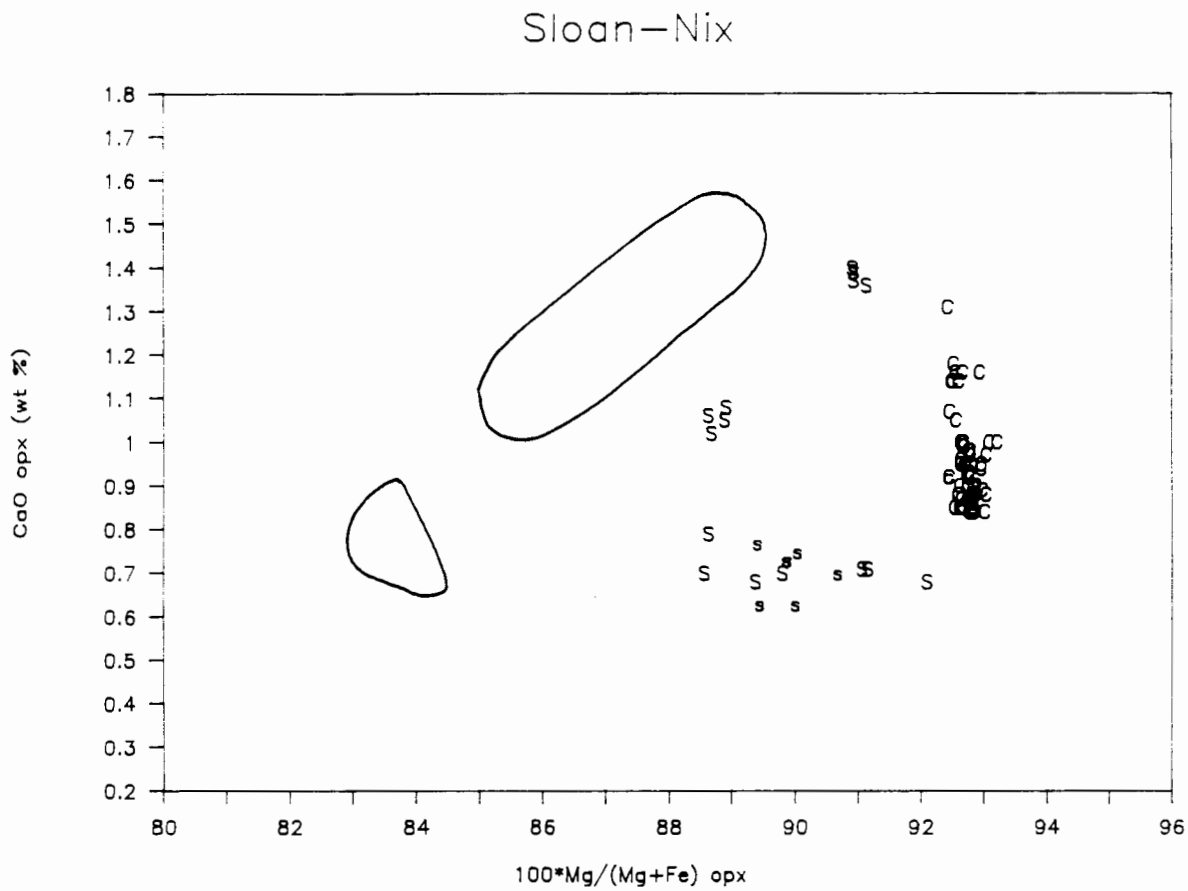

Figure 3.2.14 (b)

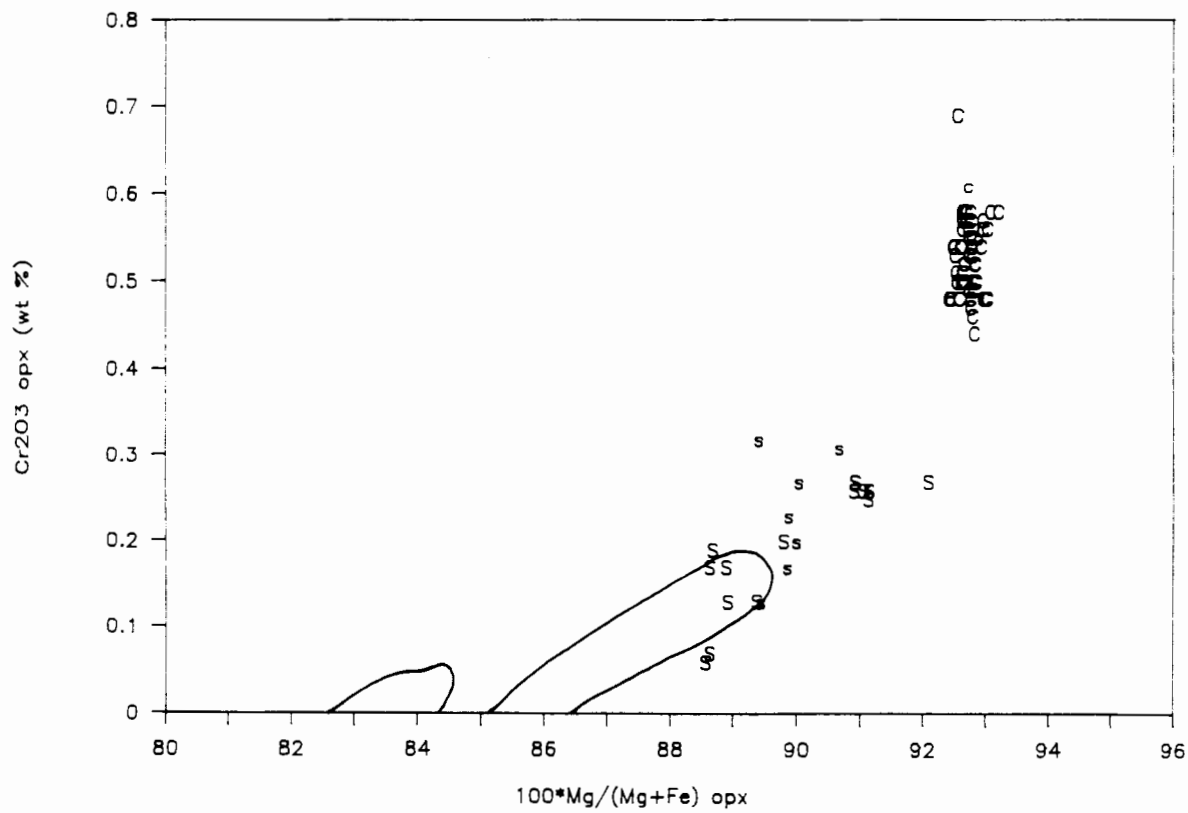

Figure 3.2.15 a and b

Mg# (atomic) versus CaO (wt%) (a) and Cr_2O_3 (wt%) (b) in orthopyroxene megacrysts from Schuller. Outlined field show compositional spreads from Monastery (solid line; Figures 3.2.9 a and b) and Sloan-Nix (stippled line; Figures 3.2.14 a and b).

Figure 3.2.15 (a)

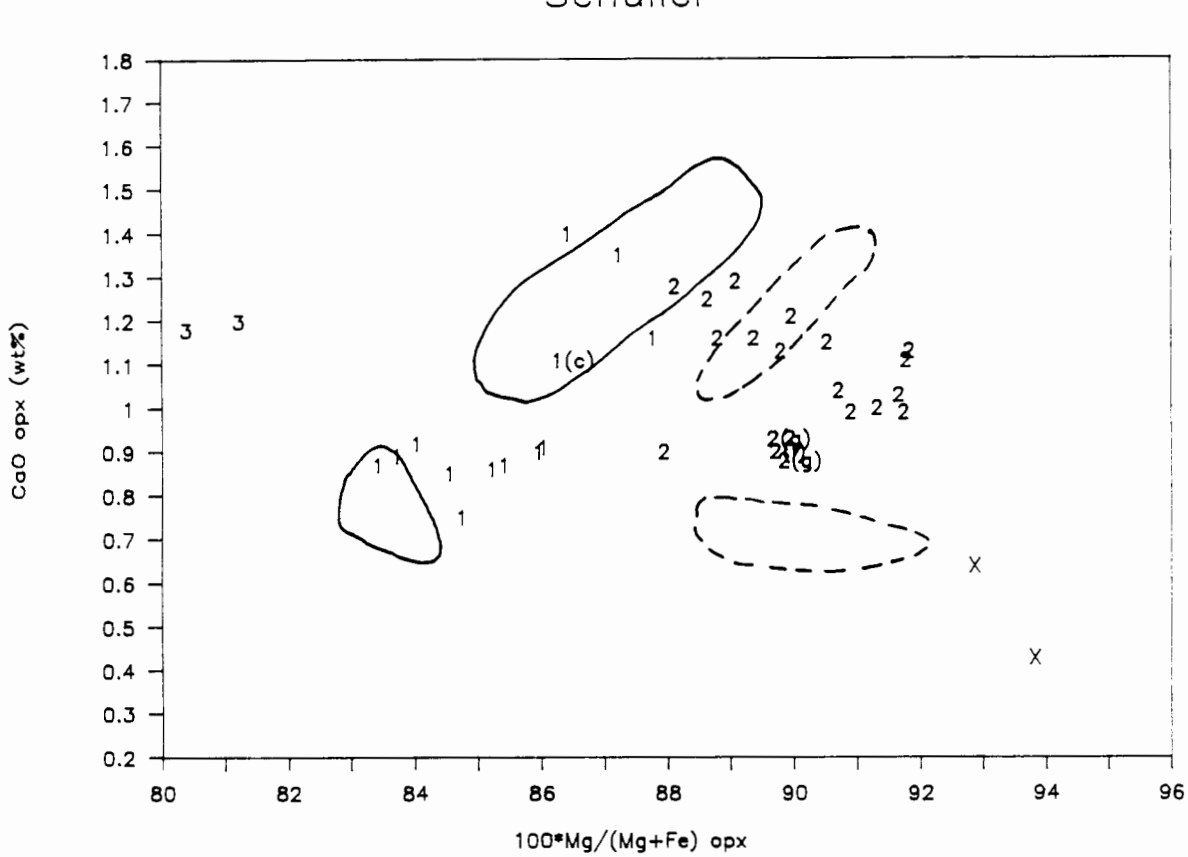

Figure 3.2.15 (b)

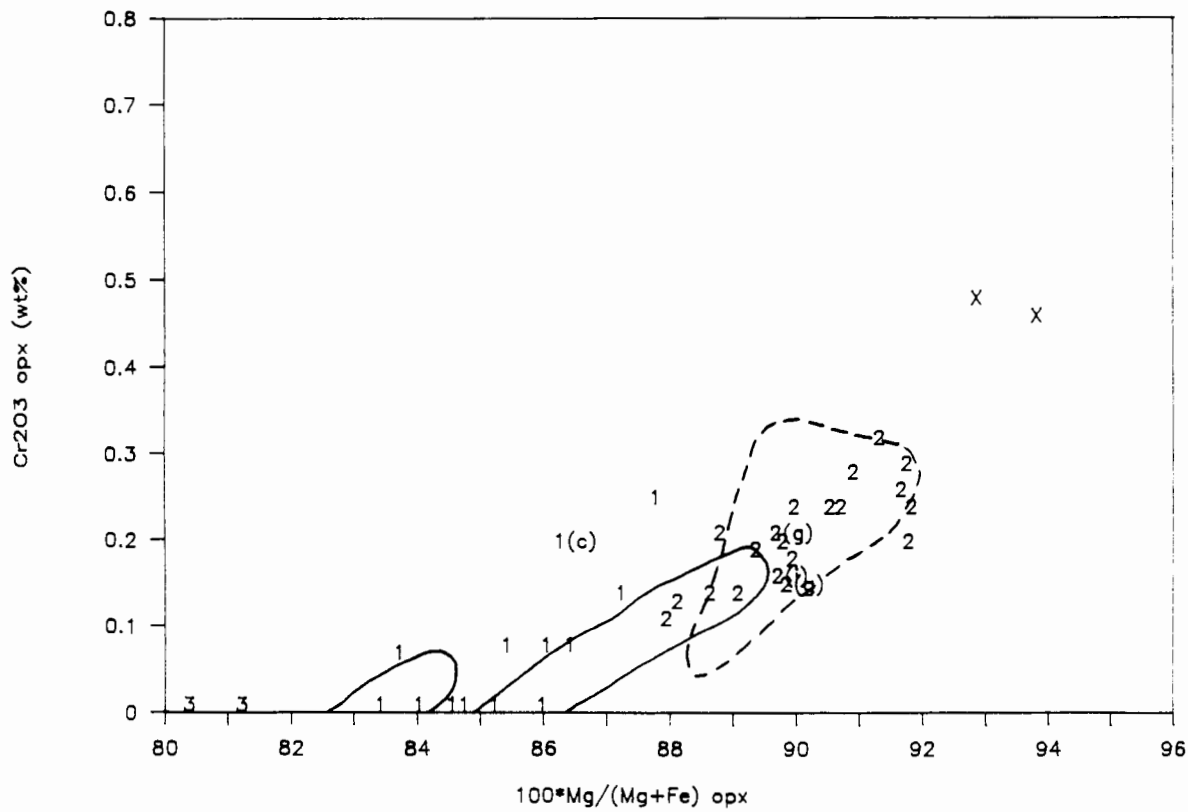

Figure 3.3.1

Mg# (atomic) versus CaO (wt%) in garnet megacrysts from the Schuller kimberlite where 1 = Fe-rich discrete megacryst; 2 = Mg-rich discrete megacryst, 3 = Calcic garnets and O = garnet inclusions in orthopyroxene megacrysts.

Figure 3.3.2

Mg# (atomic) versus Cr_2O_3 (wt%) in garnet megacrysts from the Schuller kimberlite. Symbols as in Figure 3.3.1

Figure 3.3.1

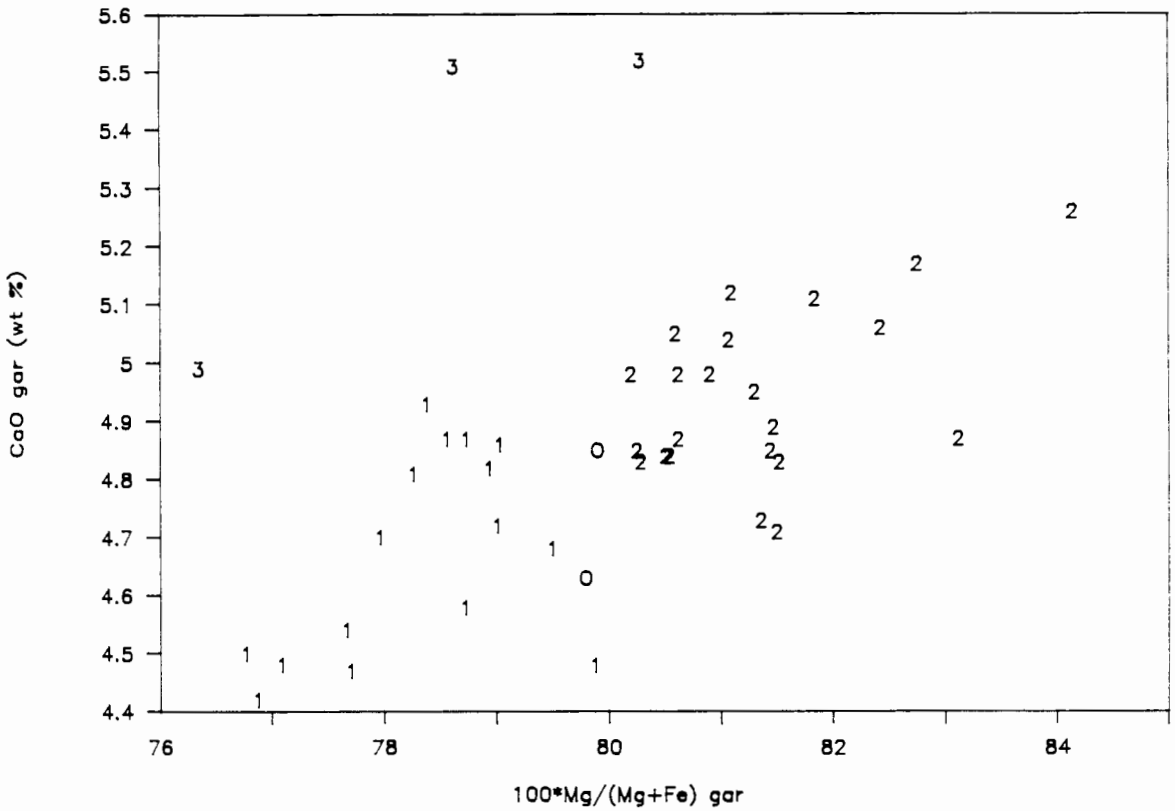

Figure 3.3.2

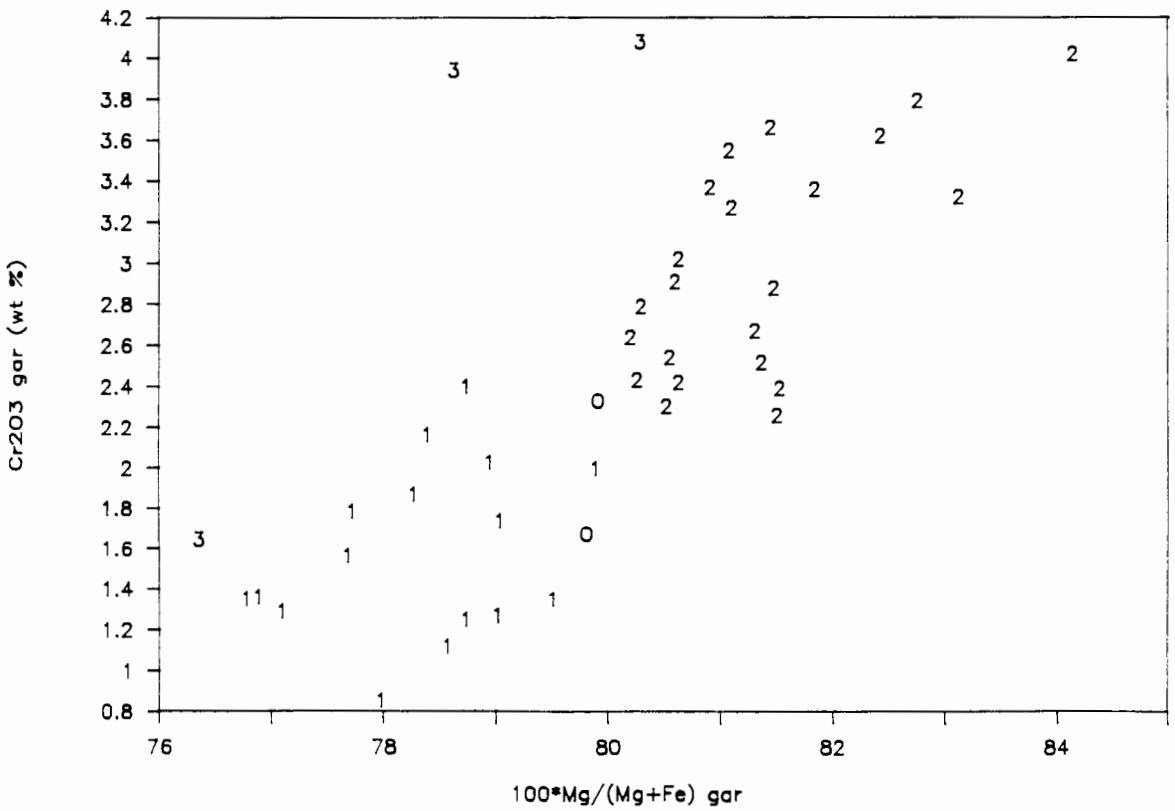

Figure 3.3.3

Mg# (atomic) versus TiO_2 (wt%) in garnet megacrysts from the Schuller kimberlite. Symbols as in Figure 3.3.1

Figure 3.3.4

Mg# (atomic) versus Na_2O (wt%) in garnet megacrysts from the Schuller kimberlite. Symbols as in Figure 3.3.1

Figure 3.3.3

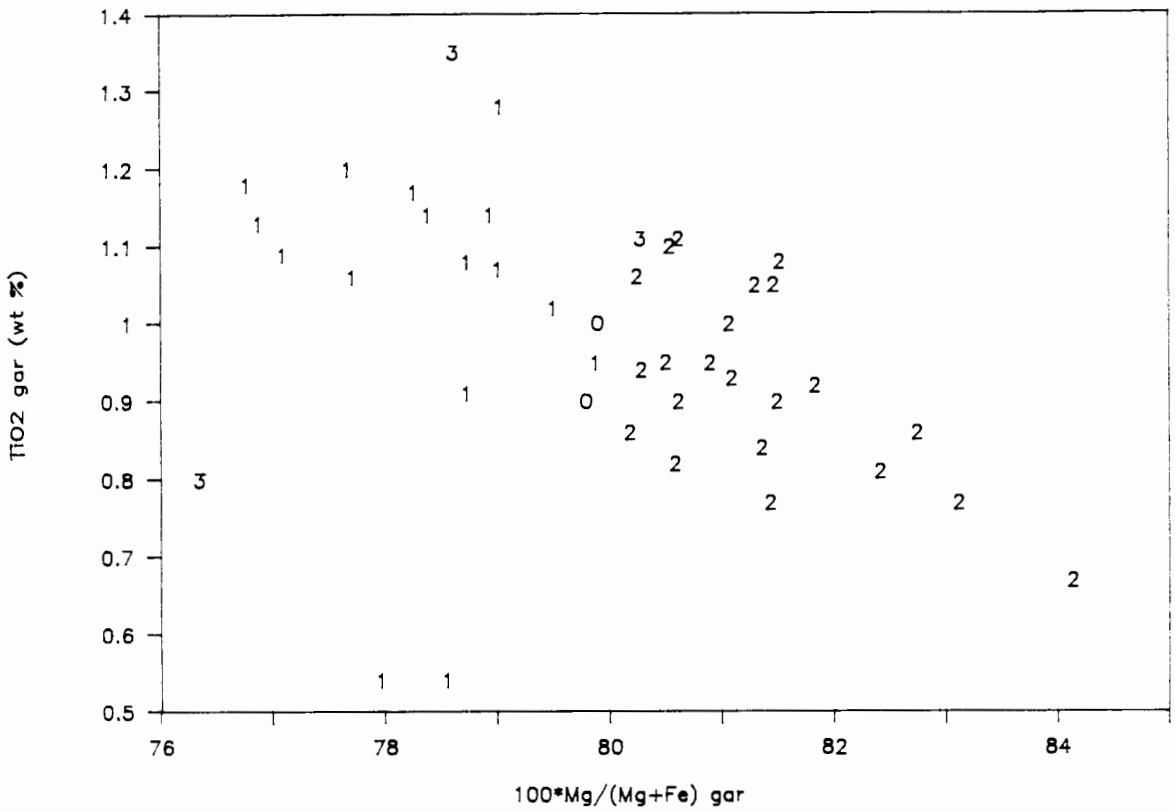

Figure 3.3.4

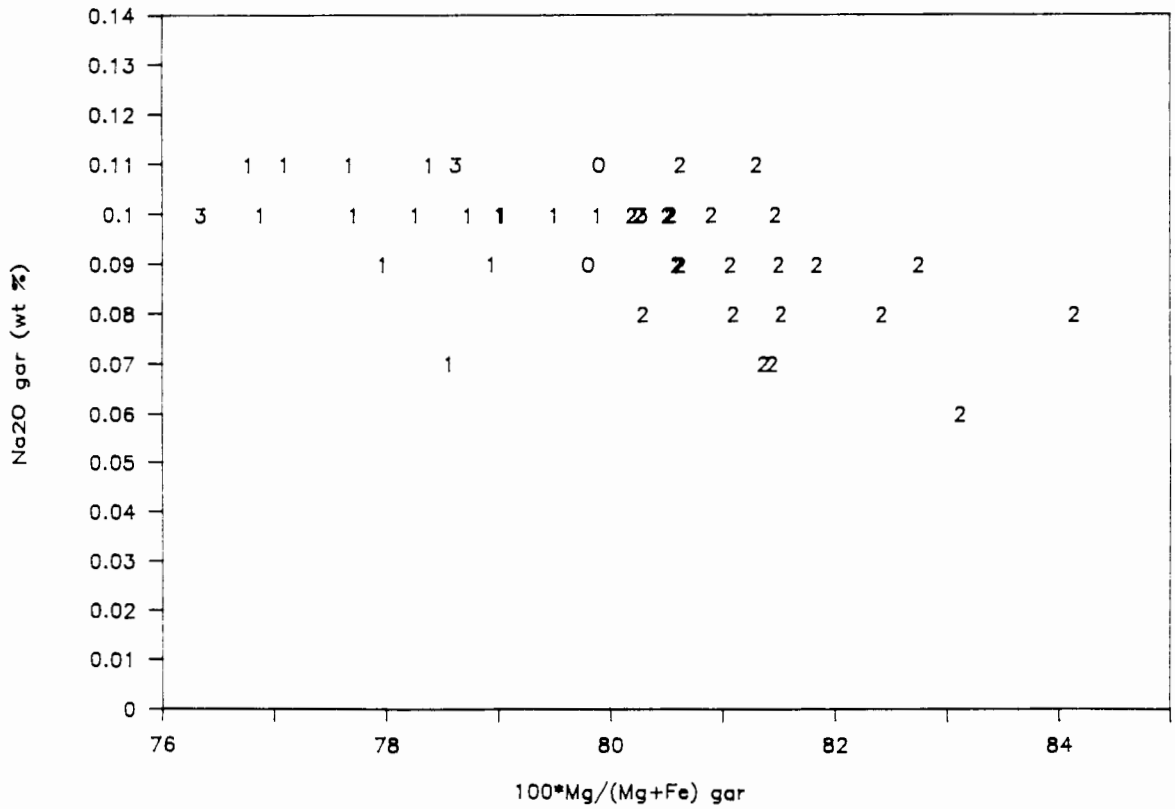

Figure 3.3.5

Mg# (atomic) versus Cr_2O_3 (wt%) in garnet megacrysts from the Schuller kimberlite and the compositional fields of garnets in deformed (solid line) and coarse (broken line) garnet lherzolites from Premier (Boyd, unpublished data) and coarse garnet lherzolites from Schuller (stippled) (de Bruin, unpublished data). Symbols for megacrysts as in Figure 3.3.1

Figure 3.3.6

Mg# (atomic) versus TiO_2 (wt%) in garnet megacrysts from the Schuller kimberlite and the compositional fields of garnets in deformed (solid line) and coarse (broken line) garnet lherzolites from Premier (Boyd, unpublished data) and coarse garnet lherzolites from Schuller (stippled) (de Bruin, unpublished data). Symbols for megacrysts as in Figure 3.3.1

Figure 3.3.5

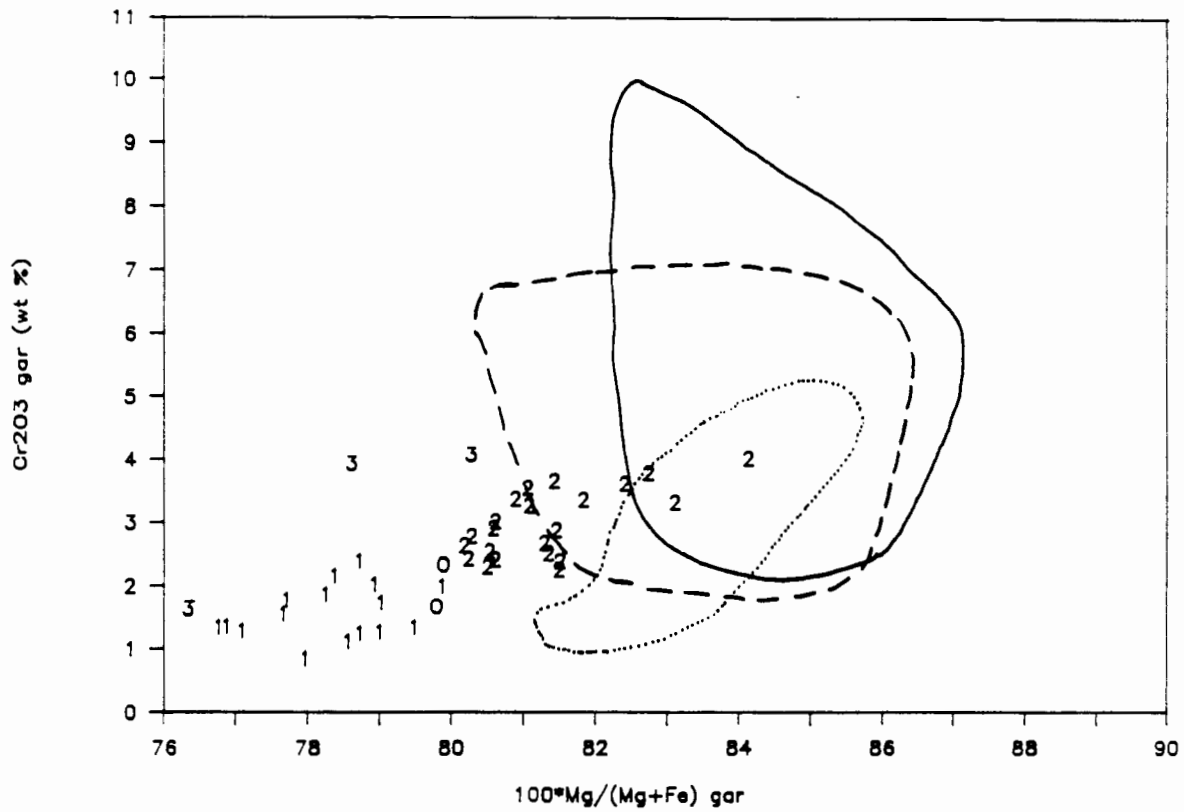

Figure 3.3.6

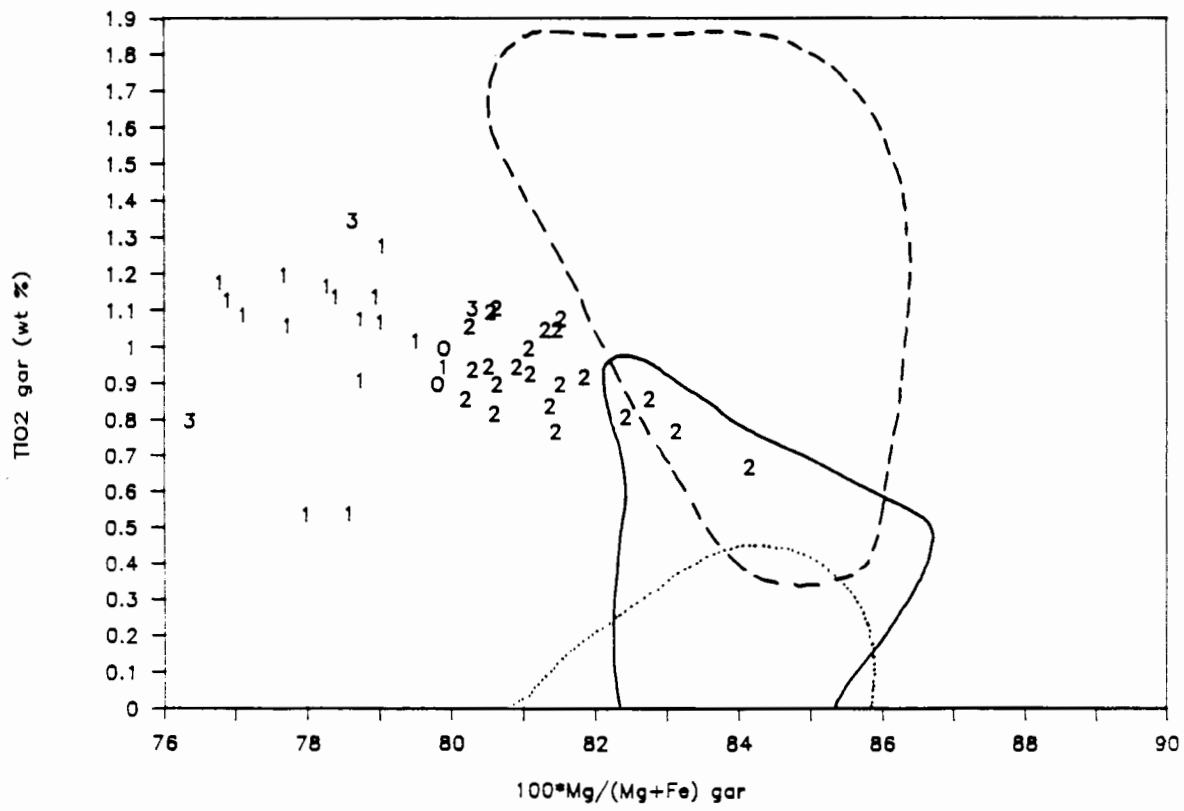

Figure 3.3.7 a and b

Ca# (atomic) versus Mg# (atomic) (a) and Cr_2O_3 (wt%) (b) in garnet megacrysts from Monastery (Jakob, 1977). M = discrete; i = association with ilmenite. Note that two samples (m) plot at much higher Cr_2O_3 in Figure (a) which might indicate that two separate trends are present.

Figure 3.3.7 (a)

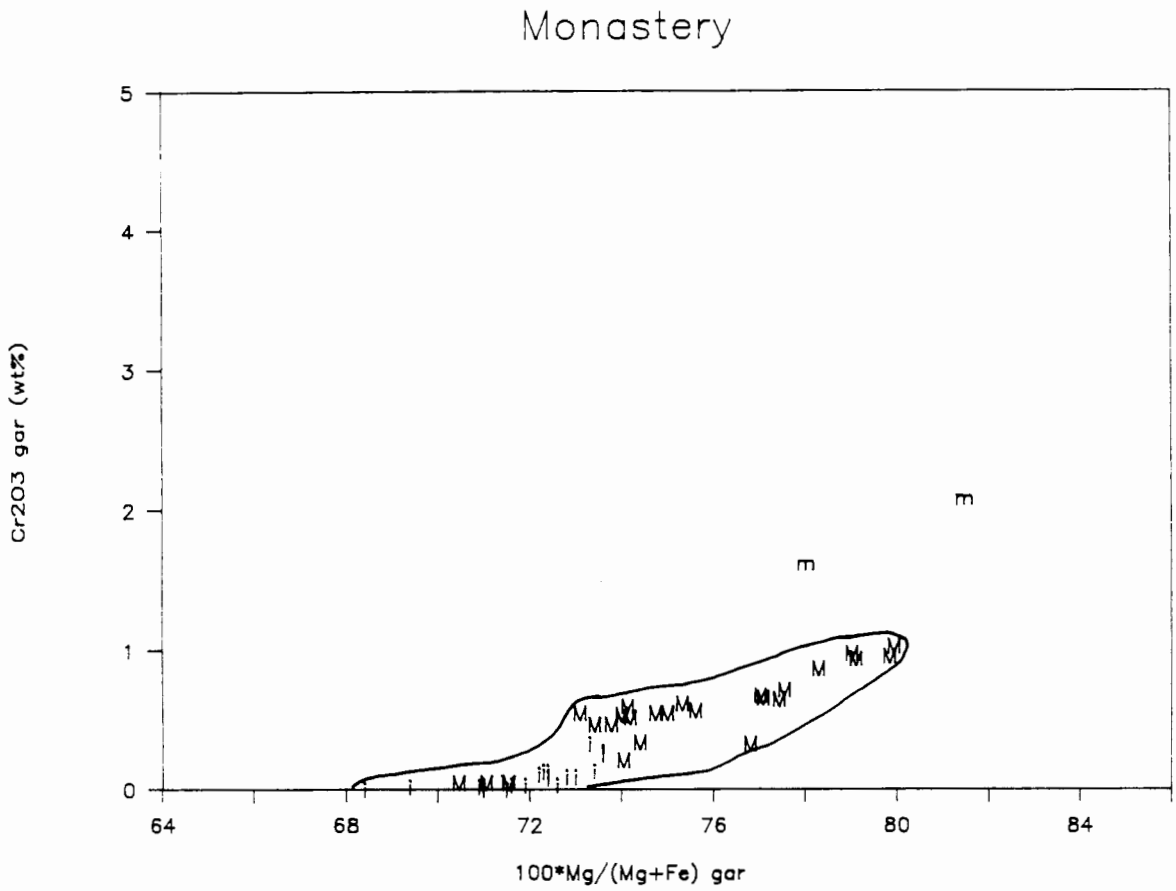

Figure 3.3.7 (b)

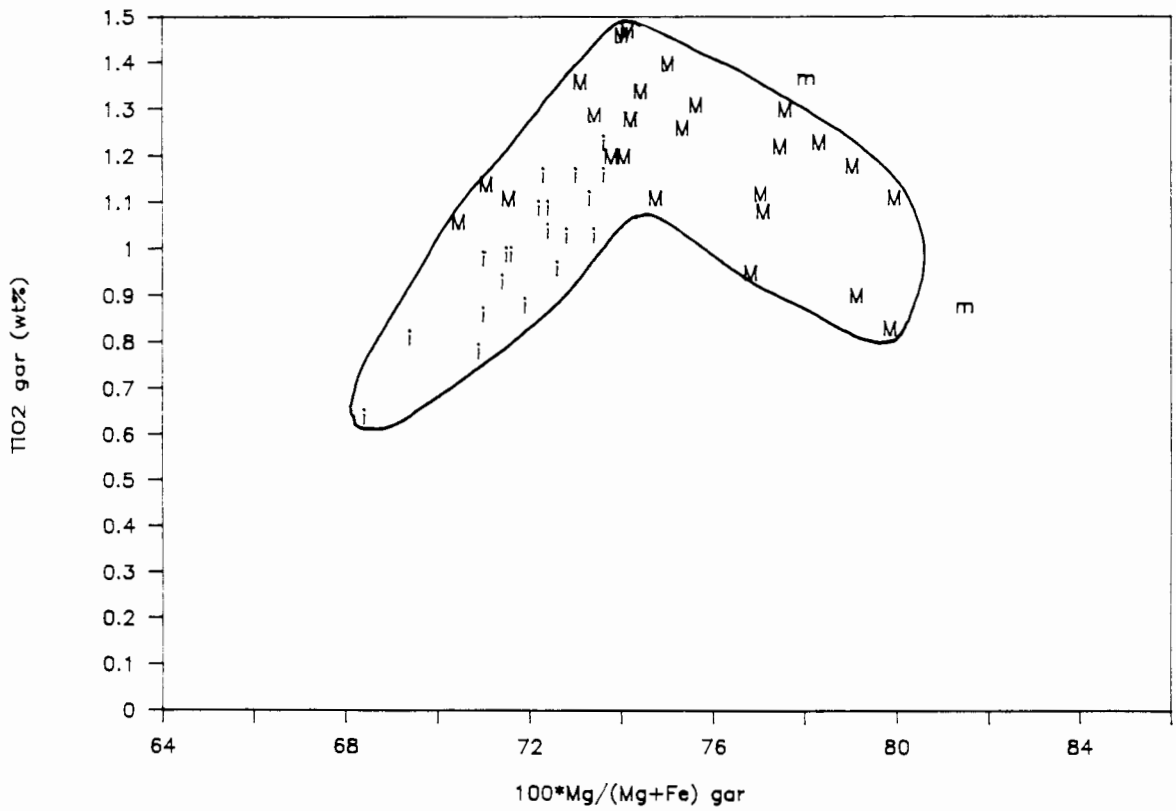

Figure 3.3.8 a and b

Ca# (atomic) versus Mg# (atomic) (a) and Cr_2O_3 (wt%) (b) in garnet megacrysts from Jagersfontein (Hops, 1989). J = discrete; j = as inclusions in another megacryst phase. The outlined field shows the compositional spread of the Cr-poor garnets from Monastery as shown in Figures 3.3.7 a and b).

Figure 3.3.8 (a)

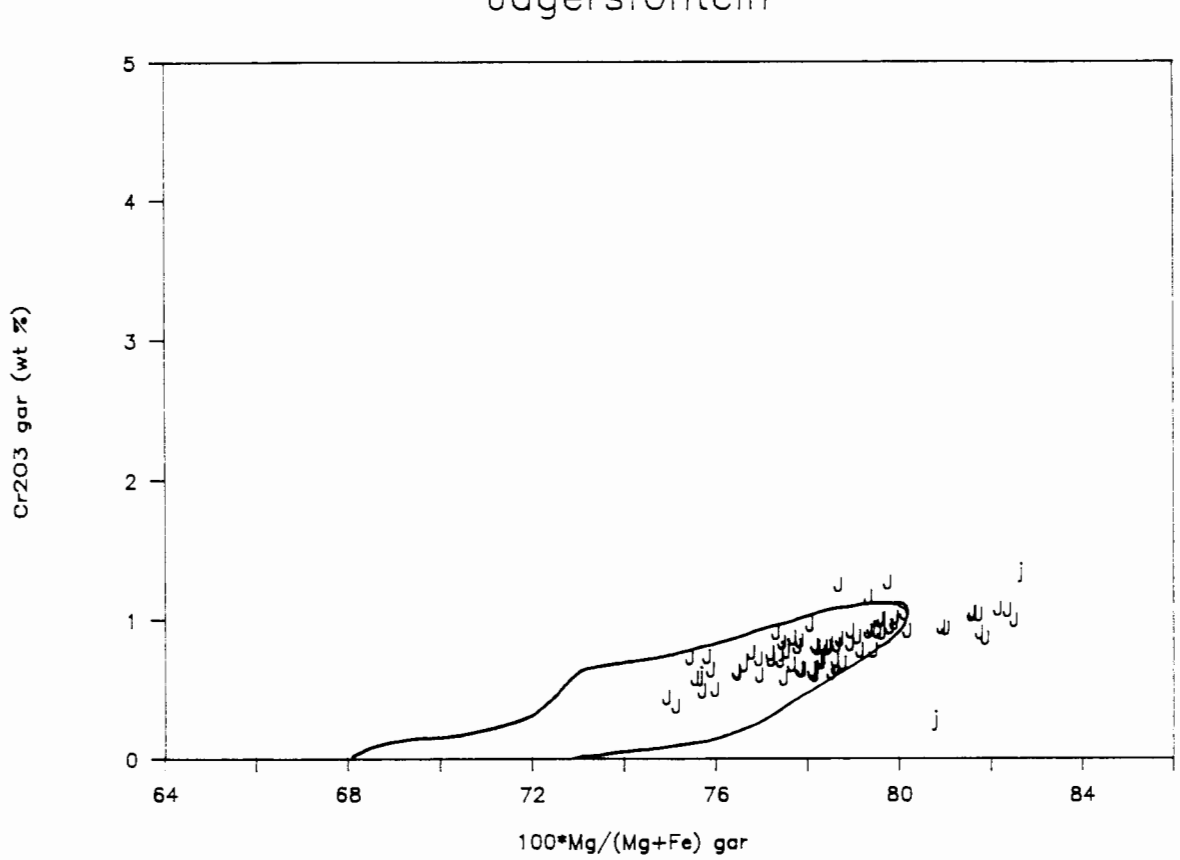

Figure 3.3.8 (b)

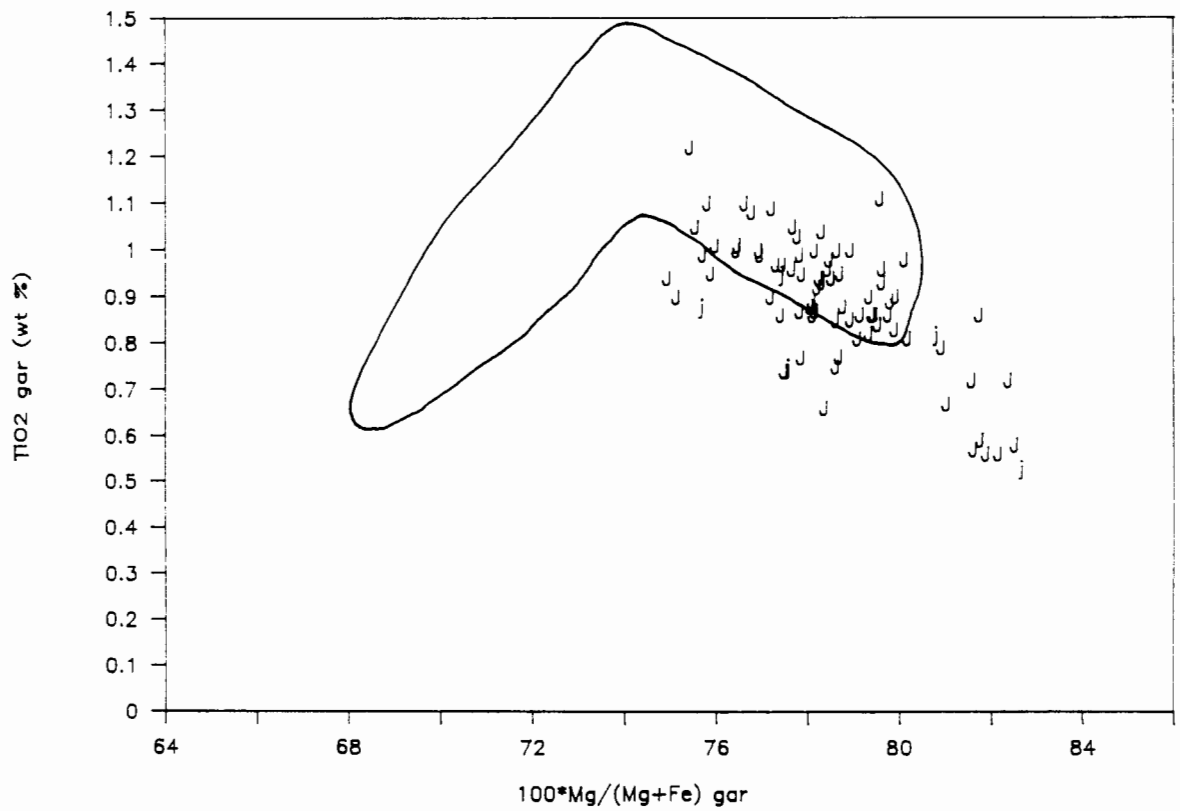

Figure 3.3.9 a and b

Ca# (atomic) versus Mg# (atomic) (a) and Cr_2O_3 (wt%) (b) in garnet megacrysts from Lekkerfontein (Robey, 1981). The outlined field shows the compositional spread of the Cr-poor garnets from Monastery as shown in Figures 3.3.7 a and b).

Figure 3.3.9 (a)

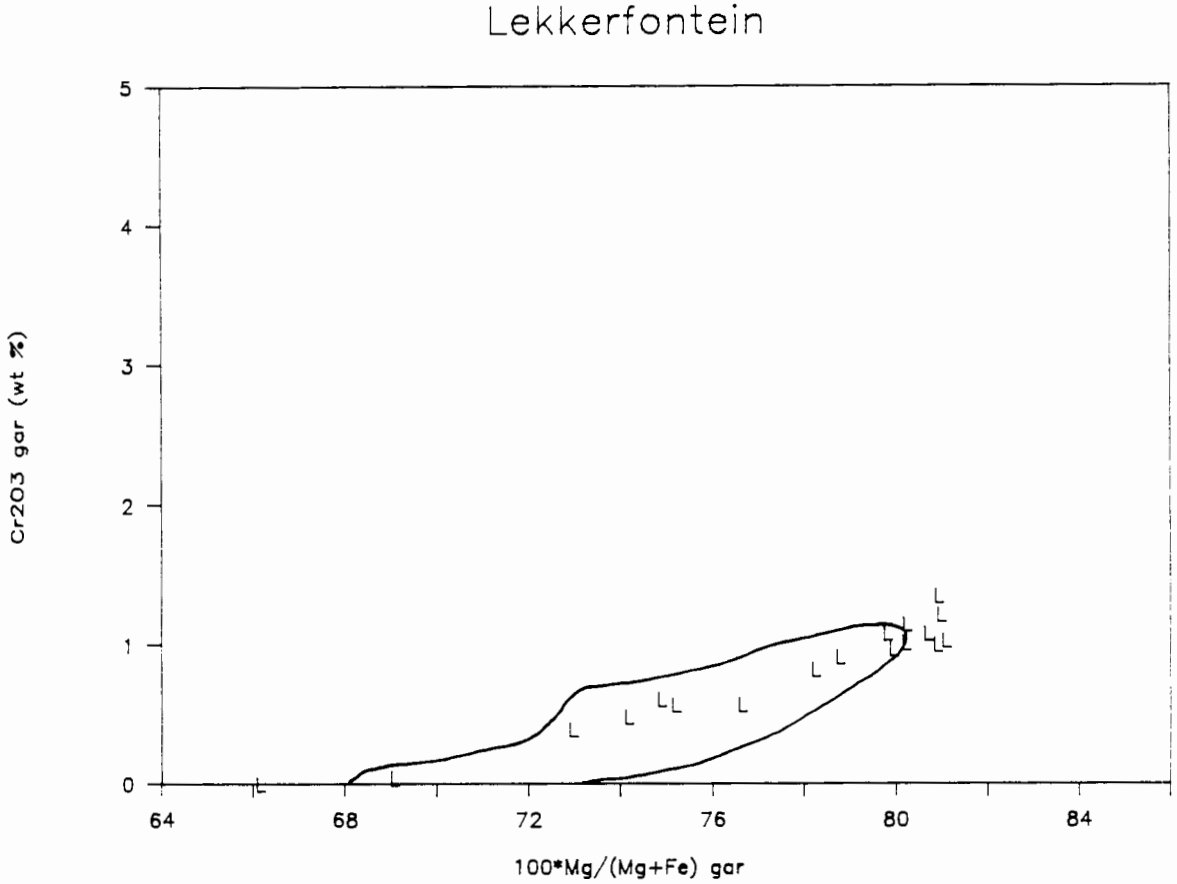

Figure 3.3.9 (b)

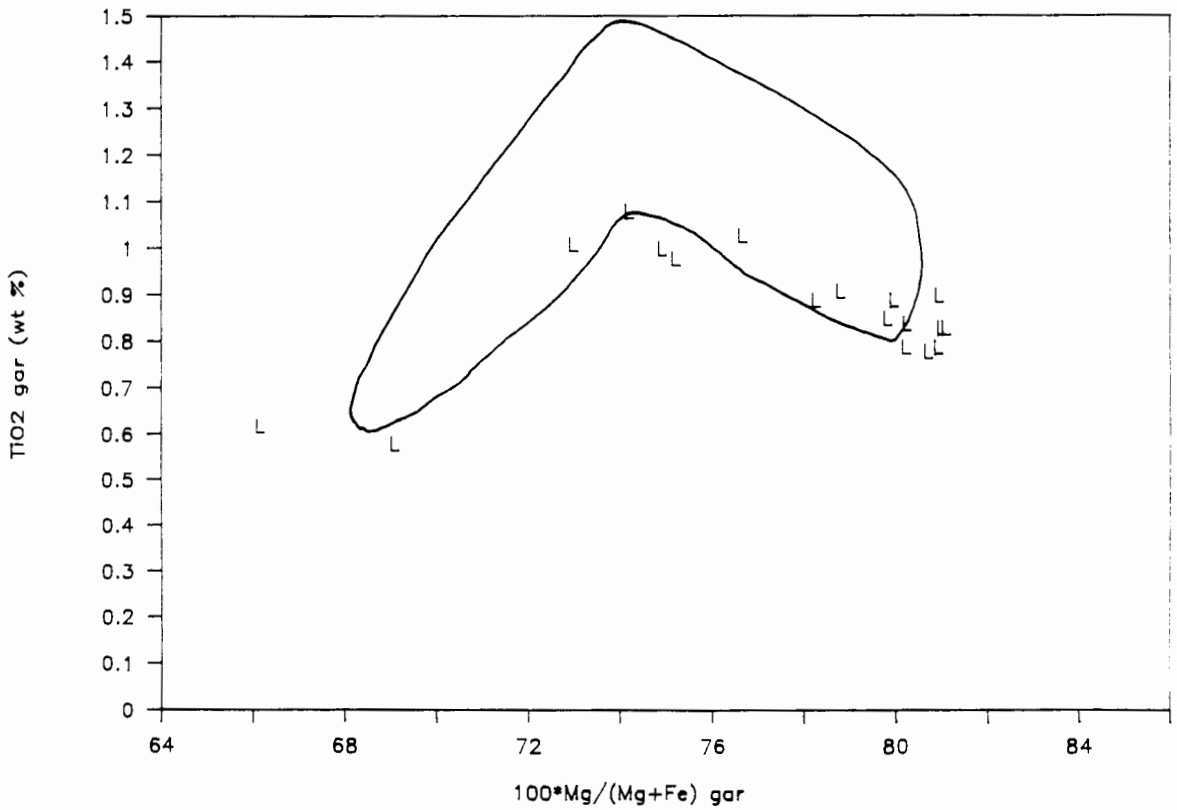

Figure 3.3.10 a and b

Ca# (atomic) versus Mg# (atomic) (a) and Cr_2O_3 (wt%) (b) in garnet megacrysts from Orapa (Shee, 1978; Tollo, 1982). O = data from Shee; o = data from Tollo. The outlined field shows the compositional spread of the Cr-poor garnets from Monastery as shown in Figures 3.3.7 a and b).

Figure 3.3.10 (a)

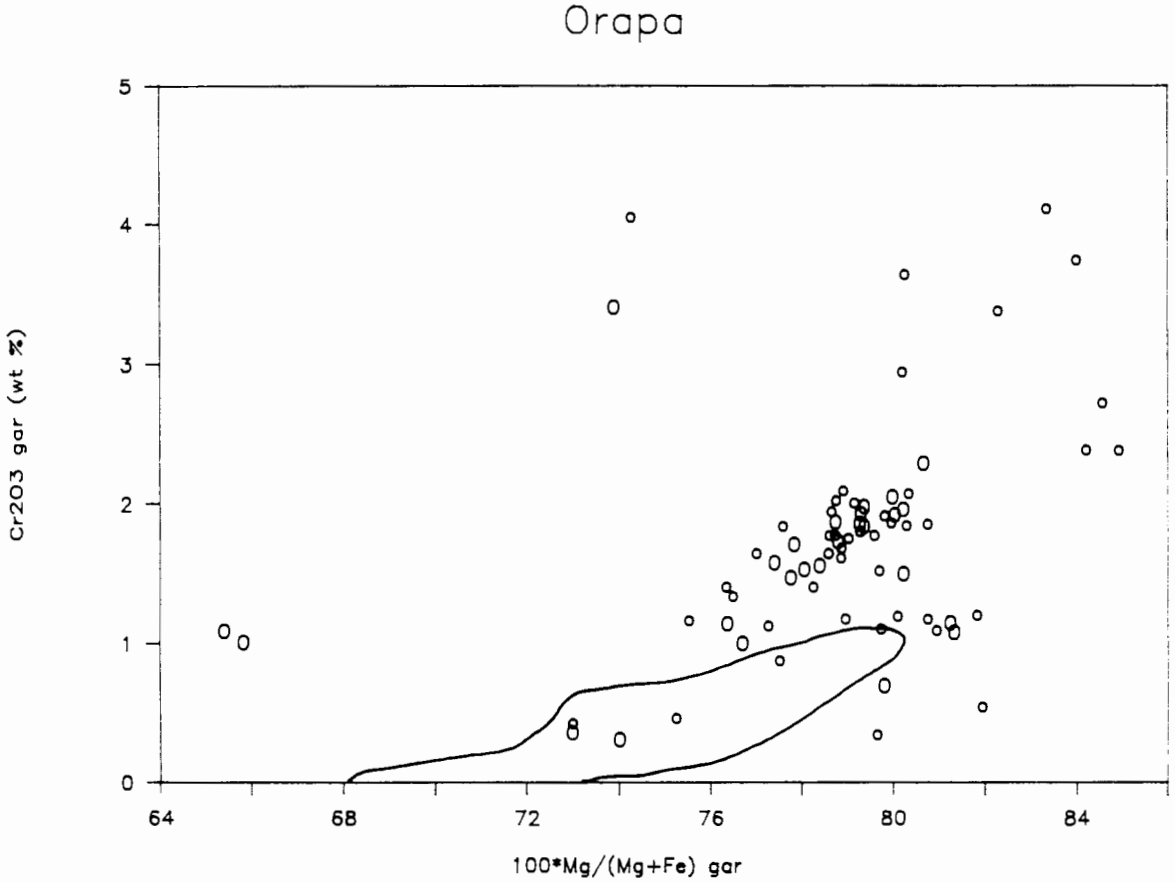

Figure 3.3.10 (b)

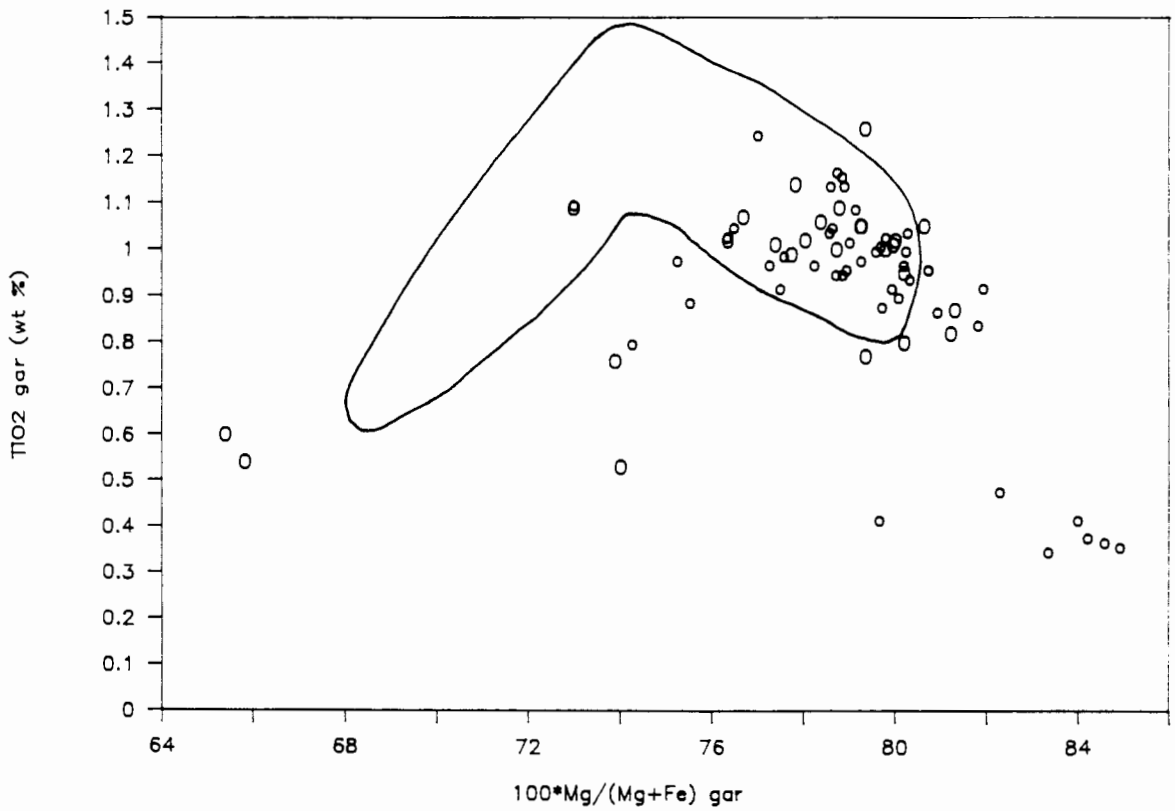

Figure 3.3.11 a and b

Ca# (atomic) versus Mg# (atomic) (a) and Cr_2O_3 (wt%) (b) in garnet megacrysts from Iron Mountain (Smith, 1977). I = discrete; i = ilmenite association. The outlined field shows the compositional spread of the Cr-poor garnets from Monastery as shown in Figures 3.3.7 a and b).

Figure 3.3.11 (a)

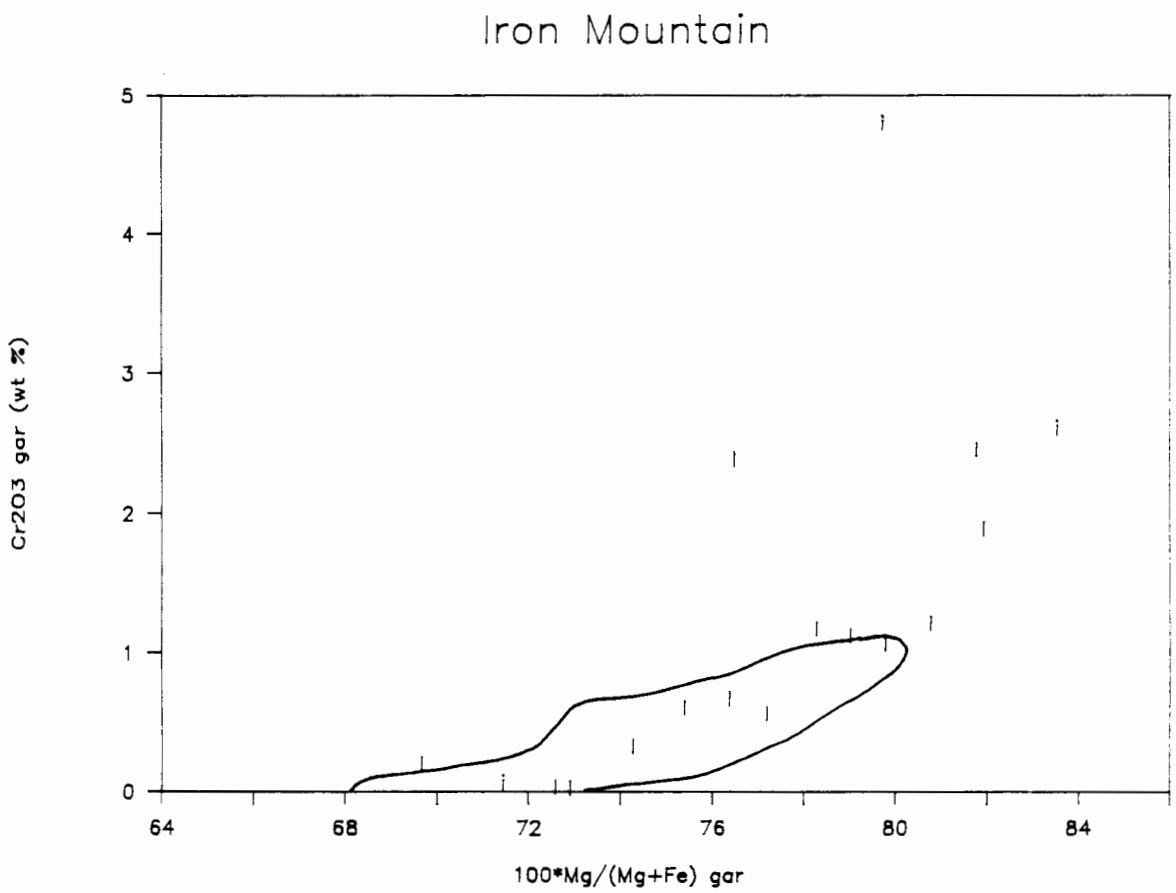

Figure 3.3.11 (b)

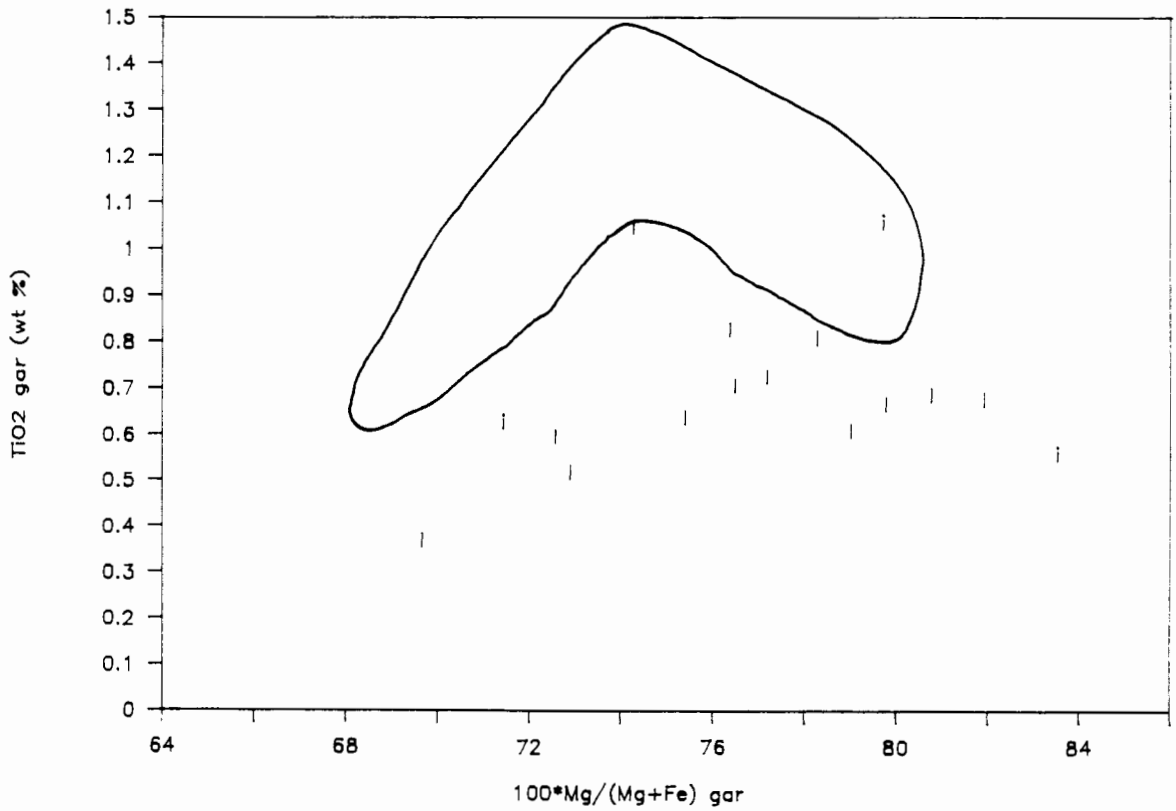

Figure 3.3.12 a and b

Ca# (atomic) versus Mg# (atomic) (a) and Cr_2O_3 (wt%) (b) in Cr-poor garnet megacrysts from Sloan-Nix (Eggler, unpublished data). S = discrete; s = inclusions. The outlined field shows the compositional spread of the Cr-poor garnets from Monastery as shown in Figures 3.3.7 a and b).

Figure 3.3.12 (a)

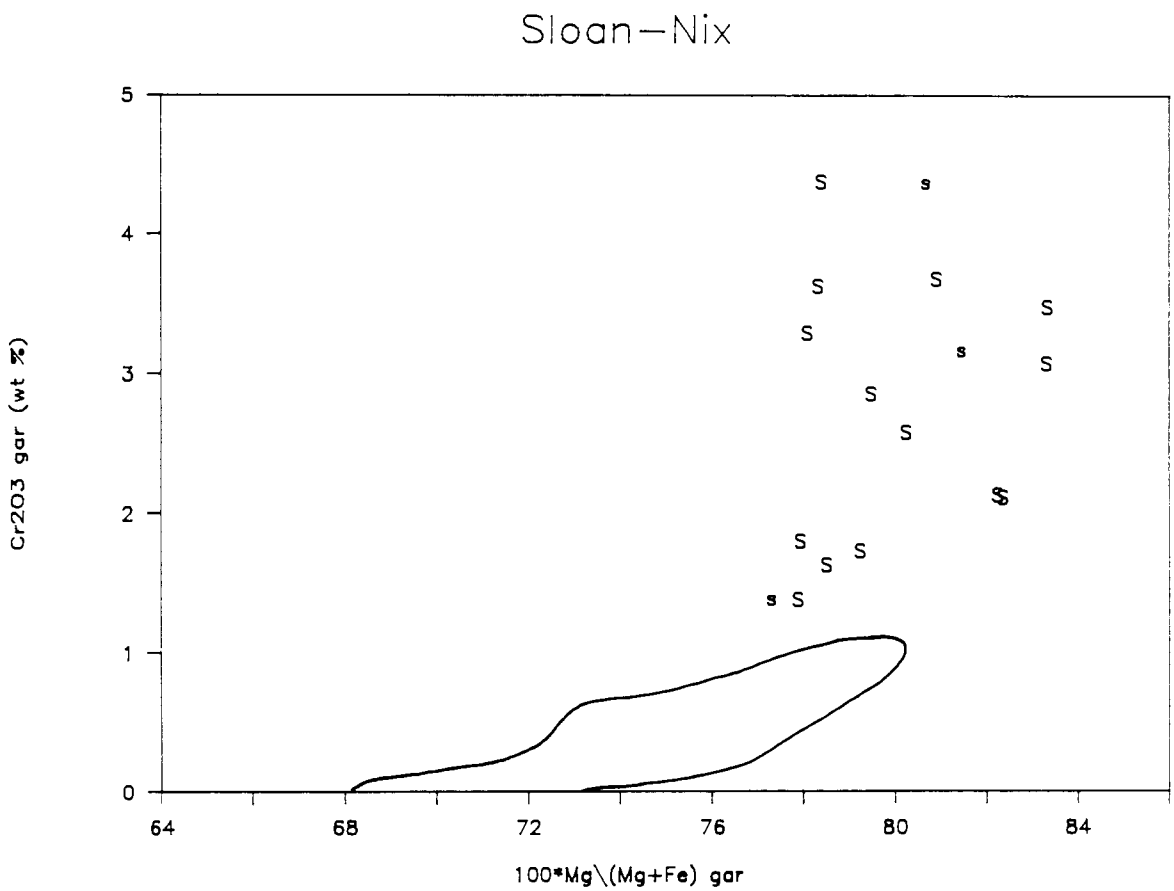

Figure 3.3.12 (b)

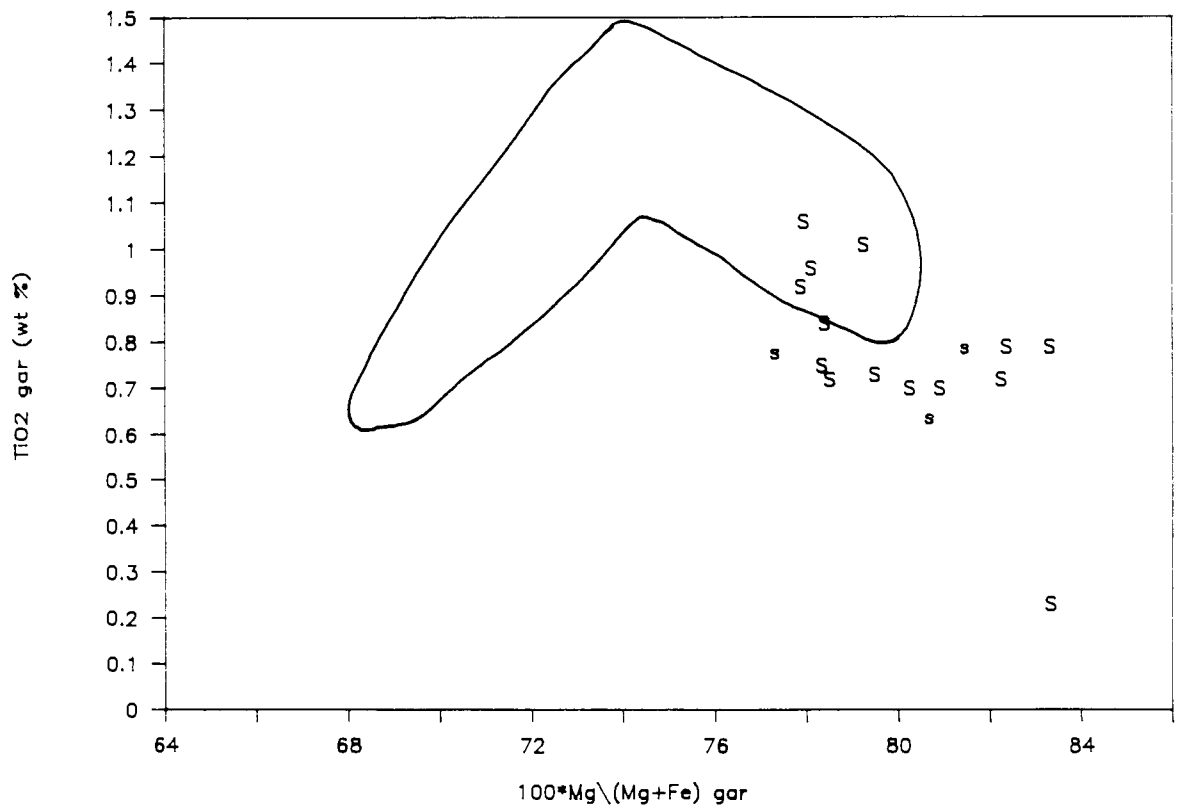

Figure 3.3.13 a and b

Ca# (atomic) versus Mg# (atomic) (a) and Cr_2O_3 (wt%) (b) in garnet megacrysts from Mukorob (Jones, 1984). The outlined field shows the compositional spread of the Cr-poor garnets from Monastery as shown in Figures 3.3.7 a and b).

Figure 3.3.13 (a)

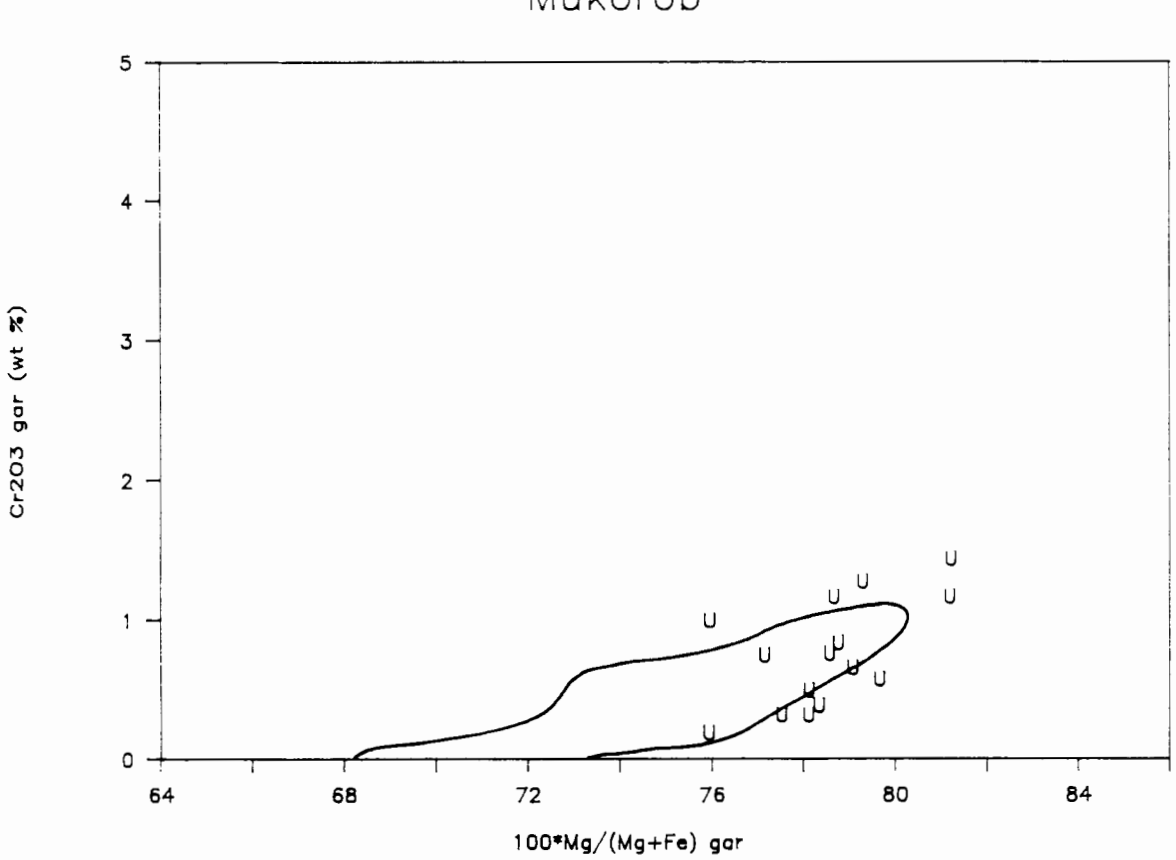

Figure 3.3.13 (b)

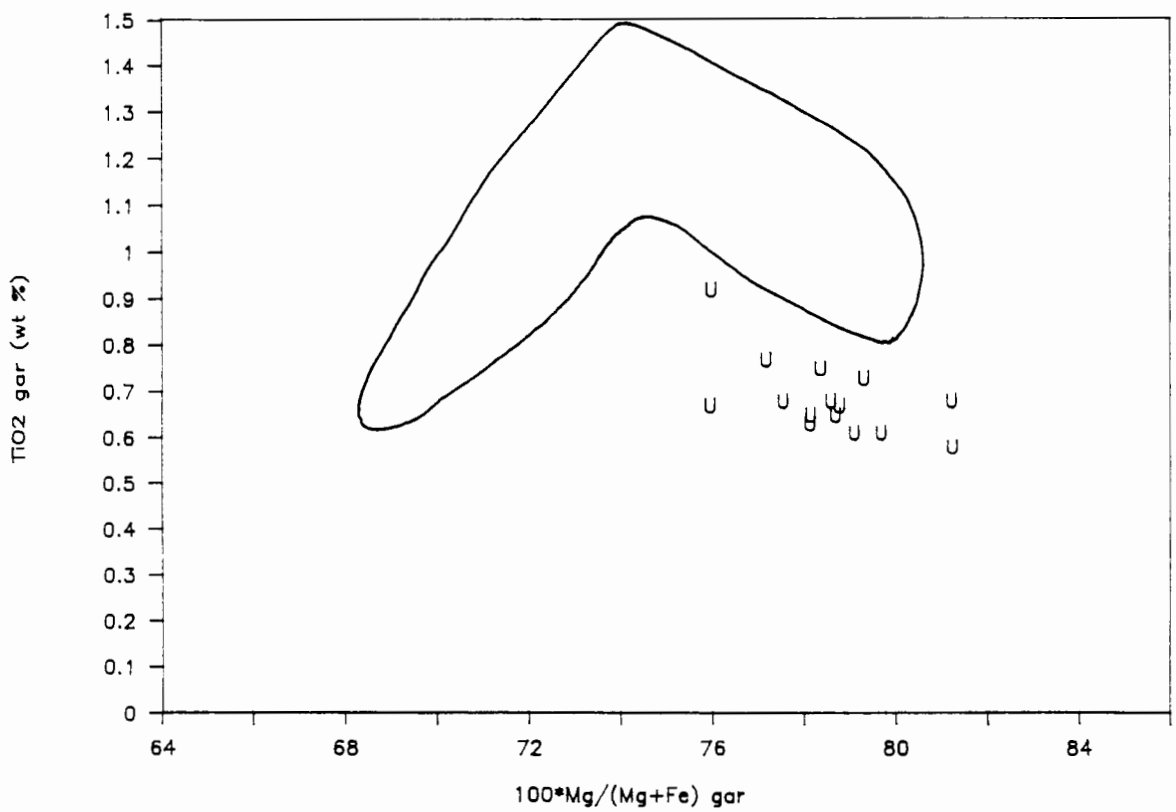

Figure 3.3.14 a and b

Ca# (atomic) versus Mg# (atomic) (a) and Cr_2O_3 (wt%) (b) in garnet megacrysts from the Eastern Griqualand kimberlites (Boyd, unpublished data). A = Abbotsford; R = Ramatseliso; C = Clarkton. The outlined field shows the compositional spread of the Cr-poor garnets from Monastery as shown in Figures 3.3.7 a and b).

Figure 3.3.14 (a)

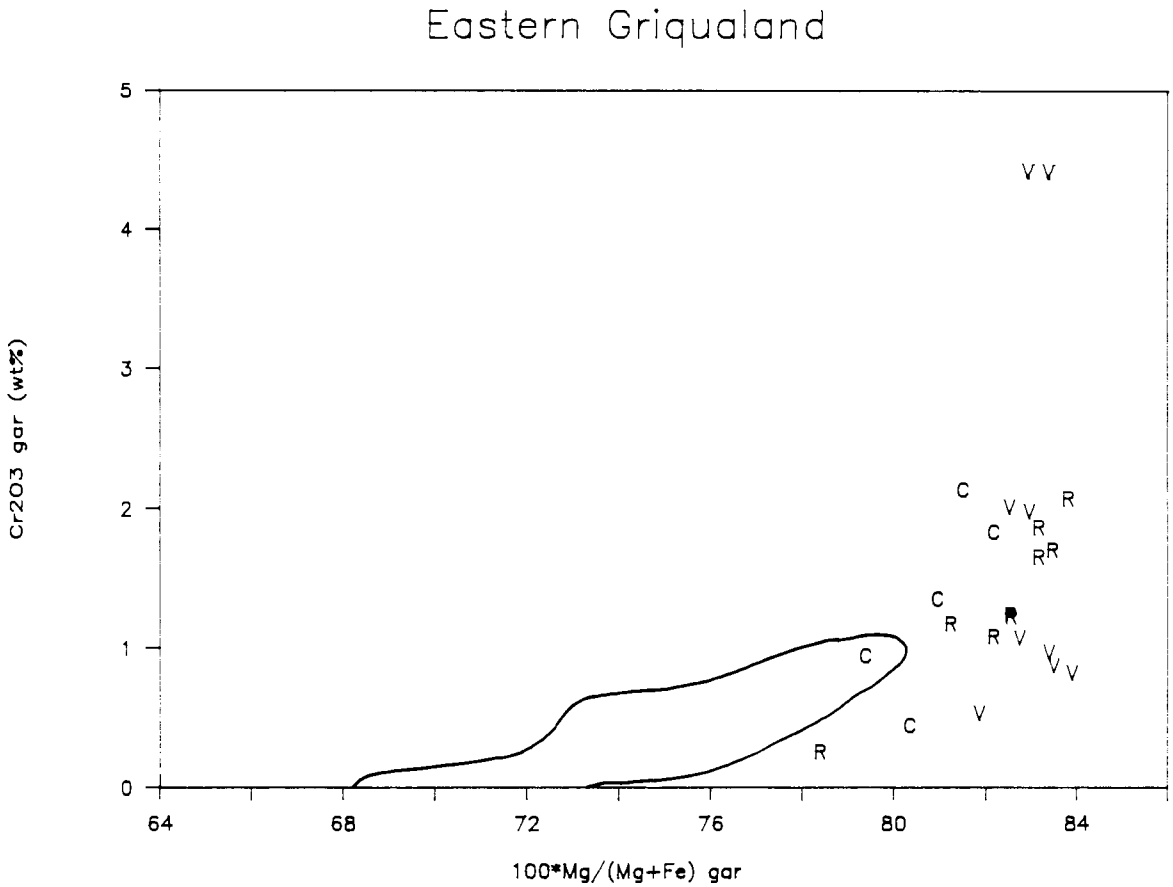

Figure 3.3.14 (b)

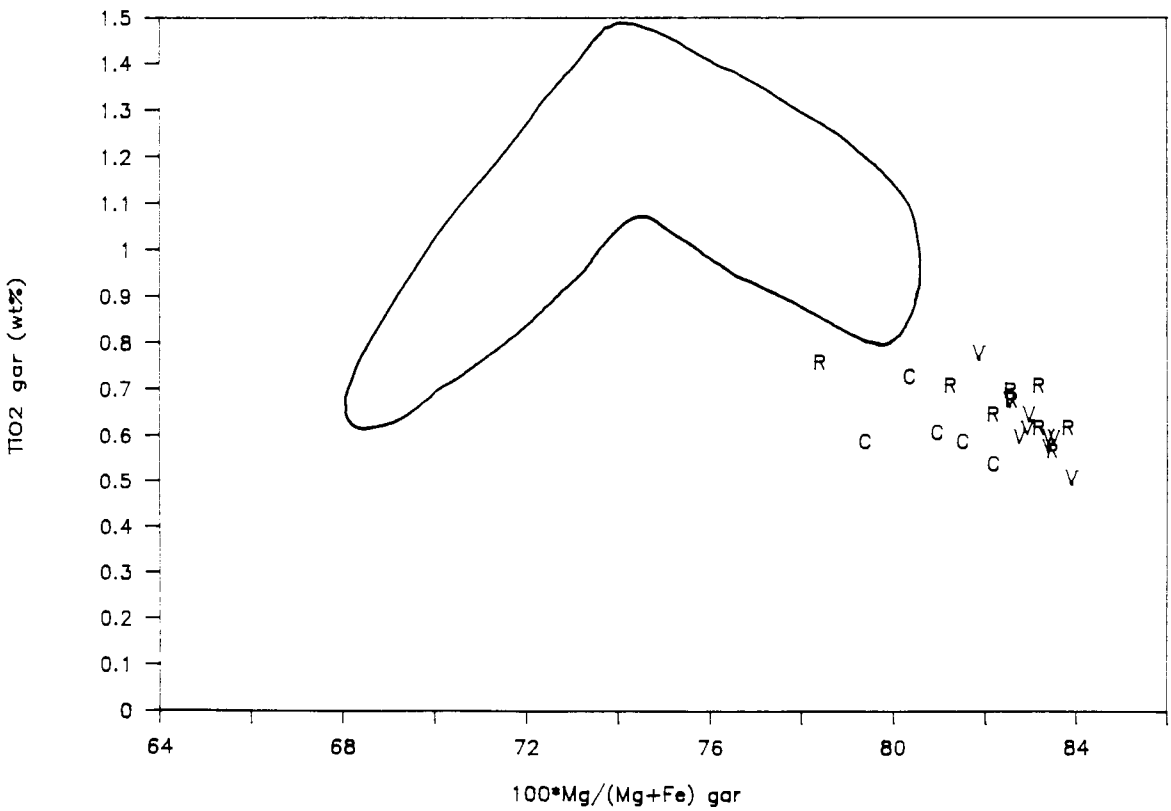

Figure 3.3.15 a and b

Ca# (atomic) versus Mg# (atomic) (a) and Cr_2O_3 (wt%) (b) in garnet megacrysts from Hamilton Branch (Schulze, 1982b). The outlined field shows the compositional spread of the Cr-poor garnets from Monastery as shown in Figures 3.3.7 a and b).

Figure 3.3.15 (a)

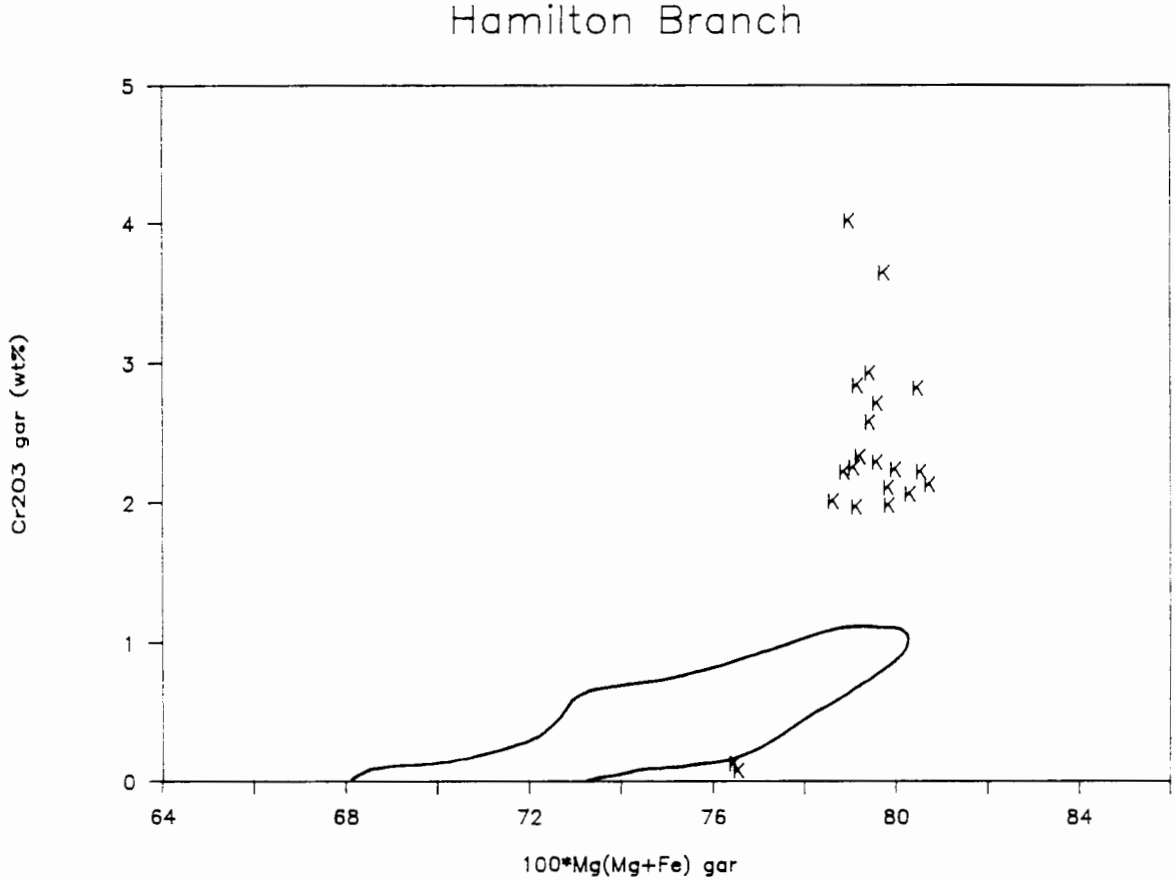

Figure 3.3.15 (b)

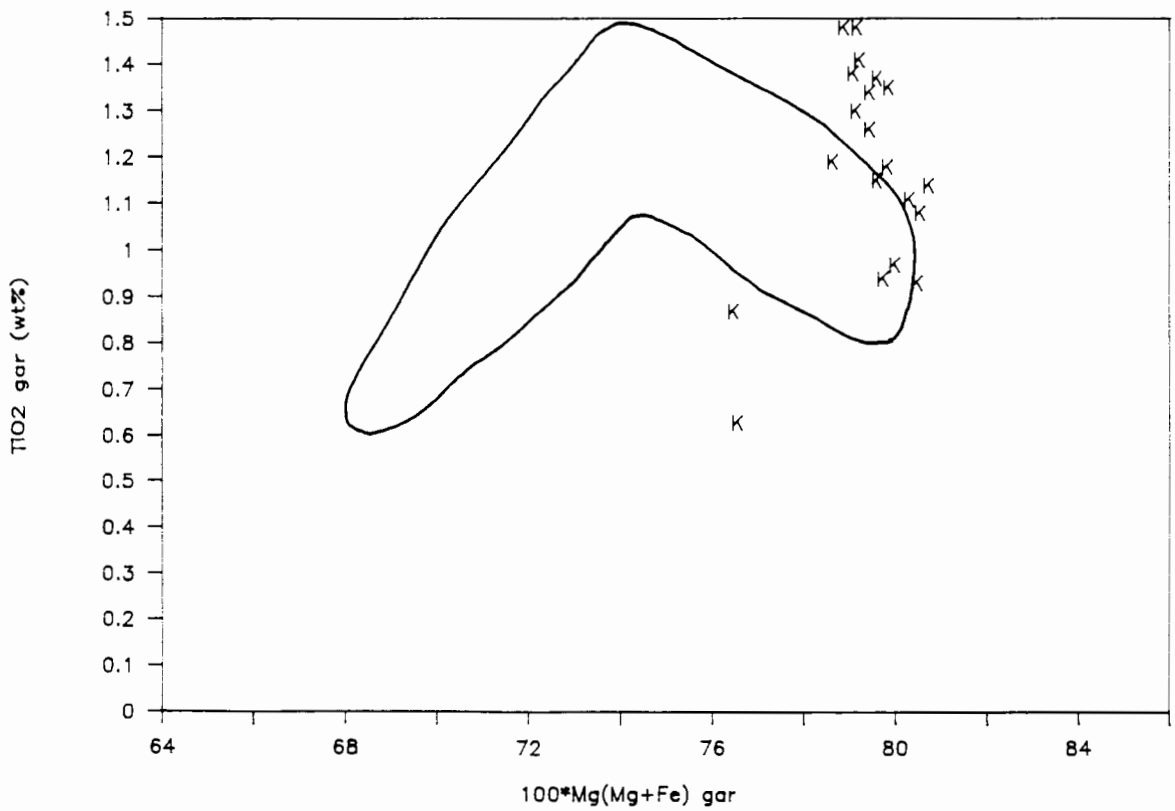

Figure 3.3.16 a and b

Ca# (atomic) versus Mg# (atomic) (a) and Cr_2O_3 (wt%) (b) in garnet megacrysts from Witberg (de Bruin, unpublished data). The outlined field shows the compositional spread of the Cr-poor garnets from Monastery as shown in Figures 3.3.7 a and b).

Figure 3.3.16 (a)

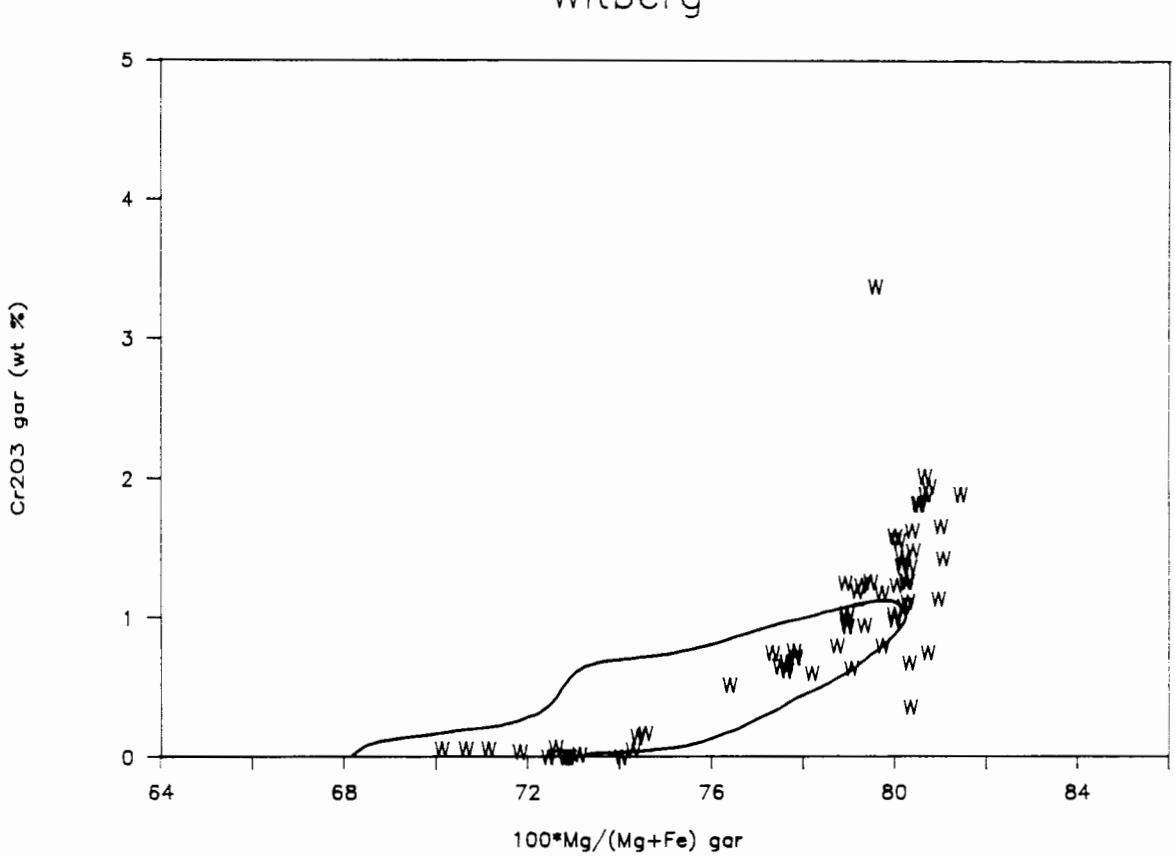

Figure 3.3.16 (b)

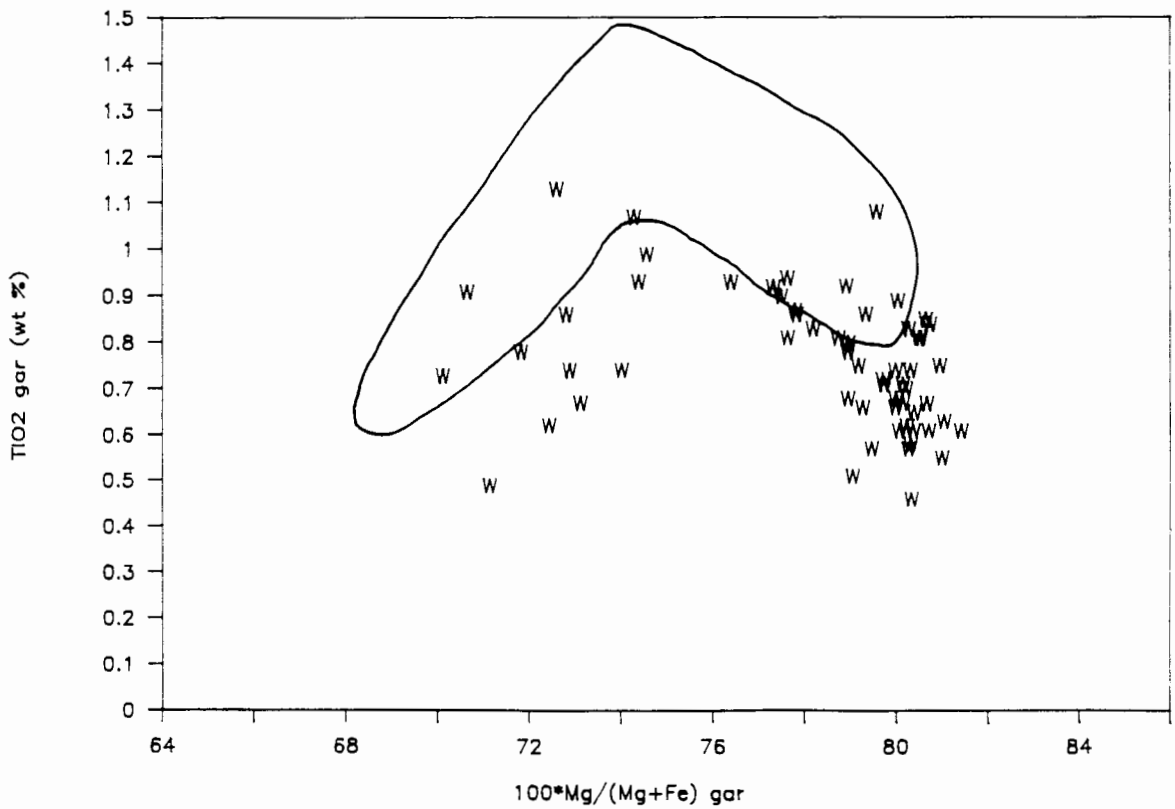

Figure 3.5.1

MgO (wt %) versus Cr_2O_3 (wt %) in ilmenite megacryst from Schuller. D = monomineralic; G = graphic intergrowth with orthopyroxene; I = ilmenites hosting inclusions of pyroxenes.

Figure 3.5.2

$Mg/(Mg+Fe^{2+})$ (atomic proportions) versus Al (atomic proportions) in ilmenite megacryst from Schuller. Fe^{2+} and Fe^{3+} were calculated from stoichiometry using the method of Droop (1987). Symbols as in Figure 3.5.1.

Figure 3.5.1

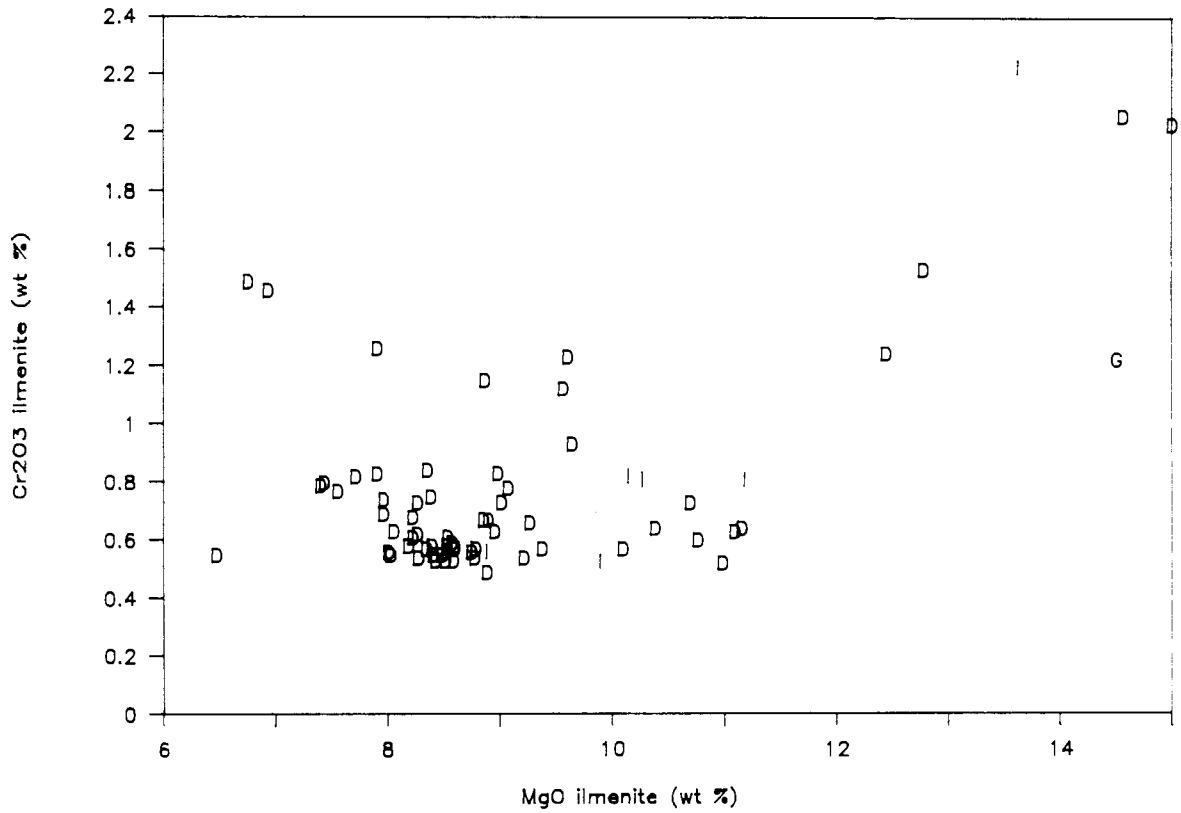

Figure 3.5.2

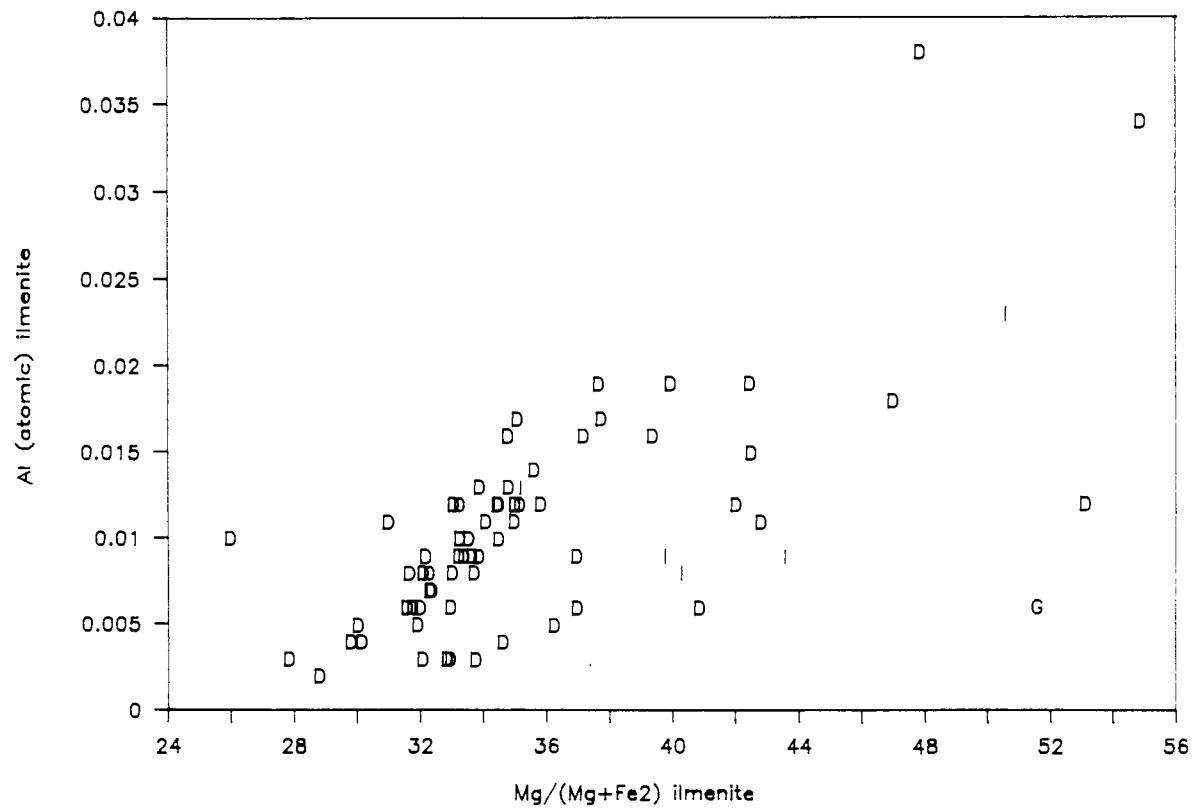

Figure 3.5.3

$Mg/(Mg+Fe^{2+})$ (atomic proportions) versus Fe^{3+} (atomic proportions) in ilmenite megacryst from Schuller. Fe^{2+} and Fe^{3+} were calculated from stoichiometry using the method of Droop (1987). Symbols as in Figure 3.5.1.

Figure 3.5.3

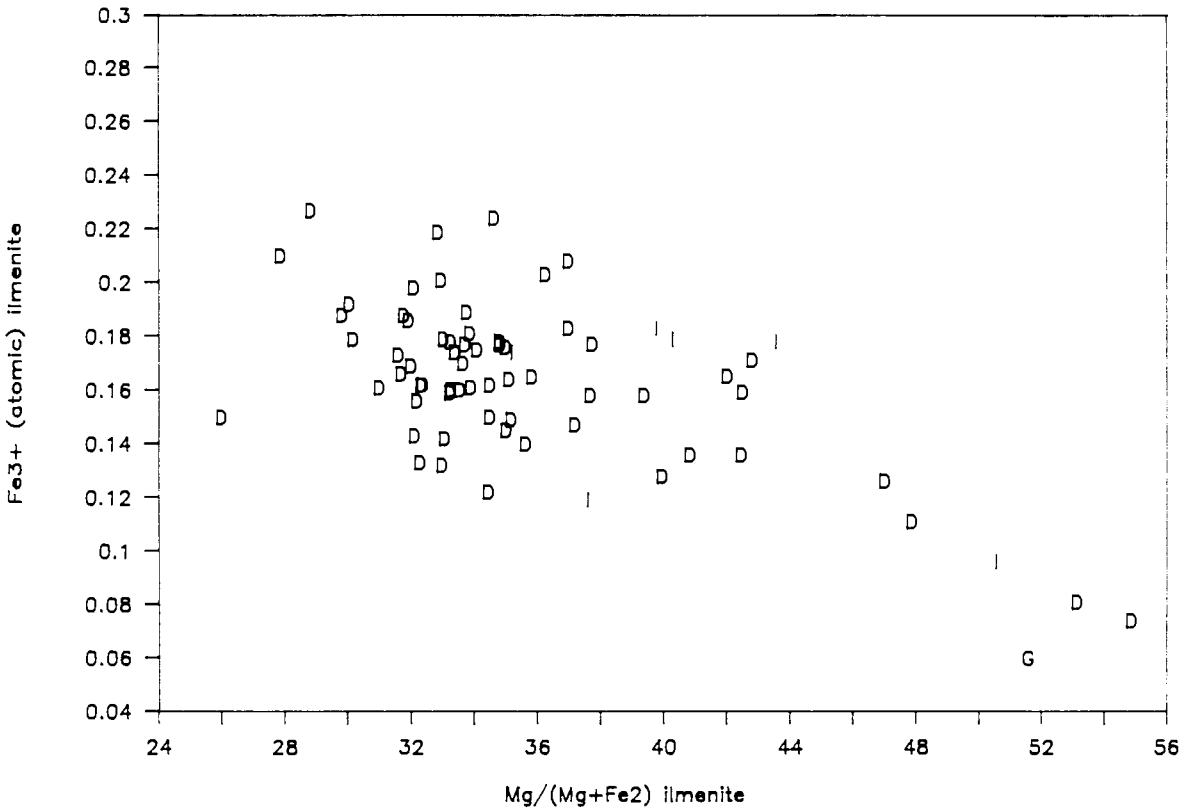
0.3
0.28
0.26
0.24
0.22
0.2
0.18
0.16
0.14
0.12
0.1
0.08
0.06
0.04
Fe3+ (atomic) ilmenite
24
28
32
36
40
44
48
52
56
Mg/(Mg+Fe2) ilmenite

Figure 4.1

Ca# (atomic) versus Mg# (atomic) in clinopyroxene megacrysts from Schuller. The solid squares show the samples selected for trace element analyses.

Figure 4.2

Ca# (atomic) versus Cr_2O_3 (wt %) in clinopyroxene megacrysts from Schuller. The solid squares show the samples selected for trace element analyses.

Figure 4.1

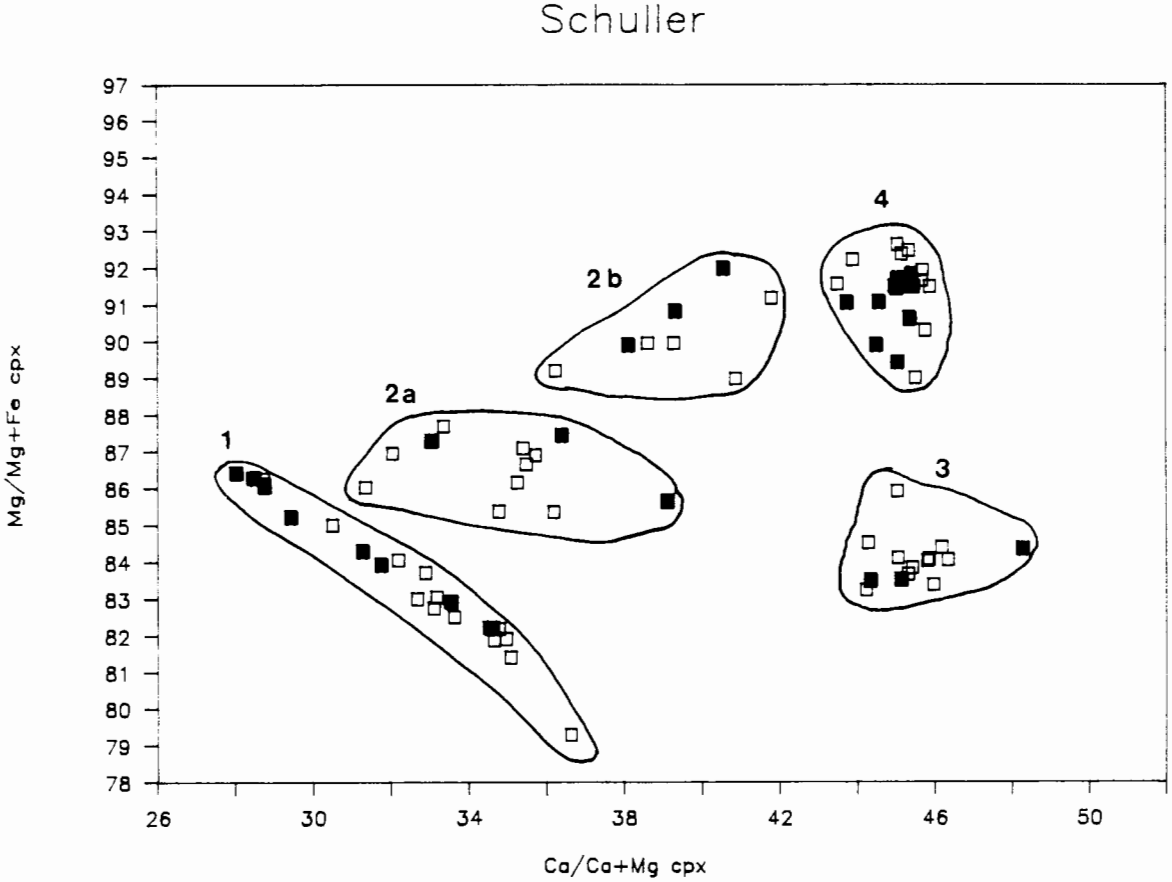

Figure 4.2

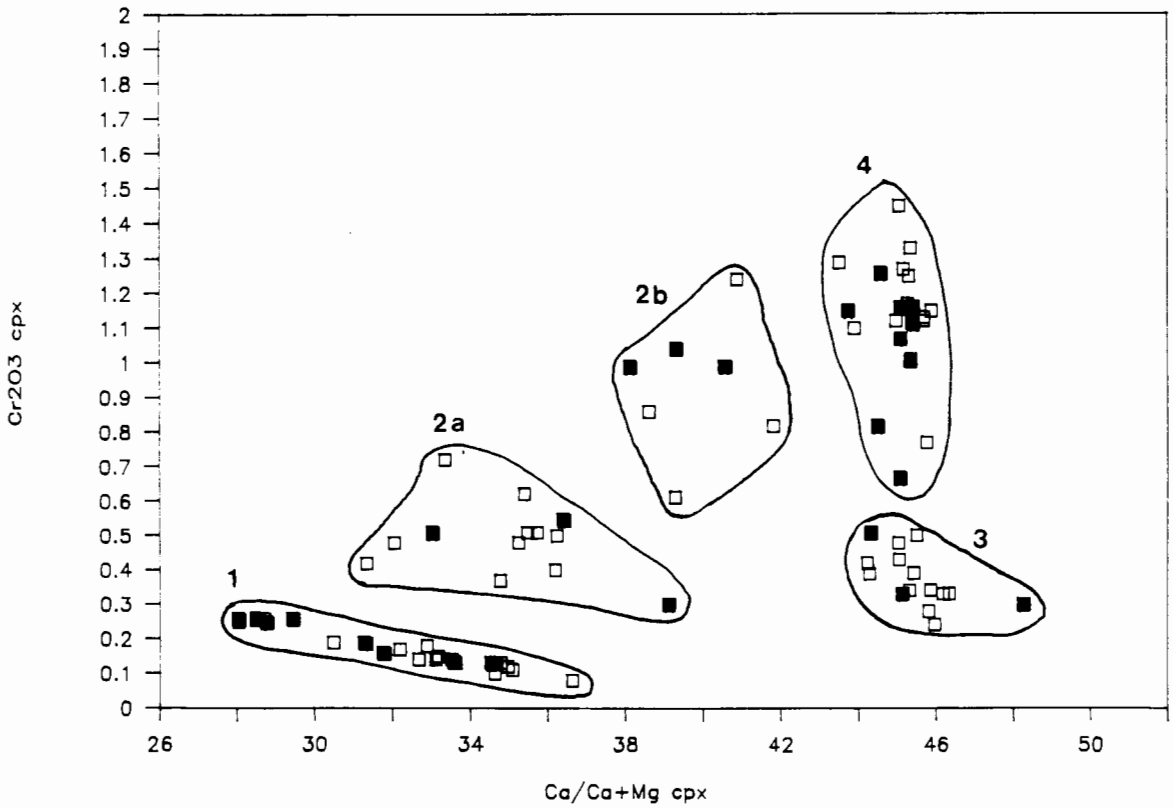

Figure 4.3

Mg# (atomic) versus CaO (wt %) in orthopyroxene megacrysts from Schuller. The solid squares show the samples selected for trace element analyses.

Figure 4.4

Mg# (atomic) versus Cr_2O_3 (wt %) in garnet megacrysts from Schuller. The solid squares show the samples selected for trace element analyses.

Figure 4.3

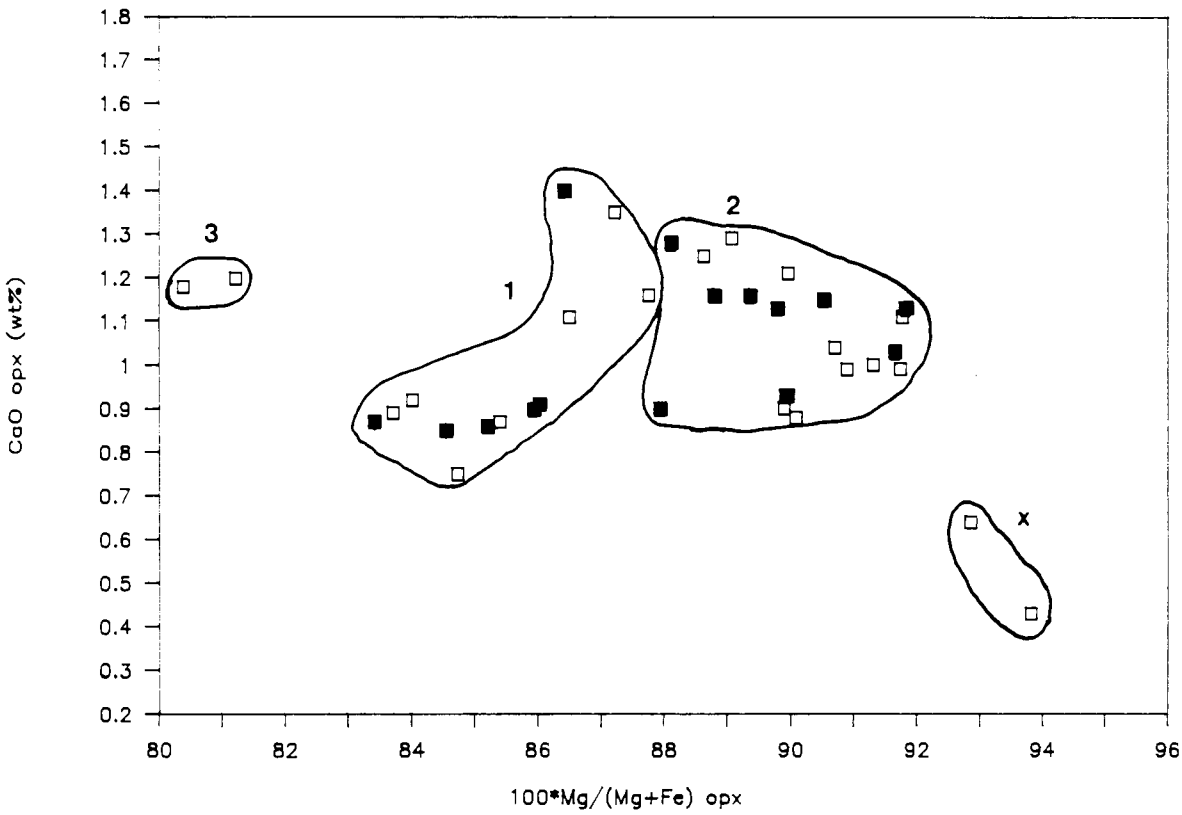

Figure 4.4

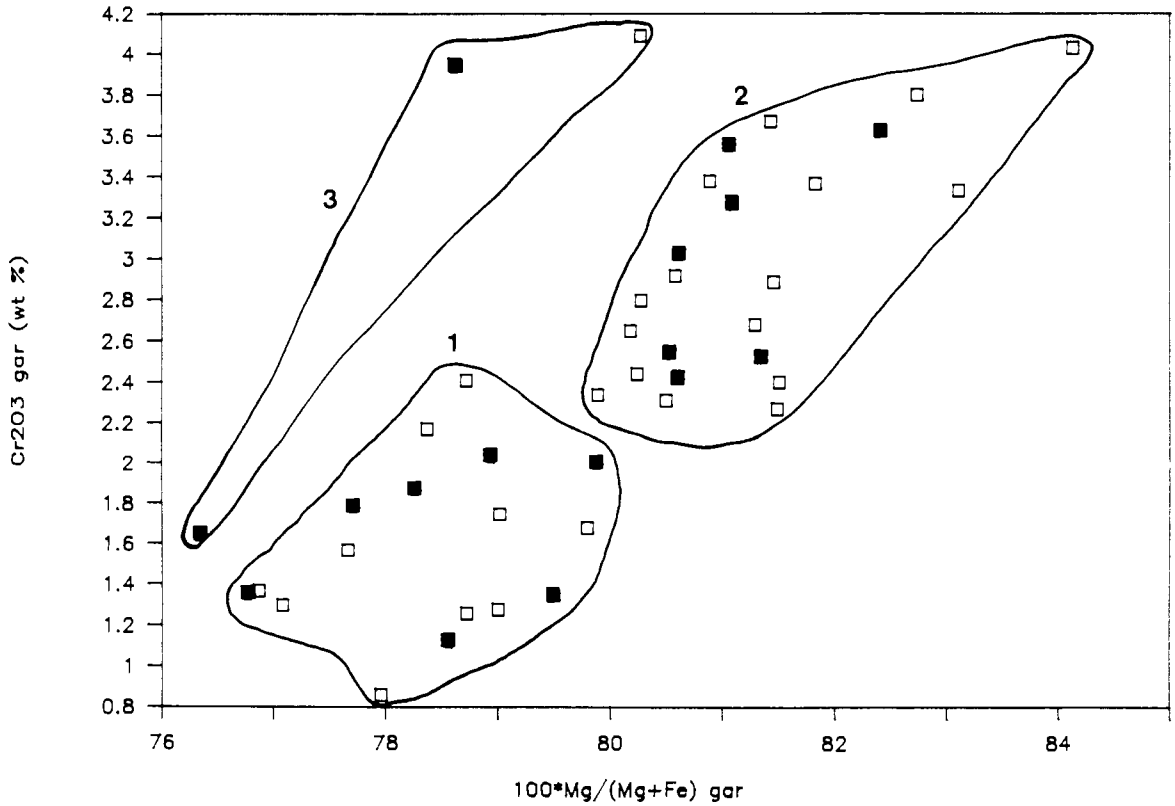

Figure 4.5

Ca# (atomic) versus Sr (ppm) in clinopyroxene megacrysts from Schuller. The symbols refer to the compositional groups discussed in the text.

Figure 4.6

Mg# (atomic) versus Sr (ppm) in clinopyroxene megacrysts from Schuller. The symbols refer to the compositional groups discussed in the text.

Figure 4.5

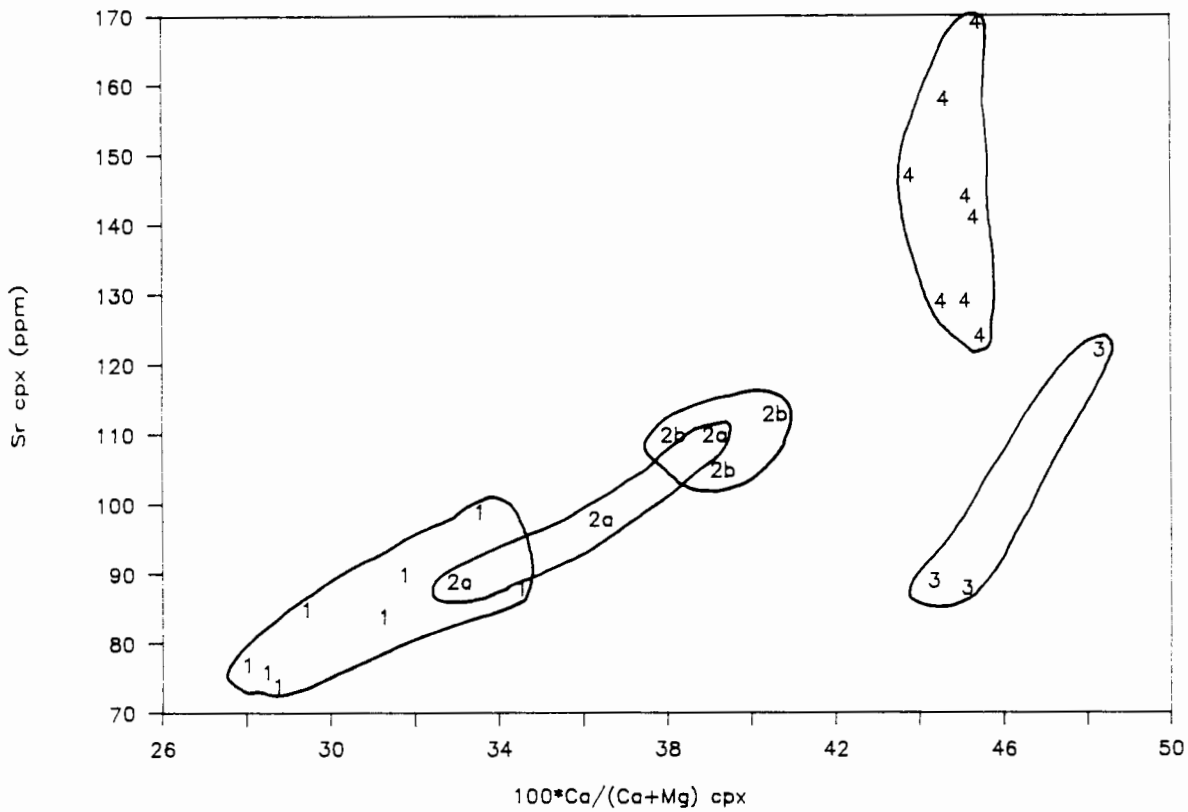

Figure 4.6

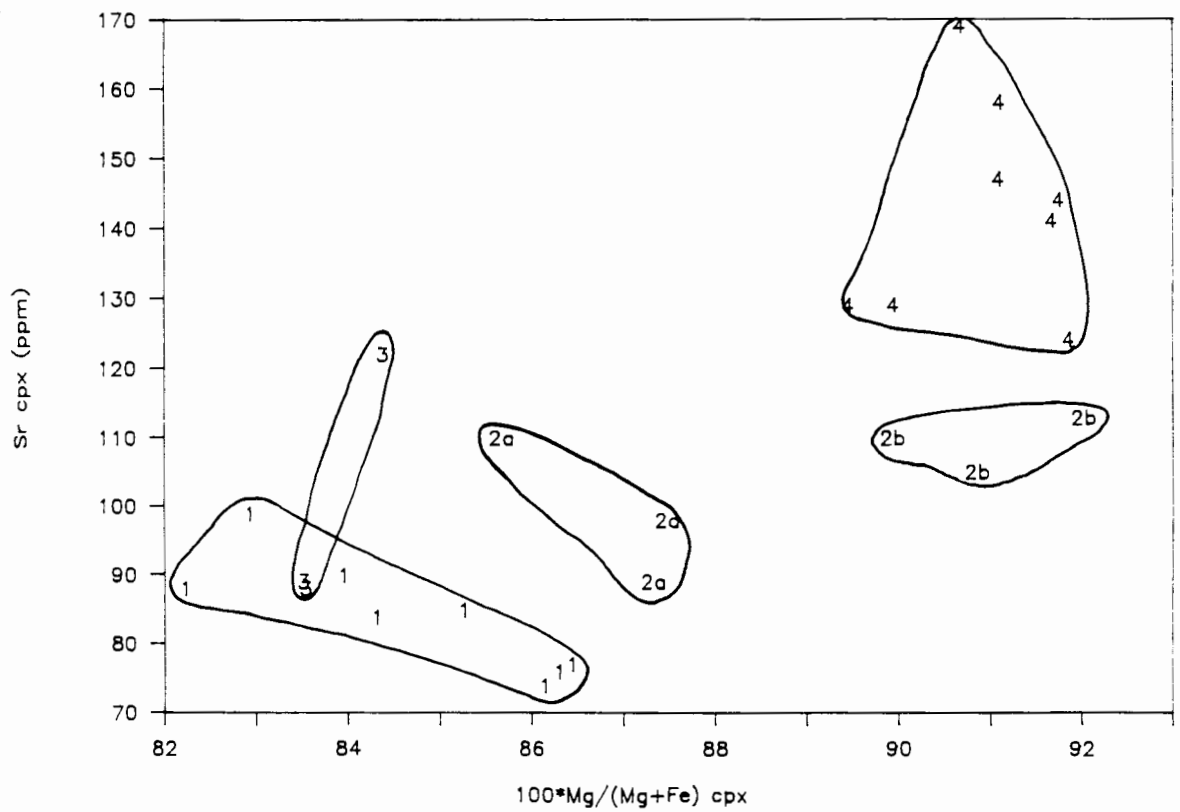

Figure 4.7

Ca# (atomic) versus Zr (ppm) in clinopyroxene megacrysts from Schuller. The symbols refer to the compositional groups discussed in the text.

Figure 4.8

Mg# (atomic) versus Zr (ppm) in clinopyroxene megacrysts from Schuller. The symbols refer to the compositional groups discussed in the text.

Figure 4.7

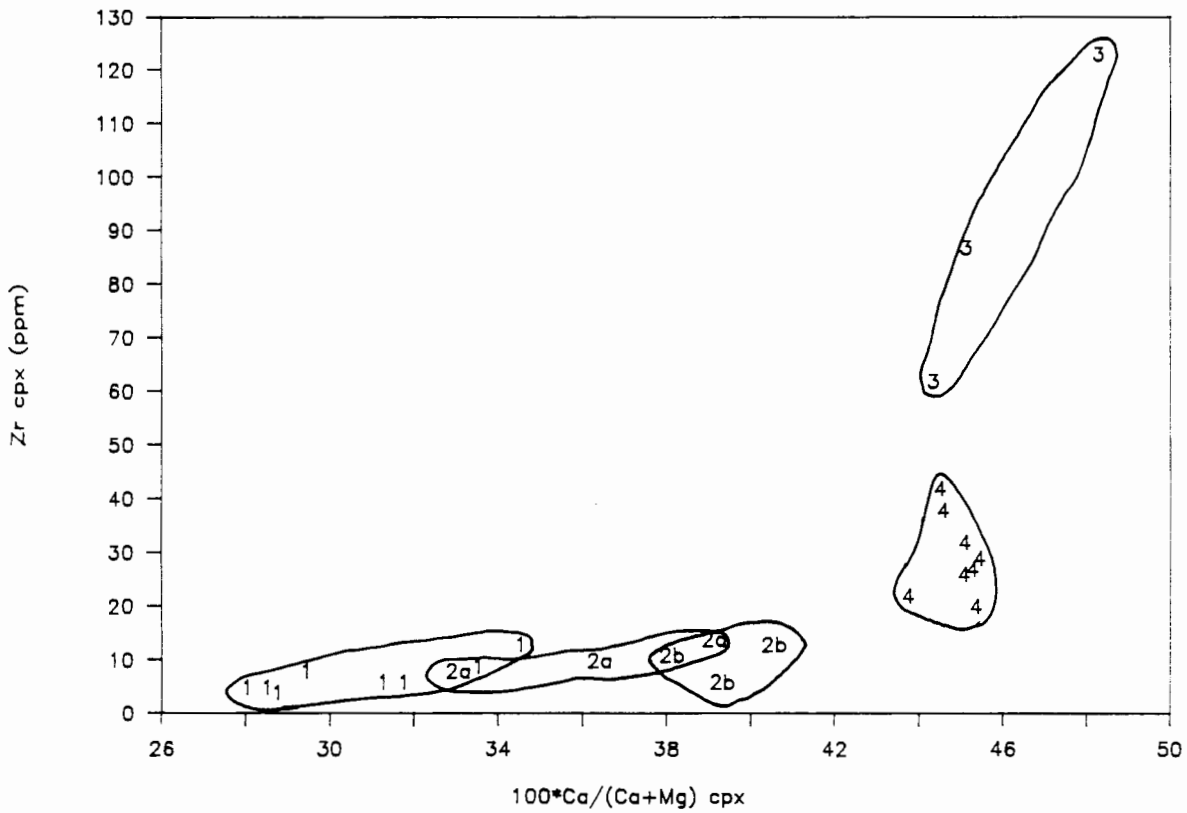

Figure 4.8

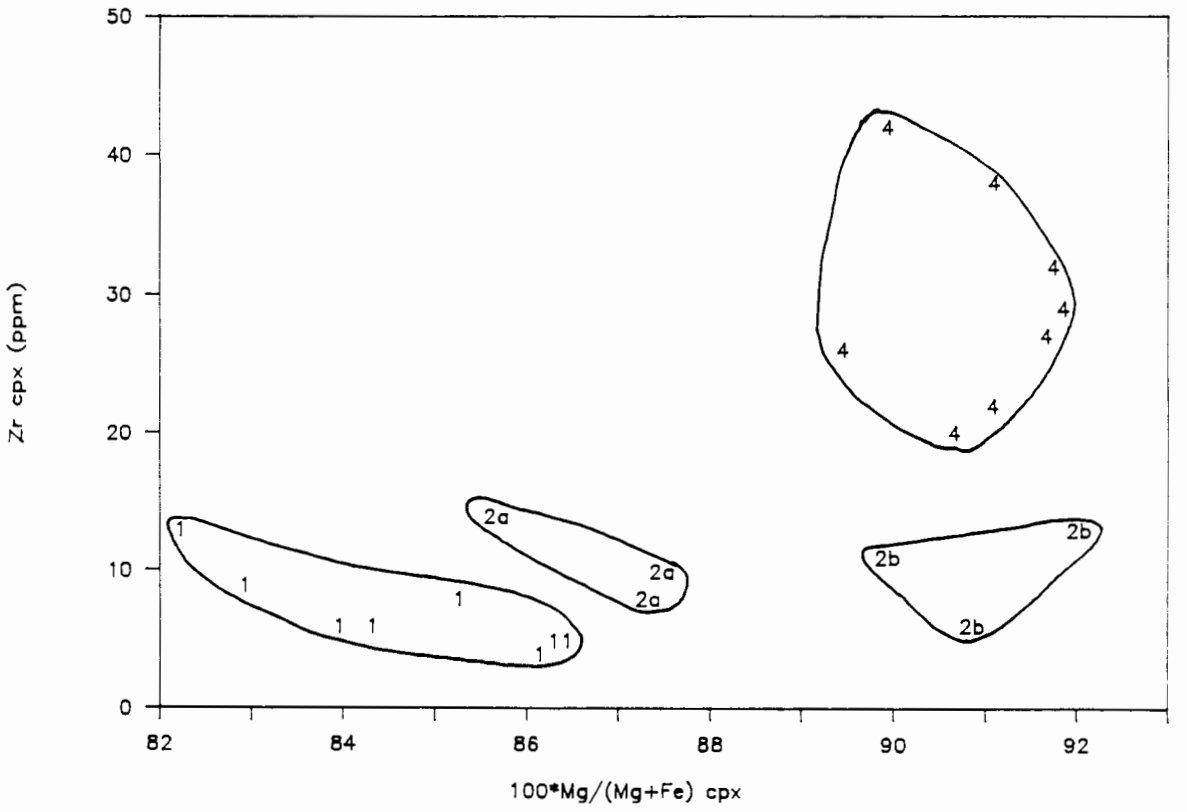

Figure 4.9

Ca# (atomic) versus Ga (ppm) in clinopyroxene megacrysts from Schuller. The symbols refer to the compositional groups discussed in the text.

Figure 4.10

Ca# (atomic) versus Ni (ppm) in clinopyroxene megacrysts from Schuller. The symbols refer to the compositional groups discussed in the text.

Figure 4.9

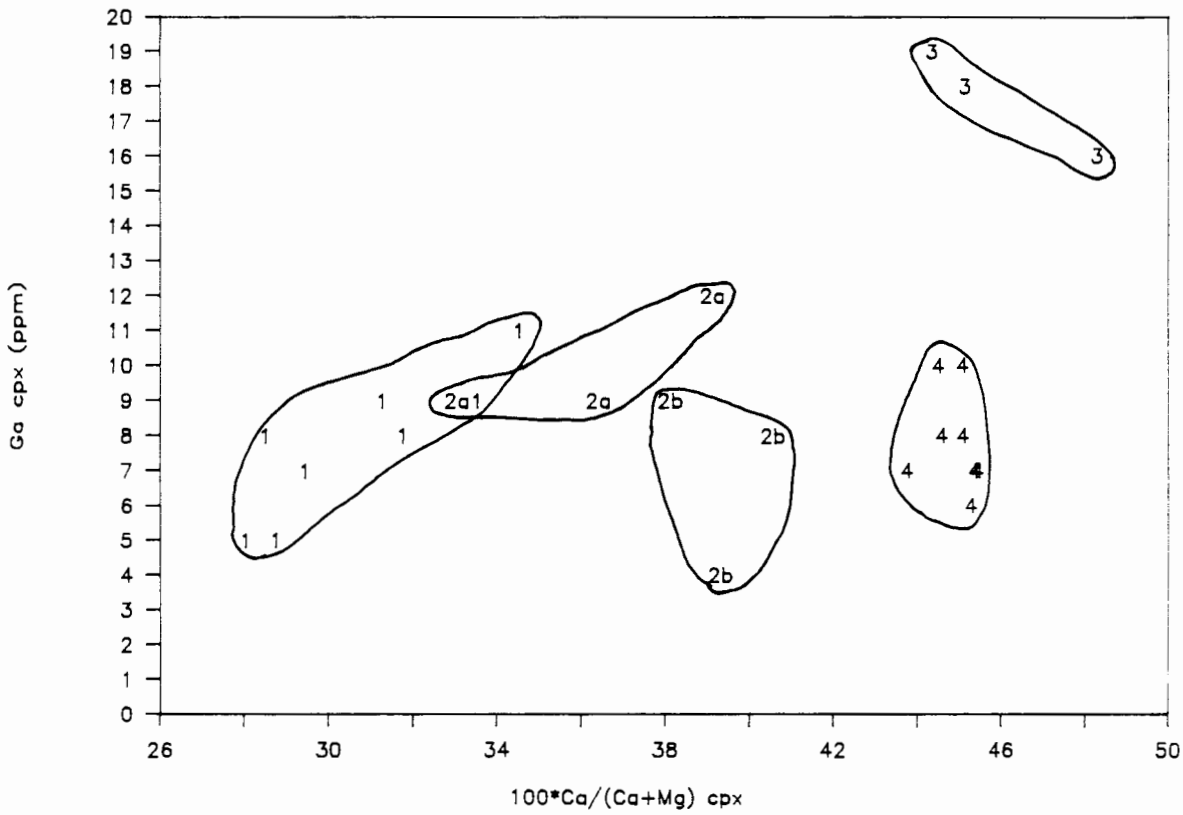

Figure 4.10

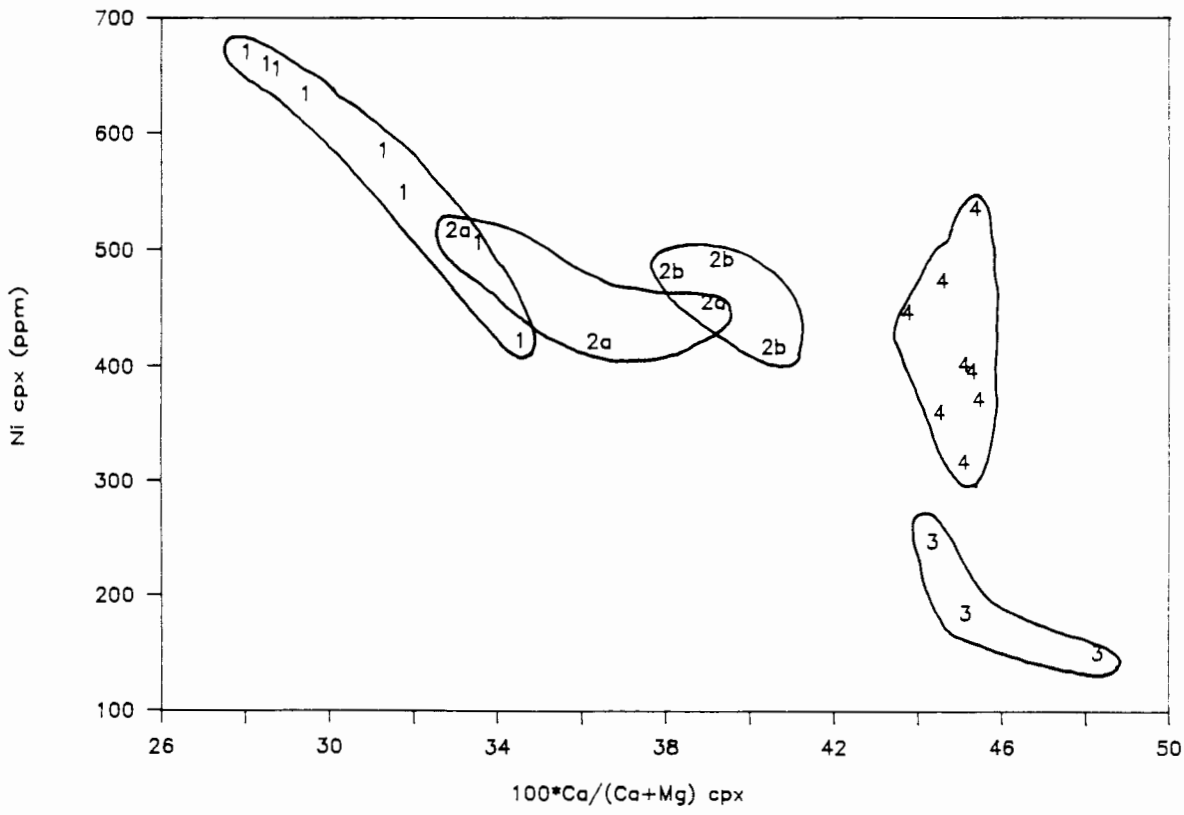

Figure 4.11

Ca# (atomic) versus Zn (ppm) in clinopyroxene megacrysts from Schuller. The symbols refer to the compositional groups discussed in the text.

Figure 4.12

FeO (wt %) versus Zn (ppm) in clinopyroxene megacrysts from Schuller. The symbols refer to the compositional groups discussed in the text.

Figure 4.11

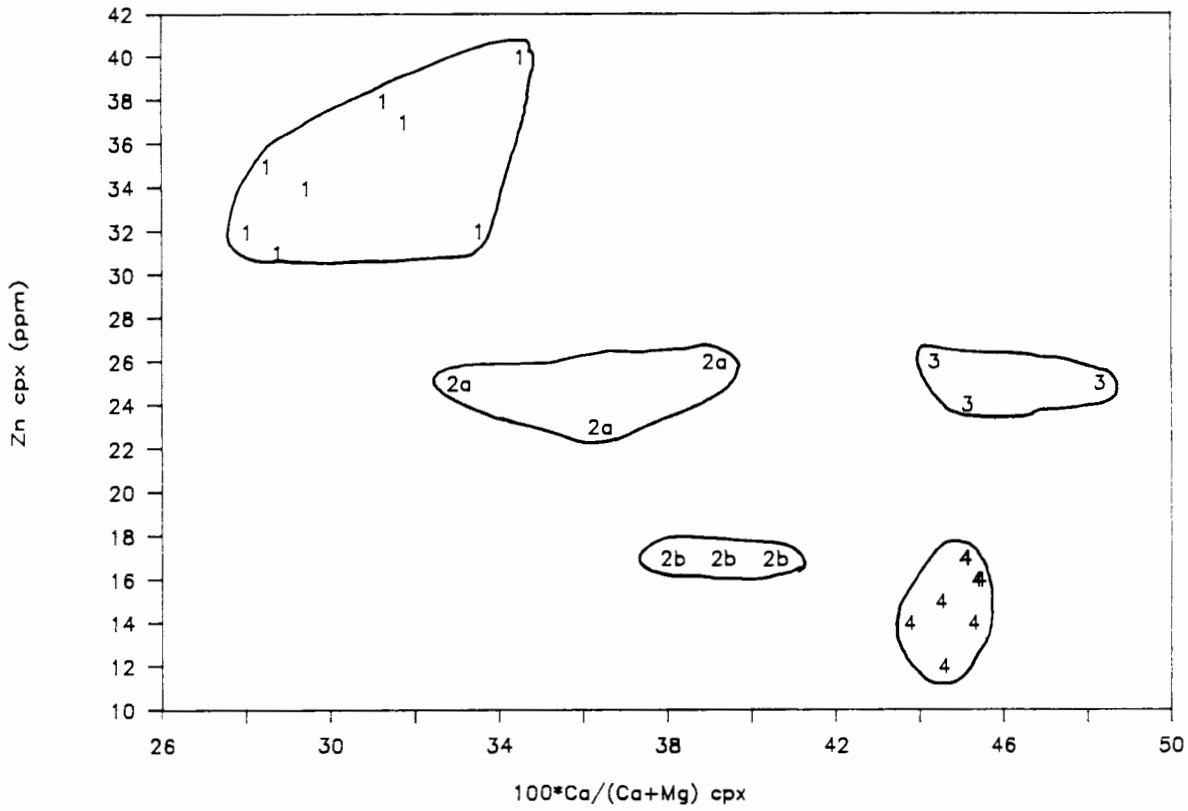

Figure 4.12

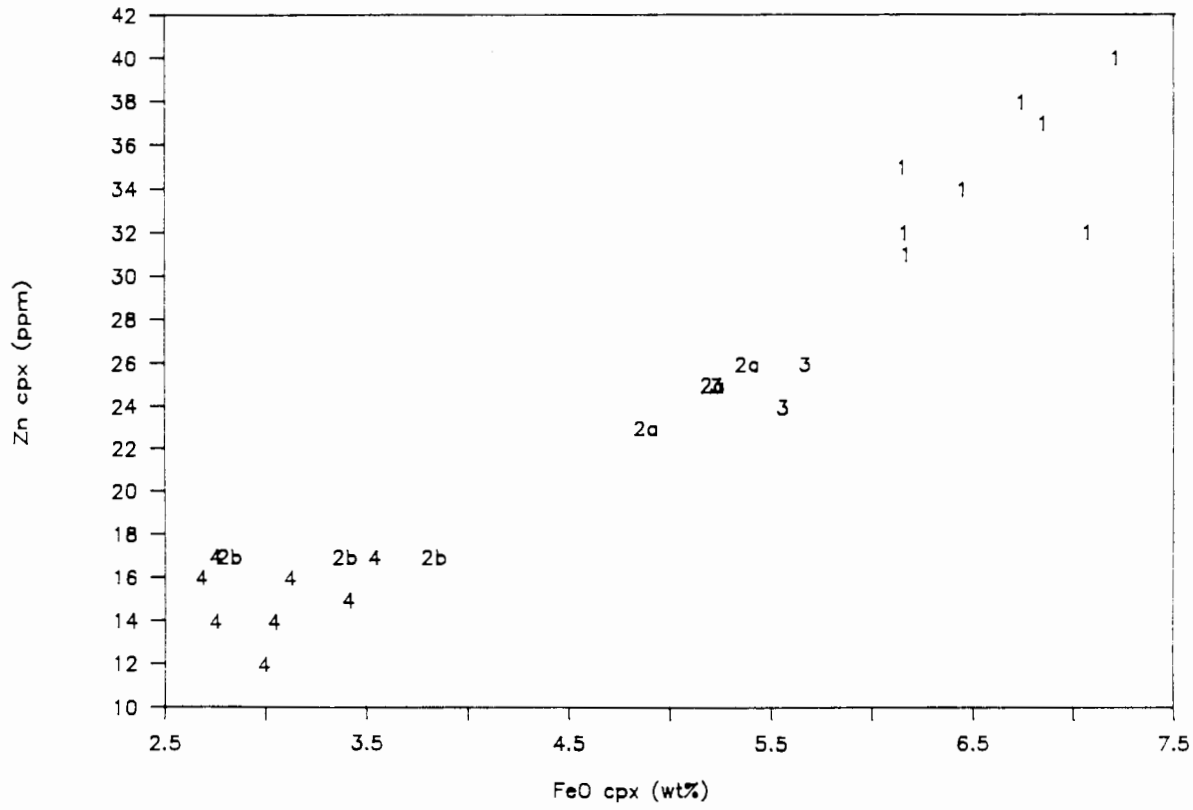

Figure 4.13

Mg# (atomic) versus Ni (ppm) in orthopyroxene megacrysts from Schuller. The symbols refer to the compositional groups discussed in the text.

Figure 4.14

Mg# (atomic) versus Zn (ppm) in orthopyroxene megacrysts from Schuller. The symbols refer to the compositional groups discussed in the text.

Figure 4.13

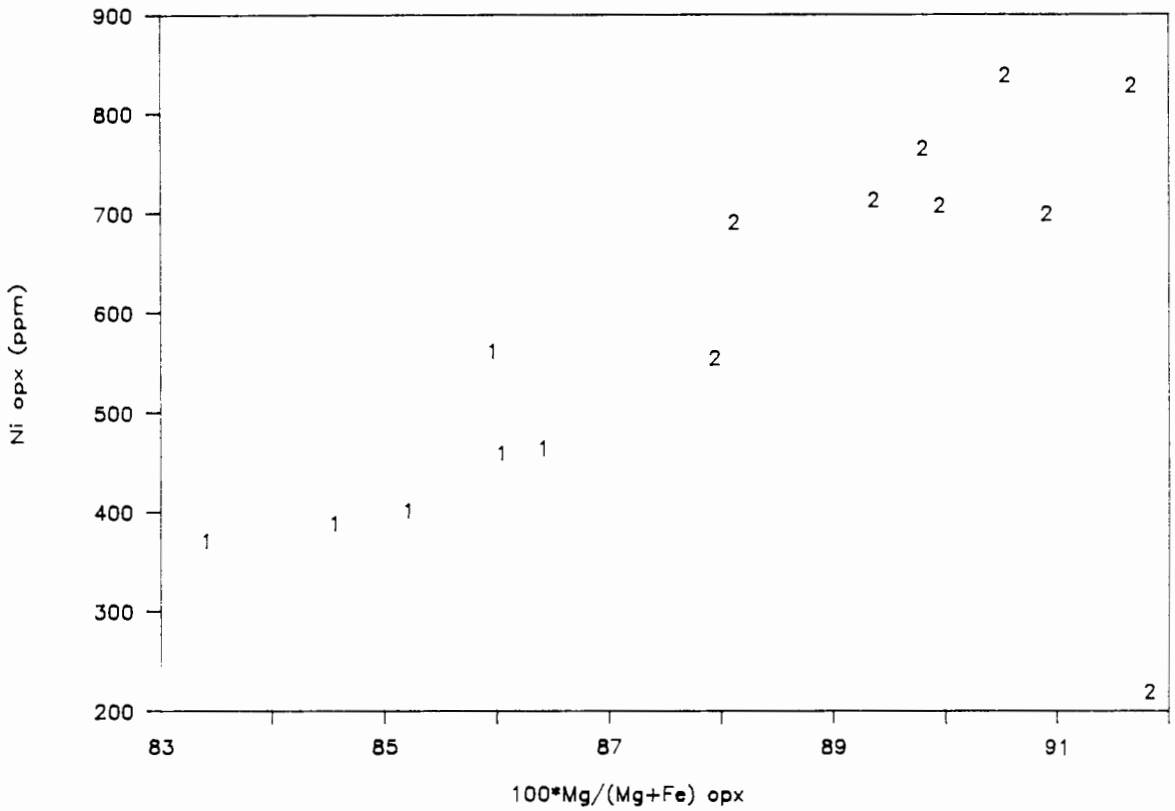

Figure 4.14

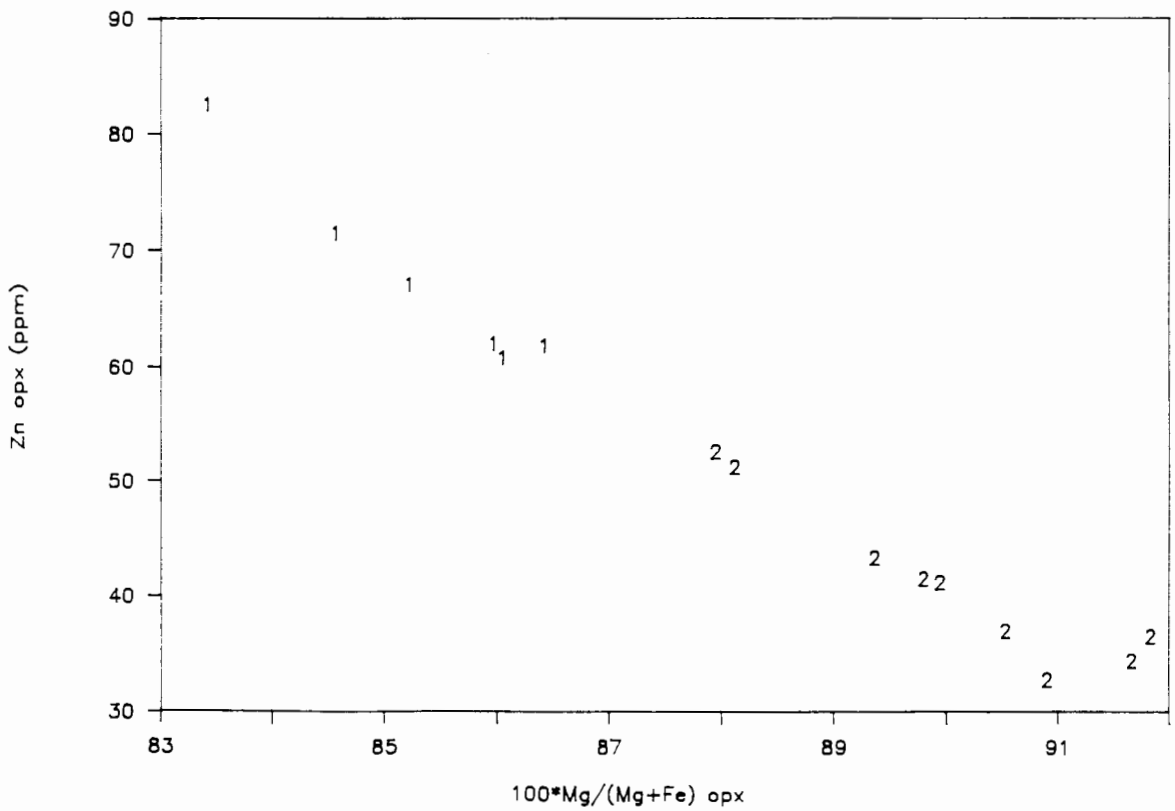

Figure 4.15

Mg# (atomic) versus Y (ppm) in garnet megacrysts from Schuller. The symbols refer to the compositional groups discussed in the text.

Figure 4.16

Mg# (atomic) versus Zr (ppm) in garnet megacrysts from Schuller. The symbols refer to the compositional groups discussed in the text.

Figure 4.15

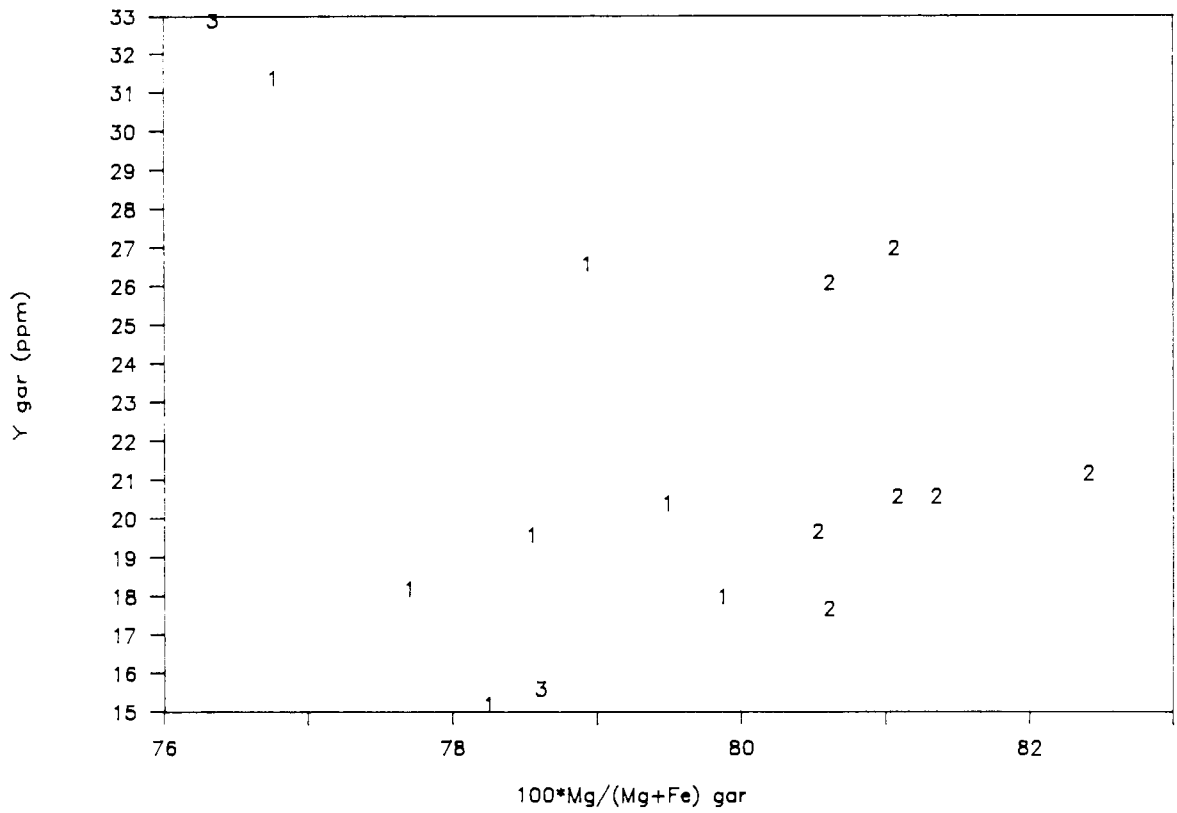

Figure 4.16

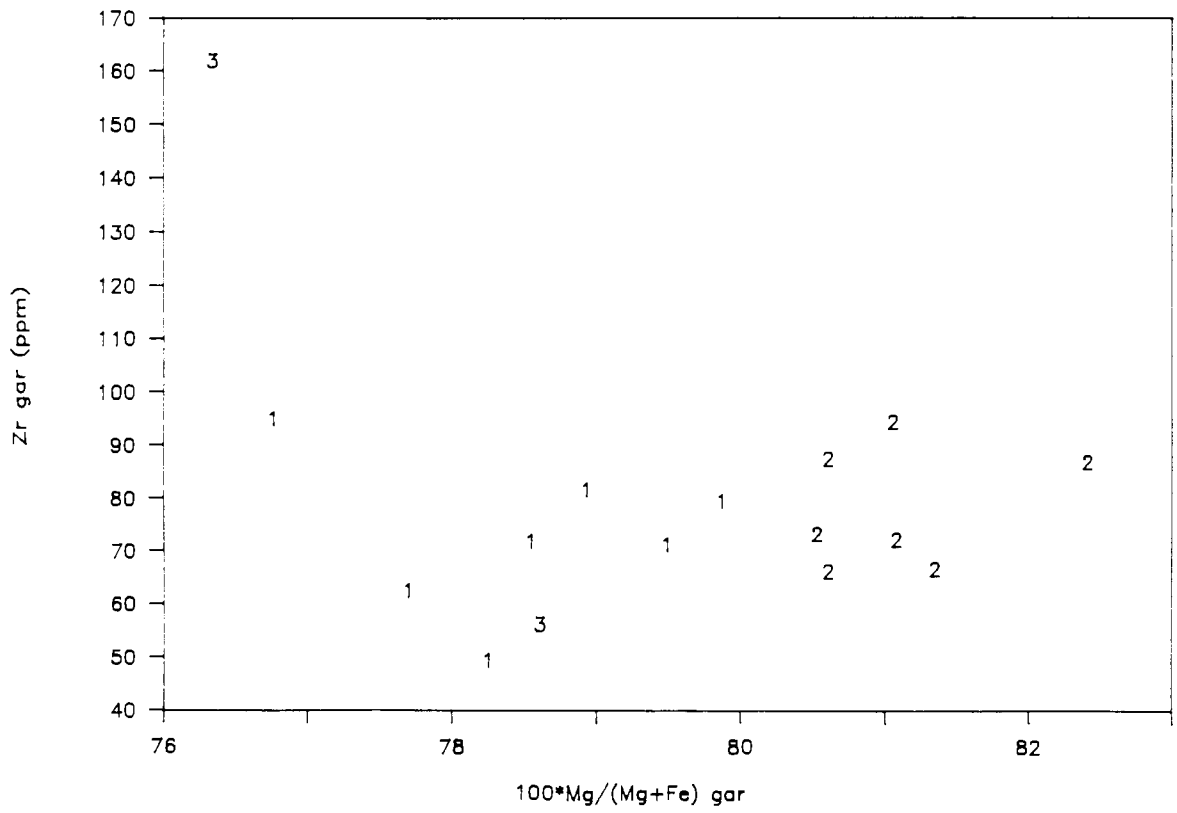

Figure 4.17

Mg# (atomic) versus Ni (ppm) in garnet megacrysts from Schuller. The symbols refer to the compositional groups discussed in the text.

Figure 4.18

Mg# (atomic) versus Ni (ppm) in garnet megacrysts from Schuller. The symbols refer to the compositional groups discussed in the text.

Figure 4.17

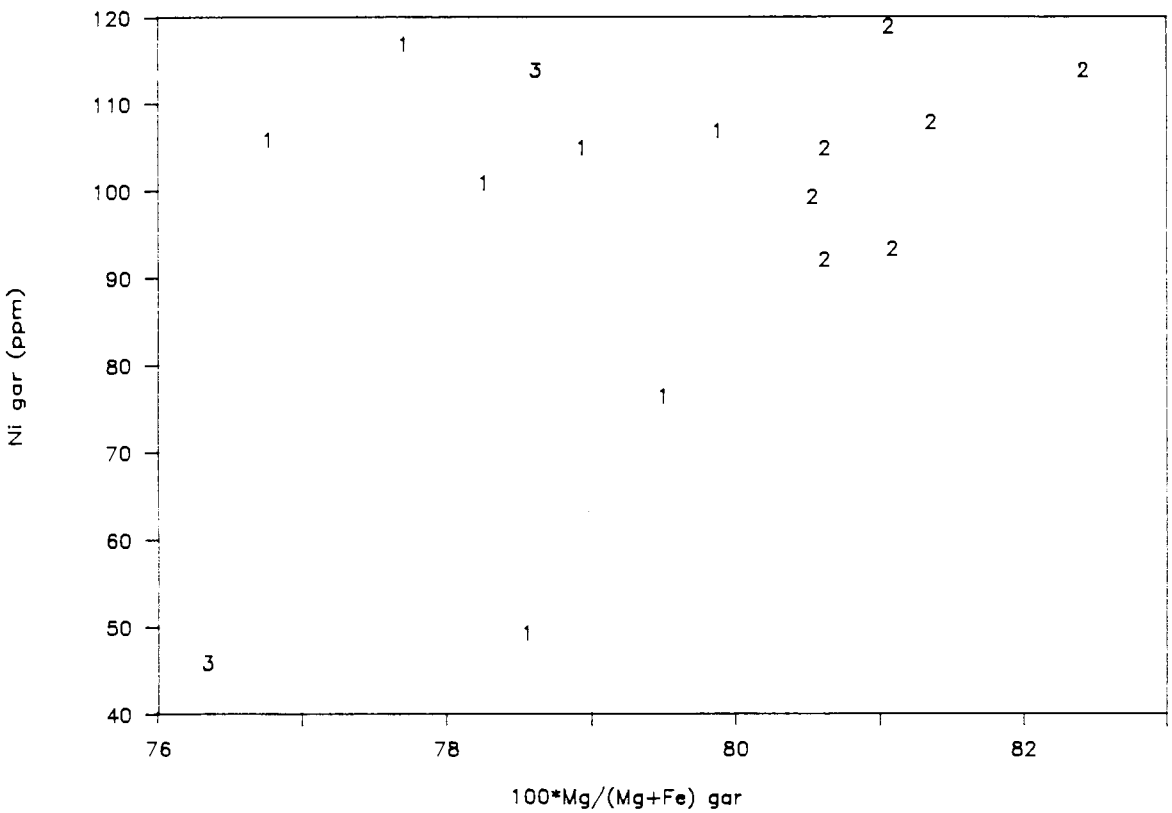

Figure 4.18

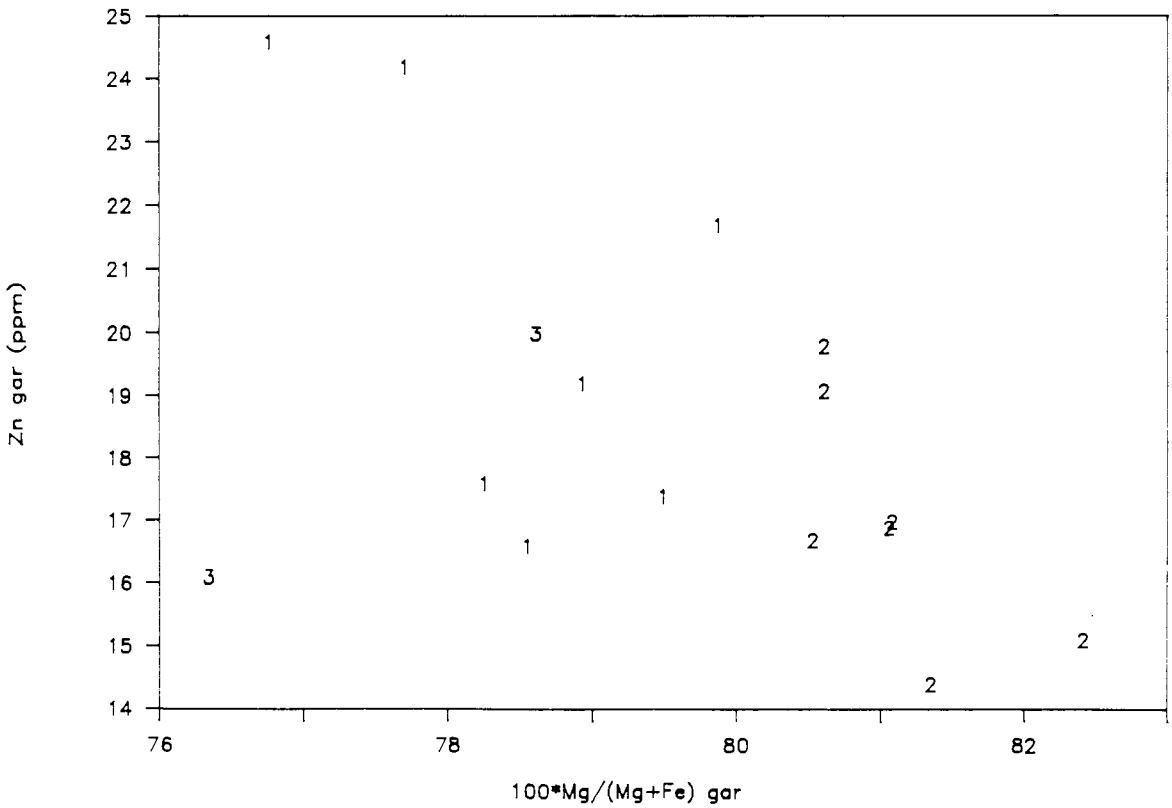

Figure 4.19

Calculated Sr and Zr liquid compositions (in ppm) in equilibrium with the group 1 clinopyroxene megacrysts from Schuller. Assuming that the least fractionated samples represent the liquidus composition, the evolution of liquid lines of descent using an equilibrium crystallisation model are shown for Sr bulk distribution coefficients of 0.1, 0.5 and 0.7 respectively. A Zr bulk distribution coefficient of 0.1 was used.

Figure 4.19

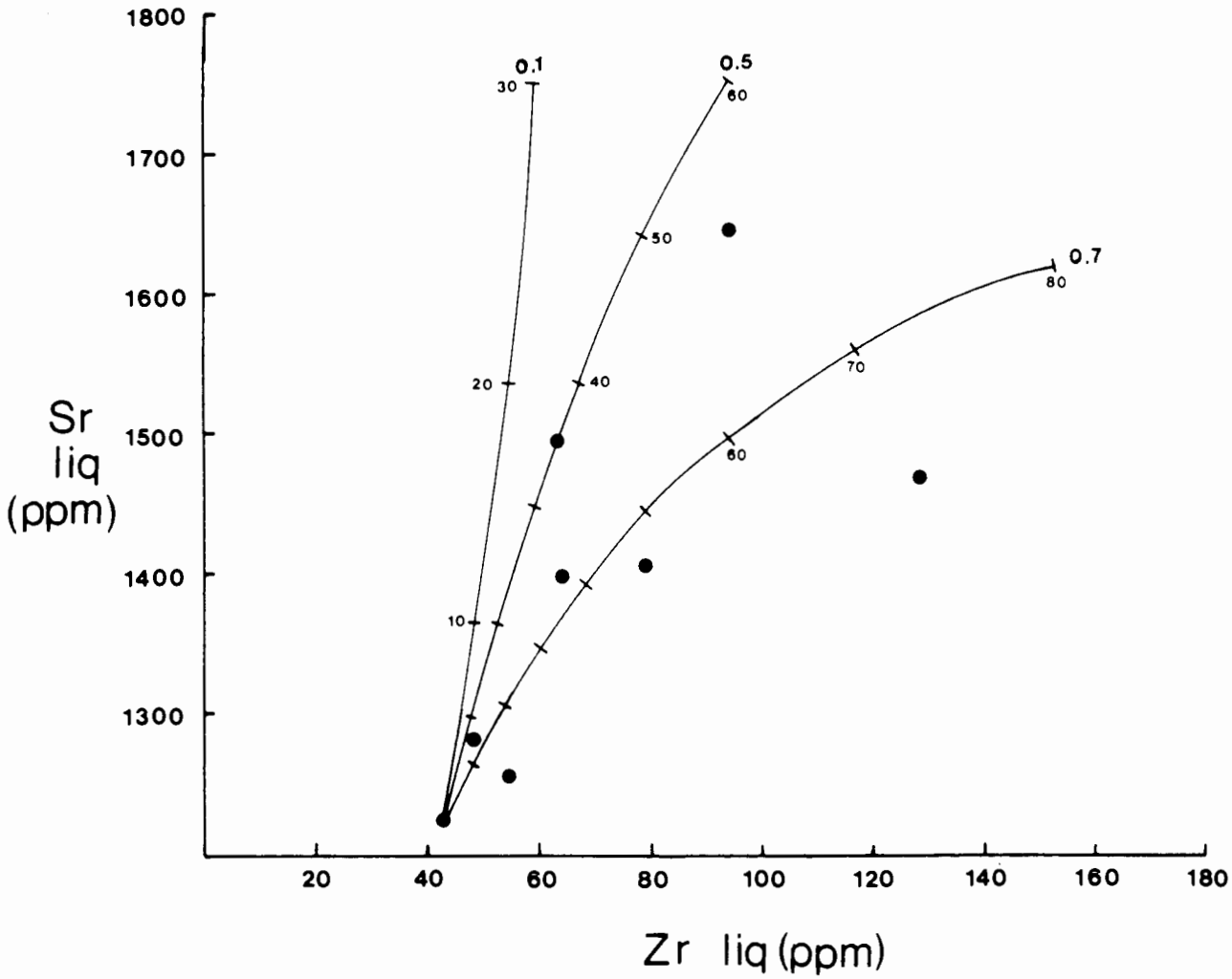
1800
1700
1600
1500
1400
1300
Sr
liq
(ppm)
0.1
0.5
0.7
10
20
30
40
50
60
70
80
20
40
60
80
100
120
140
160
180
Zr liq (ppm)

Figure 4.20

Calculated Ti and Zr liquid compositions (in ppm) in equilibrium with the group 1 clinopyroxene megacrysts from Schuller. Assuming that the least fractionated samples represent the liquidus composition, the evolution of liquid lines of descent using an equilibrium crystallisation model are shown for Ti bulk distribution coefficients of 0.3, 0.4 and 0.5 respectively. A Zr bulk distribution coefficient of 0.1 was used.

Figure 4.20

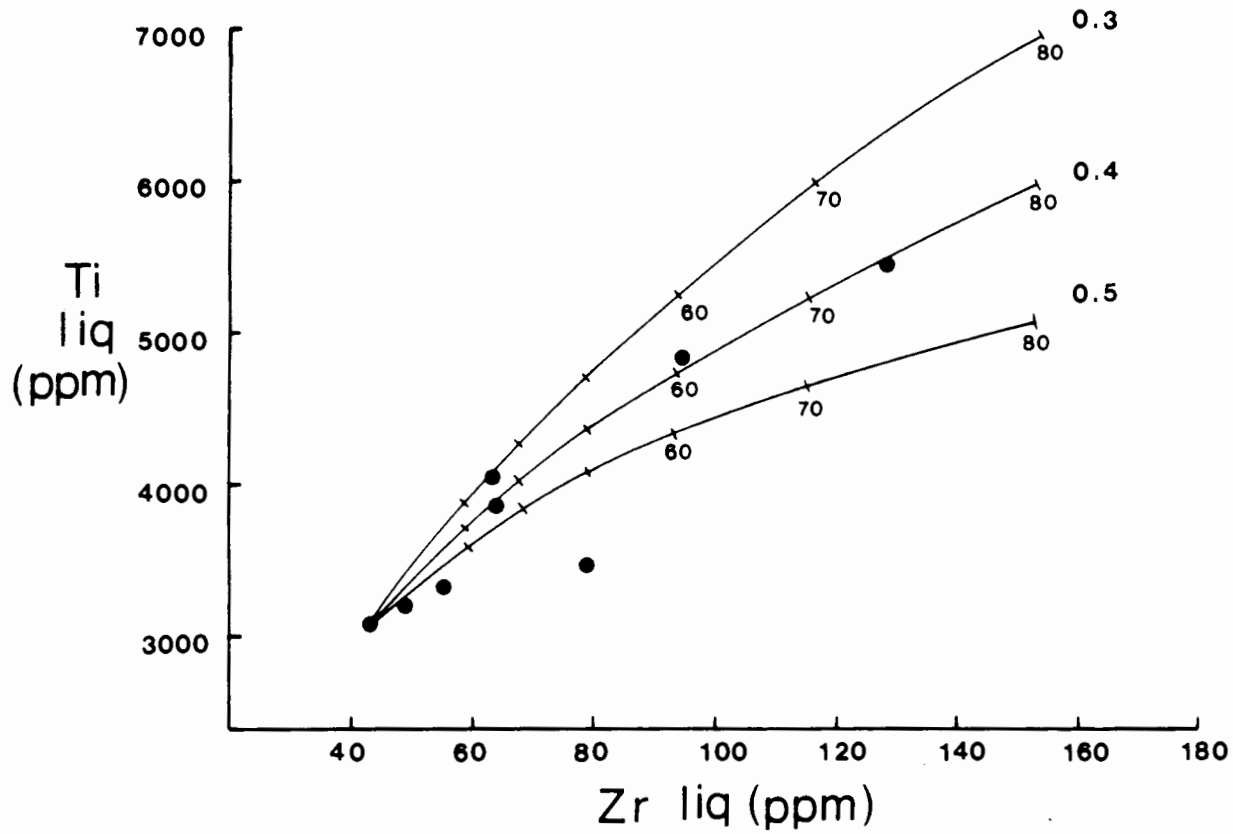
7000
6000
5000
4000
3000
Ti
liq
(ppm)
40
60
80
100
120
140
160
180
Zr liq (ppm)
0.3
0.4
0.5
60
70
80

Figure 5.1

Ca# (atomic) versus Mg# (atomic) in clinopyroxene megacrysts from Schuller. The solid circles show the samples selected for Rb/Sr and Sm/Nd isotopic analyses.

Figure 5.2

Ca# (atomic) versus Mg# (atomic) in clinopyroxene megacrysts from Premier. The solid circles show the samples selected for Rb/Sr and Sm/Nd isotopic analyses.

Figure 5.1

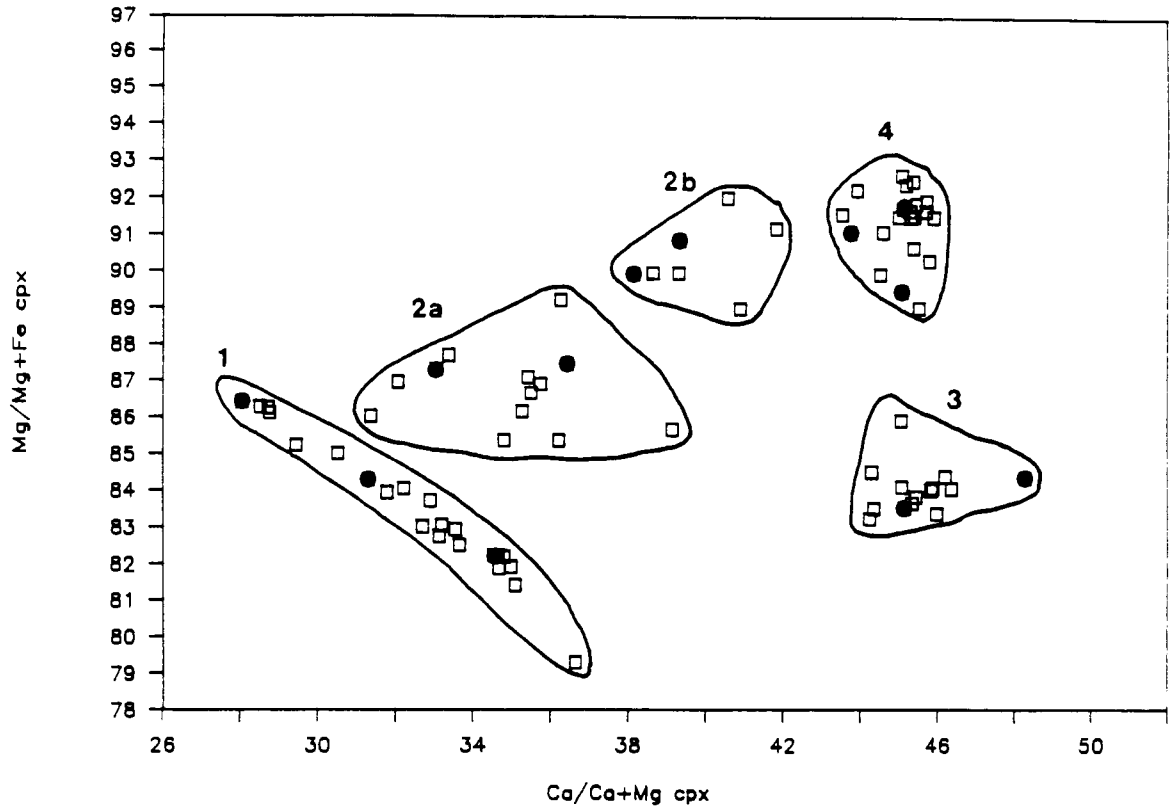

Figure 5.2

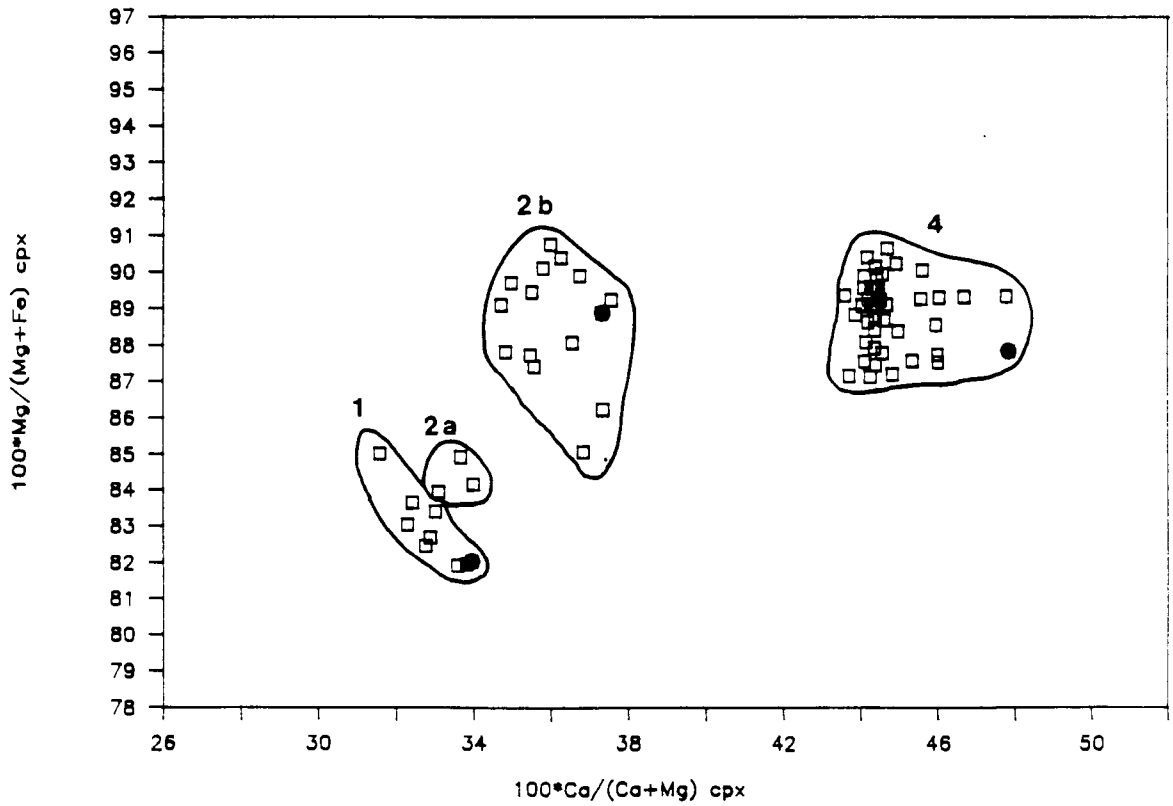

Figure 5.3

The variation of Sm (ppm) and Nd (ppm) in clinopyroxene megacrysts from the Schuller and Premier kimberlites. The symbols refer to the compositional groups discussed in the text. Note that sample 86/2 plots off scale in this diagram (Sm = 1.93 ppm ; Nd = 14.05 ppm).

Figure 5.4

Variation in the reciprocal of the Nd concentration (ppm) with the $^{143}Nd/^{144}Nd$ ratio in clinopyroxenes from megacrysts from the Schuller and Premier kimberlites. The symbols refer to the compositional groups discussed in the text.

Figure 5.3

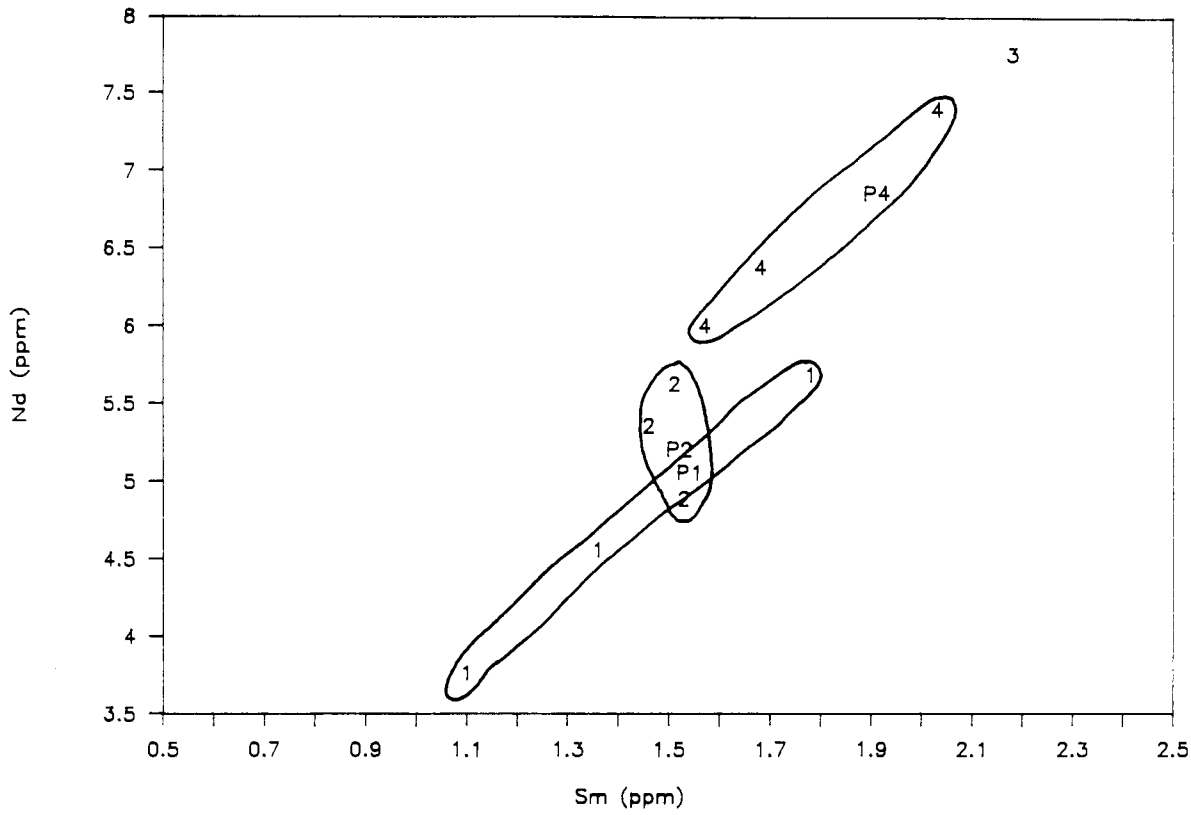

Figure 5.4

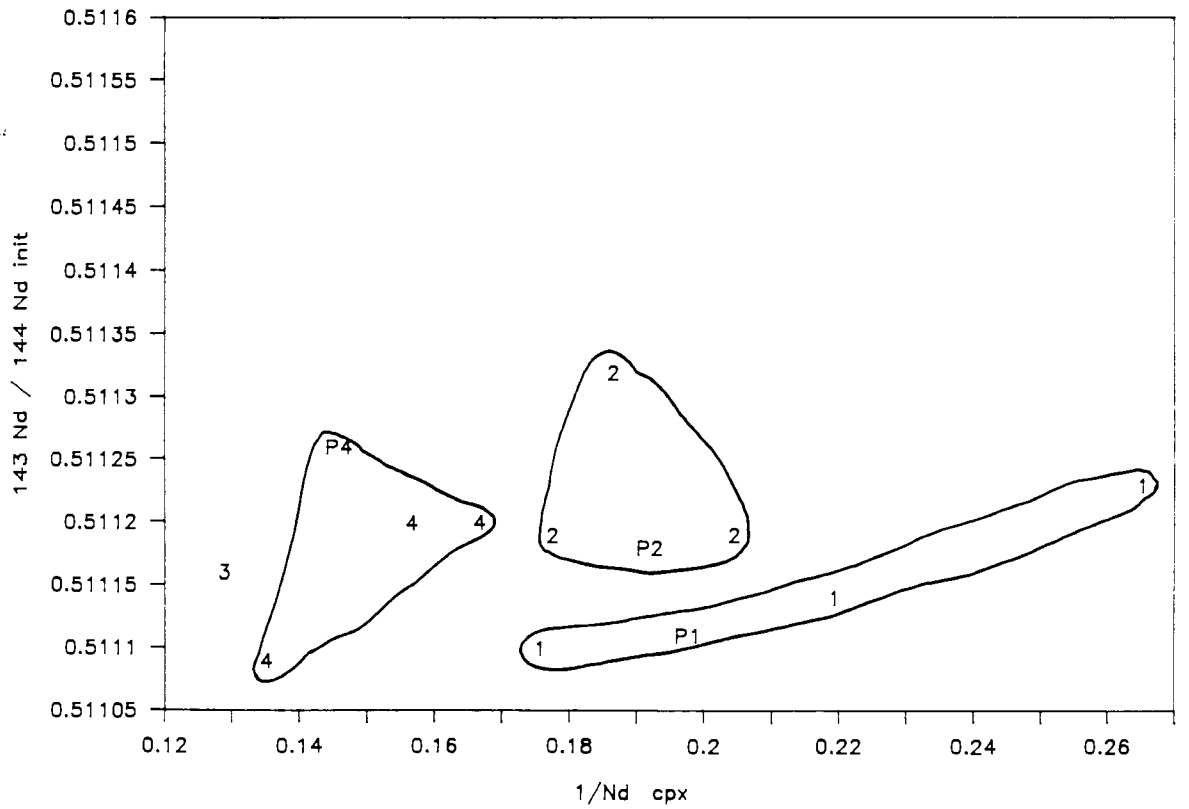

Figure 5.5

Variation in the reciprocal Sr concentration (ppm) with the $^{87}Sr/^{86}Sr$ ratio in clinopyroxenes from megacrysts from the Schuller and Premier kimberlites. The symbols refer to the compositional groups discussed in the text.

Figure 5.6

eSr versus eNd (calculated at 1198 Ma) for clinopyroxene megacrysts from the Schuller and Premier kimberlites. The symbols refer to the compositional groups discussed in the text.

Figure 5.5

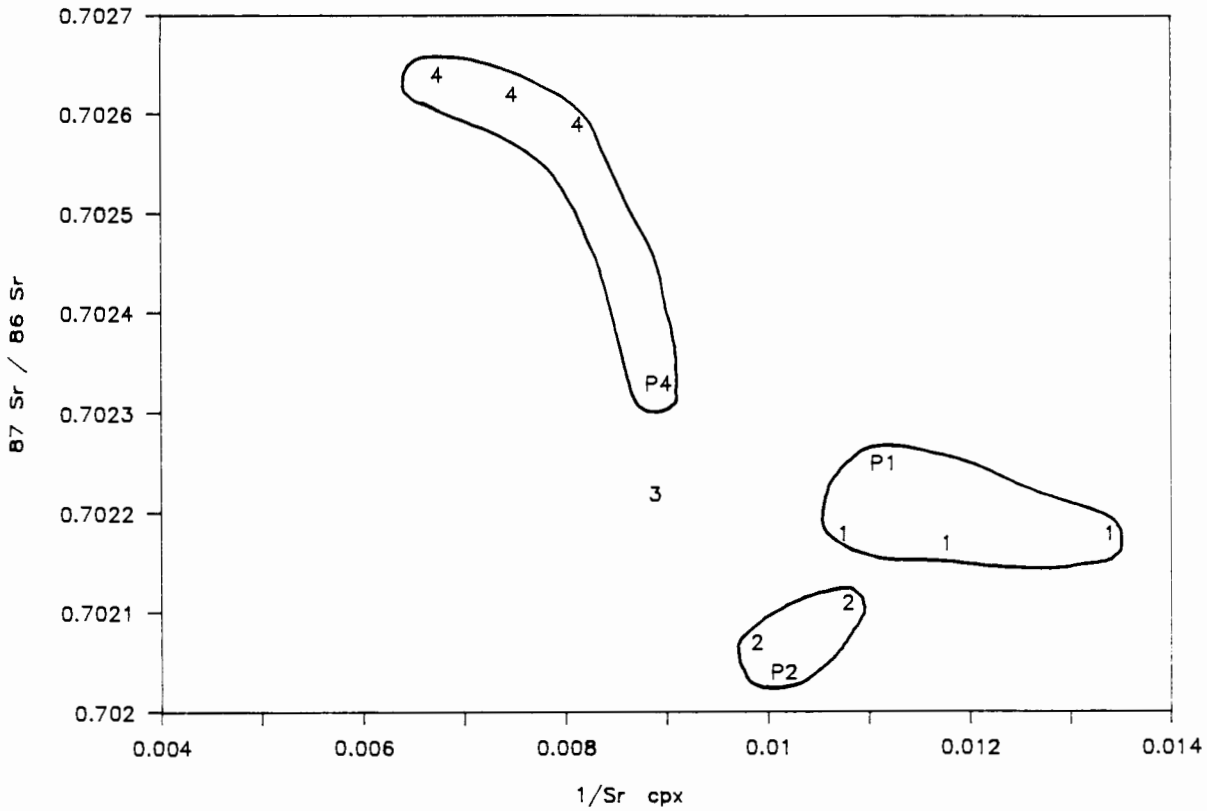

Figure 5.6

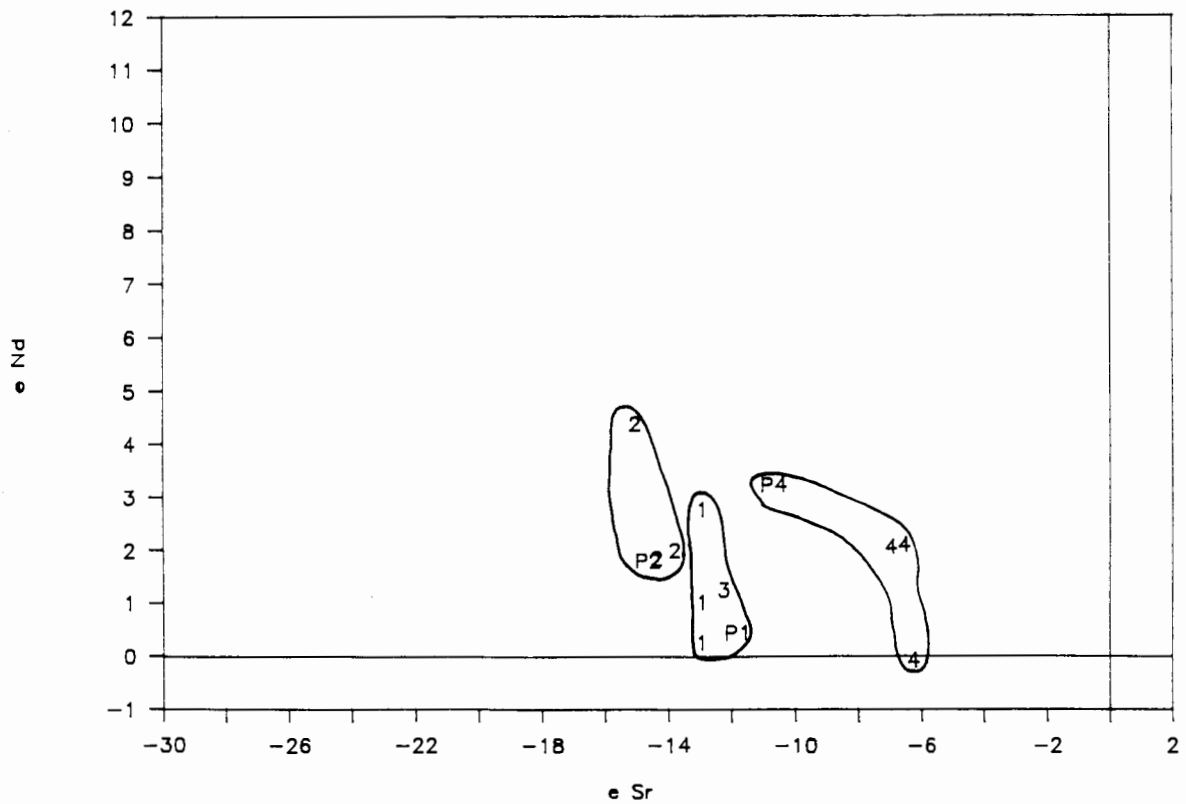

Figure 5.7

eSr versus eNd (calculated at 90 Ma) for clinopyroxene megacrysts, Granny Smith megacrysts and clinopyroxene from deformed lherzolites from the Jagersfontein kimberlite (Hops, 1989) (P = clinopyroxenes from high temperature lherzolites; M = Cr-poor clinopyroxene megacrysts; GS = Granny Smith megacrysts).

Figure 5.7

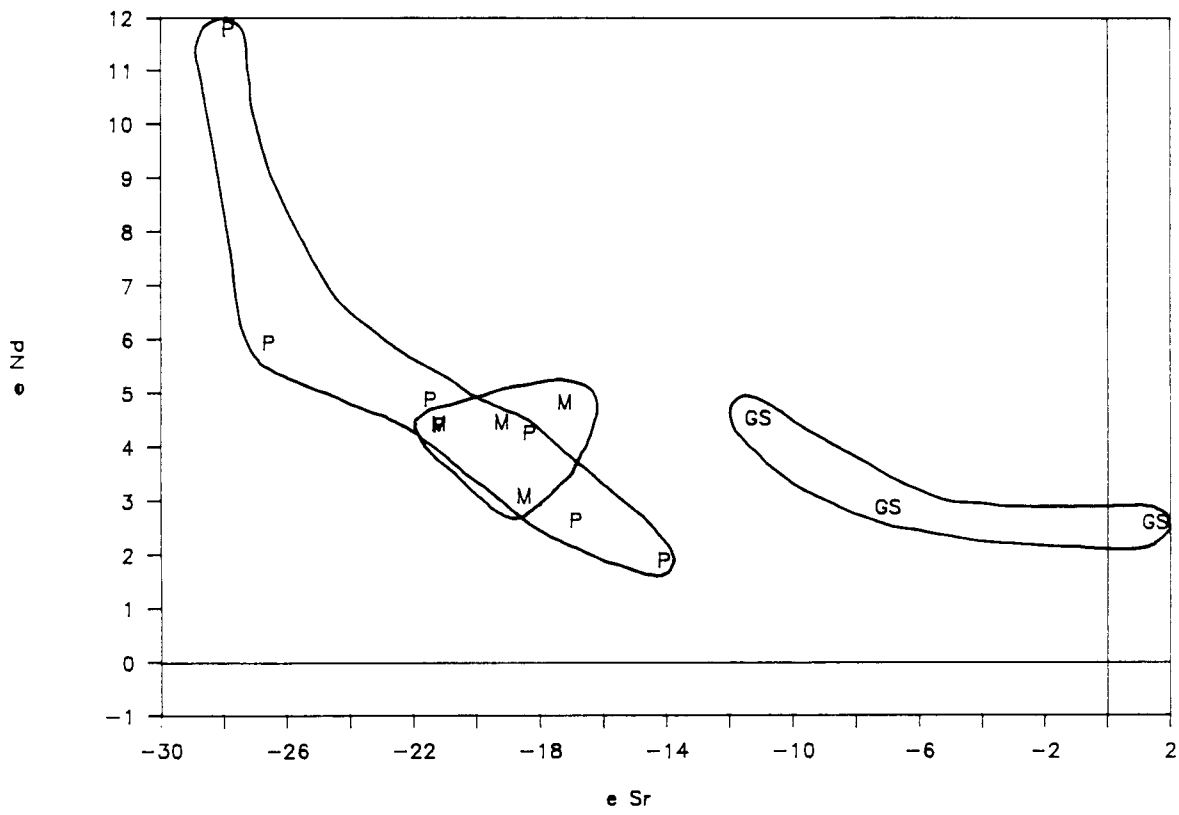
12
11
10
9
8
7
6
5
4
3
2
1
0
−1
−30
−26
−22
−18
−14
−10
−6
−2
2
e Nd
e Sr
P
P
P
M
M
P
M
P
P
GS
GS
GS

Figure 6.1

A pictorial summary of the various Schuller megacryst crystallisation events as is discussed in the text. The numbers above each crystallising phase correspond to the symbols used in the previous figures.

Figure 6.1

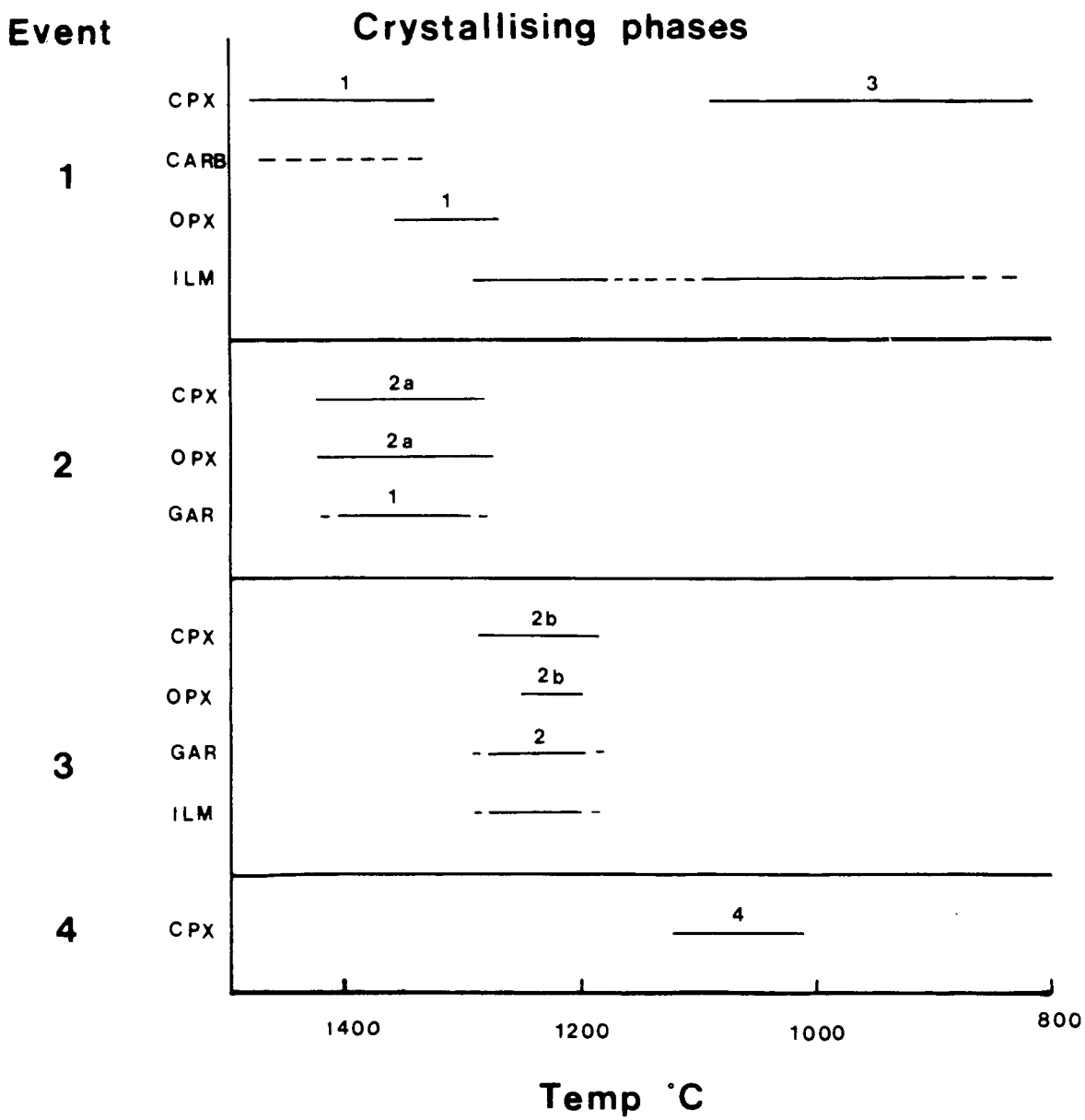
Event
Crystallising phases
CPX
CARB
OPX
ILM
1
3
1
1
2
CPX
OPX
GAR
2a
2a
1
3
CPX
OPX
GAR
ILM
2b
2b
2
4
CPX
4
1400
1200
1000
800
Temp °C

LIST OF APPENDICES

APPENDIX 1 :ANALYTICAL CONDITIONS ELECTRON MICROPROBE 200

APPENDIX 2 : MINERAL ANALYSES - MEGACRYSTS FROM SCHULLER 203

Table 1 - Clinopyroxene 205
Table 2 - Orthopyroxene 211
Table 3 - Garnet 214
Table 4 - Ilmenite 218
Table 5 - Olivine 224
Table 6 - Megacryst inclusions 225

APPENDIX 3 : CLINOPYROXENE MEGACRYSTS FROM PREMIER AND ORAPA 227

Table 1 - Premier 228
Table 2 - Orapa 234

APPENDIX 4 : TRACE ELEMENT ANALYSES OF SCHULLER MEGACRYST 237

Table 1 - Clinopyroxene 238
Table 2 - Orthopyroxene 239
Table 3 - Garnet 240

APPENDIX 5 : ANALYTICAL TECHNIQUES FOR ISOTOPE ANALYSIS 241

APPENDIX 6 : ISOTOPE RESULTS 247

Table 1 - ID and proton probe comparison 248
Table 2 - Sr isotope results 249
Table 3 - Nd isotope results 250

APPENDIX 1

ANALYTICAL CONDITIONS - ELECTRON MICROPROBE

The major element compositions were obtained either on a Cameca/Camebax microprobe at the University of Cape Town or a Jeol 733 microprobe at the South African Geological Survey.

The following instrumental conditions were used at the University of Cape Town:

Instrument	: Cameca/Camebax
Beam current	: 40 nA
kV	: 15
Peak counting	: 10 sec
Background counting	: 2 x 5 sec
Spot size	: 5 microns

Elements	Analysing crystal
Na, Mg, Si and Al	TLAP
Fe, Mn and Ni	LIF200
Ca, K, Ti and Cr	PET

Standards:	Garnet	Pyroxene	Olivine	Ilmenite
Si	K-P	DIOP	M-OL	K-P
Ti	RUT	RUT	RUT	RUT
Al	K-P	K-P	K-P	CHRO
Cr	CHRO	CHRO	CHRO	CHRO
Fe	K-P	K-P	M-OL	ILMT
Mn	RHOD	RHOD	RHOD	RHOD
Mg	K-P	DIOP	M-OL	CHRO
Ca	K-P	DIOP	K-P	K-P
NA	K-H	K-H		
K		K-H		
Ni			NISI	

The following instrumental conditions were used at the Geological Survey:

Instrument:	: Jeol 733
kV	: 15
Beam current	: 20 nA
Peak counting	: 10 sec
Background counting	: 2 x 5 sec
Spot size	: 3 - 4 microns

Elements	Analysing crystal	Counter
Si, Al, Na, Mg	TAP	Gas flow
Ti, Cr	PET	Xenon
Fe, Mn, Zn	LIF	Xenon
Ca, K	PET	Gas flow

Standards:	Garnet	Pyroxene	Ilmenite
Si	K-P	DIOP-N	K-P
Ti	RUT	RUT	RUT
Al	K-P	K-P	CHRO-T
Cr	CHRO-T	CHRO-T	CHRO-T
Fe	K-P	K-P	ILMT
Mn	RHOD	RHOD	RHOD
Mg	K-P	DIOP-N	CHRO-T
Ca	K-P	DIOP-N	K-P
NA	K-H	K-H	

CHRO :Chromite 52NL11

CHRO-T :Chromite, Teibaghi Mine : USNM 117075

DIOP :Diopside Glass S-25, Boyd

DIOP-N :Diopside, Natural Bridge : USNM 117733

K-H :Hornblende, Kakanui : USNM 143965

K-P :Pyrope, Kakanui : USNM 143968

RHOD :Rhodonite, Boyd

RUT :Rutile, synthetic Boyd

Analyses for the USNM samples can be found in Jarosewich et al. (1980).

APPENDIX 2

MINERAL ANALYSES - MEGACRYSTS FROM SCHULLER

Table 1 - Clinopyroxene

Table 2 - Orthopyroxene

Table 3 - Garnet

Table 4 - Ilmenite

Table 5 - Olivine

Table 6 - Megacrysts associated with other phases

The average composition of a at least three analyses are listed for each megacryst. Samples with a suffix of "S" were analysed on polished thin sections while the remainder were analysed on multiple grain mounts. Polished thin sections were made for all co-existing megacryst phases. The following abbreviations are used in the tables:

Clinopyroxene, orthopyroxene and garnet:

CA = 100Ca/(Ca+Mg+Fe)

MG = 100Mg/(Ca+Mg+Fe)

FE = 100Fe/(Ca+Mg+Fe)

Ca# = 100Ca/(Ca+Mg)

Mg# = 100Mg/(Mg+Ca)

Olivine:

$$FO = 100Mg/(Mg+Fe)$$

Ilmenite:

$$ILM = 200Fe^{2+}/(2Fe^{2+} + 2Mg + Fe^{3+})$$

$$GK = 200\ Mg/(2Fe^{2+} + 2Mg + Fe^{3+})$$

$$HM = 100Fe^{3+}/(2Fe^{2+} + 2Mg + Fe^{3+})$$

$$Mg\# = 100Mg/(Mg+Fe^{2+})$$

The Fe^{3+} contents of ilmenites were calculated from the stoichiometry after the method of Droop (1987).

TABLE NO: 1

CLINOPYROXENE MEGACRYST COMPOSITIONS FROM SCHULLER

SAMPLE	CPX 3	86/1	86/4	PX 4	86/21	CPX 38	CPX 19	CPX 32	CPX 31	86/141	CPX 28	CPX 10	CPX 27
TYPE	1	1	1	1	1	1	1	1	1	1	1	1	1
SiO2	55.45	55.91	55.65	55.57	55.62	55.44	55.04	55.05	55.30	54.99	54.69	54.46	54.59
TiO2	0.23	0.23	0.24	0.24	0.22	0.25	0.27	0.28	0.29	0.32	0.33	0.32	0.31
Al2O3	2.50	2.47	2.47	2.53	2.56	2.55	2.54	2.53	2.44	2.55	2.55	2.48	2.54
Cr2O3	0.26	0.25	0.26	0.26	0.25	0.26	0.19	0.19	0.16	0.17	0.14	0.18	0.14
FeO	6.16	6.14	6.15	6.20	6.17	6.45	6.56	6.74	6.85	6.77	7.16	6.91	7.17
MnO	0.12	0.17	0.14	0.14	0.17	0.13	0.14	0.14	0.12	0.18	0.15	0.16	0.16
MgO	22.04	21.99	21.74	21.87	21.51	20.93	20.87	20.34	20.10	20.03	19.64	19.94	19.30
CaO	11.94	11.92	12.05	12.25	12.07	12.14	12.74	12.87	13.01	13.23	13.26	13.59	13.29
Na2O	1.45	1.36	1.42	1.33	1.41	1.52	1.53	1.61	1.66	1.49	1.68	1.60	1.70
K2O	0.06	0.00	0.00	0.00	0.04	0.00	0.00	0.00	0.00	0.00	0.00	0.00	0.00
TOTAL	100.21	100.44	100.12	100.39	100.02	99.67	99.88	99.75	99.93	99.73	99.60	99.64	99.20
OXYGEN	6	6	6	6	6	6	6	6	6	6	6	6	6
SI	1.977	1.985	1.984	1.978	1.985	1.989	1.977	1.982	1.988	1.982	1.979	1.971	1.984
TI	0.006	0.006	0.006	0.006	0.006	0.007	0.007	0.008	0.008	0.009	0.009	0.009	0.008
AL	0.105	0.103	0.104	0.106	0.108	0.108	0.108	0.107	0.103	0.108	0.109	0.106	0.109
CR	0.007	0.007	0.007	0.007	0.007	0.007	0.005	0.005	0.005	0.005	0.004	0.005	0.004
FE	0.184	0.182	0.183	0.185	0.184	0.194	0.197	0.203	0.206	0.204	0.217	0.209	0.218
MN	0.004	0.005	0.004	0.004	0.005	0.004	0.004	0.004	0.004	0.005	0.005	0.005	0.005
MG	1.171	1.164	1.155	1.160	1.144	1.119	1.117	1.091	1.077	1.076	1.059	1.076	1.045
CA	0.456	0.454	0.460	0.467	0.462	0.467	0.490	0.497	0.501	0.511	0.514	0.527	0.518
NA	0.100	0.094	0.098	0.092	0.098	0.106	0.107	0.113	0.116	0.104	0.118	0.112	0.120
K	0.003	0.000	0.000	0.000	0.002	0.000	0.000	0.000	0.000	0.000	0.000	0.000	0.000
SUM	4.013	4.000	4.003	4.005	4.001	4.000	4.013	4.010	4.008	4.005	4.014	4.021	4.011
CA	25.19	25.20	25.59	25.79	25.79	26.23	27.17	27.72	28.09	28.53	28.72	29.09	29.06
MG	64.67	64.67	64.22	64.03	63.92	62.89	61.91	60.94	60.36	60.08	59.17	59.37	58.70
FE	10.14	10.13	10.19	10.19	10.29	10.88	10.92	11.33	11.54	11.39	12.11	11.54	12.24
Ca#	28.03	28.04	28.50	28.71	28.75	29.43	30.50	31.27	31.76	32.20	32.68	32.89	33.11
Mg#	86.44	86.45	86.30	86.27	86.14	85.26	85.01	84.32	83.95	84.06	83.02	83.72	82.75

TABLE NO: 1

CLINOPYROXENE MEGACRYST COMPOSITIONS FROM SCHULLER

SAMPLE	CPX14S	86/19	CPX 47	CPX 24	86/143	DB 5-1	CPX 3S	SN10	86/20	CPX13S	CPX 48	CPX 23	CPX 17
TYPE	1	1	1	1	1	1	1	1	1	1	2	2	2
SiO2	55.21	55.20	55.01	54.57	54.72	54.75	55.18	54.88	55.00	54.86	55.51	54.97	55.16
TiO2	0.34	0.35	0.35	0.39	0.45	0.40	0.37	0.40	0.39	0.49	0.32	0.36	0.31
Al2O3	2.45	2.64	2.48	2.55	2.53	2.41	2.78	2.46	2.46	2.62	2.44	2.46	2.30
Cr2O3	0.15	0.14	0.13	0.13	0.10	0.13	0.13	0.12	0.11	0.08	0.42	0.48	0.51
FeO	7.11	7.07	7.24	7.21	7.26	7.45	7.25	7.40	7.59	8.26	5.91	5.43	5.21
MnO	0.15	0.13	0.15	0.15	0.13	0.14	0.16	0.15	0.19	0.18	0.12	0.13	0.14
MgO	19.56	19.28	19.18	18.72	18.85	18.89	18.79	18.81	18.66	17.76	20.44	20.33	20.14
CaO	13.51	13.53	13.52	13.73	13.89	13.93	13.94	14.07	14.03	14.28	12.98	13.34	13.82
Na2O	1.51	1.57	1.59	1.70	1.76	1.62	1.74	1.58	1.62	1.79	1.67	1.67	1.53
K2O	0.00	0.00	0.00	0.00	0.04	0.04	0.04	0.00	0.00	0.04	0.00	0.00	0.04
TOTAL	99.99	99.91	99.65	99.15	99.73	99.76	100.38	99.87	100.05	100.36	99.81	99.17	99.16
OXYGEN	6	6	6	6	6	6	6	6	6	6	6	6	6
SI	1.988	1.989	1.990	1.987	1.983	1.984	1.984	1.986	1.988	1.986	1.990	1.984	1.991
TI	0.009	0.009	0.010	0.011	0.012	0.011	0.010	0.011	0.011	0.013	0.009	0.010	0.008
AL	0.104	0.112	0.106	0.109	0.108	0.103	0.118	0.105	0.105	0.112	0.103	0.105	0.098
CR	0.004	0.004	0.004	0.004	0.003	0.004	0.004	0.003	0.003	0.002	0.012	0.014	0.015
FE	0.214	0.213	0.219	0.220	0.220	0.226	0.218	0.224	0.229	0.250	0.177	0.164	0.157
MN	0.005	0.004	0.005	0.005	0.004	0.004	0.005	0.005	0.006	0.006	0.004	0.004	0.004
MG	1.050	1.035	1.034	1.016	1.018	1.020	1.007	1.014	1.005	0.958	1.092	1.093	1.083
CA	0.521	0.522	0.524	0.536	0.539	0.541	0.537	0.546	0.543	0.554	0.499	0.516	0.534
NA	0.106	0.110	0.112	0.120	0.124	0.114	0.122	0.111	0.114	0.126	0.116	0.117	0.107
K	0.000	0.000	0.000	0.000	0.002	0.002	0.002	0.000	0.000	0.002	0.000	0.000	0.002
SUM	4.001	3.999	4.002	4.006	4.013	4.009	4.006	4.005	4.004	4.008	4.002	4.006	3.999
CA	29.20	29.50	29.49	30.25	30.34	30.27	30.48	30.58	30.56	31.43	28.20	29.09	30.11
MG	58.80	58.47	58.19	57.36	57.28	57.09	57.15	56.86	56.53	54.37	61.77	61.67	61.03
FE	11.99	12.03	12.33	12.40	12.38	12.64	12.37	12.55	12.90	14.19	10.02	9.24	8.86
Ca#	33.18	33.53	33.63	34.53	34.63	34.65	34.79	34.97	35.09	36.63	31.35	32.05	33.04
Mg#	83.06	82.93	82.52	82.23	82.23	81.88	82.20	81.92	81.42	79.30	86.04	86.97	87.32

TABLE NO: 1

CLINOPYROXENE MEGACRYST COMPOSITIONS FROM SCHULLER

SAMPLE	CPX 42	CPX1S	DB 5-5	CPX 46	CPX 30	CPX 35	CPX2S	CPX16S	CPX 26	CPX 6	CPX11S	CPX 41	CPX10S
TYPE	2	2	2	2	2	2	2	2	2	2	2	2	2
SiO2	55.21	55.27	55.08	55.02	54.70	54.56	55.31	55.25	54.55	54.47	55.33	54.57	55.02
TiO2	0.33	0.42	0.41	0.39	0.39	0.41	0.47	0.34	0.44	0.39	0.21	0.50	0.32
Al2O3	2.30	2.49	2.44	2.41	2.43	2.46	2.43	2.46	2.39	2.22	2.07	2.44	2.13
Cr2O3	0.72	0.37	0.48	0.62	0.51	0.51	0.40	0.50	0.55	0.99	0.86	0.30	0.61
FeO	4.97	5.93	5.56	5.11	5.26	5.16	5.77	4.23	4.88	3.83	3.83	5.38	3.77
MnO	0.14	0.17	0.14	0.14	0.12	0.13	0.15	0.12	0.13	0.13	0.00	0.15	0.12
MgO	19.88	19.44	19.41	19.35	19.20	19.23	18.90	19.63	19.11	19.19	19.26	18.05	18.94
CaO	13.84	14.42	14.70	14.75	14.69	14.87	14.91	15.52	15.21	16.44	16.86	16.13	17.05
Na2O	1.71	1.65	1.59	1.72	1.72	1.78	1.59	1.47	1.78	1.66	1.34	1.96	1.38
K2O	0.00	0.04	0.00	0.00	0.00	0.00	0.04	0.04	0.00	0.00	0.04	0.00	0.04
TOTAL	99.10	100.20	99.81	99.51	99.02	99.11	99.97	99.56	99.04	99.32	99.80	99.48	99.38
OXYGEN	6	6	6	6	6	6	6	6	6	6	6	6	6
SI	1.993	1.984	1.983	1.985	1.984	1.979	1.990	1.986	1.980	1.972	1.988	1.981	1.987
TI	0.009	0.011	0.011	0.011	0.011	0.011	0.013	0.009	0.012	0.011	0.006	0.014	0.009
AL	0.098	0.105	0.104	0.102	0.104	0.105	0.103	0.104	0.102	0.095	0.088	0.104	0.091
CR	0.021	0.010	0.014	0.018	0.015	0.015	0.011	0.014	0.016	0.028	0.024	0.009	0.017
FE	0.150	0.178	0.167	0.154	0.160	0.157	0.174	0.127	0.148	0.116	0.115	0.163	0.114
MN	0.004	0.005	0.004	0.004	0.004	0.004	0.005	0.004	0.004	0.004	0.000	0.005	0.004
MG	1.069	1.040	1.041	1.040	1.038	1.039	1.013	1.052	1.034	1.035	1.032	0.977	1.019
CA	0.535	0.555	0.567	0.570	0.571	0.578	0.575	0.598	0.591	0.638	0.649	0.627	0.660
NA	0.120	0.115	0.111	0.120	0.121	0.125	0.111	0.103	0.125	0.117	0.094	0.138	0.097
K	0.000	0.002	0.000	0.000	0.000	0.000	0.002	0.002	0.000	0.000	0.002	0.000	0.002
SUM	3.999	4.005	4.003	4.005	4.007	4.013	3.997	3.998	4.012	4.015	3.997	4.018	3.999
CA	30.50	31.29	31.93	32.31	32.29	32.58	32.63	33.65	33.36	35.65	36.15	35.50	36.80
MG	60.94	58.67	58.64	58.95	58.69	58.60	57.52	59.19	58.29	57.87	57.44	55.26	56.85
FE	8.55	10.04	9.43	8.74	9.02	8.82	9.85	7.16	8.35	6.48	6.41	9.24	6.35
Ca#	33.36	34.78	35.25	35.40	35.49	35.73	36.19	36.24	36.40	38.12	38.63	39.12	39.29
Mg#	87.70	85.38	86.15	87.09	86.67	86.91	85.37	89.21	87.47	89.93	89.96	85.67	89.95

TABLE NO: 1

CLINOPYROXENE MEGACRYST COMPOSITIONS FROM SCHULLER

SAMPLE	CPX 11	CPX 45	CPX5S	CPX 36	CPX 4	CPX 39	CPX 33	86/5	86/2	CPX 34	CPX 37	CPX17S	CPX8S
TYPE	2	2	2	2	3	3	3	3	3	3	3	3	3
SiO2	55.22	54.88	54.70	54.30	54.63	54.06	54.29	54.67	54.72	54.16	54.07	54.36	54.67
TiO2	0.21	0.41	0.42	0.49	0.34	0.38	0.40	0.38	0.42	0.32	0.37	0.37	0.38
Al2O3	1.86	2.09	2.02	1.60	2.63	2.68	2.56	2.56	2.87	2.68	2.73	2.72	2.79
Cr2O3	1.04	0.99	1.24	0.82	0.39	0.51	0.48	0.43	0.33	0.34	0.39	0.28	0.24
FeO	3.39	2.82	4.00	3.22	5.35	5.67	4.75	5.49	5.56	5.55	5.44	5.42	5.65
MnO	0.11	0.10	0.14	0.11	0.13	0.14	0.12	0.00	0.13	0.10	0.13	0.11	0.12
MgO	18.88	18.26	18.12	18.69	16.39	16.12	16.26	16.31	15.84	15.96	15.84	16.00	15.91
CaO	17.01	17.32	17.43	18.68	18.12	17.86	18.53	18.60	18.12	18.40	18.34	18.82	18.83
Na2O	1.38	1.53	1.54	1.17	1.86	1.93	1.85	1.70	1.92	1.89	1.95	1.76	1.92
K2O	0.04	0.00	0.04	0.00	0.00	0.00	0.00	0.00	0.00	0.00	0.00	0.00	0.00
TOTAL	99.14	98.40	99.65	99.08	99.84	99.35	99.24	100.14	99.91	99.40	99.26	99.84	100.51
OXYGEN	6	6	6	6	6	6	6	6	6	6	6	6	6
SI	1.997	1.996	1.980	1.975	1.985	1.979	1.983	1.983	1.988	1.981	1.981	1.980	1.979
TI	0.006	0.011	0.011	0.013	0.009	0.010	0.011	0.010	0.011	0.009	0.010	0.010	0.010
AL	0.079	0.090	0.086	0.069	0.113	0.116	0.110	0.109	0.123	0.116	0.118	0.117	0.119
CR	0.030	0.028	0.035	0.024	0.011	0.015	0.014	0.012	0.009	0.010	0.011	0.008	0.007
FE	0.103	0.086	0.121	0.098	0.163	0.174	0.145	0.167	0.169	0.170	0.167	0.165	0.171
MN	0.003	0.003	0.004	0.003	0.004	0.004	0.004	0.000	0.004	0.003	0.004	0.003	0.004
MG	1.017	0.990	0.978	1.013	0.888	0.879	0.885	0.882	0.857	0.870	0.865	0.868	0.859
CA	0.659	0.675	0.676	0.728	0.706	0.700	0.725	0.723	0.705	0.721	0.720	0.734	0.731
NA	0.097	0.108	0.108	0.083	0.131	0.137	0.131	0.120	0.135	0.134	0.139	0.124	0.135
K	0.002	0.000	0.002	0.000	0.000	0.000	0.000	0.000	0.000	0.000	0.000	0.000	0.000
SUM	3.992	3.987	4.003	4.006	4.009	4.014	4.009	4.006	4.002	4.014	4.014	4.010	4.015
CA	37.05	38.56	38.09	39.59	40.18	39.95	41.31	40.82	40.73	40.95	41.11	41.54	41.50
MG	57.19	56.54	55.08	55.09	50.56	50.15	50.42	49.78	49.52	49.41	49.38	49.12	48.78
FE	5.76	4.90	6.82	5.33	9.26	9.90	8.27	9.40	9.75	9.64	9.52	9.34	9.72
Ca#	39.31	40.55	40.88	41.81	44.29	44.34	45.04	45.05	45.13	45.32	45.43	45.82	45.97
Mg#	90.85	92.02	88.98	91.18	84.52	83.52	85.92	84.11	83.54	83.67	83.84	84.03	83.38

TABLE NO: 1

CLINOPYROXENE MEGACRYST COMPOSITIONS FROM SCHULLER

SAMPLE	CPX 22	CPX 40	CPX 25	DB 5-6	CPX 43	86/74	CPX 2	CPX 51	CPX 5	DB 5-4	CPX 21	CPX 18	CPX9S
TYPE	3	3	3	4	4	4	4	4	4	4	4	4	4
SiO2	53.93	53.92	54.07	55.15	54.58	54.57	54.02	54.75	53.85	54.71	54.49	54.67	54.83
TiO2	0.39	0.36	0.26	0.45	0.39	0.34	0.45	0.43	0.37	0.33	0.39	0.42	0.35
Al2O3	2.70	2.62	1.25	2.09	2.15	2.23	2.53	2.16	2.46	2.38	2.39	2.28	2.32
Cr2O3	0.33	0.33	0.30	1.29	1.15	1.10	0.82	1.26	1.12	1.45	0.67	1.16	1.27
FeO	5.19	5.30	5.23	2.93	3.04	2.65	3.41	2.99	2.83	2.42	3.54	2.75	2.53
MnO	0.10	0.12	0.09	0.11	0.00	0.00	0.11	0.08	0.14	0.10	0.10	0.00	0.00
MgO	15.74	15.68	15.86	17.87	17.41	17.64	17.09	17.15	17.10	17.06	16.83	17.14	17.20
CaO	18.79	18.84	20.59	19.14	18.83	19.20	19.06	19.18	19.44	19.45	19.21	19.58	19.70
Na2O	1.92	1.92	1.39	1.44	1.59	1.58	1.73	1.66	1.73	1.65	1.62	1.61	1.54
K2O	0.00	0.00	0.00	0.06	0.00	0.05	0.00	0.00	0.00	0.04	0.00	0.00	0.00
TOTAL	99.09	99.09	99.04	100.53	99.14	99.36	99.22	99.66	99.04	99.59	99.24	99.61	99.74
OXYGEN	6	6	6	6	6	6	6	6	6	6	6	6	6
SI	1.979	1.980	1.995	1.978	1.983	1.978	1.968	1.982	1.965	1.979	1.983	1.979	1.980
TI	0.011	0.010	0.007	0.012	0.011	0.009	0.012	0.012	0.010	0.009	0.011	0.011	0.010
AL	0.117	0.113	0.054	0.088	0.092	0.095	0.109	0.092	0.106	0.102	0.103	0.097	0.099
CR	0.010	0.010	0.009	0.037	0.033	0.032	0.024	0.036	0.032	0.041	0.019	0.033	0.036
FE	0.159	0.163	0.161	0.088	0.092	0.080	0.104	0.091	0.086	0.073	0.108	0.083	0.076
MN	0.003	0.004	0.003	0.003	0.000	0.000	0.003	0.002	0.004	0.003	0.003	0.000	0.000
MG	0.861	0.858	0.872	0.955	0.943	0.953	0.928	0.925	0.930	0.920	0.913	0.925	0.926
CA	0.739	0.741	0.814	0.735	0.733	0.746	0.744	0.744	0.760	0.754	0.749	0.759	0.762
NA	0.137	0.137	0.100	0.100	0.112	0.111	0.122	0.117	0.123	0.116	0.114	0.113	0.108
K	0.000	0.000	0.000	0.003	0.000	0.002	0.000	0.000	0.000	0.002	0.000	0.000	0.000
SUM	4.015	4.017	4.016	3.999	4.000	4.006	4.015	4.001	4.017	3.999	4.003	4.001	3.997
CA	42.00	42.07	44.06	41.36	41.46	41.92	41.90	42.28	42.79	43.16	42.33	42.97	43.20
MG	48.94	48.70	47.20	53.70	53.32	53.57	52.25	52.58	52.35	52.65	51.58	52.32	52.47
FE	9.06	9.24	8.74	4.94	5.22	4.52	5.85	5.14	4.86	4.19	6.09	4.71	4.33
Ca#	46.19	46.35	48.28	43.51	43.74	43.90	44.50	44.57	44.98	45.05	45.07	45.09	45.16
Mg#	84.39	84.06	84.38	91.57	91.08	92.23	89.93	91.09	91.50	92.63	89.44	91.74	92.38

TABLE NO: 1

CLINOPYROXENE MEGACRYST COMPOSITIONS FROM SCHULLER

SAMPLE	CPX 50	CPX 49	CPX 9	86/8	86/6	CPX 8	CPX7S	86/7	DB 5-3	CPX 44	DB 5-2
TYPE	4	4	4	4	4	4	4	4	4	4	4
SiO2	54.86	54.44	54.69	55.07	55.00	54.67	54.85	54.58	54.46	54.46	54.62
TiO2	0.38	0.43	0.30	0.32	0.40	0.43	0.40	0.42	0.37	0.43	0.43
Al2O3	2.35	2.50	2.36	2.40	2.38	2.41	2.69	2.38	2.41	2.47	2.48
Cr2O3	1.17	1.25	1.33	1.01	1.15	1.11	0.50	1.12	1.13	0.77	1.15
FeO	2.75	2.78	2.47	3.12	2.84	2.68	3.71	2.75	2.64	3.19	2.78
MnO	0.00	0.00	0.00	0.14	0.00	0.00	0.00	0.10	0.00	0.10	0.00
MgO	16.95	16.77	17.01	16.99	17.18	16.95	16.84	16.93	16.90	16.66	16.77
CaO	19.50	19.32	19.63	19.62	19.85	19.63	19.56	19.81	19.78	19.56	19.78
Na2O	1.66	1.75	1.72	1.56	1.58	1.71	1.60	1.56	1.61	1.66	1.65
K2O	0.00	0.00	0.00	0.00	0.00	0.00	0.00	0.00	0.00	0.00	0.00
TOTAL	99.62	99.24	99.51	100.23	100.38	99.59	100.15	99.65	99.30	99.30	99.66
OXYGEN	6	6	6	6	6	6	6	6	6	6	6
SI	1.984	1.978	1.980	1.983	1.977	1.979	1.978	1.977	1.978	1.980	1.977
TI	0.010	0.012	0.008	0.009	0.011	0.012	0.011	0.011	0.010	0.012	0.012
AL	0.100	0.107	0.101	0.102	0.101	0.103	0.114	0.102	0.103	0.106	0.106
CR	0.033	0.036	0.038	0.029	0.033	0.032	0.014	0.032	0.032	0.022	0.033
FE	0.083	0.084	0.075	0.094	0.085	0.081	0.112	0.083	0.080	0.097	0.084
MN	0.000	0.000	0.000	0.004	0.000	0.000	0.000	0.003	0.000	0.003	0.000
MG	0.914	0.908	0.918	0.912	0.920	0.914	0.905	0.914	0.915	0.903	0.905
CA	0.756	0.752	0.762	0.757	0.764	0.761	0.756	0.769	0.770	0.762	0.767
NA	0.117	0.123	0.121	0.109	0.110	0.120	0.112	0.110	0.114	0.117	0.116
K	0.000	0.000	0.000	0.000	0.000	0.000	0.000	0.000	0.000	0.000	0.000
SUM	3.997	4.001	4.003	3.998	4.001	4.002	4.003	4.000	4.001	4.002	4.000
CA	43.12	43.11	43.41	42.95	43.19	43.34	42.63	43.53	43.62	43.25	43.69
MG	52.13	52.05	52.32	51.72	51.99	52.05	51.05	51.75	51.84	51.24	51.52
FE	4.75	4.84	4.26	5.33	4.82	4.62	6.31	4.72	4.54	5.51	4.79
Ca#	45.27	45.30	45.35	45.36	45.38	45.43	45.51	45.69	45.70	45.77	45.89
Mg#	91.66	91.49	92.47	90.66	91.51	91.85	89.00	91.65	91.94	90.30	91.49

TABLE NO: 2

ORTHOPYROXENE MEGACRYST COMPOSITIONS FROM SCHULLER

SAMPLE	86/11	OPX20	OPX16	85/73	OPX8	OPX3	OPX12	86/10	85/9	86/148	86/13	OPX13	OPX2
TYPE	1	1	1	1	1	1	1	1	1	1	1	1	2
SiO2	56.75	55.56	56.36	56.54	55.69	55.67	56.17	56.53	56.43	56.93	57.17	56.01	56.41
TiO2	0.21	0.20	0.19	0.22	0.19	0.23	0.22	0.21	0.22	0.12	0.21	0.28	0.26
Al2O3	0.94	0.90	0.93	0.97	0.92	0.93	0.94	0.94	0.94	1.19	1.11	1.07	0.89
Cr2O3	0.01	0.01	0.01	0.08	0.01	0.01	0.08	0.07	0.01	0.25	0.14	0.08	0.11
FeO	10.07	9.96	10.14	9.52	10.98	9.29	9.19	10.62	10.41	7.99	8.24	8.85	8.12
MnO	0.13	0.21	0.15	0.14	0.17	0.00	0.16	0.18	0.18	0.12	0.13	0.14	0.14
MgO	31.37	32.19	31.14	31.28	30.99	31.92	31.79	30.62	30.71	32.15	31.55	31.57	33.24
CaO	0.75	0.86	0.85	0.87	0.87	0.90	0.91	0.89	0.92	1.16	1.35	1.40	0.90
Na2O	0.18	0.18	0.21	0.19	0.23	0.21	0.22	0.20	0.23	0.42	0.32	0.48	0.19
TOTAL	100.41	100.07	99.98	99.81	100.05	99.16	99.68	100.26	100.05	100.33	100.22	99.88	100.26
OXYG	6	6	6	6	6	6	6	6	6	6	6	6	6
SI	1.983	1.954	1.980	1.983	1.966	1.967	1.973	1.984	1.983	1.977	1.988	1.966	1.962
TI	0.006	0.005	0.005	0.006	0.005	0.006	0.006	0.006	0.006	0.003	0.005	0.007	0.007
AL	0.039	0.037	0.039	0.040	0.038	0.039	0.039	0.039	0.039	0.049	0.046	0.044	0.036
CR	0.000	0.000	0.000	0.002	0.000	0.000	0.002	0.002	0.000	0.007	0.004	0.002	0.003
FE	0.294	0.293	0.298	0.279	0.324	0.274	0.270	0.312	0.306	0.232	0.240	0.260	0.236
MN	0.004	0.006	0.004	0.004	0.005	0.000	0.005	0.005	0.005	0.004	0.004	0.004	0.004
MG	1.633	1.687	1.630	1.635	1.630	1.680	1.664	1.602	1.609	1.664	1.635	1.651	1.723
CA	0.028	0.032	0.032	0.033	0.033	0.034	0.034	0.033	0.035	0.043	0.050	0.053	0.034
NA	0.012	0.012	0.014	0.013	0.016	0.014	0.015	0.014	0.016	0.028	0.022	0.033	0.013
SUM	3.999	4.028	4.003	3.996	4.018	4.015	4.008	3.997	3.999	4.006	3.993	4.020	4.018
CA	1.44	1.61	1.63	1.68	1.66	1.71	1.74	1.72	1.78	2.23	2.61	2.68	1.68
MG	83.52	83.83	83.17	83.98	82.03	84.49	84.54	82.27	82.52	85.81	84.94	84.09	86.46
FE	15.05	14.56	15.20	14.34	16.31	13.80	13.72	16.01	15.70	11.97	12.45	13.23	11.85
Ca#	1.69	1.88	1.92	1.96	1.98	1.99	2.02	2.05	2.11	2.53	2.98	3.09	1.91
Mg#	84.74	85.21	84.55	85.41	83.41	85.96	86.04	83.71	84.02	87.76	87.22	86.41	87.94

TABLE NO: 2

ORTHOPYROXENE MEGACRYST COMPOSITIONS FROM SCHULLER

SAMPLE	OPX18	86/22	OPX15	CPX7	OPX11	86/104	PX1	OPX6	OPX19	OPX17	OPX14	86/15	OPX4
TYPE	2	2	2	2	2	2	2	2	2	2	2	2	2
SiO2	57.06	57.56	57.23	57.38	57.09	57.25	57.75	57.45	55.99	56.96	56.69	57.02	56.88
TiO2	0.28	0.19	0.21	0.18	0.19	0.22	0.13	0.15	0.24	0.19	0.24	0.25	0.25
Al2O3	0.91	0.88	0.91	0.88	0.93	0.93	0.96	0.92	0.94	0.92	0.92	1.01	0.96
Cr2O3	0.18	0.29	0.28	0.32	0.26	0.24	0.20	0.24	0.20	0.24	0.19	0.21	0.24
FeO	6.82	5.45	6.01	5.71	5.57	6.21	5.43	5.45	6.81	6.27	7.02	7.33	6.70
MnO	0.11	0.15	0.11	0.13	0.08	0.00	0.13	0.12	0.14	0.16	0.14	0.14	0.14
MgO	34.20	34.03	33.70	33.73	34.37	34.02	34.02	34.37	33.61	33.63	33.09	32.58	33.71
CaO	0.93	0.99	0.99	1.00	1.03	1.04	1.11	1.13	1.13	1.15	1.16	1.16	1.21
Na2O	0.17	0.21	0.20	0.25	0.24	0.25	0.20	0.23	0.28	0.23	0.23	0.26	0.26
TOTAL	100.66	99.75	99.64	99.58	99.76	100.16	99.93	100.06	99.34	99.75	99.68	99.96	100.35
OXYG	6	6	6	6	6	6	6	6	6	6	6	6	6
SI	1.964	1.985	1.981	1.985	1.972	1.974	1.987	1.977	1.957	1.975	1.973	1.980	1.966
TI	0.007	0.005	0.005	0.005	0.005	0.006	0.003	0.004	0.006	0.005	0.006	0.007	0.006
AL	0.037	0.036	0.037	0.036	0.038	0.038	0.039	0.037	0.039	0.038	0.038	0.041	0.039
CR	0.005	0.008	0.008	0.009	0.007	0.007	0.005	0.007	0.006	0.007	0.005	0.006	0.007
FE	0.196	0.157	0.174	0.165	0.161	0.179	0.156	0.157	0.199	0.182	0.204	0.213	0.194
MN	0.003	0.004	0.003	0.004	0.002	0.000	0.004	0.003	0.004	0.005	0.004	0.004	0.004
MG	1.755	1.749	1.739	1.739	1.769	1.748	1.745	1.763	1.751	1.738	1.717	1.686	1.736
CA	0.034	0.037	0.037	0.037	0.038	0.038	0.041	0.042	0.042	0.043	0.043	0.043	0.045
NA	0.011	0.014	0.013	0.017	0.016	0.017	0.013	0.015	0.019	0.015	0.016	0.018	0.017
SUM	4.013	3.995	3.998	3.996	4.009	4.006	3.994	4.005	4.024	4.006	4.007	3.998	4.014
CA	1.73	1.88	1.88	1.91	1.94	1.95	2.11	2.12	2.12	2.18	2.20	2.22	2.27
MG	88.38	90.03	89.19	89.58	89.89	88.94	89.85	89.88	87.88	88.56	87.39	86.82	87.92
FE	9.89	8.09	8.93	8.51	8.17	9.11	8.05	8.00	9.99	9.27	10.40	10.96	9.81
Ca#	1.92	2.05	2.07	2.09	2.11	2.15	2.29	2.31	2.36	2.40	2.46	2.50	2.52
Mg#	89.94	91.75	90.90	91.32	91.66	90.71	91.78	91.83	89.79	90.53	89.36	88.79	89.97

TABLE NO: 2

ORTHOPYROXENE MEGACRYST COMPOSITIONS FROM SCHULLER

SAMPLE	86/18	OPX1	86/17	86/16	86/14	86/121	86/103
TYPE	2	2	2	3	3	X	X
SiO2	57.27	56.89	57.62	56.14	55.75	57.85	57.83
TiO2	0.24	0.25	0.24	0.25	0.21	0.01	0.09
Al2O3	1.05	1.02	1.02	0.97	1.01	0.86	0.79
Cr2O3	0.14	0.13	0.14	0.01	0.01	0.46	0.48
FeO	7.37	7.86	7.13	12.02	12.50	4.27	4.80
MnO	0.14	0.17	0.13	0.16	0.17	0.01	0.10
MgO	32.25	32.68	32.65	29.18	28.73	36.35	35.02
CaO	1.25	1.28	1.29	1.20	1.18	0.43	0.64
Na2O	0.31	0.31	0.30	0.26	0.28	0.09	0.16
TOTAL	100.02	100.59	100.52	100.19	99.84	100.33	99.91
OXYG	6	6	6	6	6	6	6
SI	1.987	1.971	1.987	1.986	1.984	1.971	1.984
TI	0.006	0.007	0.006	0.007	0.006	0.000	0.002
AL	0.043	0.042	0.041	0.040	0.042	0.035	0.032
CR	0.004	0.004	0.004	0.000	0.000	0.012	0.013
FE	0.214	0.228	0.206	0.356	0.372	0.122	0.138
MN	0.004	0.005	0.004	0.005	0.005	0.000	0.003
MG	1.668	1.687	1.678	1.539	1.524	1.846	1.791
CA	0.046	0.048	0.048	0.045	0.045	0.016	0.024
NA	0.021	0.021	0.020	0.018	0.019	0.006	0.011
SUM	3.994	4.011	3.994	3.996	3.998	4.008	3.997
CA	2.41	2.42	2.47	2.35	2.32	0.79	1.21
MG	86.50	85.97	86.88	79.32	78.51	93.07	91.74
FE	11.09	11.60	10.65	18.34	19.17	6.14	7.06
Ca#	2.71	2.74	2.76	2.87	2.87	0.84	1.30
Mg#	88.63	88.11	89.08	81.22	80.38	93.82	92.86

TABLE NO: 3

GARNET MEGACRYST COMPOSITIONS FROM SCHULLER

SAMPLE	GA18	86/38	86/28	86/30	86/37	GA9	86/36	86/35	GA27	GA16	GA8	86/34	86/33
TYPE	1	1	1	1	1	1	1	1	1	1	1	1	1
SiO2	41.62	41.85	41.30	41.53	41.87	41.06	41.57	41.39	41.61	41.26	41.44	41.64	41.88
TiO2	0.95	1.08	1.28	1.20	1.07	1.17	1.13	0.91	1.06	1.18	1.14	1.14	0.54
Al2O3	21.04	21.60	21.07	20.72	21.64	20.74	20.89	20.66	20.50	20.87	20.44	20.74	22.52
Cr2O3	2.01	1.26	1.75	1.57	1.28	1.88	1.37	2.41	1.79	1.36	2.04	2.17	0.86
FeO	9.03	9.43	9.20	9.99	9.31	9.59	10.38	9.53	10.00	10.41	9.28	9.52	9.66
MnO	0.30	0.26	0.31	0.33	0.29	0.30	0.28	0.26	0.34	0.30	0.30	0.28	0.36
MgO	20.10	19.58	19.44	19.49	19.65	19.36	19.36	19.78	19.55	19.29	19.51	19.36	19.17
CaO	4.48	4.87	4.86	4.54	4.72	4.81	4.42	4.58	4.47	4.50	4.82	4.93	4.70
Na2O	0.10	0.10	0.10	0.11	0.10	0.10	0.10	0.10	0.10	0.11	0.09	0.11	0.09
TOTAL	99.63	100.03	99.31	99.48	99.93	99.01	99.50	99.62	99.42	99.28	99.06	99.89	99.78
OXYG	12	12	12	12	12	12	12	12	12	12	12	12	12
SI	2.992	2.996	2.984	3.002	2.998	2.983	3.005	2.988	3.010	2.993	3.005	2.998	3.000
TI	0.051	0.058	0.070	0.065	0.058	0.064	0.061	0.049	0.058	0.064	0.062	0.062	0.029
AL	1.783	1.823	1.795	1.766	1.827	1.776	1.780	1.758	1.749	1.785	1.747	1.760	1.902
CR	0.114	0.071	0.100	0.090	0.072	0.108	0.078	0.138	0.102	0.078	0.117	0.124	0.049
FE	0.543	0.565	0.556	0.604	0.557	0.583	0.628	0.575	0.605	0.631	0.563	0.573	0.579
MN	0.018	0.016	0.019	0.020	0.018	0.018	0.017	0.016	0.021	0.018	0.018	0.017	0.022
MG	2.154	2.089	2.093	2.099	2.097	2.096	2.086	2.128	2.108	2.085	2.108	2.077	2.047
CA	0.345	0.374	0.376	0.352	0.362	0.374	0.342	0.354	0.347	0.350	0.374	0.380	0.361
NA	0.014	0.014	0.014	0.015	0.014	0.014	0.014	0.014	0.014	0.015	0.013	0.015	0.013
K	0.000	0.000	0.000	0.000	0.000	0.000	0.000	0.000	0.000	0.000	0.000	0.000	0.000
SUM	8.015	8.006	8.006	8.013	8.002	8.018	8.011	8.021	8.013	8.020	8.007	8.006	8.001
CA	11.35	12.34	12.44	11.51	12.00	12.26	11.20	11.59	11.33	11.41	12.30	12.55	12.08
MG	70.80	69.01	69.19	68.72	69.51	68.65	68.26	69.60	68.90	68.00	69.23	68.54	68.54
FE	17.85	18.65	18.37	19.77	18.48	19.08	20.54	18.82	19.78	20.59	18.48	18.91	19.38
Ca#	13.81	15.17	15.24	14.35	14.73	15.16	14.10	14.27	14.12	14.36	15.08	15.48	14.99
Mg#	79.87	78.72	79.02	77.66	79.00	78.25	76.87	78.72	77.70	76.76	78.93	78.37	77.96

TABLE NO: 3

GARNET MEGACRYST COMPOSITIONS FROM SCHULLER

SAMPLE	86/31	GA25	GA26	GA13	GA3	GA22	SE5	GA20	GA5	SE30	GA19	SE6	86/39
TYPE	1	1	1	2	2	2	2	2	2	2	2	2	2
SiO2	41.67	41.53	41.62	41.62	41.87	41.38	41.11	41.60	41.85	41.61	41.60	41.56	41.71
TiO2	1.09	0.54	1.02	0.90	0.84	1.11	0.94	1.05	0.77	0.77	1.10	1.08	1.06
Al2O3	20.81	21.89	21.00	21.03	20.90	20.43	20.63	20.03	20.11	20.58	20.30	20.83	20.44
Cr2O3	1.30	1.13	1.36	2.27	2.53	2.43	2.80	2.89	3.67	3.33	2.55	2.40	2.44
FeO	10.25	9.45	9.08	8.20	8.07	8.56	8.73	8.17	7.98	7.46	8.51	8.22	8.74
MnO	0.27	0.32	0.31	0.31	0.36	0.29	0.30	0.27	0.28	0.30	0.34	0.27	0.29
MgO	19.34	19.42	19.75	20.26	19.76	19.97	19.94	20.14	19.64	20.60	19.75	20.34	19.92
CaO	4.48	4.87	4.68	4.71	4.73	4.87	4.83	4.89	4.85	4.87	4.84	4.83	4.85
Na2O	0.11	0.07	0.10	0.09	0.07	0.11	0.08	0.10	0.07	0.06	0.10	0.08	0.10
TOTAL	99.32	99.22	98.92	99.39	99.13	99.15	99.36	99.14	99.22	99.58	99.09	99.61	99.55
OXYG	12	12	12	12	12	12	12	12	12	12	12	12	12
SI	3.015	2.996	3.010	2.992	3.016	2.993	2.972	3.006	3.021	2.987	3.009	2.985	3.004
TI	0.059	0.029	0.055	0.049	0.046	0.060	0.051	0.057	0.042	0.042	0.060	0.058	0.057
AL	1.775	1.862	1.791	1.782	1.775	1.742	1.759	1.707	1.712	1.741	1.731	1.764	1.736
CR	0.074	0.064	0.078	0.129	0.144	0.139	0.160	0.165	0.209	0.189	0.146	0.136	0.139
FE	0.620	0.570	0.549	0.493	0.486	0.518	0.528	0.494	0.482	0.448	0.515	0.494	0.527
MN	0.017	0.020	0.019	0.019	0.022	0.018	0.018	0.017	0.017	0.018	0.021	0.016	0.018
MG	2.085	2.088	2.129	2.171	2.121	2.152	2.149	2.169	2.113	2.204	2.129	2.177	2.138
CA	0.347	0.376	0.363	0.363	0.365	0.377	0.374	0.379	0.375	0.375	0.375	0.372	0.374
NA	0.015	0.010	0.014	0.013	0.010	0.015	0.011	0.014	0.010	0.008	0.014	0.011	0.014
K	0.000	0.000	0.000	0.000	0.000	0.000	0.000	0.000	0.000	0.000	0.000	0.000	0.000
SUM	8.009	8.016	8.007	8.010	7.984	8.014	8.023	8.008	7.981	8.011	8.000	8.013	8.008
CA	11.38	12.41	11.93	11.99	12.28	12.38	12.27	12.45	12.63	12.38	12.43	12.22	12.32
MG	68.31	68.81	70.01	71.72	71.36	70.63	70.43	71.32	71.15	72.82	70.52	71.56	70.36
FE	20.32	18.79	18.06	16.29	16.36	16.99	17.30	16.23	16.22	14.80	17.05	16.23	17.32
Ca#	14.28	15.28	14.56	14.32	14.68	14.92	14.83	14.86	15.08	14.53	14.98	14.58	14.90
Mg#	77.08	78.55	79.49	81.49	81.35	80.61	80.28	81.46	81.43	83.11	80.53	81.51	80.24

TABLE NO: 3

GARNET MEGACRYST COMPOSITIONS FROM SCHULLER

SAMPLE	86/29	86/27	85/25	SE32	SE11	86/32	86/41	86/26	GA14	GA12	GA11	GA6	GA15
TYPE	2	2	2	2	2	2	2	2	2	2	2	2	3
SiO2	42.09	42.04	42.22	41.79	41.54	41.74	41.56	41.47	40.97	41.55	41.73	41.68	41.32
TiO2	0.95	0.86	0.86	0.67	1.05	0.82	0.92	0.95	1.00	0.93	0.90	0.81	0.80
Al2O3	20.74	20.67	19.74	20.13	19.99	20.45	20.20	20.20	19.95	20.05	20.41	19.92	21.45
Cr2O3	2.31	2.65	3.80	4.03	2.68	2.92	3.37	3.38	3.56	3.28	3.03	3.63	1.65
FeO	8.63	8.72	7.47	6.93	8.33	8.40	7.89	8.39	8.28	8.20	8.39	7.65	10.30
MnO	0.31	0.30	0.28	0.30	0.33	0.29	0.29	0.26	0.31	0.33	0.32	0.29	0.40
MgO	19.99	19.80	20.10	20.61	20.31	19.56	19.94	19.93	19.88	19.72	19.57	20.11	18.65
CaO	4.84	4.98	5.17	5.26	4.95	5.05	5.11	4.98	5.04	5.12	4.98	5.06	4.99
Na2O	0.10	0.10	0.09	0.08	0.11	0.09	0.09	0.10	0.09	0.08	0.09	0.08	0.10
TOTAL	99.96	100.12	99.73	99.80	99.29	99.32	99.37	99.66	99.08	99.26	99.42	99.23	99.66
OXYG	12	12	12	12	12	12	12	12	12	12	12	12	12
SI	3.014	3.011	3.030	2.995	3.001	3.013	2.998	2.989	2.975	3.005	3.010	3.009	2.988
TI	0.051	0.046	0.046	0.036	0.057	0.045	0.050	0.052	0.055	0.051	0.049	0.044	0.044
AL	1.751	1.745	1.670	1.701	1.702	1.740	1.718	1.717	1.708	1.709	1.735	1.695	1.829
CR	0.131	0.150	0.216	0.228	0.153	0.167	0.192	0.193	0.204	0.188	0.173	0.207	0.094
FE	0.517	0.522	0.448	0.415	0.503	0.507	0.476	0.506	0.503	0.496	0.506	0.462	0.623
MN	0.019	0.018	0.017	0.018	0.020	0.018	0.018	0.016	0.019	0.020	0.020	0.018	0.025
MG	2.133	2.113	2.150	2.201	2.187	2.104	2.144	2.141	2.152	2.125	2.104	2.164	2.010
CA	0.371	0.382	0.398	0.404	0.383	0.391	0.395	0.385	0.392	0.397	0.385	0.391	0.387
NA	0.014	0.014	0.013	0.011	0.015	0.013	0.013	0.014	0.013	0.011	0.013	0.011	0.014
K	0.000	0.000	0.000	0.000	0.000	0.000	0.000	0.000	0.000	0.000	0.000	0.000	0.000
SUM	8.001	8.002	7.987	8.010	8.022	7.996	8.003	8.012	8.020	8.002	7.994	8.001	8.014
CA	12.29	12.66	13.27	13.37	12.47	13.01	13.10	12.69	12.87	13.15	12.85	12.97	12.81
MG	70.60	70.03	71.76	72.88	71.15	70.10	71.11	70.63	70.62	70.42	70.25	71.72	66.57
FE	17.10	17.31	14.97	13.75	16.38	16.89	15.79	16.68	16.51	16.43	16.90	15.31	20.63
Ca#	14.83	15.31	15.61	15.50	14.91	15.66	15.56	15.23	15.42	15.73	15.47	15.32	16.13
Mg#	80.50	80.18	82.74	84.13	81.29	80.58	81.83	80.89	81.06	81.08	80.61	82.41	76.34

TABLE NO: 3

GARNET MEGACRYST COMPOSITIONS FROM SCHULLER

SAMPLE	86/40	GA24
TYPE	3	3
SiO2	41.33	41.04
TiO2	1.11	1.35
Al2O3	19.38	18.65
Cr2O3	4.09	3.95
FeO	8.44	9.25
MnO	0.29	0.31
MgO	19.27	19.08
CaO	5.52	5.51
Na2O	0.10	0.11
TOTAL	99.53	99.25
OXYG	12	12
SI	2.997	2.999
TI	0.061	0.074
AL	1.657	1.607
CR	0.234	0.228
FE	0.512	0.565
MN	0.018	0.019
MG	2.082	2.078
CA	0.429	0.431
NA	0.014	0.016
K	0.000	0.000
SUM	8.004	8.017
CA	14.19	14.03
MG	68.88	67.58
FE	16.93	18.39
Ca#	17.08	17.19
Mg#	80.27	78.61

TABLE NO: 4

ILMENITE MEGACRYST COMPOSITIONS FROM SCHULLER

SAMPLE	IL2	IL65	IL4	IL6	IL7	IL55	IL64	IL11	IL8	IL13	IL9	IL10S	IL15
TYPE	D	D	D	D	D	D	D	D	D	D	D	D	D
SiO2	0.00	0.00	0.00	0.00	0.00	0.00	0.00	0.00	0.00	0.00	0.00	0.00	0.00
TiO2	51.42	51.48	51.61	51.29	49.98	50.48	49.74	49.84	49.75	50.55	50.38	49.59	53.14
Al2O3	0.37	0.55	0.39	0.56	0.15	0.29	0.15	0.16	0.12	0.44	0.58	0.18	1.41
Cr2O3	0.67	0.52	0.63	1.12	0.77	0.53	0.80	0.69	0.75	0.78	0.57	0.73	1.53
Fe2O3	8.42	9.01	9.78	8.32	9.89	9.91	10.42	10.29	10.46	9.20	10.01	11.31	6.49
FeO	30.12	26.50	26.44	28.81	31.20	29.87	31.20	30.30	29.33	29.00	29.35	28.25	24.81
MnO	0.27	0.22	0.21	0.27	0.29	0.35	0.28	0.33	0.47	0.29	0.30	0.28	0.22
MgO	8.89	10.98	11.09	9.56	7.55	8.51	7.43	7.96	8.38	9.07	8.78	9.01	12.77
TOTAL	100.16	99.26	100.15	99.93	99.83	99.94	100.02	99.57	99.26	99.33	99.97	99.35	100.37
OXYG	3	3	3	3	3	3	3	3	3	3	3	3	3
SI	0.000	0.000	0.000	0.000	0.000	0.000	0.000	0.000	0.000	0.000	0.000	0.000	0.000
TI	0.914	0.908	0.903	0.908	0.901	0.902	0.896	0.898	0.897	0.904	0.897	0.889	0.912
AL	0.010	0.015	0.011	0.016	0.004	0.008	0.004	0.005	0.003	0.012	0.016	0.005	0.038
CR	0.013	0.010	0.012	0.021	0.015	0.010	0.015	0.013	0.014	0.015	0.011	0.014	0.028
FE3	0.150	0.159	0.171	0.147	0.179	0.177	0.188	0.186	0.189	0.165	0.178	0.203	0.111
FE2	0.595	0.520	0.514	0.567	0.626	0.594	0.625	0.607	0.588	0.577	0.581	0.563	0.473
MN	0.005	0.004	0.004	0.005	0.006	0.007	0.006	0.007	0.010	0.006	0.006	0.006	0.004
MG	0.313	0.384	0.385	0.335	0.270	0.301	0.265	0.284	0.299	0.321	0.310	0.320	0.434
SUM	2.000	2.000	2.000	2.000	2.000	2.000	2.000	2.000	2.000	2.000	2.000	2.000	2.000
ILM	60.55	52.88	52.24	58.10	63.53	60.36	63.51	61.69	59.89	58.82	59.30	57.20	49.14
GK	31.84	39.04	39.06	34.35	27.40	30.64	26.95	28.88	30.50	32.78	31.61	32.50	45.08
HM	7.61	8.09	8.70	7.55	9.07	9.01	9.54	9.43	9.61	8.40	9.10	10.30	5.79
Mg#	34.46	42.47	42.78	37.16	30.13	33.67	29.79	31.89	33.74	35.79	34.77	36.23	47.84

TABLE NO: 4

ILMENITE MEGACRYST COMPOSITIONS FROM SCHULLER

SAMPLE	IL11S	IL16	IL8S	IL19	IL9S	IL21	86/52	IL22	IL15S	IL23	86/64	IL24	DB72
TYPE	D	D	D	D	D	D	D	D	D	D	D	D	D
SiO2	0.00	0.00	0.00	0.00	0.00	0.00	0.00	0.00	0.00	0.00	0.00	0.00	0.00
TiO2	52.32	49.91	54.57	50.07	48.22	51.16	51.60	50.09	50.72	52.59	52.78	50.34	49.65
Al2O3	0.68	0.23	0.43	0.39	0.15	0.35	0.51	0.11	0.44	0.20	0.67	0.61	0.20
Cr2O3	0.64	0.66	2.06	0.82	0.84	0.58	0.54	0.73	0.73	0.60	1.24	1.15	0.83
Fe2O3	7.75	11.67	4.74	8.92	12.32	8.98	7.86	11.27	9.27	7.74	7.22	9.19	10.41
FeO	26.96	28.16	22.91	30.62	28.14	30.51	29.71	30.00	26.32	27.80	25.02	29.24	30.28
MnO	0.22	0.22	0.21	0.66	0.34	0.31	0.28	0.27	0.24	0.31	0.27	0.24	0.29
MgO	11.15	9.26	14.56	7.71	8.35	8.52	9.21	8.26	10.69	10.76	12.44	8.86	7.90
TOTAL	99.72	100.11	99.48	99.18	98.35	100.41	99.71	100.77	98.41	100.01	99.64	99.63	99.55
OXYG	3	3	3	3	3	3	3	3	3	3	3	3	3
SI	0.000	0.000	0.000	0.000	0.000	0.000	0.000	0.000	0.000	0.000	0.000	0.000	0.000
TI	0.917	0.887	0.935	0.906	0.878	0.910	0.918	0.891	0.904	0.924	0.917	0.899	0.895
AL	0.019	0.006	0.012	0.011	0.004	0.010	0.014	0.003	0.012	0.006	0.018	0.017	0.006
CR	0.012	0.012	0.037	0.016	0.016	0.011	0.010	0.014	0.014	0.011	0.023	0.022	0.016
FE3	0.136	0.208	0.081	0.161	0.224	0.160	0.140	0.201	0.165	0.136	0.126	0.164	0.188
FE2	0.525	0.556	0.437	0.616	0.570	0.603	0.588	0.594	0.522	0.543	0.483	0.580	0.607
MN	0.004	0.004	0.004	0.013	0.007	0.006	0.006	0.005	0.005	0.006	0.005	0.005	0.006
MG	0.387	0.326	0.494	0.276	0.301	0.300	0.325	0.291	0.378	0.375	0.428	0.313	0.282
SUM	2.000	2.000	2.000	2.000	2.000	2.000	2.000	2.000	2.000	2.000	2.000	2.000	2.000
ILM	53.58	56.42	44.93	63.30	57.95	61.35	59.82	60.25	53.13	55.10	49.61	59.47	61.74
GK	39.49	33.06	50.88	28.41	30.64	30.53	33.05	29.56	38.45	38.00	43.95	32.12	28.71
HM	6.93	10.52	4.18	8.29	11.41	8.12	7.12	10.18	8.42	6.90	6.44	8.41	9.55
Mg#	42.43	36.95	53.10	30.97	34.59	33.23	35.59	32.92	41.99	40.82	46.98	35.07	31.74

TABLE NO: 4

ILMENITE MEGACRYST COMPOSITIONS FROM SCHULLER

SAMPLE	IL25	DB74	IL27	86/57	IL29	IL61	IL31	IL56	IL33	IL12	IL34	IL13S	IL35
TYPE	D	D	D	D	D	D	D	D	D	D	D	D	D
SiO2	0.00	0.00	0.00	0.00	0.00	0.00	0.00	0.00	0.00	0.00	0.00	0.00	0.00
TiO2	47.98	49.30	50.97	51.12	50.56	50.54	50.44	51.37	50.71	50.19	49.75	51.35	50.76
Al2O3	0.11	0.16	0.70	0.58	0.46	0.32	0.27	0.42	0.61	0.21	0.33	0.28	0.22
Cr2O3	1.26	0.79	0.93	0.57	0.57	0.59	0.56	0.49	1.23	0.63	0.55	0.62	0.58
Fe2O3	11.95	10.60	8.89	8.87	8.95	10.17	9.23	6.76	10.03	9.37	8.17	7.98	7.24
FeO	28.83	30.77	28.45	27.72	29.91	29.86	30.79	30.15	28.26	30.51	32.86	31.18	30.42
MnO	0.24	0.37	0.20	0.27	0.25	0.31	0.31	0.22	0.23	0.27	0.34	0.27	0.27
MgO	7.90	7.40	9.64	10.09	8.59	8.57	8.00	8.88	9.60	8.05	6.47	8.26	8.39
TOTAL	98.27	99.39	99.78	99.22	99.29	100.36	99.59	98.29	100.67	99.24	98.48	99.94	97.89
OXYG	3	3	3	3	3	3	3	3	3	3	3	3	3
SI	0.000	0.000	0.000	0.000	0.000	0.000	0.000	0.000	0.000	0.000	0.000	0.000	0.000
TI	0.877	0.894	0.903	0.908	0.908	0.899	0.908	0.928	0.892	0.906	0.915	0.919	0.925
AL	0.003	0.005	0.019	0.016	0.013	0.009	0.008	0.012	0.017	0.006	0.010	0.008	0.006
CR	0.024	0.015	0.017	0.011	0.011	0.011	0.011	0.009	0.023	0.012	0.011	0.012	0.011
FE3	0.219	0.192	0.158	0.158	0.161	0.181	0.166	0.122	0.177	0.169	0.150	0.143	0.132
FE2	0.586	0.621	0.560	0.547	0.597	0.591	0.616	0.606	0.553	0.613	0.672	0.621	0.617
MN	0.005	0.008	0.004	0.005	0.005	0.006	0.006	0.004	0.005	0.005	0.007	0.005	0.006
MG	0.286	0.266	0.338	0.355	0.306	0.302	0.285	0.318	0.335	0.288	0.236	0.293	0.303
SUM	2.000	2.000	2.000	2.000	2.000	2.000	2.000	2.000	2.000	2.000	2.000	2.000	2.000
ILM	59.70	63.15	57.33	55.78	60.73	60.08	62.58	61.51	56.65	62.18	68.36	63.01	62.55
GK	29.16	27.06	34.61	36.19	31.09	30.72	28.98	32.29	34.29	29.23	23.98	29.74	30.74
HM	11.14	9.79	8.06	8.03	8.18	9.20	8.44	6.21	9.05	8.59	7.65	7.25	6.70
Mg#	32.81	30.00	37.65	39.35	33.86	33.84	31.65	34.42	37.71	31.98	25.97	32.07	32.95

TABLE NO: 4

ILMENITE MEGACRYST COMPOSITIONS FROM SCHULLER

SAMPLE	IL6S	IL37	86/54	IL41	DB71	IL44	86/63	IL45	IL58	IL47	IL14	IL48	IL2S
TYPE	D	D	D	D	D	D	D	D	D	D	D	D	D
SiO2	0.00	0.00	0.00	0.00	0.00	0.00	0.00	0.00	0.00	0.00	0.00	0.00	0.00
TiO2	51.01	51.19	50.81	50.78	50.28	50.64	51.30	48.34	48.11	49.50	51.06	51.13	51.88
Al2O3	0.39	0.43	0.24	0.27	0.47	0.23	0.31	0.09	0.08	0.12	0.37	0.41	0.69
Cr2O3	0.63	0.83	0.68	0.61	0.54	0.55	0.54	1.49	1.46	0.74	0.53	0.55	0.64
Fe2O3	9.95	8.09	9.03	7.29	9.89	9.69	8.76	11.55	12.54	10.96	9.00	7.87	7.21
FeO	29.67	29.75	30.73	30.75	29.31	30.98	31.08	31.19	30.55	30.06	30.34	30.62	27.82
MnO	0.25	0.28	0.31	0.26	0.27	0.26	0.31	0.25	0.36	0.26	0.28	0.24	0.33
MgO	8.95	8.98	8.22	8.22	8.77	8.02	8.27	6.75	6.93	7.96	8.58	8.48	10.38
TOTAL	100.85	99.55	100.01	98.18	99.53	100.37	100.57	99.66	100.03	99.61	100.16	99.31	98.95
OXYG	3	3	3	3	3	3	3	3	3	3	3	3	3
SI	0.000	0.000	0.000	0.000	0.000	0.000	0.000	0.000	0.000	0.000	0.000	0.000	0.000
TI	0.901	0.914	0.909	0.924	0.900	0.905	0.913	0.879	0.871	0.892	0.910	0.918	0.920
AL	0.011	0.012	0.007	0.008	0.013	0.006	0.009	0.003	0.002	0.003	0.010	0.012	0.019
CR	0.012	0.016	0.013	0.012	0.010	0.010	0.010	0.028	0.028	0.014	0.010	0.010	0.012
FE3	0.176	0.145	0.162	0.133	0.177	0.173	0.156	0.210	0.227	0.198	0.160	0.142	0.128
FE2	0.583	0.591	0.612	0.622	0.583	0.616	0.615	0.631	0.615	0.603	0.601	0.612	0.549
MN	0.005	0.006	0.006	0.005	0.005	0.005	0.006	0.005	0.007	0.005	0.006	0.005	0.007
MG	0.313	0.318	0.292	0.296	0.311	0.284	0.292	0.243	0.249	0.284	0.303	0.302	0.365
SUM	2.000	2.000	2.000	2.000	2.000	2.000	2.000	2.000	2.000	2.000	2.000	2.000	2.000
ILM	59.23	60.23	62.16	63.17	59.35	62.42	62.46	64.42	62.94	61.13	61.08	62.15	56.13
GK	31.84	32.40	29.63	30.09	31.64	28.79	29.62	24.85	25.44	28.84	30.78	30.67	37.32
HM	8.93	7.37	8.21	6.74	9.01	8.78	7.92	10.73	11.62	10.03	8.15	7.19	6.55
Mg#	34.96	34.98	32.28	32.26	34.77	31.57	32.16	27.83	28.79	32.06	33.51	33.04	39.93

TABLE NO: 4

ILMENITE MEGACRYST COMPOSITIONS FROM SCHULLER

SAMPLE	IL49	DB73	IL63	IL7S	86/66	86/56	IL50	IL51	IL52	IL53	IL54	86/60	86/55
TYPE	D	D	D	D	D	D	D	D	D	D	D	I	I
SiO2	0.00	0.00	0.00	0.00	0.00	0.00	0.00	0.00	0.00	0.00	0.00	0.00	0.00
TiO2	51.24	50.44	50.24	54.42	50.58	50.56	50.51	50.48	50.22	50.39	50.30	52.35	50.33
Al2O3	0.33	0.23	0.32	1.28	0.33	0.43	0.31	0.42	0.41	0.30	0.40	0.63	0.47
Cr2O3	0.61	0.58	0.55	2.03	0.56	0.56	0.57	0.53	0.67	0.57	0.58	0.53	0.56
Fe2O3	8.93	8.96	9.65	4.33	9.48	9.04	10.29	9.99	8.18	10.03	9.77	6.72	9.70
FeO	30.57	30.50	29.91	21.99	29.99	29.63	28.49	30.17	29.12	30.20	29.64	29.24	29.15
MnO	0.30	0.28	0.30	0.21	0.31	0.26	0.23	0.22	0.27	0.25	0.28	0.21	0.28
MgO	8.53	8.18	8.40	15.00	8.52	8.74	9.37	8.42	8.85	8.34	8.59	9.89	8.88
TOTAL	100.51	99.17	99.37	99.26	99.77	99.22	99.77	100.23	97.72	100.07	99.56	99.57	99.37
OXYG	3	3	3	3	3	3	3	3	3	3	3	3	3
SI	0.000	0.000	0.000	0.000	0.000	0.000	0.000	0.000	0.000	0.000	0.000	0.000	0.000
TI	0.910	0.910	0.903	0.928	0.905	0.908	0.899	0.900	0.913	0.901	0.901	0.927	0.901
AL	0.009	0.007	0.009	0.034	0.009	0.012	0.009	0.012	0.012	0.008	0.011	0.017	0.013
CR	0.011	0.011	0.010	0.036	0.011	0.011	0.011	0.010	0.013	0.011	0.011	0.010	0.011
FE3	0.159	0.162	0.174	0.074	0.170	0.162	0.183	0.178	0.149	0.179	0.175	0.119	0.174
FE2	0.604	0.612	0.598	0.417	0.597	0.591	0.564	0.598	0.589	0.600	0.591	0.576	0.580
MN	0.006	0.006	0.006	0.004	0.006	0.005	0.005	0.004	0.006	0.005	0.006	0.004	0.006
MG	0.300	0.293	0.299	0.507	0.302	0.311	0.330	0.297	0.319	0.295	0.305	0.347	0.315
SUM	2.000	2.000	2.000	2.000	2.000	2.000	2.000	2.000	2.000	2.000	2.000	2.000	2.000
ILM	61.40	62.11	60.76	43.41	60.66	60.14	57.19	60.74	59.95	60.92	60.07	58.61	59.08
GK	30.53	29.68	30.41	52.75	30.71	31.61	33.52	30.21	32.47	29.98	31.02	35.33	32.07
HM	8.07	8.21	8.82	3.84	8.63	8.25	9.29	9.05	7.58	9.10	8.91	6.06	8.85
Mg#	33.21	32.34	33.36	54.86	33.61	34.46	36.95	33.22	35.13	32.98	34.06	37.61	35.18

TABLE NO: 4

ILMENITE MEGACRYST COMPOSITIONS FROM SCHULLER

SAMPLE	86/85	86/59	86/98	86/97
TYPE	I	I	I	I
SiO2	0.00	0.00	0.00	0.00
TiO2	50.79	53.70	51.06	50.70
Al2O3	0.32	0.84	0.34	0.30
Cr2O3	0.82	2.23	0.81	0.81
Fe2O3	10.35	5.61	10.08	10.07
FeO	27.37	23.73	25.80	27.11
MnO	0.23	0.29	0.19	0.18
MgO	10.14	13.62	11.18	10.27
TOTAL	100.02	100.01	99.46	99.44
OXYG	3	3	3	3
SI	0.000	0.000	0.000	0.000
TI	0.897	0.921	0.899	0.899
AL	0.009	0.023	0.009	0.008
CR	0.015	0.040	0.015	0.015
FE3	0.183	0.096	0.178	0.179
FE2	0.537	0.452	0.505	0.535
MN	0.005	0.006	0.004	0.004
MG	0.355	0.463	0.390	0.361
SUM	2.000	2.000	2.000	2.000
ILM	54.64	46.96	51.34	54.28
GK	36.07	48.04	39.64	36.65
HM	9.29	4.99	9.02	9.07
Mg#	39.77	50.57	43.57	40.30

TABLE NO: 5

OLIVINE MEGACRYST COMPOSITIONS FROM SCHULLER

SAMPLE	85/95	85/90	85/86	85/39	85/53
SiO2	39.37	39.22	39.40	39.25	39.30
TiO2	0.00	0.00	0.00	0.00	0.00
Al2O3	0.00	0.00	0.00	0.00	0.00
Cr2O3	0.00	0.00	0.00	0.00	0.00
FeO	17.17	19.03	18.40	17.67	17.90
MnO	0.21	0.22	0.21	0.13	0.21
MgO	42.38	41.25	42.15	41.99	41.51
CaO	0.03	0.03	0.06	0.03	0.04
NiO	0.15	0.14	0.20	0.00	0.11
TOTAL	99.31	99.89	100.42	99.07	99.07
OXYG	4	4	4	4	4
SI	1.006	1.005	1.001	1.006	1.009
TI	0.000	0.000	0.000	0.000	0.000
AL	0.000	0.000	0.000	0.000	0.000
CR	0.000	0.000	0.000	0.000	0.000
FE	0.367	0.408	0.391	0.379	0.384
MN	0.005	0.005	0.005	0.003	0.005
MG	1.613	1.575	1.596	1.605	1.589
CA	0.001	0.001	0.002	0.001	0.001
NI	0.003	0.003	0.004	0.000	0.002
SUM	2.995	2.997	2.999	2.994	2.990
FO	81.47	79.44	80.32	80.90	80.52

TABLE NO: 6

CO-EXISTING MEGACRYST COMPOSITIONS FROM SCHULLER

SAMPLE	86/3	86/3	85/08	85/08	86/118	86/118
TYPE	Cpx	Opx	Gar	Opx	Gar	Opx
SiO2	54.65	56.71	41.57	57.37	41.21	56.96
TiO2	0.36	0.26	1.00	0.27	0.90	0.25
Al2O3	2.68	1.10	20.95	0.93	21.62	0.91
Cr2O3	0.34	0.20	2.34	0.21	1.68	0.15
Fe2O3	0.00	0.00	0.00	0.00	0.00	0.00
FeO	5.40	8.87	8.95	6.64	8.96	6.70
MnO	0.12	0.16	0.31	0.12	0.33	0.12
MgO	16.01	31.90	19.95	33.24	19.85	34.19
CaO	18.87	1.11	4.85	0.93	4.63	0.88
Na2O	1.84	0.19	0.11	0.19	0.09	0.19
K2O	0.00	0.00	0.00	0.00	0.00	0.00
TOTAL	100.27	100.50	100.03	99.90	99.27	100.35
OXYG	6	6	12	6	12	6
SI	1.982	1.973	2.983	1.985	2.972	1.966
TI	0.010	0.007	0.054	0.007	0.049	0.006
AL	0.115	0.045	1.772	0.038	1.838	0.037
CR	0.010	0.006	0.133	0.006	0.096	0.004
FE3	0.000	0.000	0.000	0.000	0.000	0.000
FE2	0.164	0.258	0.537	0.192	0.540	0.193
MN	0.004	0.005	0.019	0.004	0.020	0.004
MG	0.865	1.654	2.133	1.714	2.133	1.758
CA	0.733	0.041	0.373	0.034	0.358	0.033
NA	0.130	0.013	0.015	0.013	0.013	0.013
K	0.000	0.000	0.000	0.000	0.000	0.000
SUM	4.011	4.001	8.019	3.993	8.019	4.014

TABLE NO: 6

CO-EXISTING MEGACRYST COMPOSITIONS FROM SCHULLER

SAMPLE	86/83	86/83	86/114	86/114
TYPE	Cpx	Ilm	Opx	Ilm
SiO2	54.45	0.09	57.28	0.00
TiO2	0.39	50.26	0.26	56.00
Al2O3	2.73	1.02	0.91	0.21
Cr2O3	0.42	1.49	0.16	1.22
Fe2O3	0.00	0.63	0.00	3.52
FeO	5.86	34.3	6.76	24.28
MnO	0.12	10.34	0.10	0.24
MgO	16.33	0.24	33.75	14.50
CaO	18.01	0.08	0.90	0.00
Na2O	1.95	0.00	0.19	0.00
K2O	0.04	0.00	0.00	0.00
TOTAL	100.30	98.45	100.31	99.96
OXYG	6	3	6	3
SI	1.976	0.002	1.976	0.000
TI	0.011	0.961	0.007	0.956
AL	0.117	0.031	0.037	0.006
CR	0.012	0.031	0.004	0.022
FE3	0.000	0.012	0.000	0.060
FE2	0.178	0.731	0.195	0.461
MN	0.004	0.223	0.003	0.005
MG	0.883	0.009	1.735	0.491
CA	0.700	0.002	0.033	0.000
NA	0.137	0.000	0.013	0.000
K	0.002	0.000	0.000	0.000
SUM	4.019	2.001	4.003	2.000

APPENDIX 3

CLINOPYROXENE MEGACRYSTS FROM PREMIER AND ORAPA

Table 1 - Premier

Table 2 - Orapa

The average composition of at least three analyses are listed for each megacryst. Samples were analysed on multiple grain mounts. The following abbreviations are used in the tables:

Clinopyroxene :

CA = 100Ca/(Ca+Mg+Fe)

MG = 100Mg/(Ca+Mg+Fe)

FE = 100Fe/(Ca+Mg+Fe)

Ca# = 100Ca/(Ca+Mg)

Mg# = 100Mg/(Mg+Ca)

TABLE NO: 1

CLINOPYROXENE MEGACRYST COMPOSITIONS FROM PREMIER

SAMPLE	P3	P4	P5	P6	P7	P8	P9	P10	P11	P12	P13	P14	P15
TYPE	4	4	4	2	2	1	1	1	1	1	4	4	4
SiO2	54.37	54.30	54.40	54.93	55.01	54.87	54.52	54.97	54.83	54.77	54.42	54.70	54.42
TiO2	0.28	0.46	0.38	0.31	0.36	0.40	0.41	0.39	0.39	0.35	0.42	0.38	0.44
Al2O3	1.46	2.29	2.55	2.01	2.25	2.55	2.52	2.53	2.41	2.46	2.34	2.37	2.57
Cr2O3	0.29	0.51	0.42	0.82	0.84	0.29	0.15	0.26	0.26	0.37	0.32	0.21	0.33
FeO	4.08	3.46	3.79	4.30	4.36	6.84	7.45	6.76	7.23	6.37	3.87	3.55	4.38
MnO	0.09	0.08	0.08	0.16	0.09	0.12	0.17	0.17	0.14	0.12	0.05	0.06	0.08
MgO	16.52	17.31	16.44	19.28	19.99	19.32	18.96	19.47	19.42	20.33	17.05	16.66	16.73
CaO	21.08	19.24	19.44	15.95	14.79	13.25	13.34	13.00	13.24	13.06	19.10	20.29	18.90
Na2O	1.27	1.57	1.77	1.45	1.66	1.70	1.76	1.73	1.65	1.70	1.51	1.44	1.78
TOTAL	99.44	99.22	99.27	99.21	99.35	99.34	99.28	99.28	99.57	99.53	99.08	99.66	99.63
OXYG	6	6	6	6	6	6	6	6	6	6	6	6	6
SI	1.989	1.976	1.982	1.988	1.982	1.987	1.983	1.990	1.985	1.977	1.984	1.984	1.978
TI	0.008	0.013	0.010	0.008	0.010	0.011	0.011	0.011	0.011	0.010	0.012	0.010	0.012
AL	0.063	0.098	0.110	0.086	0.096	0.109	0.108	0.108	0.103	0.105	0.101	0.101	0.110
CR	0.008	0.015	0.012	0.023	0.024	0.008	0.004	0.007	0.007	0.011	0.009	0.006	0.009
FE	0.125	0.105	0.115	0.130	0.131	0.207	0.227	0.205	0.219	0.192	0.118	0.108	0.133
MN	0.003	0.002	0.002	0.005	0.003	0.004	0.005	0.005	0.004	0.004	0.002	0.002	0.002
MG	0.901	0.939	0.893	1.040	1.074	1.043	1.028	1.050	1.048	1.094	0.926	0.901	0.906
CA	0.826	0.750	0.759	0.618	0.571	0.514	0.520	0.504	0.514	0.505	0.746	0.789	0.736
NA	0.090	0.111	0.125	0.102	0.116	0.120	0.124	0.122	0.116	0.119	0.107	0.101	0.126
SUM	4.013	4.010	4.009	4.000	4.006	4.003	4.011	4.002	4.007	4.016	4.003	4.002	4.013
CA	44.62	41.81	42.95	34.58	32.15	29.15	29.30	28.66	28.85	28.20	41.67	43.89	41.46
MG	48.64	52.32	50.52	58.14	60.45	59.11	57.93	59.71	58.85	61.06	51.74	50.12	51.04
FE	6.74	5.87	6.54	7.28	7.40	11.74	12.77	11.63	12.30	10.74	6.59	5.99	7.50
Ca#	47.85	44.42	45.95	37.30	34.72	33.02	33.59	32.43	32.89	31.59	44.61	46.68	44.82
Mg#	87.83	89.91	88.54	88.88	89.10	83.43	81.93	83.69	82.72	85.05	88.70	89.32	87.19

TABLE NO: 1

CLINOPYROXENE MEGACRYST COMPOSITIONS FROM PREMIER

SAMPLE	P16	P17	P18	P19	P20	P21	P22	P23	P24	P25	P26	P27	P28
TYPE	2	2	4	4	4	4	4	2	4	4	2a	2a	2
SiO2	54.87	55.11	54.42	54.37	54.56	54.54	54.48	54.74	54.36	54.16	54.71	54.80	54.93
TiO2	0.32	0.17	0.39	0.44	0.46	0.47	0.43	0.40	0.45	0.46	0.39	0.38	0.29
Al2O3	2.38	2.09	2.41	2.57	2.45	2.46	2.32	2.09	2.37	2.35	2.31	2.39	2.11
Cr2O3	0.26	0.65	0.27	0.41	0.38	0.61	0.56	1.06	0.59	0.62	0.45	0.43	0.58
FeO	5.90	3.82	3.59	4.40	4.07	3.13	3.37	5.00	3.55	3.37	6.48	6.61	3.95
MnO	0.15	0.12	0.07	0.12	0.09	0.08	0.07	0.13	0.10	0.09	0.13	0.15	0.12
MgO	18.87	20.18	16.81	16.72	16.87	17.05	17.28	19.46	17.15	17.33	19.34	19.43	19.76
CaO	15.30	15.97	19.94	18.46	18.54	19.16	19.18	14.94	18.95	19.24	13.85	13.37	15.97
Na2O	1.58	1.36	1.48	1.84	1.67	1.68	1.57	1.68	1.62	1.60	1.60	1.80	1.48
TOTAL	99.63	99.47	99.38	99.33	99.09	99.18	99.26	99.50	99.14	99.22	99.26	99.36	99.19
OXYG	6	6	6	6	6	6	6	6	6	6	6	6	6
SI	1.985	1.983	1.980	1.981	1.988	1.982	1.980	1.979	1.979	1.972	1.985	1.986	1.984
TI	0.009	0.005	0.011	0.012	0.013	0.013	0.012	0.011	0.012	0.013	0.011	0.010	0.008
AL	0.102	0.089	0.103	0.110	0.105	0.105	0.099	0.089	0.102	0.101	0.099	0.102	0.090
CR	0.007	0.018	0.008	0.012	0.011	0.018	0.016	0.030	0.017	0.018	0.013	0.012	0.017
FE	0.179	0.115	0.109	0.134	0.124	0.095	0.102	0.151	0.108	0.103	0.197	0.200	0.119
MN	0.005	0.004	0.002	0.004	0.003	0.002	0.002	0.004	0.003	0.003	0.004	0.005	0.004
MG	1.017	1.082	0.911	0.908	0.916	0.923	0.936	1.048	0.931	0.940	1.046	1.049	1.064
CA	0.593	0.616	0.777	0.721	0.724	0.746	0.747	0.579	0.739	0.751	0.538	0.519	0.618
NA	0.111	0.095	0.105	0.130	0.118	0.119	0.111	0.118	0.115	0.113	0.113	0.127	0.104
SUM	4.007	4.006	4.006	4.011	4.001	4.003	4.006	4.009	4.006	4.013	4.005	4.010	4.007
CA	33.15	33.96	43.23	40.89	41.04	42.28	41.84	32.54	41.58	41.85	30.24	29.35	34.32
MG	56.87	59.69	50.69	51.51	51.93	52.33	52.43	58.96	52.34	52.43	58.72	59.32	59.06
FE	9.98	6.34	6.08	7.61	7.03	5.39	5.74	8.50	6.08	5.72	11.04	11.33	6.62
Ca#	36.83	36.26	46.03	44.25	44.14	44.69	44.38	35.57	44.27	44.39	33.99	33.10	36.75
Mg#	85.07	90.40	89.30	87.13	88.08	90.66	90.14	87.40	89.59	90.16	84.17	83.97	89.91

TABLE NO: 1

CLINOPYROXENE MEGACRYST COMPOSITIONS FROM PREMIER

SAMPLE	P29	P30	P31	P32	P33	P34	P35	P36	P37	P38	P39	P40	P41
TYPE	2a	2	4	2	2	4	4	4	4	2	4	4	2
SiO2	54.69	54.95	54.32	55.06	54.88	54.34	54.39	54.41	54.44	54.73	54.33	54.25	55.01
TiO2	0.44	0.36	0.44	0.39	0.27	0.45	0.44	0.44	0.44	0.20	0.38	0.47	0.17
Al2O3	2.37	2.41	2.51	2.14	1.93	2.29	2.35	2.47	2.55	2.05	2.07	2.58	1.61
Cr2O3	0.44	0.56	0.75	1.05	0.86	0.55	0.37	0.76	0.41	0.56	0.39	0.59	1.36
FeO	6.15	4.89	3.89	4.07	4.16	3.61	3.89	3.79	3.93	4.97	3.46	4.42	3.65
MnO	0.14	0.14	0.09	0.10	0.13	0.09	0.11	0.12	0.08	0.12	0.09	0.13	0.09
MgO	19.46	19.79	16.65	19.91	19.36	17.39	17.28	16.91	16.77	19.92	16.27	16.83	20.15
CaO	13.74	14.72	18.47	14.90	16.20	19.07	19.18	18.38	19.06	15.23	20.71	18.17	15.76
Na2O	1.68	1.68	1.90	1.66	1.48	1.59	1.52	1.84	1.75	1.35	1.41	1.82	1.36
TOTAL	99.11	99.50	99.02	99.28	99.27	99.38	99.53	99.12	99.43	99.13	99.11	99.26	99.16
OXYG	6	6	6	6	6	6	6	6	6	6	6	6	6
SI	1.984	1.981	1.982	1.984	1.986	1.975	1.976	1.982	1.980	1.983	1.986	1.978	1.987
TI	0.012	0.010	0.012	0.011	0.007	0.012	0.012	0.012	0.012	0.005	0.010	0.013	0.005
AL	0.101	0.102	0.108	0.091	0.082	0.098	0.101	0.106	0.109	0.088	0.089	0.111	0.069
CR	0.013	0.016	0.022	0.030	0.025	0.016	0.011	0.022	0.012	0.016	0.011	0.017	0.039
FE	0.187	0.147	0.119	0.123	0.126	0.110	0.118	0.115	0.120	0.151	0.106	0.135	0.110
MN	0.004	0.004	0.003	0.003	0.004	0.003	0.003	0.004	0.002	0.004	0.003	0.004	0.003
MG	1.052	1.063	0.906	1.069	1.044	0.942	0.936	0.918	0.909	1.075	0.886	0.914	1.085
CA	0.534	0.568	0.722	0.575	0.628	0.743	0.747	0.717	0.743	0.591	0.811	0.710	0.610
NA	0.118	0.118	0.135	0.116	0.104	0.112	0.107	0.130	0.124	0.095	0.100	0.129	0.095
SUM	4.006	4.009	4.008	4.003	4.006	4.011	4.010	4.007	4.010	4.008	4.003	4.010	4.002
CA	30.13	31.96	41.35	32.55	34.93	41.39	41.47	40.97	41.93	32.53	44.98	40.35	33.79
MG	59.35	59.76	51.85	60.50	58.07	52.50	51.97	52.43	51.32	59.18	49.15	51.99	60.10
FE	10.53	8.29	6.80	6.94	7.00	6.12	6.56	6.59	6.75	8.29	5.87	7.66	6.11
Ca#	33.67	34.84	44.37	34.98	37.56	44.09	44.38	43.87	44.97	35.47	47.79	43.70	35.99
Mg#	84.94	87.82	88.41	89.71	89.24	89.57	88.78	88.83	88.38	87.72	89.34	87.16	90.77

TABLE NO: 1

CLINOPYROXENE MEGACRYST COMPOSITIONS FROM PREMIER

SAMPLE	P42	P43	P44	P46	P47
TYPE	4	2	2	1	4
SiO2	53.93	54.92	54.72	54.62	54.40
TiO2	0.40	0.32	0.32	0.34	0.44
Al2O3	2.55	2.13	2.14	2.48	2.30
Cr2O3	0.30	0.82	0.70	0.15	0.32
FeO	4.18	4.18	4.70	7.39	3.60
MnO	0.13	0.12	0.14	0.14	0.08
MgO	16.45	19.89	19.47	18.95	17.31
CaO	19.49	15.23	15.60	13.55	19.27
Na2O	1.67	1.46	1.54	1.70	1.50
TOTAL	99.10	99.07	99.33	99.32	99.22
OXYG	6	6	6	6	6
SI	1.974	1.985	1.980	1.986	1.980
TI	0.011	0.009	0.009	0.009	0.012
AL	0.110	0.091	0.091	0.106	0.099
CR	0.009	0.023	0.020	0.004	0.009
FE	0.128	0.126	0.142	0.225	0.110
MN	0.004	0.004	0.004	0.004	0.002
MG	0.897	1.071	1.050	1.027	0.939
CA	0.764	0.590	0.605	0.528	0.751
NA	0.119	0.102	0.108	0.120	0.106
SUM	4.015	4.001	4.010	4.010	4.008
CA	42.71	33.00	33.66	29.67	41.75
MG	50.14	59.94	58.43	57.71	52.16
FE	7.15	7.07	7.91	12.63	6.09
Ca#	46.00	35.51	36.55	33.95	44.46
Mg#	87.52	89.45	88.07	82.05	89.55

TABLE NO: 1

CLINOPYROXENE MEGACRYST COMPOSITIONS FROM PREMIER

SAMPLE	JJG 3160	JJG 3161	JJG 3162	JJG 3163	JJG 3164	JJG 3165	JJG 3166	JJG 3167	JJG 3168	JJG 3170	JJG 3171	JJG 3172	JJG 3173
TYPE	4	4	4	4	4	4	4	1	1	4	4	4	1
SiO2	54.70	54.20	54.44	54.43	54.22	54.58	54.13	55.13	54.54	54.61	54.71	54.38	54.74
TiO2	0.45	0.42	0.40	0.39	0.41	0.43	0.40	0.36	0.31	0.46	0.44	0.41	0.35
Al2O3	2.33	2.23	2.28	2.57	2.34	2.39	2.63	2.41	2.43	2.37	2.37	2.35	2.48
Cr2O3	0.27	0.30	0.33	0.41	0.21	0.30	0.32	0.30	0.19	0.33	0.57	0.31	0.12
FeO	3.72	3.81	3.59	4.18	3.64	3.79	4.09	7.11	7.35	3.71	3.66	3.71	7.46
MnO	0.08	0.10	0.12	0.08	0.09	0.11	0.09	0.17	0.12	0.09	0.12	0.11	0.15
MgO	17.09	17.38	17.29	16.51	16.98	17.34	16.42	19.59	19.42	17.26	17.27	17.28	19.02
CaO	19.19	19.33	19.14	19.05	19.77	18.98	19.45	13.00	13.17	19.26	18.57	19.04	13.51
Na2O	1.52	1.45	1.51	1.77	1.47	1.55	1.66	1.70	1.68	1.51	1.60	1.48	1.73
TOTAL	99.35	99.22	99.10	99.39	99.13	99.47	99.19	99.77	99.21	99.60	99.31	99.07	99.56
OXYG	6	6	6	6	6	6	6	6	6	6	6	6	6
SI	1.987	1.975	1.983	1.982	1.978	1.981	1.977	1.989	1.983	1.980	1.986	1.981	1.986
TI	0.012	0.012	0.011	0.011	0.011	0.012	0.011	0.010	0.008	0.013	0.012	0.011	0.010
AL	0.100	0.096	0.098	0.110	0.101	0.102	0.113	0.103	0.104	0.101	0.101	0.101	0.106
CR	0.008	0.009	0.010	0.012	0.006	0.009	0.009	0.009	0.005	0.009	0.016	0.009	0.003
FE	0.113	0.116	0.109	0.127	0.111	0.115	0.125	0.215	0.224	0.112	0.111	0.113	0.226
MN	0.002	0.003	0.004	0.002	0.003	0.003	0.003	0.005	0.004	0.003	0.004	0.003	0.005
MG	0.925	0.944	0.938	0.896	0.923	0.938	0.894	1.053	1.052	0.933	0.934	0.938	1.028
CA	0.747	0.755	0.747	0.743	0.773	0.738	0.761	0.503	0.513	0.748	0.722	0.743	0.525
NA	0.107	0.103	0.107	0.125	0.104	0.109	0.118	0.119	0.119	0.106	0.113	0.105	0.122
SUM	4.001	4.012	4.006	4.009	4.010	4.007	4.010	4.005	4.013	4.005	4.000	4.005	4.011
CA	41.84	41.59	41.62	42.08	42.77	41.21	42.77	28.39	28.68	41.72	40.86	41.42	29.51
MG	51.83	52.01	52.29	50.72	51.09	52.37	50.22	59.50	58.82	52.00	52.85	52.28	57.78
FE	6.33	6.40	6.09	7.21	6.15	6.42	7.02	12.12	12.49	6.27	6.29	6.30	12.72
Ca#	44.67	44.43	44.32	45.34	45.57	44.04	45.99	32.30	32.78	44.51	43.60	44.20	33.81
Mg#	89.11	89.05	89.56	87.56	89.26	89.07	87.74	83.08	82.48	89.24	89.37	89.25	81.96

TABLE NO: 1

CLINOPYROXENE MEGACRYST COMPOSITIONS FROM PREMIER

SAMPLE	JJG 3174	JJG 1538	JJG 1542	JJG 1545	JJG 1557	JJG 1559	JJG 1561	JJG 1563	JJG 1564	JJG 1567	JJG 1569	JJG 1579
TYPE	4	4	4	2	4	4	4	4	4	2	4	4
SiO2	54.56	54.50	54.66	54.75	54.15	54.34	54.32	54.45	54.37	55.07	54.34	54.58
TiO2	0.42	0.45	0.42	0.44	0.44	0.40	0.37	0.45	0.42	0.24	0.42	0.42
Al2O3	2.29	2.32	2.29	2.08	2.35	2.11	2.48	2.43	2.46	1.86	2.34	2.47
Cr2O3	0.35	0.66	0.29	0.83	0.38	0.34	0.50	0.58	0.53	1.15	0.33	0.47
FeO	3.92	3.27	3.80	5.34	3.77	3.41	4.27	3.55	4.28	3.89	3.69	4.12
MnO	0.11	0.09	0.13	0.13	0.11	0.11	0.15	0.10	0.13	0.10	0.13	0.09
MgO	17.15	17.30	17.41	18.76	17.31	17.34	16.70	17.14	16.87	19.91	17.25	16.83
CaO	18.89	19.04	19.06	15.54	19.14	20.21	18.53	19.02	18.51	15.44	19.20	18.66
Na2O	1.51	1.59	1.43	1.72	1.52	1.24	1.80	1.64	1.79	1.45	1.57	1.72
TOTAL	99.20	99.22	99.49	99.59	99.17	99.50	99.12	99.36	99.36	99.11	99.27	99.36
OXYG	6	6	6	6	6	6	6	6	6	6	6	6
SI	1.986	1.981	1.983	1.983	1.974	1.975	1.983	1.978	1.980	1.989	1.978	1.985
TI	0.011	0.012	0.011	0.012	0.012	0.011	0.010	0.012	0.012	0.007	0.011	0.011
AL	0.098	0.099	0.098	0.089	0.101	0.090	0.107	0.104	0.106	0.079	0.100	0.106
CR	0.010	0.019	0.008	0.024	0.011	0.010	0.014	0.017	0.015	0.033	0.009	0.014
FE	0.119	0.099	0.115	0.162	0.115	0.104	0.130	0.108	0.130	0.118	0.112	0.125
MN	0.003	0.003	0.004	0.004	0.003	0.003	0.005	0.003	0.004	0.003	0.004	0.003
MG	0.930	0.937	0.941	1.013	0.940	0.939	0.909	0.928	0.916	1.072	0.936	0.912
CA	0.737	0.741	0.741	0.603	0.748	0.787	0.725	0.740	0.722	0.598	0.749	0.727
NA	0.107	0.112	0.101	0.121	0.108	0.088	0.128	0.116	0.127	0.102	0.111	0.121
SUM	4.002	4.004	4.003	4.009	4.012	4.007	4.010	4.007	4.011	3.999	4.011	4.005
CA	41.24	41.70	41.22	33.93	41.47	43.01	41.10	41.68	40.85	33.44	41.67	41.21
MG	52.08	52.70	52.37	56.97	52.16	51.33	51.51	52.24	51.78	59.98	52.08	51.69
FE	6.68	5.59	6.41	9.10	6.37	5.66	7.39	6.07	7.37	6.58	6.25	7.10
Ca#	44.19	44.17	44.04	37.33	44.29	45.59	44.38	44.38	44.10	35.80	44.45	44.36
Mg#	88.63	90.41	89.09	86.23	89.11	90.06	87.45	89.59	87.54	90.12	89.28	87.92

TABLE NO: 2

CLINOPYROXENE MEGACRYST COMPOSITIONS FROM ORAPA

SAMPLE	JJG 4134a	JJG 4134b	JJG 4134d	JJG 4134e	JJG 4134f	JJG 4134g	JJG 4134h	JJG 4134i	JJG 4134j	JJG 4134k	JJG 4134l	JJG 4134m	JJG 4134n
TYPE	C	C	C	C	C	C	C	C	C	C	C	C	C
SiO2	54.08	54.80	54.52	54.39	54.65	54.13	54.42	54.43	54.43	54.94	54.24	54.54	54.33
TiO2	0.32	0.17	0.20	0.24	0.25	0.35	0.22	0.31	0.42	0.23	0.39	0.31	0.23
Al2O3	4.03	2.95	2.63	2.64	2.70	2.21	2.78	2.69	2.37	2.69	2.31	2.75	2.60
Cr2O3	0.35	0.45	0.40	0.32	0.39	0.95	0.38	0.22	0.53	0.44	0.62	0.21	0.42
FeO	2.56	4.73	5.10	5.10	4.80	3.05	4.79	5.48	4.85	4.85	3.33	5.66	5.07
MnO	0.00	0.14	0.13	0.90	0.13	0.00	0.12	0.15	0.12	0.15	0.09	0.12	0.13
MgO	15.34	20.86	20.78	20.44	20.15	17.22	20.47	19.42	18.88	21.35	17.16	19.17	20.98
CaO	19.46	12.96	13.41	13.84	13.85	19.21	13.47	14.38	15.85	12.89	18.97	14.48	13.23
Na2O	2.43	1.85	1.72	1.74	1.78	1.77	1.81	1.85	1.72	1.67	1.74	1.89	1.73
TOTAL	98.57	98.91	98.89	99.61	98.70	98.89	98.46	98.93	99.17	99.21	98.85	99.13	98.72
OXYG	6	6	6	6	6	6	6	6	6	6	6	6	6
SI	1.974	1.975	1.972	1.964	1.980	1.976	1.975	1.977	1.976	1.975	1.980	1.978	1.969
TI	0.009	0.005	0.005	0.007	0.007	0.010	0.006	0.008	0.011	0.006	0.011	0.008	0.006
AL	0.173	0.125	0.112	0.112	0.115	0.095	0.119	0.115	0.101	0.114	0.099	0.118	0.111
CR	0.010	0.013	0.011	0.009	0.011	0.027	0.011	0.006	0.015	0.013	0.018	0.006	0.012
FE	0.078	0.143	0.154	0.154	0.145	0.093	0.145	0.166	0.147	0.146	0.102	0.172	0.154
MN	0.000	0.004	0.004	0.028	0.004	0.000	0.004	0.005	0.004	0.005	0.003	0.004	0.004
MG	0.834	1.121	1.120	1.100	1.088	0.937	1.107	1.051	1.022	1.144	0.934	1.036	1.133
CA	0.761	0.501	0.520	0.535	0.538	0.752	0.524	0.560	0.617	0.496	0.742	0.563	0.514
NA	0.172	0.129	0.121	0.122	0.125	0.125	0.128	0.130	0.121	0.117	0.123	0.133	0.122
SUM	4.012	4.016	4.021	4.030	4.013	4.016	4.018	4.019	4.015	4.014	4.012	4.018	4.024
CA	45.47	28.38	28.97	29.92	30.36	42.18	29.49	31.49	34.54	27.80	41.75	31.78	28.53
MG	49.86	63.54	62.43	61.47	61.43	52.59	62.33	59.15	57.22	64.04	52.53	58.52	62.93
FE	4.67	8.08	8.60	8.61	8.21	5.23	8.18	9.37	8.25	8.16	5.72	9.70	8.53
Ca#	47.70	30.88	31.69	32.74	33.07	44.51	32.12	34.74	37.64	30.27	44.28	35.19	31.20
Mg#	91.44	88.71	87.89	87.72	88.21	90.96	88.39	86.33	87.40	88.69	90.18	85.79	88.06

TABLE NO: 2

CLINOPYROXENE MEGACRYST COMPOSITIONS FROM ORAPA

SAMPLE	JJG 4134o	JJG 4134p	JJG 4134q	JJG 4134r	JJG 4135b	JJG 4135c	JJG 4135d	JJG 4135f	JJG 4135g	JJG 4135h	JJG 4135i	JJG 4135j	JJG 4135k
TYPE	C	C	C	C	C	C	C	C	C	C	C	C	C
SiO2	54.61	54.86	54.16	54.60	54.03	54.09	54.37	54.57	53.95	54.24	54.07	54.23	54.14
TiO2	0.32	0.23	0.37	0.24	0.38	0.37	0.27	0.37	0.33	0.38	0.29	0.39	0.32
Al2O3	2.11	2.64	2.31	2.79	2.17	2.32	2.81	2.50	3.39	2.35	2.76	2.23	2.19
Cr2O3	0.82	0.43	0.62	0.39	1.32	0.80	0.23	0.50	0.25	0.70	0.53	0.89	1.32
FeO	4.11	4.73	4.74	5.02	2.71	3.01	5.41	4.84	5.96	3.28	5.80	2.64	2.79
MnO	0.10	0.14	0.14	0.13	0.00	0.10	0.14	0.14	0.15	0.12	0.11	0.00	0.00
MgO	19.63	20.86	19.08	19.97	17.00	16.87	19.37	19.13	14.65	17.09	15.59	17.09	16.94
CaO	15.78	13.35	15.26	13.60	19.03	19.82	14.44	15.11	17.26	19.07	17.60	19.40	19.43
Na2O	1.61	1.61	1.68	1.80	1.80	1.80	1.89	1.73	2.93	1.87	2.41	1.73	1.82
TOTAL	99.09	98.85	98.36	98.54	98.44	99.18	98.93	98.89	98.87	99.10	99.16	98.60	98.95
OXYG	6	6	6	6	6	6	6	6	6	6	6	6	6
SI	1.978	1.980	1.979	1.981	1.979	1.973	1.975	1.981	1.986	1.977	1.985	1.982	1.976
TI	0.009	0.006	0.010	0.007	0.010	0.010	0.007	0.010	0.009	0.010	0.008	0.011	0.009
AL	0.090	0.112	0.100	0.119	0.094	0.100	0.120	0.107	0.147	0.101	0.119	0.096	0.094
CR	0.023	0.012	0.018	0.011	0.038	0.023	0.007	0.014	0.007	0.020	0.015	0.026	0.038
FE	0.124	0.143	0.145	0.152	0.083	0.092	0.164	0.147	0.184	0.100	0.178	0.081	0.085
MN	0.003	0.004	0.004	0.004	0.000	0.003	0.004	0.004	0.005	0.004	0.003	0.000	0.000
MG	1.060	1.122	1.039	1.080	0.928	0.917	1.048	1.035	0.804	0.928	0.853	0.931	0.922
CA	0.612	0.516	0.597	0.529	0.747	0.775	0.562	0.588	0.681	0.745	0.692	0.760	0.760
NA	0.113	0.113	0.119	0.127	0.128	0.127	0.133	0.122	0.209	0.132	0.172	0.123	0.129
SUM	4.013	4.008	4.012	4.010	4.008	4.019	4.021	4.009	4.032	4.018	4.026	4.008	4.013
CA	34.09	28.99	33.54	30.03	42.49	43.43	31.66	33.21	40.82	42.00	40.17	42.89	43.02
MG	58.98	63.00	58.33	61.32	52.79	51.42	59.08	58.48	48.18	52.36	49.49	52.55	52.16
FE	6.93	8.02	8.13	8.65	4.72	5.15	9.26	8.30	11.00	5.64	10.33	4.56	4.82
Ca#	36.63	31.51	36.51	32.87	44.59	45.79	34.90	36.22	45.86	44.51	44.80	44.94	45.20
Mg#	89.49	88.71	87.76	87.64	91.79	90.90	86.45	87.57	81.41	90.28	82.73	92.02	91.54

TABLE NO: 2

CLINOPYROXENE MEGACRYST COMPOSITIONS FROM ORAPA

SAMPLE	JJG 4135l	JJG 4135m	JJG 4135n
TYPE	C	C	C
SiO2	54.64	54.85	54.65
TiO2	0.26	0.20	0.38
Al2O3	2.82	2.82	3.50
Cr2O3	0.29	0.46	0.22
FeO	5.15	4.71	5.64
MnO	0.17	0.14	0.11
MgO	19.49	20.95	18.26
CaO	14.22	13.15	13.41
Na2O	1.88	1.80	2.51
TOTAL	98.92	99.08	98.68
OXYG	6	6	6
SI	1.980	1.975	1.985
TI	0.007	0.005	0.010
AL	0.120	0.120	0.150
CR	0.008	0.013	0.006
FE	0.156	0.142	0.171
MN	0.005	0.004	0.003
MG	1.053	1.124	0.989
CA	0.552	0.507	0.522
NA	0.132	0.126	0.177
SUM	4.014	4.016	4.015
CA	31.36	28.61	31.03
MG	59.78	63.39	58.78
FE	8.86	8.00	10.19
Ca#	34.41	31.10	34.56
Mg#	87.09	88.80	85.23

APPENDIX 4

TRACE ELEMENT ANALYSES OF SCHULLER MEGACRYSTS

Table 1 : Clinopyroxene megacrysts

Table 2 : Orthopyroxene megacrysts

Table 3 : Garnet megacrysts

TABLE NO: 1
TRACE ELEMENTS IN CLINOPYROXENE MEGACRYSTS FROM SCHULLER

SAMPLE	CPX 3	86/4	86/21	CPX 38	CPX 32	CPX 31	86/19	CPX 24	CPX 17	CPX 26	CPX 6	CPX 41	CPX 11
TYPE	1	1	1	1	1	1	1	1	2a	2a	2a	2a	2b
SiO2	55.45	55.65	55.62	55.44	55.05	55.30	55.20	54.57	55.16	54.55	54.47	54.57	55.22
TiO2	0.23	0.24	0.22	0.25	0.28	0.29	0.35	0.39	0.31	0.44	0.39	0.50	0.21
Al2O3	2.50	2.47	2.56	2.55	2.53	2.44	2.64	2.55	2.30	2.39	2.22	2.44	1.86
Cr2O3	0.26	0.26	0.25	0.26	0.19	0.16	0.14	0.13	0.51	0.55	0.99	0.30	1.04
FeO	6.16	6.15	6.17	6.45	6.74	6.85	7.07	7.21	5.21	4.88	3.83	5.38	3.39
MnO	0.12	0.14	0.17	0.13	0.14	0.12	0.13	0.15	0.14	0.13	0.13	0.15	0.11
MgO	22.04	21.74	21.51	20.93	20.34	20.10	19.28	18.72	20.14	19.11	19.19	18.05	18.88
CaO	11.94	12.05	12.07	12.14	12.87	13.01	13.53	13.73	13.82	15.21	16.44	16.13	17.01
Na2O	1.45	1.42	1.41	1.52	1.61	1.66	1.57	1.70	1.53	1.78	1.66	1.96	1.38
K2O	0.06	0.00	0.04	0.00	0.00	0.00	0.00	0.00	0.04	0.00	0.00	0.00	0.04
TOTAL	100.21	100.12	100.02	99.67	99.75	99.93	99.91	99.15	99.16	99.04	99.32	99.48	99.14
Ni (ppm)	671	661	657	635	586	550	507	423	518	422	483	456	493
Zn (ppm)	32	35	31	34	38	37	32	40	25	23	17	26	17
Ga (ppm)	5	8	5	7	9	8	9	11	9	9	9	12	4
Sr (ppm)	77	76	74	85	84	90	99	88	89	98	110	110	105
Y (ppm)	3	5	4	4	3	5	5	3	3	5	4	5	3
Zr (ppm)	5	5	4	8	6	6	9	13	8	10	11	14	6
Co (ppm)	139	151	173	142	160	194	168	183	126	116	99	137	82

SAMPLE	CPX 45	CPX 39	86/2	CPX 25	CPX 43	CPX 51	CPX 18	CPX 50	CPX 8	CPX 2	CPX 21	86/8
TYPE	2b	3	3	3	4	4	4	4	4	4	4	4
SiO2	54.88	54.06	54.72	54.07	54.58	54.75	54.67	54.86	54.67	54.02	54.49	55.07
TiO2	0.41	0.38	0.42	0.26	0.39	0.43	0.42	0.38	0.43	0.45	0.39	0.32
Al2O3	2.09	2.68	2.87	1.25	2.15	2.16	2.28	2.35	2.41	2.53	2.39	2.40
Cr2O3	0.99	0.51	0.33	0.30	1.15	1.26	1.16	1.17	1.11	0.82	0.67	1.01
FeO	2.82	5.67	5.56	5.23	3.04	2.99	2.75	2.75	2.68	3.41	3.54	3.12
MnO	0.10	0.14	0.13	0.09	0.00	0.08	0.00	0.00	0.00	0.11	0.10	0.14
MgO	18.26	16.12	15.84	15.86	17.41	17.15	17.14	16.95	16.95	17.09	16.83	16.99
CaO	17.32	17.86	18.12	20.59	18.83	19.18	19.58	19.50	19.63	19.06	19.21	19.62
Na2O	1.53	1.93	1.92	1.39	1.59	1.66	1.61	1.66	1.71	1.73	1.62	1.56
K2O	0.00	0.00	0.00	0.00	0.00	0.00	0.00	0.00	0.00	0.00	0.00	0.00
TOTAL	98.40	99.35	99.91	99.04	99.14	99.66	99.61	99.62	99.59	99.22	99.24	100.23
Ni (ppm)	417	248	186	151	447	474	402	396	372	361	317	536
Zn (ppm)	17	26	24	25	14	12	17	14	16	15	17	16
Ga (ppm)	8	19	18	16	7	8	8	6	7	10	10	7
Sr (ppm)	113	89	88	122	147	158	144	141	124	129	129	169
Y (ppm)	5	5	4	10	3	3	4	0	0	4	0	3
Zr (ppm)	13	62	87	123	22	38	32	27	29	42	26	20
Co (ppm)	71	98	110	130	79	83	108	51	71	79	90	114

TABLE NO :2
TRACE ELEMENTS IN ORTHOPYROXENE MEGACRYSTS FROM SCHULLER

SAMPLE	OPX13	OPX16	OPX3	OPX8	OPX20	OPX12	OPX17	OPX2	OPX19	OPX6	OPX15	OPX11	OPX18
TYPE	1	1	1	1	1	1	2	2	2	2	2	2	2
SiO2	56.01	56.36	55.67	55.69	55.56	56.17	56.96	56.41	55.99	57.45	57.23	57.09	57.06
TiO2	0.28	0.19	0.23	0.19	0.20	0.22	0.19	0.26	0.24	0.15	0.21	0.19	0.28
Al2O3	1.07	0.93	0.93	0.92	0.90	0.94	0.92	0.89	0.94	0.92	0.91	0.93	0.91
Cr2O3	0.08	0.01	0.01	0.01	0.01	0.08	0.24	0.11	0.20	0.24	0.28	0.26	0.18
FEOT	8.85	10.14	9.29	10.98	9.96	9.19	6.27	8.12	6.81	5.45	6.01	5.57	6.82
MnO	0.14	0.15	0.00	0.17	0.21	0.16	0.16	0.14	0.14	0.12	0.11	0.08	0.11
MgO	31.57	31.14	31.92	30.99	32.19	31.79	33.63	33.24	33.61	34.37	33.70	34.37	34.20
CaO	1.40	0.85	0.90	0.87	0.86	0.91	1.15	0.90	1.13	1.13	0.99	1.03	0.93
Na2O	0.48	0.21	0.21	0.23	0.18	0.22	0.23	0.19	0.28	0.23	0.20	0.24	0.17
K2O	0.23	0.00	0.00	0.00	0.00	0.00	0.00	0.00	0.00	0.00	0.00	0.00	0.00
TOTAL	100.11	99.99	99.18	100.06	100.08	99.65	99.76	100.27	99.35	100.07	99.65	99.77	100.67
Ni (ppm)	465	389	562	372	402	460	839	555	766	220	700	829	708
Zn (ppm)	62	72	62	83	67	61	37	53	42	37	33	34	41

SAMPLE	OPX1	OPX14
TYPE	2	2
SiO2	56.89	56.69
TiO2	0.25	0.24
Al2O3	1.02	0.92
Cr2O3	0.13	0.19
FEOT	7.86	7.02
MnO	0.17	0.14
MgO	32.68	33.09
CaO	1.28	1.16
Na2O	0.31	0.23
K2O	0.00	0.00
TOTAL	100.60	99.69
Ni (ppm)	691	714
Zn (ppm)	51	43

TABLE NO: 3
TRACE ELEMENTS IN GARNET MEGACRYSTS FROM SCHULLER

SAMPLE	GA16	GA9	GA25	GA27	GA8	GA26	GA18	GA19	GA6	GA3	GA12	GA11	GA14
TYPE	1	1	1	1	1	1	1	2	2	2	2	2	2
SiO2	41.26	41.06	41.53	41.61	41.44	41.62	41.62	41.60	41.68	41.87	41.55	41.73	40.97
TiO2	1.18	1.17	0.54	1.06	1.14	1.02	0.95	1.10	0.81	0.84	0.93	0.90	1.00
Al2O3	20.87	20.74	21.89	20.50	20.44	21.00	21.04	20.30	19.92	20.90	20.05	20.41	19.95
Cr2O3	1.36	1.88	1.13	1.79	2.04	1.36	2.01	2.55	3.63	2.53	3.28	3.03	3.56
FeO	10.41	9.59	9.45	10.00	9.28	9.08	9.03	8.51	7.65	8.07	8.20	8.39	8.28
MnO	0.30	0.30	0.32	0.34	0.30	0.31	0.30	0.34	0.29	0.36	0.33	0.32	0.31
MgO	19.29	19.36	19.42	19.55	19.51	19.75	20.10	19.75	20.11	19.76	19.72	19.57	19.88
CaO	4.50	4.81	4.87	4.47	4.82	4.68	4.48	4.84	5.06	4.73	5.12	4.98	5.04
Na2O	0.11	0.10	0.07	0.10	0.09	0.10	0.10	0.10	0.08	0.07	0.08	0.09	0.09
TOTAL	99.28	99.01	99.22	99.42	99.06	98.92	99.63	99.09	99.23	99.13	99.26	99.42	99.08
Ni (ppm)	106	101	49	117	105	76	107	99	114	108	93	92	119
Zn (ppm)	25	18	17	24	19	17	22	17	15	14	17	19	17
Ga (ppm)	22	21	15	14	24	18	14	16	17	15	13	16	14
Ge (ppm)	4	4	6	4	5	4	0	0	5	5	6	4	4
Y (ppm)	31	15	20	18	27	20	18	20	21	21	21	18	27
Zr (ppm)	95	50	72	63	82	71	80	74	87	67	72	66	95

SAMPLE	GA22
TYPE	2
SiO2	41.38
TiO2	1.11
Al2O3	20.43
Cr2O3	2.43
FeO	8.56
MnO	0.29
MgO	19.97
CaO	4.87
Na2O	0.11
TOTAL	99.14
Ni (ppm)	105
Zn (ppm)	20
Ga (ppm)	19
Ge (ppm)	4
Y (ppm)	26
Zr (ppm)	88

APPENDIX 5

ANALYTICAL TECHNIQUES FOR ISOTOPE ANALYSIS

1.1 PREPARATION OF SAMPLES

The samples were wrapped in clean tissue paper and broken by hammer. Further crushing was done in an agate mortar and pestle which was solely reserved for the clinopyroxene isotope work. Samples were crushed gently in order to minimise the dust fraction with resultant maximum yields of material suitable for hand picking. All samples were crushed to pass through a 600 um nylon screen after which the -600 +500 and -500 +425 size fractions were collected. These were subjected to ultrasonic agitation in reagent grade ethanol to clean surface contamination and to remove the residual dust fraction. All processing implements including the mortar and pestle, glassware and nylon screens were carefully cleaned and examined between successive samples to minimise the possibility of cross contamination between samples.

Samples were hand-picked while immersed in reagent grade ethanol using a binocular microscope fitted with both brightfield and darkfield illumination. Immersion in alcohol and the type of illumination used minimised surface reflections and allowed the interiors of grains to be inspected. Only grains free of inclusions and free of

fracture- or crystallographic planes containing alteration material were selected. Under brightfield illumination the alteration zones shows up as brown discolorations at the crystallographic or internal fracture surfaces while under darkfield illumination these appear as brighter reflection areas. Grains with any surface films or with an irregular pitted or frosted surfaces were excluded. All grains were examined from all sides to exclude grains with any possible defects. Each sample was subjected to an additional screening to select only the purest fraction. The grains selected for isotope work were clear fresh grains bounded by conchoidally fracture surfaces or clear cleavage planes. The resulting material were estimated to be better than 99% clean. Sample yields for the initial picking varied between 2 and 5 % by mass of the sieved fraction of which between 30 to 50 % were discarded during the final picking. Sample masses of between 12 and 60 mg were finally processed for isotope work.

1.2 ISOTOPE PREPARATION

1.2.1 Leaching

The hand-picked material was leached overnight on a hot plate at 50 deg C in double distilled 6N HCl in a closed Savillex beaker. The leachate solution was decanted and the clinopyroxene grains were cleaned by 5 minutes of ultrasonic agitation in double distilled water followed by

several washes in distilled water. Sample masses were determined before and after leaching.

1.2.3 Dissolution

The leached grains were dissolved in a mixture of double distilled HF, $HClO_4$ and HNO_3 in the ratio 20:1:2 per volume in clean 15 ml Savillex beakers. The samples were heated on a hot plate for 20 minutes, cooled and placed in a 30 ml Savillex pressure vessel in and oven at 100 deg C for 6-7 days. Following this, the excess liquid was evaporated on a hot plate. Double distilled 6 N HCl was added to the residue and the mixture was heated until a clear yellow solution was obtained. The solution was then split into two aliquots for isotope dilution (ID) and isotope composition (IC) determinations in ratio 1/3 : 2/3. The ID aliquot was heated to homogenise with pre-weighed spikes of enriched ^{87}Rb, ^{84}Sr, ^{146}Nd and ^{149}Sm. Both aliquots were dried in separate clean air boxes under thermal lamps in order to prevent cross-contamination.

1.3 COLUMN WORK

All separations were done on small columns which are reserved for low level small mineral samples. Separate columns were used for natural and spiked samples. The Rb, Sr and REE fractions were successively eluted in a 5 mm diameter column containing 10 cm of Biorad AG 50 Wx8,

200-400 mesh, resin. The samples were taken into solution with 0.5 ml of 2.59 N HCl and left overnight to equilibrate. The solutions were centrifuged in plastic test tubes and pipetted onto pre-cleaned and preconditioned columns.

REE separations were done on a 5mm diameter column packed with teflon particles coated with a solution of di-2-ethylhexyl orthophosphoric acid (HDEHP) (Richard et al, 1976). The REE fraction from the cation exchange column was dried in clean air boxes under thermal lamps, cooled and equilibrated in 250 ul 0.21 N HCl and pipetted onto pre-cleaned and pre-conditioned columns.

1.3.1 Calibration of columns

The primary columns were periodically calibrated with a mixture of Ca-Sr-Rb-Fe salts whereas a Ba-Nd-Sm mixture was used for the REE column. Aliquots of 0.5 ml or 1.0 ml of the eluant were collected and subsequently analysed by atomic absorption to determine element peak positions and ranges.

Due to the high calcium concentration and low Sr concentrations of clinopyroxenes and short length of the cation exchange columns, an extensive overlap was found between the calcium and strontium elution peaks. This necessitated the strontium fraction to be processed through the column for a second time.

1.4 FILAMENTS and MASS SPECTROMETRY

1.4.1 Sr

The residue from the columns were converted to nitrides with a few drops of concentrated HNO_3, dried and loaded on single Ta filaments using a mixture of phosphoric and nitric acids. The isotope determinations were performed with a with VG 354 mass spectrometer for both ID and IC.

1.4.2 Rb

The Rb fraction collected from the columns were loaded on double Ta filaments with distilled water. The isotopic ratios were determined with a with MAT 261 mass spectrometer. All measurements were found to be within blank levels.

1.4.3 REE

Both Sm and Nd were loaded on single Re filaments with Pt activated charcoal following the method of Noble et al. (1989). The Nd isotopic compositions were determined on VG 354 mass spectrometer whereas Nd and Sm concentrations were determined on MM30 mass spectrometer.

1.5 CALCULATION OF RESULTS

Values for Bulk Earth used in calculations:

$(^{87}Sr/^{87}Sr)$bulk earth (present) = 0.7045

$(^{87}Rb/^{86}Sr)$bulk earth (present) = 0.0827

$(^{143}Nd/^{144}Nd)$CHUR (present) = 0.51264

$(^{147}Sm/^{144}Nd)$CHUR = 0.1967

Blanks:

Total procedure blanks for Sr, Sm and Nd were found to be less than 0.6, 0.2 and 0.5 ng respectively.

Nd is reported relative to $^{143}Nd/^{144}Nd$ = 0.511850 +/- 30 for the La Jolla standard. Sr is reported relative to $^{87}Sr/^{86}Sr$ = 0.708002 +/- 35 for the E&A standard.

APPENDIX 6

Table 1 - Comparison of Sr concentration results obtained by isotope dilution and the proton probe.

Table 2 - Sr isotope results from Schuller and Premier.

Table 3 - Nd and Sm isotope results from Schuller and Premier.

TABLE 1: Comparison of Sr concentration results obtained by isotope dilution (ID) and the proton probe (PIXE).

Sample	Sr (ID)	Sr (PIXE)	PIXE (1 sigma)
CPX 3	74.75	77	3.5
CPX 32	85.07	84	3.9
CPX 24	93.10	88	4.4
CPX 17	92.7	89	2.5
CPX 6	101.11	110	4.2
CPX 39	85	89	2.9
86/2	95	88	4.3
CPX 25	112.64	122	4.5
CPX 18	148.65	144	5.3
CPX 43	133.83	147	5.8
CPX 21	123.22	129	3.9

TABLE 2 : Sr isotope results from Schuller and Premier.

	Sr ppm	$^{87}Sr/^{86}Sr$ ID	$^{87}Sr/^{86}Sr$ IC
SCHULLER			
GROUP 1			
CPX 3	74.75	0.70219 +/- 2	0.70217 +/- 2
CPX 32	85.07	v. poor run	0.70217 +/- 2
CPX 24	93.10	0.70217 +/- 2	0.70218 +/-2
GROUP 2			
CPX 17	-	failed	0.70202 +/- 2
CPX 26	92.7	0.70211 +/- 2*	failed
CPX 6	101.11	0.70264 +/- 5*	0.70207 +/- 3
CPX 11	na	na	0.70214 +/- 3
GROUP 3			
86/2	(95.5)	0.70286 +/- 2*	0.70222 +/- 2
CPX 25	112.64	0.70235 +/- 2*	0.70222 +/- 2
GROUP 4			
CPX 18	148.65	0.70264 +/- 2	0.70264 +/- 2
CPX 43	failed	failed	failed
CPX 43#	133.83	0.70262 +/- 2	na
CPX 21 a	failed	failed	0.70259 +/- 3
CPX 21 b	123.22	0.70258 +/- 2	0.70255 +/- 3
CPX 21 b#	122.89	0.70240 +/- 1	0.70243 +/- 1
PREMIER			
GROUP 1			
P46	na	0.70222 +/- 2	failed
P46a	89.79	0.70216 +/- 5	0.70225 +/- 2
P46a#	89.75	0.70222 +/- 1	na
GROUP 2			
P6a	98.57	0.70204 +/- 5	0.70195 +/- 2
P6a#	98.24	0.70205 +/- 1	na
GROUP 4			
P3c	112.2	0.70233 +/- 2	failed

na = not analysed
# = samples analysed at the Geological Survey
* = inconsistent analyses

TABLE 3 : Nd and Sm isotope results from Schuller and Premier.

	Sm	Nd	$^{147}Sm/^{144}Nd$	$^{143}Nd/^{144}Nd_m$	$^{143}Nd/^{144}Nd_i$	eNd
SCHULLER						
GROUP 1						
CPX 3	1.10	3.77	0.17622	0.51262 +/- 4	0.51123	+2.80
CPX 32	1.36	4.56	0.18012	0.51256 +/- 4	0.51114	+1.03
CPX 24	1.78	5.69	0.18893	0.51259 +/- 3	0.51110	+0.26
GROUP 2						
CPX 17	1.46	5.36	0.16451	0.51261 +/- 2	0.51132	+4.41
CPX 26	1.53	4.89	0.18896	0.51268 +/- 5	0.51119	+2.01
CPX 6	1.51	5.63	0.16198	0.51246 +/- 6	0.51119	+1.86
CPX 11	na	na	-	0.51237 +/- 4	-	-
GROUP 3						
86/2	1.93	14.05	0.08296	failed	-	-
CPX 25	2.18	7.76	0.16966	0.51249 +/- 7	0.51116	+1.26
GROUP 4						
CPX 18	2.03	7.40	0.16568	0.51239 +/- 6	0.51109	-0.08
CPX 43	1.68	6.38	0.15903	0.51245 +/- 6	0.51120	+2.12
CPX 21a	1.52	6.06	0.15148	0.51242 +/- 3	0.51123	+2.69
CPX 21b	1.57	6.00	0.15803	0.51244 +/- 5	0.51120	+2.08
PREMIER						
P46	1.52	5.06	0.18142	na	-	-
P46a	1.54	5.08	0.18308	0.51256 +/- 3	0.51112	+0.57
P6a	1.52	5.21	0.17620	0.51257 +/- 3	0.51118	+1.82
P3c	1.91	6.86	0.16815	0.51258 +/- 2	0.51126	+3.26
P3d	1.89	6.81	0.16761	failed	-	-